Net Current Measurements and Secondary Electron Emission Characteristics of the Voyager Plasma Science Experiment and Their Impact On Data Interpretation

RALPH L. MCNUTT, JR.

Department of Physics and Center for Space Research
Massachusetts Institute of Technology
Cambridge, MA 02139

September, 1988

CSR-TR-88-6

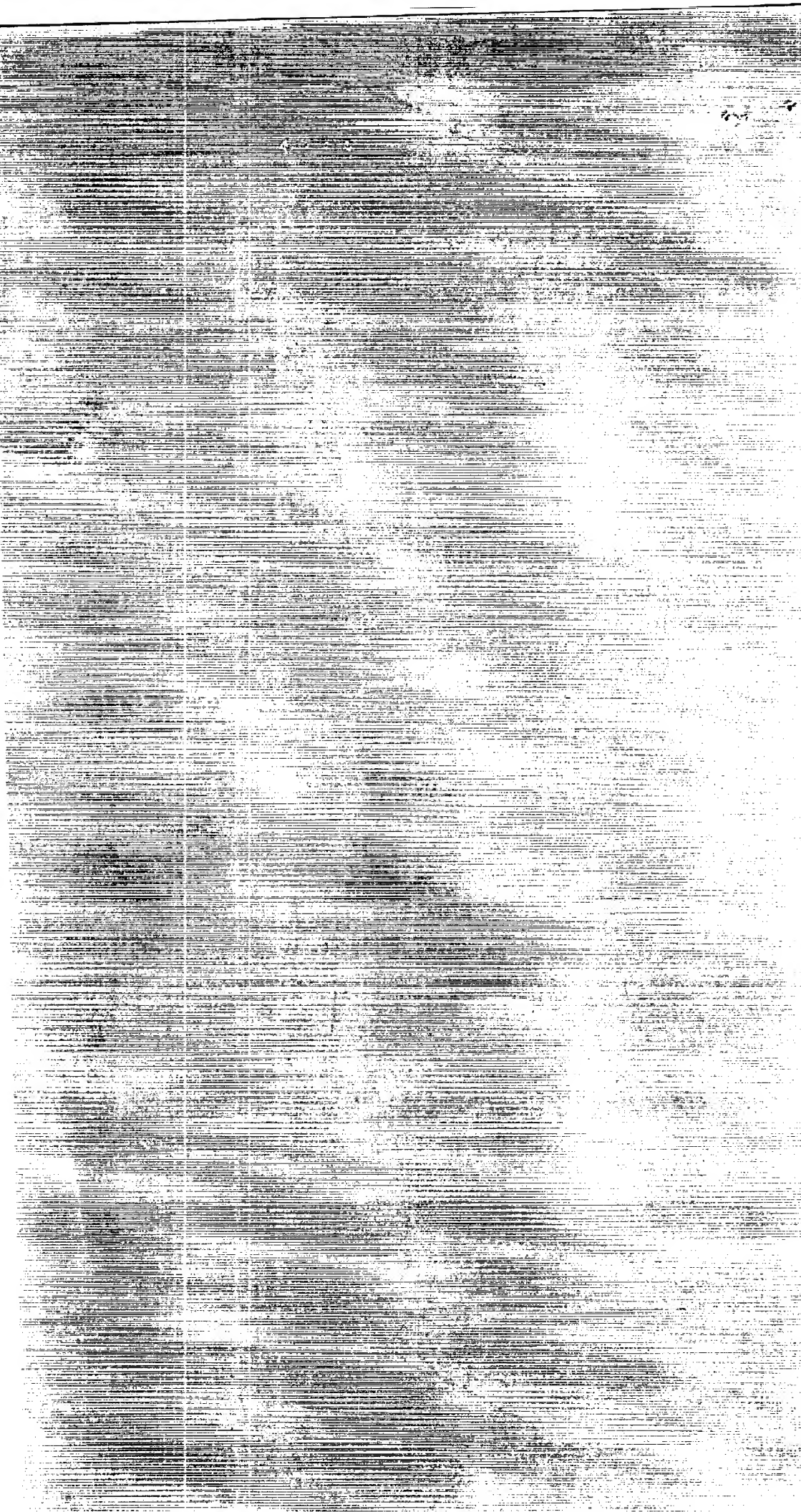

Net Current Measurements and Secondary Electron Emission Characteristics of the Voyager Plasma Science Experiment and Their Impact On Data Interpretation

RALPH L. MCNUTT, JR.

Department of Physics and Center for Space Research
Massachusetts Institute of Technology
Cambridge, MA 02139

September, 1988

CSR-TR-88-6

Net Current Measurements and Secondary Electron Emission Characteristics of the Voyager Plasma Science Experiment and Their Impact On Data Interpretation

RALPH L. MCNUTT, JR.

Department of Physics and Center for Space Research, Massachusetts Institute of Technology, Cambridge

The Voyager Plasma Science (PLS) instrument is capable of returning integral (DC) current measurements as well as normal plasma measurements. These measurements are similar in some respects to measurements made with a Langmuir probe or a retarding potential analyzer, although there are significant differences. The integral measurements have been made during calibration sequence in the solar wind, during Cruise Science Maneuvers, and within the magnetospheres of Jupiter and Saturn by Voyager 1. After the failure of the PLS experiment after the Saturn encounter, that instrument was placed in the DC return mode and returned possibly usable data from early 1981 through early 1985. The DC return measurements are difficult to interpret and are above threshold values only for relatively large fluxes; the determination of the measured current level is dependent on the operating temperature of the preamplifiers which further complicates the interpretation. Nevertheless, these measurements can be used to determine the efficiency of the suppressor grid at preventing the loss of secondary electrons off of the collector plate. Some DC return measurements have been invaluable in aiding in the interpretation of some electron plasma measurements which had not previously been understood. We find that the electron spectra can be significantly modified by the presence of second generation secondary electrons produced by the production of either first generation secondaries or photoelectrons on the support ring of the negative high voltage modulator grid within the instrument housing. This accounts for electron spectra obtained when the PLS side sensor is illuminated by sunlight while in one of the electron modes. The effect also explains the characteristics of electron spectra obtained by Voyager 2 in the plasma voids near Ganymede during the Jupiter encounter and in the "charging region" while that spacecraft was outbound from Uranus. As a result, we have also identified other regions in which the Voyager spacecraft was charged to −1 kV and have noted regions in which care must be taken in the analysis of the suprathermal component of the measured electron distributions.

INTRODUCTION

The Plasma Science (PLS) experiment on the two Voyager spacecraft has returned a wealth of scientific information concerning the state of the interplanetary medium [*Gazis*, 1984] and the plasma populations of the magnetospheres of the outer planets visited to date [*Belcher*, 1983 and references therein; *Sittler et al.*, 1981; *Lazarus and McNutt*, 1983; *Sittler et al.*, 1983; *Richardson*, 198 ; *McNutt et al.*, 1987; *Selesnick and McNutt*, 1987]. In addition to the plasma measurements made most of the time by the instrument upon which all previously reported analyses are based, there are integral (DC return) measurements. These measurements effectively bypass the action of the modulator grid in the instrument and are only taken over a limited dynamical range [*Bridge et al.*, 1977]. These measurements are also difficult to interpret as is made clear in the body of this paper. However, they have proven to be an invaluable diagnostic tool in better understanding the effects due to the production of secondary electrons within the instrument housing itself. In particular, there are electron spectra which do not "make sense" given the normal operating characteristics and environment of the PLS instrument. Using the DC return measurements and the production of photoelectrons within the instrument as guides and diagnostics, we have been able to explain semi-quantitatively data which had previously defied explanation.

DC RETURN MEASUREMENTS

DC return currents and normal plasma data are returned from the A and D cups of the PLS instrument in the DC return mode; plasma data from the B and C cups is replaced by A cup DC return and D cup DC return currents, respectively. The quantization steps for DC return currents are large to accommodate both large fluxes and currents of both positive and negative sign. The nominal sensitivity/range of the DC amplifiers (there are 2 DC measurement chains) is $\pm$ (10^{-10} to 10^{-7}) amperes [*Bridge et al.*, 1977]. In the main PLS analysis software package (VGRANL), there is a conversion lookup table from DN to femtoamperes. This table, in the common block PLCONS, has negative currents from -1.00×10^5 fA (femtoamperes; 1 fA = 10^{-15} A) for DN=0 to -1.00×10^8 fA for DN=127 and positive currents from $+7.5 \times 10^4$ fA for DN=128 to $+1.00 \times 10^8$ fA for DN=255. A listing of these currents is included as Table 1 and a graph of the absolute value of these currents versus DN is included as Figure 1. The calibration curve from which this table was constructed is not known, but it is probably based upon a laboratory calibration curve (A. Mavretic, private communication) which was made at a temperature of +25° C (this is the most detailed curve which is available to me and is for SN003, the flight spare; there is also a "quick check" measurement which was made for SN002, launched on Voyager; SN001 is on Voyager 2 - the spacecraft numbers and instrument serial numbers *really are* reversed). This curve is appended as Figure 2; note that for negative

currents there is a small difference between the conversions for the A and D cups.

From another laboratory notebook (A. Mavretic, private communication), a full set of I_{DC} calibration have been found for SN002 (also designated Flight 1 or F1). These are from the summer of 1977. Figures 3 through 5 plot DC current (positive and negative) versus DN for both A and D cups. These were made for three different temperatures: -10°C, +27°C, and +50°D. Figures 6 through 9 show DC current versus temperature for constant DN values. Figures 6 and 7 are for the A cup (negative and positive current) and Figures 8 and 9 are for the D cup (negative and positive current). The calibration changes as a function of temperature (the preamplifier temperature) can be significant for the DC measurements; this is (thankfully!) not the case for the AC, i.e., plasma, measurements.

DC return spectra typically show a DN value of 128 (positive threshold) in the D cup and a flat spectrum at the upper positive levels in the A cup (from DC return measurements in the L and M - positive modulator voltage - modes). At lower positive voltages in the A cup, higher positive currents indicative of the solar wind are apparent (at small enough heliographic distances). The currents at large potentials in the A cup have been ascribed to photoelectron production in the A cup, presumably off of the gold-plated collector plate. The D cup is usually in shadow so no photoelectrons should be produced. Considerable structure is found in the DC return spectra (all modes) from the Voyager 1 encounters with Jupiter and Saturn when particle fluxes into the cups were large; the PLS-A science link (the nomenclature may have been different for the Saturn encounter) included DC return measurements about every 45 minutes. No DC measurements were made routinely during the Voyager 2 encounters with Jupiter, Saturn or Uranus. The few DC return measurements made during the Voyager 2 encounter with Jupiter occurred far from the planet when particle fluxes were low and exhibit the same flat structure as found in the solar wind.

R. S. Selesnick attempted to verify the photoelectron hypothesis by plotting the DC return current from the A cup (channel 128) as a function of spacecraft distance from the sun. At these voltages, there should be no contribution from the solar wind, even if the particle flux in the wind is very large. Selesnick's plots are appended as Figures 10 (Voyager 1) and 11 (Voyager 2). Although the current tends to follow an r^{-2} line for both spacecraft, there are unexplained deviations. Two possible effects not taken into account are i) the angle at which the sunlight is incident upon the collector and ii) changes in the DN to current conversion as the spacecraft moves out from the sun and cools (the calibration curve for a temperature of +25° C is used to do all of the conversions). The last point on the Voyager 1 plot is for day 236 of 1984 (corresponding to a heliocentric distance of 20.8 AU). In spot checking the printout of currents made at JPL (O. Divers, private communication), I found that in the L mode measurements in the A cup, the DN values in channel 16 are down to 128 by this time (Selesnick was using M mode spectra). In the lower channels, DC levels apparently due to the solar wind are being measured. The DN value in channel 1 is down to 129 (1 DN above positive threshold) on day 25 of 1985. The corresponding heliocentric distance is 22 AU. **Information on the solar wind velocity and flux (hence, density) is apparently available from the DC return measurements through this time.** The M mode measurements seem to be clamped to a constant value indicative of the solar wind; in other words, the M mode measurements do seem to have been effected adversely by the failure.

In Voyager Memorandum #153, I gave a rough estimate that the DC return values should be near threshold at ~24 AU. This distance was reached near the end of 1985, so the available numbers are roughly consistent. At 400 km s^{-1}, 10^5 fA corresponds to a charge density of ~0.23 cm^{-3} (see Table 3 of Voyager Memorandum #99).

Photoelectron Yields

The photoelectron yield can vary as secθ although this effect is dependent on both polarization and wavelength of the incident light in a complicated fashion (see *Whipple* [1981]). The energy distribution of photoelectrons can be well represented by a Maxwellian energy distribution,

$$f(E) = \frac{2}{\pi^{1/2} E_0^{3/2}} E^{1/2} e^{-E/E_0} \qquad (1)$$

Here $\int_0^\infty f(E) = 1$ and E_0 is the "temperature" of the photoelectrons.

In dealing with both photoelectron and secondary electron emission, a flux "distribution function" is used [*Grard*, 1973; *Hachenberg and Brauer*, 1959]. In this case the Maxwellian energy distribution is

$$j(E) = E/E_0^2 e^{-E/E_0} \qquad (2)$$

Again, the normalization is such that $\int_0^\infty j(E) = 1$. Note that the most probable energy E_{mp} - defined at the maximum of $j(E)$ - is E_0. Hence, when a "most probable" secondary electron energy is quoted in the literature, it is *almost always* with respect to $j(E)$ and. therefore, is the same as the secondary "temperature."

Grard [1973] finds values of E_0 ("most probable energy") of 0.88 eV for gold (appropriate for the collector plate) and 1.02 for graphite (appropriate more or less for the black conducting paint - up to 12% carbon by weight (A. C. Whittlesey, private communication, Feb. 20, 1987) - used on the Voyager spacecraft; secondary and photoemission characteristics of the paint are not known).

PLS Instrument Temperatures

Three instrument temperatures are routinely telemetered to Earth in the PLS engineering records. Knowledge of the temperature decreases during the missions of Voyagers 1 and 2 as they move away from the sun is of both general interest as well as necessary for the proper interpretation of DC return measurements: the calibration curves for translating DN (data numbers) to I_{DC} values is dependent upon the temperature of the preamplifier and measurement chain.

The temperature readouts from the PLS instruments on both

spacecraft have been indicating decreasing temperature with increasing distance from the sun. Temperatures and other readouts are returned in engineering records and are plotted to produce engineering plots. Such plots have been made for both spacecraft for a great deal of the two missions and are in a notebook in the programmers' office. Printout of the engineering records consists of 9 integer fields (IENG) and 3 real fields (TEMPS). The integer fields are data numbers, and 8 of these are plotted on engineering plots with the not terribly illuminating labels ESUP, VREF, VCOM, PSUP, TSEN, TPMC, TMOD, and MODE. The non-temperature data is part of the PLS analog multiplexer output. The latter is comprised of the PLS backup science data ("a 0 to 3 volt representation of the four decade plasma measurement to be used in the event that the PLS ADC ceases to function"), the internal reference voltage of 10 volts, the suppressor voltages, and a combination of the positive and negative 15 volt supply voltages; correspondence with the engineering plots is obvious given this information. Backup science data DNs are not routinely plotted; backup science data is also not well documented at this juncture. What documentation I have found is in JPL document 618-505, Vol. IV, Rev. B.

The temperature data are interpreted as follows

Label	Description	IENG( )	TEMP( )
TMOD	Modulator Temperature	1	1
TPMC	Preamp and Measurement Chain	2	2
TSEN	Sensor Temp. (A cup Housing ?)	3	3

The units of TEMP are °C; the conversion algorithm from DN to °C is not documented but buried in the subroutine MJSTEM. The DN values are first converted to resistance values. These are then converted to temperatures via interpolation from a lookup table stored with the subroutine. The sensor temperature conversion is different from the other two. Lookup tables and graphs for the conversion for the sensors on S/C 31 are included as Appendix A (from JPL document 618-301).

Engineering plots were not routinely made during the encounter periods; they have been recently run for one day periods during the encounters. Variation during these periods was minimal; typical temperatures from the encounters are listed in the following table.

S/C	Date	Planet	TSEN (°C)	TPMC (°C)	TMOD (°C)
1	1979/ 64	Jupiter	-123.58	9.07	11.18
1	1980/318	Saturn	-148.22	4.14	6.95
2	1979/189	Jupiter	-122.39	9.07	11.18
2	1981/237	Saturn	-147.17	4.84	6.95
2	1986/ 24	Uranus	-160.35	3.43	6.95

Selesnick's numbers (referred to above) have not been corrected for the temperature shift; how much this will "help" his curves is not yet known.

Photocurrent Loss From DC Return Measurements

At the Earth *Garrett* [1981] lists the photoelectron flux from solar spectrum photons incident on gold as $j_{ph} = 2.9 \times 10^{-9}$ A cm^{-2} (see his Table 4). The effective area of each of the main sensor cups is $A_{eff} = 66$ cm^2 (see p.12 of *Barnett*, [1984]), and the photoelectron flux at Jupiter is down from that at Earth by a factor of 5.2^{-2}. This should produce a photocurrent at the collector plate of

$$I_{ph} = j_{ph,Earth} A_{eff} r^{-2} \qquad (3)$$

or 7.08×10^6 fA. I have looked at the L mode DC return measurements from the Voyager 1 Jupiter encounter (DC return measurements were made every 45 minutes as part of the PLS-A science link). The following table lists DC return times and the A cup current and the D cup current in channel 16 (the D cup current was at the positive threshold of 7.5×10^4 fA for most of the spectra). Note that the currents listed are nominal values using the lookup table exhibited in Table 1 and Figure 1.

Time	$I_{A,16}$ fA	DN, A	$I_{D,16}$ fA
62 0601	1.71×10^6	192	7.50×10^4
63 1924	1.38×10^6	191	7.50×10^4
64 0503	8.20×10^5	184	7.50×10^4
64 0737	1.38×10^6	191	7.50×10^4
64 0921	1.38×10^6	191	7.50×10^4
64 1426	1.38×10^6	191	7.50×10^4
64 1829	-2.40×10^6	66	-2.0×10^6
64 1922	-2.40×10^6	66	-4.9×10^6
65 0629	4.14×10^5	164	-2.0×10^6

The difference between the fluxes into A and D should be representative of the current measured due to the loss of photoelectrons within the instrument (i.e. those not returned to the collector plate by the potential on the suppressor grid). If we take 1.5×10^6 as a representative photocurrent, this implies an internal loss of ~ 20 %, consistent with more detailed calculations on secondary electron losses in the side sensor. From Voyager Bulletin #37, entrance into solar occultation was 1637 and exit from solar occultation was 1849. This is consistent with the no photoelectron production and the measured negative current at 1829. The very large negative currents at 1922 of day 64 are apparently due to photoelectron production in the side sensor; due to a maneuver, the angle between the D cup normal and the sun decreased to just under a critical angle discussed elsewhere. The large negative currents on 65 are presumably from the hot electron population near the spacecraft, but this needs further investigation (and use of the proper DN to current curve). Four DC return measurements at Saturn on day 317 of 1980 (at 0736, 0738, 0828, and 0919) all gave the D cup at positive threshold and the A cup at 5.80×10^5 fA, somewhat larger than predicted than a simple r^{-2} scaling from Jupiter would predict, but, again, this could be related to the change in the preamplifier temperature.

There are a few other things to note about the Voyager 1 encounter with Saturn. The first is that there was one 360° yaw turn at Saturn, similar to the PLOMAN and FLOMAP maneuvers by Voyager 1 at Jupiter. For the record, appropriate information about the maneuver (FSMAN-5) is as follows:

Voyager 1 Yaw Maneuver at Saturn	
Type of Rotation	Start Time of Rotation
Roll	318/2117:02
Yaw	318/2128:24
Yaw	318/2146:29
Roll	318/2210:42

My notes indicate that the first yaw went through 132° and the second completed the 360° turn.

In addition, it should be noted that the sun occultation ingress for Voyager 1 was 1980-318/0153:23 and the sun occultation egress was 1980-318/0240:01. In occultation, there is no evidence from a cursory examination of the 1800 plots that any charging of the spacecraft to high negative levels was occurring. This is probably not surprising in that the bulk of the electrons had a relatively low (< 50 eV) temperature during this time. It should also be noted that of DC return spectra were acquired around ~ 318/0200 within the occultation period. The spectra from the A cup do show that the photoelectron current from the collector plate was turned off. They also indicate large negative currents at positive potentials up to several tens of volts. If such a signature has occurred elsewhere in the DC return spectra, I have not yet run across it.

Secondary Electron Emission From the Collector Plate

I am also investigating the possibility of "experimentally" obtaining the suppressor efficiency from looking at DC return measurements made early in the mission when sunlight illuminated the D cup collector plate. In addition, George and I are working on a quantitative model of secondary electron loss from the D cup. Secondary electrons can also be modeled with Maxwellian distribution functions [*Whipple*, 1981].

The collector plate is electroplated gold on an electrolous Ni-Cu phosphate substrate on Al. The substrate prevents the "leeching" of the magnesium structure into the gold plating. Plating details (from the instrument specifications) are as follows: 1) flash Cu to thickness of 100 ±50 micro in., 2) underplate non-magnetic electroless Ni per Mil-C-26074 Class I to thickness of 500 ± 100 micro in., 3) overplate bright Au per Mil-G-45204 Type I Class II to thickness of 100 ± 25 micro in. (from drawing 21-8001, rev. C). Hence the gold plating has a thickness of at least 2×10^{-4} cm.

Secondary electrons are emitted from a surface layer much thinner than this, ~ 10^{-6}cm (see p. 423 of *Dekker* [1957]); hence the secondary emission characteristics of gold are appropriate for determining the secondary yield and energy spectrum.

The most extensive compilation of the secondary emission characteristics of metals appears to be due to *Kollath* [1947, 1956]. The best "temperature" for secondaries emitted from gold is ~2 to 3 eV (from table 1 of [*Kollath*, 1956]) obtained from a primary electron energy of 150 eV. The secondary emission spectra are not very sensitive to the energy of the primary for primary energies above ~ 20 eV [*Hachenberg and Brauer*, 1959] and at least up to ~ 1.6 MeV [*Schultz and Pomerantz*, 1963]; these are well outside the energy range for which the total secondary electron yield is significant (see below). A temperature of ~ 3 eV is also consistent with the theoretical treatment of *Chung and Everhart* [1973]. For quantitative modeling of the loss of secondaries from the collector, we have assumed a temperature of 2.5 eV; as this is small compared to the instrument suppressor voltages of ~ -8 V and -95 V, small errors in the temperature have a negligible effect on our results.

The loss of secondary electrons (i.e. those produced at the collector and not returned to the collector by the suppressor grid) was considered in detail for the PLS instrument by Sittler in 1979 (E. C. Sittler, Jr., private communication). The geometrical problem is illustrated in Figure 12 (figure due to E. C. Sittler). For a given radial location r on the collector plate (of radius r_c), an impact by a primary electron will cause the emission of secondary electrons with an energy distribution as discussed above and an angular distribution which is isotropic [*Whipple and Parker*, 1969] (for an extended emitting surface) with respect incidence angle θ and azimuthal angle ϕ] (early work, see e.g. *Hachenberg and Brauer* [1959] and *McDaniel* [1964], suggested a cos θ emission distribution, but isotropy seems to now be accepted by most workers in the field [ ]). Consider a secondary electron of energy E_s emitted at angle θ. The trajectory will follow a straight line in the field-free region between the collector plate and the grounded grid (Grid 1 - this is the "normal suppressor" electrical configuration). Grid 2, held at the suppressor potential V_{sup} will decelerate the electron motion perpendicular to the collector plate, resulting in the parabolic trajectory shown in the figure for $E_{s\perp} < V_{sup}$; higher energy electrons penetrate the potential barrier and are immediately lost from the system. The parabolic trajectory will again intersect grid 1 a distance R from the position at which it first crossed the grid plane. If d_{sup} is the distance between the grounded grid and the suppressor grid (equivalent to $z_2 - z_1$ in Fig. 12), then an elementary calculation shows that

$$R = 2d_{sup}\frac{E_s}{eV_{sup}} \sin 2\theta \qquad (4)$$

The electron will again move in a straight line until it crosses the plane of the collector plate. If d (z_1 in the figure) is the separation of the collector plate and the ground grid, the electron will intersect the plane of the collector plate a distance a (equal to Δx in the figure) from where it was created where

$$a = 2d \tan\theta + R \qquad (5)$$

If the impact point is outside of the collector, the secondary electron is lost, giving rise to a spurious (positive) current in the data. From Figure 12, it is obvious that the electrons emitted in a cone of half angle θ map to a circle in the plane of the

collector plate. As long as $a - r < r_c$ there will be a range of azimuthal angles ϕ such that $|\phi| \leq \phi_{max}$ for which the secondaries will be lost. For larger values of a (corresponding to smaller values of θ), all of the secondaries will be lost.

Noting again that both the angular and energy distributions of the secondary electrons is independent of the energy and angular distributions of the primary electrons, we can calculate a solid angle $\Omega_{loss}(r)$ corresponding to secondaries which are lost. Define the angular limit $\theta_1(E_s)$ as the smallest value of θ for which $a = r_c$ using equations 4 and 5 (found numerically); define $\theta_2(E_s)$ as the largest value of θ for which $a = r_c$ or $\pi/2$, whichever is smaller (N.B. θ considered as a function of R is a double-valued function). Define ϕ_0 by

$$\phi_0(\theta,E_s) \equiv \cos^{-1}\left[\frac{r_c^2 - r^2 - a^2}{2ra}\right] \quad \text{for } a < r + r_c \qquad (6)$$

$$\phi_0(\theta,E_s) \equiv \pi \quad \text{for } a \geq r + r_c \qquad (7)$$

The angular limits are, of course, dependent upon the energy of the secondaries due to the parabolic section of their trajectories. The solid angle for lost current (integrated over the secondary electron energy spectrum) is

$$\Omega_{loss}(r) = 2 \int_0^{eV_{sup}} f(E_s)dE_s \int_{\theta_1(E_s)}^{\theta_2(E_s)} h(\theta)\, \phi_0(\theta,E_s)\, \sin\theta\, d\theta \qquad (8)$$

where $h(\theta)$ is the angular distribution of secondaries, and $f(E_s)$ is their energy distribution function with respect to current, given by equation 2. We have computed $\Omega_{loss}(r)$ both for the case of isotropically emitted secondaries, i.e., $h(\theta) = 1$ and for a cosine distribution (normalized to unity over a hemisphere), $h(\theta) = 2\cos\theta$ for the various operating modes of the instrument.

There are four relevant operating modes of the instrument for which $\Omega_{loss}(r)$ has been evaluated: the normal suppressor configuration, described above, and the "reversed suppressor" configuration, in which the grounded grid and suppressor grid are reversed; for each configuration there are two suppressor voltages, one for the low energy electron measurements (E1) and one for the high energy electron (E2) and ion (L, M) measurements (see *Bridge et al.* [1977]). Relevant parameters are listed in the table below.

Mode	Configuration	V_{sup} (V)	d (cm)	d_{sup} (cm)
E1	Normal	-8.05	0.996	0.417
E1	Reversed	-7.70	0.000	0.996
E2, L, M	Normal	-95.2	0.996	0.417
E2, L, M	Reversed	-85.9	0.000	0.996

The distances between the grids are from Figure 2.12 of *Barnett* [1984]. The cups of the main sensor only have a "normal" configuration and use a suppressor voltage of -95.2 V (these numbers are from Voyager Memorandum #69 of 1/8/80 which indicates the data source as Mavretic's notebook #4. The voltages quoted are within 50 mV for SN002 and SN003; it is assumed that SN001 has the same values, but these are not documented).

Note that for $\phi_0 = \pi$, $\theta_1 = 0$, and $\theta_2 = \pi/2$, $\Omega_{loss}(r) = 2\pi$, i.e. the solid angle in a hemisphere. G. S. Gordon, Jr. has normalized $\Omega_{loss}(r)$ to 2π to find the fraction of secondaries lost per unit incident current as a function of radial distance r from the center of the D cup collector plate. E. C. Sittler, Jr. performed the same calculations in 1979; his results for the fraction of secondary electrons lost in the E1 and E2 modes are shown in Figures 13 and 14, respectively. Sittler normalized the losses to their maximum values and expressed radial distance as a fraction of the collector radius. The maximum loss occurs at the edge of the collector plate. In E1 Ed found a loss of 26.3% for the normal suppressor configuration and 12.5% for reversed suppressor configuration. For E2 the loss fractions at the edge are 25.3% and 3.5%, respectively.

The results of Gordon's calculation are shown in Figures 15 through 19. Again the *normalized* value of $\Omega_{loss}(r)$ is plotted. In Figure 15, results for all of the cases noted in the table above are plotted. The notations "iso" and "cos" refer to isotropic and cosine angular distributions of the emitted secondaries, respectively. The notations "std" and "rev" refer to whether the suppressor voltage is on the standard or reversed grid. The suppressor potentials are also indicated. Figures 16 through 19 show the loss fraction for cosine and isotropic secondary distributions for each of the four suppressor modes; the dotted lines indicate the isotropic results and the solid line cosine results. Note that in the standard configuration - denoted by "s" in the label on the graph - the isotropic distribution produces more losses as there are more electrons emitted at large angles of incidence which are not reflected back to the collector until they have moved relatively far from their point of emission. In the reversed configuration - denoted by an "r" - the cosine distribution gives rise to more losses as there are more "forward emitted" secondaries which simply penetrate the potential barrier in the forward direction; electrons emitted at large angles of incidence are immediately "shoved" back into the collector plate by the suppressor potential. Note that "i" refers to the case of L, M, or E2 and "e" in the label refers to the E1 potential, e.g., the label "is" identifies the normal, or standard, suppressor configuration with -95.2 volts on the suppressor grid.

Listings of the loss fraction as a function of radial distance across the collector plate are included in Appendix B. The file "out.rlme15ci" contains numerical output for the isotropic cases; the file "out.rlme15cc" contains the the corresponding numbers for the case of a cosine angular distribution. The parameters used for each table are listed at the top: "ds", "d", and "volts" correspond to d_{sup}, d, and V_{sup}, respectively. The parameter "e0" refers to the assumed energy of the secondary electrons, here 2.5 eV for each case.

We have not included either elastically scattered (reflected) primaries or inelastically scattered (rediffused or "backscattered" primaries) electrons [*Hachenberg and Brauer*, 1959; *Dekker*, 1957]. Reflected primaries have the same energy as the incident electrons and display a maximum in the direction of the incident beam [*Hachenberg and Brauer*, 1959]. According to *Whipple* [1981], reflection is only significant at primary energies less than ~10 eV. Backscattered electrons occupy the energy range

between ~50 eV and the energy of the primary. They obey the same angular distribution law as the true secondaries [*Hachenberg and Brauer*, 1959] and can contribute a net backscattered current ~ 0.3 of the incident current [*Whipple*, 1981]. As the true secondaries contribute most of the current at the collector, we only consider their effect here; it should be noted that a sizable fraction of the backscattered electrons will be lost in any event if the energy of the primaries substantially exceeds eV_{sup}.

Secondary Yield and Lost Secondary Current

The loss of secondary electrons produced at the collector plate is measured as a positive current by the DC measurement chain, and, if modulated, as a positive current by the AC measurement chain (see *Bridge et al.* [1977]). This current is superimposed on the "direct" current produced by the primary flux of charged particles on the collector plate. It is convenient to consider separately the "direct" or primary current as opposed to the secondary current. This is done in terms of the secondary yield function δ where

$$j_s = \delta j_p \tag{9}$$

and the subscripts refer to the current density of the primary particles and that of the secondary particles [*Hachenberg and Brauer*, 1959]. In what follows we concentrate on the production of secondary electrons by primary electrons; at primary energies above several keV the production of secondary electrons by primary ions can also give rise to significant effects [*Whipple*, 1981].

The yield of secondary electrons form primary electrons is, in general, a function of both the primary energy E_p and angle of incidence θ_p. However, the yield curve tends to be universal, i.e., independent of the emitting material, if parameterized in terms of the maximum yield δ_m and the energy at this maximum E_m (see e.g., *Dekker* [1957]). The yield function is further characterized by the energies E_I and E_{II} corresponding, respectively, to the lowest and highest primary energy for which the secondary yield exceeds unity. For gold δ_m is 1.45 at E_m of 800 eV, and E_I and E_{II} are 150 eV and > 2000 eV, respectively [*Kollath*, 1956]. An analytic form for the yield is given by *Whipple* [1981] which we use here

$$\delta(E_p,\theta_p) = \frac{1.114\delta_m}{\cos\theta_p}\left[\frac{E_m}{E}\right]^{0.35} \times \left\{1 - \exp\left[-2.28\cos\theta\left[\frac{E}{E_m}\right]^{1.35}\right]\right\} \tag{10}$$

Note that for small energies or angles of incidence near 90°, $\delta(E_p,\theta_p) \propto E_p$.

The response of the PLS side sensor to electrons is a convolution of the the distribution function of the electrons with the "response" function of the detector. The response function can be conveniently separated into a transparency function T and an area overlap function A; the latter contains the effects of the refraction of particle trajectories by the various grids as well as the decrease in effective collector area due to particle trajectories within the detector [*Barnett*, 1984; *Barnett and Olbert*, 1986].

If we define a coordinate system with the z axis along the symmetry axis of the side sensor, or D cup, then the angle of incidence of a primary electron with respect to the collector plate is the same as that with respect to the entrance aperture of the detector (both the grid at the entrance aperture and the collector plate are at the spacecraft "ground" (which is the potential of the conducting surface of Voyager; the latter can, of course, have some floating potential with respect to the surrounding plasma). Hence $\theta_p = \tan^{-1}(v_t/v_z)$ where v_z is the component of electron velocity into the sensor and v_t is the component of velocity transverse to the sensor. The energy dependence of the yield follows from $E_p = 1/2\ m_e\ (v_t^2 + v_z^2)$.

For a given angle of incidence and given primary energy, the region of the collector plate illuminated by electrons passing through the aperture grid, will, in general, be the common overlap area of three circles whose centers are colinear [*Barnett*, 1984]. This is a two parameter function $A(d_{ag},d_{gc})$ which can be described by the distance between the centers of the aperture image and the guard ring image d_{ag} and between the centers of the guard ring image and collector image d_{gc}, respectively; the function can be written in closed analytic form [*Barnett*, 1984]. The distances are offsets determined by the refraction effects which are, in turn, functions of v_z, v_t, V_{sup}, and V_{mod} the modulator potential. The current measured due to electrons more energetic than eV_{mod} is

$$I_{DC,m} = e\int_{v_m}^{\infty} dv_z\, v_z \int_{-\infty}^{\infty}\int_{-\infty}^{\infty} d^2v_t\, f(\mathbf{v})\, T\, A \tag{11}$$

where $v_m \equiv (2eV_{mod}/m_e)^{1/2}$. The DC return current actually measured by the instrument is $I_{DC} = 1/2\ (I_{DC,m} + I_{DC,m+1})$, i.e. the average current in a given channel (when the modulator is on, which is usually the case).

To calculate the effect of secondary current loss, we have modified the area overlap function as follows. We have numerically integrated the solid angle for secondary loss $\Omega_{loss}(r)$ over the overlap area to find an effective "loss area" A_{loss},

$$A_{loss} \equiv \int_{overlap\ area} \Omega_{loss}(r)\, dA \tag{12}$$

The secondary current lost due to primary electrons more energetic than eV_{mod} is given by the current density at the collector plate multiplied by the secondary yield and the loss area, viz.

$$I_{sec} = e\int_{v_m}^{\infty} dv_z\, v_z \int_{-\infty}^{\infty}\int_{-\infty}^{\infty} d^2v_t\, f(\mathbf{v})\, T\, \delta\, A_{loss} \tag{13}$$

(Note that the lost secondary current density per velocity space volume is simply the primary current density at the collector plate $\times\ \delta \times\ \Omega_{loss}$).

In the DC return mode, the current measured for modulator voltage V_{mod} is given by $I_{DC} - I_{sec}$. In the normal plasma mode, the measured current is the modulated part of this current.

To incorporate this effect into the simulation of electron

spectra, Gordon computed a set of eight loss tables (low and high suppressor potential; normal and reverse suppressor configuration; isotropic and cosine law for the angular distribution of the secondary electrons). The numerical integrations of eqn. 12 for these 8 cases were run on a Sun Microsystems Workstation on the weekend preceding May 18, 1987. The jobs were run in the background beginning on the preceding Friday and completed late on Sunday, May 17.

The loss tables have been incorporated into the PMODEL package via modified versions of the subroutine REDART (which reads the tables into the SUN from the disk where they are stored) and the functions ARSIDE and CPRESP. In CPRESP, the overlap area A (refer to eqn. 11 above) has been replaced by $A - \delta A_{loss}$ (refer to eqn. 12 above). The output from PMODEL then produces synthesized electron spectra which are corrected for the inefficiency of the suppressor. Listings of the relevant code are included as Appendix C. Note that the hand lettering on the listing for CPRESP is only applicable to using the code to simulate the effects of photoelectrons; the code as printed on the laser printer was implemented for the case of secondary electrons made from primary electron (rather than photon) impacts. Equation 10 with $\delta_m = 1.45$ and $E_m = 800$ eV is used to compute the yield.

Figure 20 displays a contour map of the normal area overlap function; the two axes are the relative displacement of the aperture and shield circle centers (DAS) and the relative displacement of the shield and collector circle centers (DSC) (these correspond to the coordinates X and Y, respectively, which appear in the call to ARSIDE in the function CPRESP). Figures 21 and 22 show the area (in cm^2) as a function of one of these two parameters (labeled "1" and "2") for a constant value of the other. The distance from one side of the aperture to the other side of the shield is 10.8 cm, and the distance from one side of the shield to the other side of the collector plate is 11.5 cm; hence, these are the values of DAS and DSC for which the area overlap goes to zero. Parameter 1 is therefore DAS, and parameter 2 is DSC. A three-dimensional projection of the overlap area function is shown in Figure 23.

Figures 24 through 39 are plots of A_{loss} versus DAS (="1") and DSC (="2"), in an analogous fashion to the plots of A in Figures 21 and 22. Each plot is labeled with a four character alphanumeric label: "vcan", where "v" is "e" (E1 suppressor voltage) or "i" (L, M, and E2 suppressor voltage), "c" is "s" (normal suppressor configuration) or "r" (reversed suppressor configuration), "a" is "i" (isotropic angular distribution of secondaries) or "c" (cosine angular distribution of secondaries) and "n" is "1" or "2" depending upon whether DAS or DSC is the independent variable plotted along the abscissa. Note that in each case in which the independent parameter is DSC, the effective loss area is a minimum for DSC=0. As this parameter is increased, the losses increase (refer to Figure 15), but the overlap area decreases (Figures 21 and 22). Hence, there is a maximum loss for some nonzero value of DSC. Also note that the scale along the ordinate is different for Figures 24 through 39.

Figures 40 and 41 are contour plots for the E2, normal configuration case, for isotropic and cosine distributions of the secondaries, respectively. Corresponding three-dimensional representations for these two cases are shown (on the same scale) in Figures 42 and 43, respectively. Figure 44 reproduces Figure 42 but on the same scale as Figure 23; from this last comparison, it is obvious that the loss of secondary electrons from the collector plate can decrease the measured electron current but cannot change its sign (a seemingly trivial point which is important in accounting for some of the PLS electron spectra).

We simulated electron spectra (E2 mode) by using PMODEL and including the loss portion for assumed isotropic and cosine distributions in the normal suppressor configuration. Figures 45, 46, and 47 show simulated currents for an isotropic Maxwellian distribution of electrons at a temperature of 400 eV assuming, respectively, no losses, isotropic emission of secondaries, and a cosine law for the emission of secondaries. The losses decrease the measured currents by ~20% or less. Note that the apparent discontinuity between channels 3 and 4 is due to the suppressor grid; the threshold of channel 4 is -92.3 volts whereas the suppressor potential is -95.2 volts. The currents in the first three channels are due entirely to modulation of the trajectories of the electrons in the input distribution with energies greater than 95 eV (this is the so-called feedthrough effect). To further investigate this effect, we also simulated a κ distribution with a most probable speed corresponding to an energy of 9.85 eV. The case for no losses is shown in Figure 48. This spectrum is qualitatively similar to those observed in the vicinity of the "voids" in the Jovian magnetosphere by Voyager 2 [*McNutt et al.*, 1987]. The high energy cutoff is due to numerical cutoffs used in simulating the spectrum. The spectrum including losses from isotropic secondaries is shown in Figure 49 and the loss current itself in Figure 50.

Experimental Verification of the Suppressor Efficiency

General Considerations

The calculation of the apparent current due to the inefficiency of the suppressor grid is complex enough that it is desirable to verify it experimentally. Efforts are currently underway at M.I.T. to do so in a vacuum chamber using the side sensor of the Flight Spare PLS experiment (as of this writing, Sept. 17, 1988, these have not yet begun). In addition to what can be done in a laboratory (which can approach but not really duplicate the environment of interplanetary space), we can look for this effect in some of the plasma measurements themselves, in which the local environment is correct but the types of measurements were not really optimized for looking for this effect. We noted previously that photoelectrons and secondary electrons have similar energy distributions for production from gold surfaces, the mean energy of the photoelectrons being smaller (0.88 eV versus ~2.5eV). These energies are small with respect to typical potentials within the PLS detectors; hence, the emitted electrons should follow similar trajectories. No experimental information on the angular distribution of emitted photoelectrons appears to be readily available; however, it is reasonable to assume that the angular distributions are also similar. We can thus use sunlight into the instrument hitting the collector plate as a probe to determine the suppressor loss as a function of the illuminated part of the collector plate.

When the instrument is in an electron measurement mode, photoelectrons are emitted by the support ring for the negative high voltage grid whenever the angle between the cup normal and the sun is less than 78.5°. If sunlight also hits the collector plate, photoelectrons will also be emitted there, but the loss current is small compared to that produced by those photoelectron coming from the negative modulator support. To eliminate this effect, the instrument must be in a positive ion detection mode. In this case, the only surfaces with negative potentials are the suppressor grid, which has a small cross sectional area, and the buckout grid. The latter has only a small negative potential which alternates with a positive potential. As the suppressor grid is between it and the collector plate, any electrons from the buckout grid cannot reach the collector plate in any case.

The loss of photoelectron current from the collector plate cannot be affected by the modulator potential and will give rise to only a DC signal as the modulator steps. This is the source of the DC current in the high channels of the A cup measured during cruise. The geometry of the A cup is complex enough that a good mathematical model for the suppressor losses, while possible to construct, will also be very complex. Fortunately, there were a series of cruise maneuvers conducted during the cruise phase of both spacecraft during which the D cup collector plate is illuminated by the sun, and the instrument is in DC return mode.

Cruise Maneuvers

Several types of changes in spacecraft attitude are made during cruise. Early in the mission Cruise Science Maneuvers (CRSMVR) were performed, consisting of 25 roll turns (counterclockwise about the +Z axis of the spacecraft, which points opposite to the high gain antenna) and 10 yaw turns (counterclockwise about the +Y axis of the spacecraft, which is aligned with the projection of the science boom perpendicular to the +Z axis - see Figure 51). Later in the mission these were changed to mini-Cruise Science Maneuvers (Mini-CRSMVR) which included fewer revolutions of the spacecraft. The original idea was to partially roll the spacecraft so as to bring the D cup directly across the sun during the yaws. As far as I can tell this was not done, probably as the result of operational constraints of which I am not aware. A listing of all maneuvers through a complete revolution for both spacecraft as well as a memo describing our original thoughts on PLS measurements (from J.D. Sullivan, dated June 14,1978) are included as Appendix D.

I have looked in some detail at the CRSMVR yaw turns on Voyager 1 on day 258 of 1978. There is one sequence of DC return measurements (normal suppressor) for one full yaw early on day 258. Other measurements during the yaws are normal plasma and current calibrations (CURCAL) with both modulator on and off, all with normal suppressor. The minimum angle between the D cup normal and the sun is 43.3°, corresponding to the angle between the D cup normal and the +X axis of the spacecraft (refer to Figure 51). Sunlight reaches the collector plate in the D cup when the sun-cup angle is less than 63.1°. Due to the fairly rapid rotation rate of the spacecraft (~32 minutes to rotate through 360°), this limits the available DC return spectra for which the theory and observations can be compared.

The DC return measurements were removed from the sequence when the change was made to mini-CRSMVRs. From the maneuver list in Appendix D, this limits the comparison to 11 maneuvers on Voyager 1 and 6 maneuvers on Voyager 2. The comparison is further limited by the distance between the spacecraft and the sun. The suppressor in the D cup is apparently more efficient at returning photoelectrons to the collector plate than is the suppressor in the A cup. In addition, the geometry during the yaws limits the illuminated area of the collector in the D cup. These effects combined with the relatively high threshold for detectable current in the DC return mode further limits the availability of data. As the spacecraft both receded from the sun, the observed current decreased to threshold before the CRSMVRs were changed to mini-CRSMVRs and the DC return measurements were deleted from the measurement sequence. The following tables list the CRSMVRs by date, the maximum DC return DN in the D cup in channel 16 of the L mode, and whether evidence of photoelectrons in the DC returns in the electron modes is present.

Voyager 1			
SCET	Max DN (IDC)	Photoelectrons	Range (AU)
1978-048	172	Yes	2.4
1978-257/8	151	Yes	4.1
1979-034	146	Yes	5.1
1979-288/9	130	Yes	6.4
1980-031	N/A	N/A	7.1
1980-168	128	Yes	8.2
1981-041	128	??	9.9

More information concerning the DC return levels after the Voyager 1 failure can be found in Voyager Memorandum #157. No maneuver data could be found from the tape logs on day 31 of 1980.

Voyager 2			
SCET	Max DN (IDC)	Photoelectrons	Range (AU)
1977-362	177	Yes	1.9
1978-275	N/A	N/A	4.0
1979-155	136	Yes	5.2
1980-024	128	Yes	6.1
1980-136	128	Yes	6.7
1981-148	128	Yes	9.0
1982-103	128	No	10.0

Data from a maneuver on day 275 of 1978 could not be located and the mini-CRSMVR on day 155 of 1979 does have DC return data during a yaw turn. The SOEs have not been

investigated closely to clear up these discrepancies. During the yaw turn on day 24 of 1980, the lower channels of the D cup registered 134 DN and fell off to 128 at the location of the solar wind peak in the normal plasma data for the D cup. The same behavior occurred on day 136 of 1980, with the first channel of the D cup showing a maximum of 132 DN. On day 148 of 1981, the solar wind can no longer be seen in the DC return measurements from the D cup. N.B. the "Range" is actually the heliocentric distance of the spacecraft.

In spite of the entry for 1982-103 there were photoelectrons observed in the E1 and E2 modes during the Uranus encounter during a spacecraft maneuver (day 24 of 1986). In addition, the threshold for detecting the solar wind in the DC return A cup currents is apparently lower for Voyager 2 than for Voyager 1 (refer to discussion above). As of day 160 of 1987, Voyager 2 was 23.0 AU from the sun, and the first channel of the L mode (A cup) showed a DN of 132 in DC return. Channel 16 registered a DN of 130 from photoelectrons. The "break" in the L mode spectrum occurs at the location of the solar wind peak in the A cup as indicated by the normal plasma data.

To attempt to test the numerical loss calculations, we have concentrated on the Voyager 1 Cruise Science Maneuver from day 258 of 1978. From the PLS engineering output for this time of the maneuver, the electronics temperature (TPMC) 12.6°C and the sensor temperature (TSEN) was -117.5°C. Modulation of the temperatures during the maneuver is clear from the engineering plots from this period (Figure 52). The times of the L mode spectra used, the DN value in channel 16, the corresponding current (corrected for temperature using interpolated values from Figure 9), and the angle between the D cup normal and the sun (using the nominal sensor orientation with respect to the spacecraft) are shown in the following table.

I_{DC} From CRSMVR 1978-258			
SCET	DN	I (fA)	$\theta_{D,\,sun}$
0132:25.276	128	$< 10^5$	75.0°
0134:01.276	128	$< 10^5$	63.3°
0135:37.276	128	$< 10^5$	53.2°
0137:13.276	144	2.50×10^5	45.9°
0138:49.276	151	3.25×10^5	43.1°
0140:25.276	151	3.25×10^5	45.6°
0142:01.276	145	2.58×10^5	52.7°
0143:37.276	128	$< 10^5$	62.8°
0145:13.276	128	$< 10^5$	74.4°

It is immediately obvious that the variation in current does not exactly track the variation in angle; whether this is related to the motion of the cup, shading of the instrument, bias in the timing information, hysteresis in the electronics or whatever is unknown. Another feature which is not understood is that when both the A and D cups are in shadow, at 0156:25.276 - angles between the sun and the normals of the A and D cups 66.6° and 136°, respectively, negative currents were measured in both cups. At other angles, DN of 128 were recorded in shadow.

To see if this behavior was peculiar to this maneuver (and to check for errors in the analysis), a cruise maneuver on Voyager 2 was also examined in some detail. The first one, from day 362 of 1977, was examined; the electronics temperature is not readily available so only the DN values from channel 16 (L mode, DC return, normal suppressor) are listed. The angles are obviously incorrect; the changes in the DN values are well-centered in the time period during which photoelectrons are observed in the E1 and E2 modes. Examination of the trajectory data indicates that the time labels are off by about the round–trip light time between the spacecraft and Earth (to within a minute). This error in the trajectory data precludes a better analysis. The trajectory data corresponding to the Voyager 2 Cruise Science Maneuver on day 155 of 1979 and the Voyager 1 maneuver on day 34 of 1979 are in Jupiter encounter format; the pointing information is supposed to be updated every 48 s, rather than every 4 m on the usual CRSMVR tapes (which is interpolated to provide the angles listed in the tables).

I_{DC} From CRSMVR 1977-362		
SCET	DN	$\theta_{D,\,sun}$
0606:00.350	128	97.2°
0607:36.350	128	109.0°
0609:12.350	128	121.0°
0610:48.350	170	130.0°
0612:24.350	177	136.0°
0614:00.350	175	137.0°
0615:36.350	169	132.0°
0617:12.350	140	124.0°
0618:48.350	128	113.0°
0620:24.350	128	101.0°

Examination of these maneuvers in more detail should provide better estimates on the angles through which the sunlight was entering the side sensor as a function of time.

Predicted Photocurrent at the Collector Plate

To compare the theoretical predictions of suppressor loss with the data, the quantity A_{loss} of equation 12 must be computed for the illuminated area of the D cup collector plate. As photons are not refracted by the fields between the intervening grids as electrons are, *Aloss* is a one parameter function; the parameter can be taken to be the angle from the D cup normal at which sunlight enters the cup. To perform this calculation, the subroutine CPRESP was modified as shown by the handwritten notes in Appendix C. The actual code used is appended in Appendix E along with the effective loss area for both isotropic and cosine angular distributions of the secondaries. The optical transparency of the intervening grid wires is also listed. As the measured currents are from the positive ion mode, the lookup tables used are for -95.2 volts on the suppressor grid in the normal suppressor configuration.

Comparison of Measured Currents with the Data

The saturation photoelectron current density for gold under solar irradiation is $j_{photo,\,Au} = 2.9 \times 10^{-9}$ amperes cm^{-2} [*Grard*, 1973]. For the Cruise Science Maneuver by Voyager 1 on day

258 of 1978 (the maneuver used by *Barnett* [1984] in testing the algorithm for the response function), this must be corrected for the heliocentric distance of the spacecraft, 4.152 AU. At Voyager, the expected photocurrent density from the illuminated part of the collector plate is $j_{photo,\,Au\,corr} = 1.7 \times 10^{-10}$ amperes cm^{-2}. Predicted currents as a function of angle, using this current density and values from the table in Appendix E are given in the following table; the loss current is in fA for both isotropic and cosine angular distributions. The illuminated area is corrected for the grid transparency.

I_{DC} Predicted for CRSMVR 1978-258			
SCET	$\theta_{D,\,sun}$	$I_{loss,\,iso}$ (10^5 *fA*)	$I_{loss,\,cos}$ (10^5 *fA*)
0135:37.276	53.2°	5.20	3.37
0137:13.276	46.0°	8.35	4.85
0138:49.276	43.3°	9.20	5.19
0140:25.276	45.8°	8.40	4.88
0142:01.276	52.9°	5.36	3.45
0143:37.276	63.0°	0.055	0.047

Note that the angles used are slightly different than those quoted above (pointing accuracy is no better than ~0.02° in any case); the difference comes from a somewhat crude linear interpolation of the angles which are used in the table immediately above; the "better" values used in the table previously were not available when the predictive calculations were done.

All of the predicted currents are larger than those actually measured; however, there is an additional effect which lowers the calculated predicted current. Sunlight on the suppressor grid will also produce photoelectrons; some of these (one can estimate roughly half) will be accelerated toward the collector plate while the rest will be accelerated in the direction of the buckout grid and eventually lost to the sides of the cup (more details of where secondaries go after they are produced is discussed below). The grid wires are woven tungsten mesh. The expected photoelectron saturation current for tungsten at 1 AU is bracketed by [*Whipple*, 1981] 2.1×10^{-9} A $cm^{-2} < j_{photo,\,W} < 8.1 \times 10^{-9}$ A cm^{-2}. Correcting for the distance of the spacecraft from the sun yields 1.2×10^{-10} A $cm^{-2} < j_{photo,\,W\,corr} < 4.7 \times 10^{-10}$ A cm^{-2}. To have reached the suppressor grid, the light must pass through 6 grids, and to reach the collector plate from the suppressor grid another grid must be passed (which is at ground potential). The associated transparency can be estimated as $(1 - 1/[42 \cos 43.3])^7 \times (1 - \frac{1}{42})^7 = 0.6693$. The area of suppressor grid illuminated with sunlight is given by the overlap area of the aperture and the guard rings multiplied by $1 - (1 - 1/[42 \cos 43.3]) \times (1 - \frac{1}{42}) = 0.0558$. The overlap area is 46.0 cm^2; hence, the area for emission is 2.56 cm^2. Multiplying by the transparency yields an effective area of 1.72 cm^2, which is smaller than but not negligible compared to the effective area for photoelectron loss.

If we take half of the average current density suggested for tungsten and combine it with this effective area, we obtain a negative current of 2.5×10^5 fA.

From the table above, at 43.3°, the total predicted current is 6.5×10^5 fA using the numbers for isotropic emission and 2.5×10^5 fA assuming the emission follows a cosine law. Given the uncertainty in the photoemission properties of the grid wires as well as the uncertainty in the fraction of photoelectrons emitted by the suppressor grid that will travel toward the collector, the predicted current (especially for the cosine distribution) is in excellent agreement with the maximum measured positive current of 3.25×10^5 fA during the Cruise Science Maneuver in question.

We note that the DC return current should be negative in the reversed suppressor configuration due to the vastly increased suppressor efficiency. Unfortunately, no cruise full yaw turns were performed in the DC return mode with the suppressor position reversed; hence, this prediction cannot be verified.

Other Sources of Photo- and Secondary Electron Currents

Electrical Configuration of the Side Sensor

Figure 53 is a scaled working drawing of the D cup showing the placement and support structures for the various grids. A comparably detailed drawing of one of the main sensor cups can be found in *Barnett* [1984] and in *Barnett and Olbert* [1986]. A less detailed drawing of the side sensor, in similar format, can be found in *Barnett* [1984]. The original version of that drawing is included as Figure 54. There are some differences in the dimensions which should be noted; they are probably too small to have any effect on any analysis done to date or contemplated for the future using the algorithm developed by *Barnett* [1984].

Although the dimensions in Figure 53 are quoted to the nearest thousandth of an inch (inches because those are the units in which the original mechanical specifications were made), the quoted uncertainties on all of the machine drawings for the various pieces of the assembly are typically ± 0.002", if not larger. In labeling Figure 53, the intergrid spacings were computed from the nominal dimensions on the final machine drawings (including all of the Engineering Change Orders - ECOs) from the top surface of one grid to the top of the next (or to the top of the collector plate); the reference line is the top surface of the aperture grid. An expanded detail in the lower left corner illustrates the assembly of the 1 mil tungsten mesh (woven like nylon hose) to the grid support rings. There is a nominal 0.009" space between the top surface of the outer support ring and the top surface of the grid wires. This spacing has been included in calculating the between the grids and the top of the collector plate; it was not included in the dimensions on Figure 54. The mesh is stretched over each inner support ring and then secured with the outer ring (press fit). Excess mesh was then trimmed away at the bottom surface of both rings which were positioned to be flush. The nominal size of the openings in the mesh is 0.042" × 0.042". Variations from this are small and are documented in the appropriate engineering notebooks which record details of the grid assemblies.

The thickness of the insulating spacers which electrically

isolate the bottom four grids were not specified exactly, rather, a range was given; to compute the spacing, the relative spacing of the centers of the holes for the anchor screws was used. These values were generally consistent with those inferred from the thicknesses of the grid support rings and the insulators.

The intergrid spacings are listed in the table at the lower right in inches. The computed values are in the column labeled nominal. The column labeled Flight 1 (i.e., SN002) are values measured after assembly of the cup using a microscope. The grid wires were brought into focus and the spacings computed. Most of the dimensions are fairly close and give a better idea of the range of error involved. The measured dimension F is almost certainly in error; not only does it differ from the computed value by 0.0049" (a lot), but also the difference between F and G is 0.0120", which is smaller than the specified machine thickness of the outer support ring for the second suppressor grid.

The intergrid spacings shown on Figures 53 and 54 are consistent to better than 0.002" for five of the spacings and not as consistent on the other three. The spacing E - D on Figure 53 (based on the screw hole spacing) is 0.159" as compared to 0.164" on Figure 54. This difference of 0.005" is annoying and probably small due to an error but follows directly from the dimensions to the anchor holes as given on the machine drawing for the lower housing. The spacing F - E is probably correct on Figure 53 and too large by 0.010" on Figure 54 (from including too much thickness for the shield ring). Finally, the spacing from the second suppressor grid and the top of the collector plate is 0.015" larger on Figure 54 than on Figure 53. I have triple and quadruple checked the distance from the aperture grid to the top of the collector plate; I believe that 2.338" is correct as shown on Figure 53. The collector plate thickness is 0.020" so this does not seem to be the source of the problem. The standoffs which separate the lower housing and collector plate come in two sizes 0.250" and 0.235". There are two of each; the shorter ones also support solder lugs which come between them and the collector plate (these are used to connect the wires to the collector plate to make the electrical connection from the plate to the input amplifiers). If the shorter length were assumed for all of the standoffs, the grid to collector spacing would be larger by 0.015"; this is the likely source of the error on Figure 54.

This latter discrepancy is probably the most important, as it would lead to more secondary electrons escaping from the collector plate than were found in the calculations discussed above. In other words, the suppressor is probably slightly more efficient than the numerical calculations done to date imply. This difference is probably not great enough to justify a recalculation of the tables for A_{loss} however.

Overall, the aperture grid - to - collector plate spacing may be in error by up to 0.030" in the algorithms of *Barnett* [1984]. This maximum error is only 1.3% and certainly smaller than other uncertainties in the algorithm.

Characteristics of the Buckout Grid

The so-called "buckout" grid was included in the instrument design to fine tune the instrument to depress the electrical noise level. The effect of the buckout potential was not included in the algorithms of *Barnett* [1984] and *Barnett and Olbert* [1986]. Given the very small potentials involved and other uncertainties, such treatment is easily justified. However, the buckout potential may be important in understanding one of the features in the "photospectrum", and is not documented elsewhere in an easily accessible way. For reference then, we discuss it here.

In the real instrument there is a certain amount of capacitative coupling between the modulator grid and collector plate, i.e., some field lines from the modulator grid "leak" through the grounded grids to the collector plate. As a result, the changing modulator voltage can produce a spurious current at the collector. The buckout grid is "tuned" to cancel this effect. The voltage applied to the buckout comes from the secondary winding of a transformer in the AC portion of the circuit for the modulator; hence, the buckout voltage is proportional to the AC part of the modulator voltage. The waveform is quasi-square and out of phase with the square wave voltage on the modulator grids. There are separate adjustments for the buckout potential for the main sensor and for the side sensor. The first failure (in 1978) of the PLS instrument on Voyager 1 occurred in the buckout transformer for the main sensor, effectively degrading the sensitivity by a large amount which varied in time (the failure was "repaired" by thermally cycling the instrument, presumably cold soldering a connection which had come loose).

After assembly, the voltage to the buckout grids was trimmed to minimize the modulator to collector feedthrough. For the 16th channel of the L mode the buckout signal was measured to be 5 volts peak-to-peak for the main sensor and 2 volts peak-to-peak for the side sensor for SN001, the PTM or "Proof Test Model" which was flown on Voyager 2 (H.S. Bridge, private communication, July 14, 1987). These values can be scaled by the modulator voltage (AC component) to the other channels of the L mode and to the other operating modes (E1, E2, and M) as well.

It should be noted somewhere that SN003 was to be flown on Voyager 2 but was replaced with SN001 shortly before launch (the substitution was made June 17,1977 at ETR, i.e., the Eastern Test Range). Hence, SN003 was not flown on either spacecraft and is the "flight spare" in the group's possession at M.I.T.

A calculation of the capacitive coupling based upon planar grids rather than a mesh (and invoking other assumptions and approximations which are reasonable) is included as Appendix G. The solution follows the treatment presented on pp. 1235-7 of *Morse and Feshbach* [1953].

Measured Currents in the Presence of Sunlight

Angular Dependence

If the angle between the D cup normal and the direction to the sun decrease to less than a critical angle when a negative potential is present on the negative modulator grid (refer to Figure 53), large modulated currents are measured at the collector plate in the E1 and E2 plasma modes. The spectra have a peculiar character in that some of the channels register threshold, i.e., 0 DN, regardless of the magnitude of the currents in the other channels.

During 1977 and 1978 there were extended periods of time

during which sunlight entered the D cup at a fairly large angle, and these currents were measured in the electron modes for ~100 days at both spacecraft during each year. The effect turned on and off suddenly in 1977 due to spacecraft rolls through relatively small angles; the cutoff occurred when both Voyagers were reoriented to acquire the DSN stations with the spacecraft high gain antenna (HGA). The turn on and turn off of the effect occurred due to very gradual changes in the D cup sun angle. As the spacecraft HGA stays pointed at the Earth, the angular separation of the sun and Earth on the sky change as the Earth orbits the sun; the amplitude of this variation decreases as the spacecraft recede from the Earth. In 1978 the photoelectron signal changed between the off and on states as the angle between the side sensor normal and the sun decreased from 78.5° to 77.5°. As the angle again increased through this range the effect shut off. This behavior was seen on both spacecraft, and is consistent with the range of angles over which the photo-induced currents have bee seen during the Cruise Science Maneuvers and special yaw maneuvers which have taken place as part of planetary encounter operations. It should also be noted that during 1978 while the effect was "on" the sun-D cup angle never decreased to less than 74°. In 1979, the minimum angle for the Voyager 2 spacecraft was 78.7° and no effect was seen; the minimum angle for Voyager 1 during 1979 was larger. As both spacecraft have receded from the sun and the angular separation of the Earth and sun have decreased, the corresponding minimum angles have increased; the effect has not been observed again during cruise (all angles quoted are accurate to better than 0.5° and are probably accurate to 0.2° as found from observations of the steady solar wind during cruise maneuvers, H.S. Bridge, private communication, 1987). More details and documented evidence concerning the value of the critical angle can be found in Voyager Memorandum #156.

Character of DC Return Spectra

The DC return mode of the spacecraft has been referred to previously, and must be discussed again because they provide an important clue to the production of the observed modulated current. Figures 55 and 56 show DC return spectra from the cruise phase for Voyager 1 and Voyager 2, respectively. During this phase of the mission sunlight was entering the D cup at less than the critical angle referred to previously. Both figures are a generalized version of the usual display of (the logarithm of) the current versus channel number (~logarithmic in energy per charge). The ordinate here is scaled to the logarithm of the magnitude of the measured current. As the DC return currents can be positive or negative, regardless of the operating mode (i.e., the potential on the modulator grids), the plot format has been generalized to take into account both signs of the current. The abscissa is a similar generalization of the channel number. The basic unit is one channel width in the M mode. The width of an L or E2 channel is 8 basic units and the width of an E1 channel is 2 basic units (one E2 channel is spanned by four E1 channel widths where the two overlap in coverage).

The "generalized data number" 1 through 8 corresponds to channel 16 of the E2 mode, 9 through 16 to channel 15 and so on, with decreasing magnitude of negative modulator potential. Data numbers 121 through 128 correspond to channel 1 of the E2 mode and numbers 127 and 128 correspond to channel 1 of the E1 mode; the "lower edge" of data number 1 is (a nominal) -5950 volts and the "upper edge" of data number 128 is -10 volts. A 16 unit gap is included to represent the gap in coverage from -10 V to +10 V. Data number 145 then corresponds to channel 1 of the M mode (positive modulator potentials), and numbers 145 through 152 correspond to channel 1 of the L mode. Channel 128 of the M mode corresponds to data number 272 and channel 16 of the L mode corresponds to data numbers 265 through 272. The "upper edge" of data number 272 corresponds to +5950 volts.

The conversion between channel number and voltage is discussed in *Bridge et al.* [1977]; for the sake of completeness, we give it here. Let n be the channel number, which can take on values of 1 to 16 for the E1, E2, and L modes and 1 to 128 for the M mode. Let M be an integer with values of 8 for E2 and L modes, 32 for E1 and 64 for M. Then the potential ϕ_n at the lower edge ("bottom") of channel n, which is equal to the voltage at the upper edge ("top") of channel $n + 1$ (the upper edge potentials follow from considering "channel" 129 for the M mode and 17 for the other modes), is given by

$$\phi_n = 60\ 10^{n/M} - 50 \qquad (14)$$

where ϕ_n is in volts.

In Figures 55 and 56, data from the E1, E2, and L modes are plotted; the times of the spectra are indicated across the bottom (the title "NEPTUNE MAGNETOSPHERE" is, of course, erroneous, and a glitch left over from rapidly converting some software to make these plots). Data from the M mode is not shown on these particular plots. The two traces for positive modulator potential are from the A and D cups, the D cup trace being at the positive threshold value. To plot the data as current, the conversion used is that of Figure 1 and Table 1. No temperature correction was made because it is not generally available.

In the DC return mode, the PLS instrument works similarly to a Langmuir plasma probe but only in a superficial way. First because the aperture grid is grounded, the modulator potential can have no direct effect on the surrounding plasma; it can only effect plasma which drifts into the aperture. The exposed aperture grid is always at the spacecraft potential, so there is no way of using these measurements to directly infer the spacecraft potential by adjusting the modulator potential until zero current is measured. At large positive modulator potential, the positive ions should all be excluded, leaving a saturated negative current due to the electrons. At large negative potentials, all electrons should be excluded and a positive saturation current should be measured. This behavior does not usually occur in the DC return measurements although there are exceptions.

For positive modulator potentials, the current saturates at a positive current which is due to the suppressor inefficiency (discussed previously). At lower positive modulator potentials, higher currents are measured as the solar wind is excluded less and less from the collector plate. For the times considered, the solar wind is more obvious on Figure 56 than on Figure 55 even though it is present in both. From the discussion in the previous paragraph, this curve should have started at a large

negative value, increasing toward zero as the positive solar wind is included with decreasing potential. The curve is shifted up due to the suppressor potential. In the solar wind, most of the negative current reaching the spacecraft is due to electrons with energies substantially less than the 95.2 volts (negative) on the suppressor; hence, in this case the suppressor acts as a rectifier allowing no negative current to reach the collector. There are a few cases, in the magnetospheres of Jupiter and Saturn when DC return currents were measured, that the electrons carrying most of the current through the aperture had energies in excess of 95 volts; in these cases, the expected behavior does occur; the total current to the collector plate is negative at large positive modulator potentials.

For negative modulator potentials the expected behavior again does not occur. In this case, an increasing negative modulator potential should exclude more and more electrons while not affecting the ion current to the collector. At large negative potentials, all electrons should be excluded and the current measured should just be the positive saturation current due to the positive ions. In figures 55 and 56, increasing negative current is measured with increasing negative modulator voltage for the first channel of the E1 mode (data numbers 128 and 127) and the first 9 channels (data numbers 128 through 56) of the E2 mode. Due the way that currents are synchronously detected in the normal plasma mode [*Bridge et al.*, 1977], the currents in the first 9 channels of a regular plasma measurement in the E2 mode (and the first channel of E1) will not be detected because the current is out of phase with the detector; a level of 0 DN, i.e., threshold, will be entered into the telemetry stream. The modulator potential at the upper edge of channel 9 is -750 volts. This corresponds to an energy close to the maximum in the secondary emission yield curve for gold, an important clue to the origin of this effect. At higher negative potentials, the negative current is decreasing in magnitude, but is still large and negative at -5950 volts, a potential sufficiently large to easily exclude all ambient electrons.

The switch in suppressor potential between -95.2 volts in E2 and -8.05 volts in E1 introduces a subtle change. The two traces from E1 and E2 are different just below -95 volts (data number less than 103), although they are approximately continuous at the "top" of the E1 mode. Another effect is present also in that channel 3 of E2 (data numbers 111 to 104) corresponds to nominal potentials from -56.7 to -92.3 volts. However, electrons in this energy range cannot pass the -95.2 volt potential barrier of the suppressor grid, so a current with the modulator at this channel is also a mystery. These changes imply that both the modulator and suppressor potentials determine the current measured at the collector plate.

The position of the suppressor potential also affects the currents. For both Voyager 1 and Voyager 2 there are sets of DC return spectra acquited within two hours of those spectra shown in Figures 55 and 56. Figures 57 and 58 show DC return spectra for Voyagers 1 and 2, respectively, in the reversed suppressor configuration. In both cases, there are qualitative changes in the shapes of the curves and the current is larger in magnitude by roughly 50% in the reversed configuration. This behavior suggests that in the normal configuration, the suppressor excludes more current from reaching the collector plate.

In Figures 59 through 69 are DC return scans from the Voyager 1 encounters with Jupiter and Saturn. They illustrate (sometimes) the "correct" behavior of the spectra and also some of the difficulties of interpretation. Figure 59 is from the middle magnetosphere of Jupiter. Photoelectron current dominates the A cup signal. E2 and D are continuous (both use the same suppressor voltage); note that E2 exhibits an increasing (positive) current with decreasing (negative) potential in the lowest 4 channels. This out of phase behavior is similar to that produced by photoelectrons and is, presumably, due to secondaries produced by hot energetic electrons in the ambient medium. The side sensor was in not illuminated with solar UV at this time (UV reflected from Jupiter might be able to enter the cup - I haven't checked the geometry - but is probably of too low an intensity to have an effect). Note that the transition through zero net current occurs in the E1 scan. That it does not occur at zero modulator potential is not surprising; the spacecraft is not illuminated uniformly with the positive ion and electron fluxes, and this will be manifested in the zero current potential. The "crossover" is in no way related to the floating potential of the spacecraft with respect to the plasma due to the grounded aperture grid.

Figures 60 through 64 contain data from the warm Io torus. Effects of photocurrent loss in the A cup, hot electrons, and the change in the ram direction of the positive ions are all present, as well as what appears to be the effect of rapid time variations resulting in time aliasing of the A cup data in Figure 61.

Figure 65 is illustrative of (but not the best example of) data from the cold torus, and Figure 66 is from the torus outbound just prior to the encounter with the Io flux tube. Figure 67 is the from the period of solar occultation; at large positive modulator potentials the A and D cups track each other well as the shadow of the planet has cut off the photoelectron production in the A cup. With both the A and D cups looking away from the positive ion flow direction, the positive ion flux reaching the spacecraft is poorly sampled. As a result the transition through zero current occurs at a relatively large negative modulator potential (the entire trace should be shifted up) and the A and D cup spectra are relatively flat (neither cup is pointed in the correct direction to sample ions which a positive modulator potential would exclude). Figure 68 shows the first set of spectra back in sunlight; the A cup is still low, presumably due to a large electron flux.

Finally, Figure 69 is one of the more interesting ones from the Saturn encounter. It is from the outbound crossing of the Dione - Tethys plasma torus. The positive potential traces appear to have the wrong sign for the current; at least that would make more sense than the data as displayed. The effect of the suppressor voltage in excluding electrons is illustrated nicely by the E1 and E2 data in this case.

In principle, it should be possible to use plasma parameter determinations from the normal plasma data in conjunction with the DC return spectra along with the condition of zero current at zero modulator potential (equivalent to modulator off DC measurements, of which we have none in the magnetospheres) to estimate the net current to the spacecraft due to the (subsonic) electrons and ions with energies per charge above

5950 volts. In practice this would be difficult because the electron plasma and DC measurements would have to be corrected for contamination by secondaries within the housing itself. More troublesome than that is the fact that the secondary electron emission characteristics of the materials from which the spacecraft is made are not really known (discussed above in the section on photoelectron yields).

Electric Fields Within the Side Sensor Housing

For the purpose of calculating the instrument response to a variety of plasma conditions, *Barnett* [1984] and *Barnett and Olbert* [1986] make the simplifying assumption of uniform electric fields between the various grid planes. For most purposes this is adequate. Further refinements, such as taking into account the nonuniformity of the field in the immediate vicinity of the grid wires, effective makes the problem enormously more complicated, if not impossible due to the small differences between the sensors as designed and as actually configured once assembled. An example (the subject of grid spacing) has been mentioned above. There are two examples where the effects of the field nonuniformities may play important roles in the effects of photoelectrons and secondary electrons within the instrument housing. We can also give some quantitative estimates of these nonuniformities, if we make some approximations. The regions in question are in the vicinity of the modulator grid support ring and in the vicinity of the suppressor grids.

Fringing Electric Field Near the Negative Modulator Grid Support

In light of the evidence presented, the currents produced when the PLS side sensor is appropriately illuminated with sunlight must be due to photoelectrons produced on the inner surface of the inner support ring of the negative high voltage modulator grid. Referring to Figure 53, it does not appear possible for such electrons to reach the collector directly due to the presence of the shield ring. A more important objection to a direct collection of these electrons is the fact that all electrons produced at this location will be "born" at the modulator potential; photoelectrons are cold, with an average energy of less than~1 eV, small compared to the other potentials which are present. To assess the possibility of a direct contribution to the current, it is necessary to consider the electric field configuration in the vicinity of the ring.

The actual boundary conditions for the appropriate Dirichlet problem are rather complicated even though there is cylindrical symmetry. To simplify the problem so that it is more easily treated numerically, we can replace the true boundary value problem with a two-dimensional analogue. If the scale length of changes in the potential is small compared to the support ring radius, this approximation should be adequate for our purposes. Figure 70 shows the boundary conditions for the two-dimensional problem. The electrostatic potential is sought for the indicated surface at some potential V_{mod}; all other surfaces are at ground potential. Equipotentials were calculated numerically and are displayed in Figure 71, and electric field lines in the near vicinity of the support are displayed in Figure 72 (from a Laplacian problem solver available on Project Athena, C. K. Clark, private communication, June, 12, 1987). The modeling used a fairly coarse grid spacing but does indicate that the "fringing" effect around the support rings dies out after a displacement toward the center of the cup equal to about twice the width of the combined inner and outer ring supports. This is, also roughly, half of the distance from the inner surface of the inner ring to the inner edge of the shield ring.

An approximate solution to the problem is available in analytic form using conformal mapping techniques. This approximation includes only the inner wall of the support ring with their surface facing the shield ring extended to infinity. The appropriate map (inverted) is from *Kober* [1957] and is shown in Figure 73.

A detailed calculation of electron trajectories from the surface of the support to the the plane of the shield ring has not been carried out; however, it appears unlikely that the fringe field can impart enough of a "kick" to the electrons to enable them to clear the shield ring. A proper calculation would need to take into account the drift space between the various ground grids and buckout grid. The intergrid spacing is small enough and the modulator frequency low enough that the problem can be treated as a static one with photoelectrons first produced at the upper potential and then at the lower potential for a given modulator step.

The problem is simplified somewhat by the low energy of the photoelectrons. As the energy the electrons gain from the modulator potential is large compared to the energy with which they are "born" and the buckout potential is a small fraction of the modulator potential, the trajectories of the photoelectrons are independent of the modulator potential. This statement is true only above the ground grid above the first suppressor grid in the normal suppressor configuration. As discussed immediately below, the suppressor potential, which is independent of the modulator potential, produces a nonuniform field in this region. The effect of this constant field will tend to deflect toward the cup wall the electrons coming from the modulator grid. The deflection will then determine where on the shield ring the electrons impact; the deflection should decrease with increasing modulator potential.

Further Work on the Fringing Problem

After the initial assessment of the "fringing field" problem discussed in the section immediately above, it became obvious that the question of whether electrons produced on the relatively large surface area of the modulator support ring can indeed reach the collector plate. As of January, 1988, an experimental answer based on the characteristics of the Flight Spare PLS instrument is still unavailable. In December, 1987 an extensive set of calculations was undertaken (by G. S. Gordon, Jr.) to find a theoretical answer to this question. Details and results of this calculation are outlined in this section (note that the figures referred to herein are out of numerical order with some of those referred to in following sections).

The problem is solved in a two-dimensional approximation using the map from *Korber* [1957] depicted in Figure 73 (this mapping function is also given in problem 10.21 on p. 1315 of

Morse and Feshbach [1953]. The appropriate Schwarz-Christoffel transformation is specified by (note that the numbering of the equations is out of sequence)

$$\frac{dz}{dw} = \frac{k\sqrt{w-1}}{\pi w\sqrt{w-c}} \tag{22}$$

with $k \equiv hc^{-1/2}$ and $c > 1$, $k > 0$. The solution is

$$z(w) = \frac{k}{\pi}\cosh^{-1}\left[\frac{2w-c-1}{c-1}\right] - \frac{k}{\pi}\frac{1}{\sqrt{c}}\cosh^{-1}\left[\frac{[c+1]w-2c}{[c-1]w}\right] \tag{23}$$

In this problem $k = 0.452$ inches, $h = 0.312$ inches, and $c = 2.0988$; the dimensions again correspond to the nominal values given in Figures 53 and 75. Details of the computer routines used to make the plots discussed immediately below and to obtain $w(z)$ from eqn. (23) can be found in Appendix F.

Contour maps of Re $[z(w)]$ are shown in Figures 78 through 81 for different regions with contour lines at 0.1 and 0.01 levels. Corresponding maps of Im $[z(w)]$ are shown in Figures 82 through 85. The inverse mapping $w(z)$ was found using a variation on the Newton-Rapson technique (see Appendix F and the appropriate source listings for further details). Contour plots of Re $[w(z)]$ and Im $[w(z)]$ are shown in Figures 86 and 87, respectively. The contour levels are powers of 2 in these two figures. In Figure 86, heavy lines indicate the contour levels of -1, 0, and +1; heavy lines in Figure 87 show the contours at 0 (along the periphery) and +1. Note that the rectangular region in the upper left hand corner indicates the modulator grid support. Dimensions are given in inches in these figures with the 0.0 along the vertical scale located at the ground grid just below the negative modulator grid (cf. Figure 53).

Given the mapping function, Laplace's equation can be solved in the w plane and the solution mapped into the z plane. From p. 1245 of *Morse and Feshbach* [1953], we choose the complex potential

$$F \equiv \psi + i\chi = \frac{V}{i\pi}\ln w \tag{24}$$

which gives zero potential on the positive real w axis and potential V on the negative real w axis. Hence,

$$w(F) = e^{i\pi F/V} \tag{25}$$

and contours of constant Re $F = \psi$ are lines of constant potential which can be mapped to the z plane. These are shown in Figure 88. Contours of constant Im $F = \chi$ give the electric field lines; these are shown in Figure 89.

Given the electrostatic potential of Figure 88, we assume photo- or secondary electrons are "born" on the inner edge of the modulator support ring. For a given set of initial conditions, the trajectories of these electrons can then be integrated to the plane containing the shield ring to see what fraction pass the ring and can continue to the collector plate (this, of course, assumes that the electron energy is greater than that expended in climbing the potential barrier of the suppressor grid. To make a set of representative calculations, we have assumed that the suppressor potential is zero (representative of the reversed suppressor configuration) and that the electrons are emitted normal to the surface. Figures 90 and 91 show the resulting trajectories for -10 volts on the modulator grid and initial electron energies of 0 eV and 2 eV, respectively. Figures 92 and 93 show trajectories for modulator potentials of -6000 volts and the same two initial electron energies.

On Figures 90 through 93, the inner edge of the support ring is in the upper left corner. Small tic marks on the y axis locate the two ground grids and buckout grid located at dimensions C, D, and E on Figure 53. For the purposes of this calculation, the buckout grid was also assumed to be at ground potential. As the electrons have been accelerated through the modulator potential before reaching it, this potential should produce a negligible effect on the trajectories. The edge of the shield ring is indicated by the rectangle on the lower left. Again all dimensions are in inches. The information of the previous figures is summarized in Figure 94. The equipotential contours in the region between the negative modulator grid and the first grounded grid are shown at the top; the trajectories shown in Figures 90 through 93 are shown below with the physical region covered to the same scale.

The immediate and obvious conclusion to be drawn from the figures is that the electrons get enough of a sideways "kick" to make it past the shield ring. Therefore, such electrons will reach the collector plate and contribute a negative current. This current is a constant, i.e., has no modulated component. To attempt to determine the origin of the modulated component detected in the normal plasma mode, we must now consider the effects of the suppressor potential.

Electric Fields in the Space Above the Suppressor Grid

In both the reversed suppressor configuration and in the normal suppressor configuration, the field line configuration within the cup is somewhat complicated due to the details of the cup design. In the usual analysis algorithms, the electric field lines are all assumed to be parallel with the symmetry axis; this approximation is not necessarily as good in dealing with the effect of electrons produced on the modulator support ring. In the reversed suppressor configuration, the previously computed suppressor efficiencies will be modified by the fact that edge of the collector does not extend as far as the edge of the second suppressor grid itself (see Figure 53); there are modifications in the vicinity of the collector plate edge because, past the edge, the suppressor potential must drop across a greater distance, i.e., the distance to the bottom of the cup housing which is also at ground potential. Between the second suppressor grid and the first suppressor grid (clamped to ground in the reversed suppressor configuration) the field lines should indeed be straight (ignoring all of the incalculable second order effects present in the real cup). It is important to note that the (approximate) plane occupied by the shield ring and the first suppressor grid is at ground potential in this case.

In the normal suppressor configuration, the second suppressor grid is held at ground potential, and the field lines between the second suppressor and first suppressor grid are straight, to first order. A complication in the field structure now arises in the space between the plane occupied by the first suppressor and

shield ring on the one hand and the ground grid which separates the first suppressor and buckout grids on the other.

The space in question can be modeled as a circular cylinder whose sides and one end are at a potential of zero and whose other end is at a finite potential out to some radius a (the hole in the shield ring) and held to zero potential from radius a out to the edge of the cylinder at radius b (the space above the shield ring). The configuration exhibits sufficient symmetry that the potential can be written explicitly as a Fourier-Bessel series. Choose $z = 0$ as the plane of the ground grid just below the buckout grid, and let positive z be in the direction toward the collector plate; the boundary condition of $\Phi = 0$ at $z = 0$ is satisfied by taking the potential to be proportional to sinh kz. The combination of cylindrical symmetry and finite potential at $r = 0$ imposes a radial dependence of $J_0(kz)$. The boundary condition $\Phi = 0$ at $r = b$ is satisfied by taking $k = x_{0,n}/b$ where $x_{0,n}$ is the n *th* zero of the Bessel function of order zero. Let the spacing between the plane of the ground grid and that of the shield ring be denoted by L. Again, we ignore the 0.024" difference between the top surface of the shield ring (gold plate on a copper-clad piece of epoxy glass) and the top surface of the first suppressor grid. Then using the expansion

$$\Phi(r, z) = \sum_{n=1}^{\infty} A_n J_0(k_n r) \sinh k_n z \qquad (15)$$

where $k_n \equiv x_{0,n}/b$ and applying the boundary condition

$$\Phi(r, L) = V \text{ for } 0 < r < a \qquad (16)$$

and zero otherwise, we can find A_n. After some algebra

$$A_n \equiv 2V \frac{a}{b} \frac{csch\, k_n L}{x_{0,n}} \frac{J_1(k_n a)}{J_1(x_{0,n})^2} \qquad (17)$$

The series does not converge very rapidly (for n = 1 to 4, A_n is +10.7, -0.53, -1.0, and +0.99, respectively).

The same calculation can be made for a two-dimensional geometry, i.e., eqn. (15) is now replaced by

$$\Phi(r, z) = \sum_{n_{odd}=1}^{\infty} A_n \cos(k_n r) \sinh k_n z \qquad (15a)$$

with $k_n \equiv n\pi/2b$. Applying the boundary condition eqn. (16) for this formulation yields

$$A_n \equiv \frac{4V}{\pi} \frac{csch\, k_n L}{n} \sin(k_n r) \qquad (17a)$$

which is an equally unenlightening result.

An integral formulation can be found by letting $b \to \infty$. An analysis of this case yields

$$\Phi(r, z) = V \int_0^{\infty} J_0(kr)\, J_1(ka) \frac{\sinh kz}{\sinh kL}\, d(ka) \qquad (18)$$

which is more elegant but no more illuminating. This case can also be approximated by a two-dimensional analogue. In this case we obtain

$$\Phi(r, z) = \frac{2V}{\pi} \int_0^{\infty} \frac{\cos kx \sin ka}{k} \frac{\sinh kz}{\sinh kL}\, dk \qquad (19)$$

This integral can be evaluated in terms of simple functions by noting that $\cos kx \sin ka = 1/2(\sin k(x + a) - \sin k(x - a)$ and using 4.114.1 of *Gradshteyn and Ryzhik* [1980], viz.

$$\int_0^{\infty} \frac{\sin \alpha k}{k} \frac{\sinh kz}{\sinh kL}\, dk = \tan^{-1}\left[\tan \frac{\pi z}{2L} \tanh \frac{\pi \alpha}{2L}\right] \qquad (20)$$

A plot of the field lines is shown in Figure 76 (note that the numbering is off, Figures 74 and 75 have not yet been introduced). The fact that the field lines are not really parallel to the symmetry axis of the cup is not included in either the algorithm of *Barnett* [1984] for the side sensor or in the numerical integration scheme PMODEL. Note that the effect on charged particles entering the cup will be to focus ions and defocus electrons. Put differently, the effect is to make the hole in the shield ring larger for ions and smaller for electrons with the effect becoming less important with increasing particle energy.

To better assess the potential configuration, eqns. (15) and (17) were numerically evaluated by G. S. Gordon, Jr. to produce a contour plot of $\Phi(r, z)$. This is shown in Figure 77; note that the figure is inverted with the suppressor grid at the top and the ground plane at the bottom. The dimensions are in inches, and the plot space (0.165 x 2.765) corresponds to the dimensions on Figure 75 (the vertical dimension used in Figure 76 does not include the 0.015 inch thickness of the shield ring). The contours are at 10% intervals, except for those nearest the boundaries, which are at 1% above/below the boundary value. The mesh used is 999 x 999 and the sum of eqn. (15) was terminated at either the 999th term or when the next term gave a further correction of less than 10^{-6}, whichever came first.

At this time, a rigorous, quantitative analysis of the difference between switching between normal and reversed configurations cannot be given. Qualitatively, one might think that the reversed configuration should lead to more electrons in the vicinity of the hole in the shield ring actually passing through the hole. This is consistent with the increased negative current observed in the DC return mode, reversed suppressor configuration, when sunlight is illuminating the negative modulator support ring.

From early in the mission of Voyager 2 on day 243 of 1977 (11 days after launch), there are DC return spectra for both the normal and reversed suppressor configurations. At this time the angle between the sun and the D cup normal was 73.3°, hence, the negative modulator support was illuminated but not the shield ring (and suppressor grid) or collector plate. A plasma measurement from 1977-238:2011, normal suppressor, modulator on, shows the "turn on" in channel 10, i.e., channel 9 is at threshold, as are channels 3, 4, 6-9, 15, and 16. This is in sharp contrast to the turn on location in the PLOMAN 2 spectra (see below). A corresponding DC return measurement on 1977-249:1340 indicates a maximum (negative) current of -7.04×10^6 fA in channels 9 and 10, i.e., a maximum at ~750 volts (negative) on the modulator grid. This is consistent with the turn on in one of the "voids" in the Jovian magnetosphere

(see below). An earlier DC measurement at 1977-243:1856, gave a broad maximum of -6.40×10^6 fA in channels 7 through 11, indicating that the maximum is flat to ~10% (resolution in this current range for the DC currents, cf. Table 1).

About an hour after the DC measurement in the normal configuration, at 1977-243:1954, there is a DC return measurement in the reversed suppressor configuration. Here the maximum current is -9.60×10^6 fA and extends from channel 6 through channel 10. This is an increase of 50% in the current; the fractional increase in other channels is less, ranging down to % for channel 16. The only logical explanation is that increased refraction of secondary electron trajectories in the normal configuration prevents more electrons from reaching the collector. Given that additional refraction of electrons emitted from the modulator support ring should direct them farther toward the center of the cup, this is also consistent with most of the electrons originating on the underside of the modulator grid itself, presumably due to internally reflected photons.

It is interesting to note that the next available plasma measurement in the reversed suppressor configuration, at 1977-242:2332, shows a turn on in channel 8, i.e., at a modulator voltage of 400 volts. This is consistent with the movement downward (in modulator potential) of the broad maximum in the DC return current; it is not simply consistent with the yield curve for any exposed materials in the interior of the cup. We return to this point below in considering the fractional modulation in the presence of sunlight.

A Qualitative Explanation of the Effect

Illuminated Area of the Support Ring for the Modulator Grid

To quantitatively evaluate the spectra due to photoelectrons, we need to know the illuminate area of the inner surface of the inner ring supporting the negative high voltage modulator grid as a function of the angle of illumination. The geometry is illustrated in Figure 74. Let the inner radius of the ring be a (= 2.457" from Figure 53) and let the height of the ring be h (= 0.140"). Assume the ring is tilted at an angle θ with respect to the viewing direction. The illuminated area (in projection) appears as the intersection of two ellipses of semi-major axis a and semi-minor axis $a \cos\theta$ whose centers are displaced by an amount $h \sin\theta$. The geometry is illustrated in Figure 74. Note that the illuminated area is conveniently divided into Regions A and B as indicated in the figure. The point where the lower branch of the upper ellipse $y_1(x)$ coincides with the upper branch of the lower ellipse $y_2(x)$ separates the two regions; its x coordinate is given by $x_0 = \sqrt{a^2 - (h \tan\theta/2)^2}$.

A straightforward, but tedious, integration gives the projection of the illuminated area A_{illum}. Define the parameter $\beta \equiv h \tan\theta/(2a)$. The illuminated area is then given by

$$A_{illum} = ah \sin\theta \sqrt{1-\beta^2} + 2a^2 \cos\theta \sin^{-1}\beta \qquad (21)$$

For small θ, $A_{illum} \rightarrow 2ah\sin\theta$ as expected.

We have investigated the variation with angle of the modulated part of the current in the E2 spectra acquired during the PLOMAN 2 maneuver within the Jovian magnetosphere. The following table lists the times of the spectra, the angle θ, the illuminated area of the modulator support from equation 21, and the peak current. For the first two spectra the peak current appeared in channels 10 and 11 (i.e., from 750 to 1373 volts); the peak current was located in channel 11 for the rest of the spectra (1017 to 1373 volts).

E2 Spectra From PLOMAN 2 Maneuver 1979-062

SCET	θ	A_{illum} cm^{-2}	I_{peak} (10^4 fA)
1825:19.471	75.3°	4.28	1.59
1826:55.471	63.6°	3.97	2.63
1828:31.471	53.4°	3.56	3.15
1830:07.471	46.1°	3.19	3.26
1831:43.471	43.2°	3.04	3.15

The change in illuminated area of the support ring is obviously not the major factor in causing the current to increase as θ decreases; the illuminated area is actually decreasing due to projection effects. If we assume that the photoelectron current varies as the secant of the angle between the incident photons and the normal to the support ring surface, we still cannot account for the factor of two increase in current as the cup is rotated more into the sunlight.

Let α be the angle of incidence of the photons with respect to the normal to the inner surface of the ring. Then

$$\left\langle \frac{A_{illum}}{\cos\alpha} \right\rangle = 2ah\left(\frac{\pi}{2} - \sin^{-1}\beta\right) + 4a^2 \cot\theta \left(1 - \sqrt{1-\beta^2}\right) \qquad (26)$$

where β is defined as above and $\langle \cdots \rangle$ indicates an average over the illuminated angle. In this case we obtain

E2 Spectra From PLOMAN 2 Maneuver 1979-062

SCET	θ	$\left\langle \frac{A_{illum}}{\cos\alpha} \right\rangle$ cm^{-2}	I_{peak} (10^4 fA)
1825:19.471	75.3°	6.73	1.59
1826:55.471	63.6°	6.84	2.63
1828:31.471	53.4°	6.89	3.15
1830:07.471	46.1°	6.91	3.26
1831:43.471	43.2°	6.91	3.15

The averaging over $\cos\alpha$ increases the effective illuminated area by about 50%; dividing A_{illum} by $\sin\theta$ gives a roughly constant value of 4.4 cm^{-2}. These variations show that even including the angular dependence of the electron yield per photon, the variation cannot be accounted for.

To produce a modulated current, electrons produced at the modulator potential must be involved. A final source for such electrons is the modulator grid itself illuminated by photons reflected from the inside of the cup (E. C. Sittler, Jr, private communication, December, 1987). Photoelectrons produced on the underside of the grid wires will be accelerated toward the collector plate while those produced by direct illumination on

the top will tend to be accelerated toward the aperture grid and leave the cup.

In the review on reflectivity in the ultraviolet by *Koller* [1965], the reflectivity of thin gold film is ~20% for photons of energies between 6 and 10 eV. Such photons form the bulk of the solar spectrum in the energy range for which photoelectron yields are appreciable for many materials [*Grard*, 1973]. Although photoelectron yield versus photon energy is not readily available for tungsten, it is reasonable to assume that ~1/5 of the photons incident on the inner surfaces of the cup will be reflected back to illuminate the negative modulator grid wires. In this case the illuminating flux goes like cos θ. At normal incidence, the grid wire area is $\pi a^2 [1 - (1 - \frac{1}{42})^2] = 5.76$ cm^{-2}, i.e., comparable to the directly illuminated area of the modulator support ring. At angles of incidence of 75.3° and 43.2°, respectively, the areas of the modulator grid wires illuminated by sunlight are 1.46 and 4.20 cm^{-2}, respectively. These values should be reduced by a factor of 0.2 (the reflectivity coefficient). Adding the values from the table apparently again give too low a modulation with angle.

One final correction is the transparency of the aperture grid, positive modulator grid (grounded), and negative modulator grid to the photons hitting the support ring. The transmission probability can be estimated as

$$T = (1 - \frac{1}{42})^3 (1 - \frac{1}{42} \sec \theta)^3 \qquad (27)$$

This effect also yields too small a modulation with angle of incidence: in changing the angle of incidence from 75.3° to 43.2°, respectively, the transparency increases from 0.692 to 0.842 if estimated from eqn. (27).

It is important to note that as the PLOMAN 2 maneuver occurred within the magnetosphere of Jupiter, the positive ions were flowing about at right angles to the spacecraft-sun line [*Sands and McNutt*, 1988]. This is not an important consideration for the plasma mode measurements as such; however, it identifies the problem with attempting to determine the angular modulation of the unmodulated electron current produced by photoelectrons. This component is only available from DC return measurements during a period in which the spacecraft is rotating. Such measurements are made during the Cruise Science Maneuvers mentioned earlier. These maneuvers are made only in the solar wind, so the angular modulation of the photocurrent also includes the positive contribution of the current due to the solar wind at the smaller angles of incidence (<–63° at which the solar wind can reach the collector plate - cf. Figure 53). In addition, there is the positive current which results from photons on the collector plate and escape due to the inefficiency of the suppressor grid, an effect discussed in detail above. We can attempt to disentangle these effects by differencing DC return currents from the L and E2 modes in the same channel acquired at about the same angle (there is some difference in angle due to the finite rotational speed of the spacecraft and the non-simultaneity of the L and E2 measurements).

We again consider the Cruise Science Maneuver on Voyager 1 from day 258 of 1978. If we use the nominal DN to current conversion of Table 1, the currents are smaller than those listed in the above table in the text. It does appear that the time delay between L and E2 acquisition is too slow compared to the angular change in spacecraft orientation to use this technique to come to a definitive conclusion about the angular variation of the DC photocurrent.

The variations are plotted as a function of angle in Figure 95. The modulated current is fairly consistent with a cosine variation, except for the turnover at angles of incidence of less than ~50°. The DC curve indicates an even larger variation at larger angles, but this could be due to not correctly incorporating the electronics temperature in the DN to current conversion. The obvious conclusion to be drawn is that the internally reflected photons illuminating the underside of the negative modulator grid must play a major role in producing the photoelectrons in the instrument. In light of the lack of information in the literature on the photoelectron yield of tungsten as a function of photon energy, as well as the geometric complexities of internal reflection within the instrument, it is likely that a quantitative model of the photoelectron response could only be derived from extensive laboratory calibrations of the flight spare (under appropriate conditions). If back illumination of the modulator grid is the major source of photoelectrons, then their utility as tracers of secondary electrons produced inside the instrument must also be considered limited.

Production of Intermediate Secondaries

Given the photoelectrons produced at the support ring and/or on the modulator grid itself, we turn to the question of how this can give rise to a modulated current at the collector plate. As the modulator potential increases, the photoelectron current produced will increase somewhat but reaches a saturation value at an applied potential of a few volts. This could explain the initial increase in current with negative modulator potential, but cannot explain the peak at ~750 volts. The location of the peak current in the DC return spectra during the Cruise Science Maneuver on day 258 of 1978 is located in channels 8 and 9. PLOMAN 2 spectra shows a "turn on" of the effect in channel 9, which is consistent with the location of the peak in the DC return spectra. The thresholds of channels 9 and 10 are 550 and 750 volts, respectively, so 750 volts is certainly past the maximum. According to *Kollath* [1956], the peak in the secondary yield curve for gold is 800 volts and for tungsten 650 volts. Hence, the location of the peak in current versus modulator potential is consistent with secondaries produced from a tungsten surface, i.e., from the grid wires, but not from a gold surface, i.e., the plating on the cup surface.

An exception to this occurs on Voyager 2 during its encounter with Jupiter in 1979 on day 190 from ~1150 to ~1155. This period is during the crossing of one of the "voids" identified in the Voyager plasma data [*McNutt et al.*, 1987; *Khurana et al.*, 1987]. During this period, the E2 current is apparently out of phase with the synch detector for all channels through channel 9, i.e., the "turn on" occurs in channel 10 above its threshold of 750 volts. This suggests that at very high electron temperatures, the secondary electrons produced off of the gold plating can produce a significant effect.

Secondary electrons capable of reaching the collector plate

must have an energy in excess of ~95 volts to pass the potential barrier established by the suppressor potential (secondary electrons can also be produced on the grounded grid between the suppressor and collector in the normal suppressor mode). This implies that the electrons must originate on either the modulator grid itself (or the support ring) on on the suppressor grid. The fact that sunlight produces a modulated current means that this current must be produced on a surface whose potential varies with respect to the modulator as the modulator voltage is stepped. By elimination, this surface must be the suppressor grid itself. At the peak current, the suppressor is at a potential of 0 - 95 = ~650 volts with respect to the modulator; this, of course, corresponds to the energy of the peak in secondary yield from tungsten.

Most of the secondaries produced at the suppressor grid will be produced on the sunlit, or outward facing, side (along with photoelectrons which constitute another unmodulated component). These will be accelerated by the suppressor potential out of the cup; however, if the modulator voltage is greater than the suppressor voltage (as is the case except for the lowest 3 channels of the E2 mode), these will be reflected back into the cup by the modulator potential. Furthermore, they will have just enough energy to climb over the potential barrier between the suppressor grid wires, which is fractionally smaller than that on the wires themselves. Only those electrons initially emitted nearly parallel to the cup axis will not drift to the sides of the cup and be lost; however, those that do make it through will reach the collector plate. For a given lighting condition, the number of electrons striking the collector will be proportional to the secondary electron yield of tungsten at an energy corresponding to the difference between the modulator and suppressor voltages. Some of the possible electron trajectories and secondary production sites are illustrated qualitatively in Figure 96.

The other case of real interest concerns the production of secondary electrons within the instrument by energetic secondary electrons in the local plasma environment. Again, to produce a modulated signal (which can either add to or subtract from the modulated primary electron current) the modulator potential must be involved. As noted by *Vasyliunas* [1968], a component of secondary flux in phase with the primary flux (and therefor simply adding to it) will be produced at both the suppressor grid (proportional to the yield at energy $E_{primary} - eV_{sup}$) and the grounded grid between the suppressor grid and collector plate (proportional to the yield at energy $E_{primary}$).

More importantly, secondary electrons can be produced at the modulator grid or support ring. In fact, given the relatively large area of the modulator support ring compared to the area of the grid, most of the secondaries presumably would originate on the inner surface of the support structure. Here, of course, the underside of the grid cannot be illuminated by primary electrons as it can by reflected photons. The current so produced will be proportional to the yield at the energy $E_{primary} - eV_{mod}$. The total current so produced is actually given by (cf. eqn. 13)

$$I_{sec} = e \int_{v_m}^{\infty} dv_z\, v_z \int_{-\infty}^{\infty}\int_{-\infty}^{\infty} d^2v_t\, f(\mathbf{v})\, T\delta\left(\tfrac{1}{2} mv^2 - eV_{mod}\right) \quad (28)$$

This current will flow with an annular cross section (cf. Figure 94), intersect the suppressor with an energy of $E_{primary} - eV_{sup}$ (recall that the secondaries are "born" with energies on the order of 1 eV), and continue to the collector plate with this intermediate population of "daughter" secondaries. The current reaching the collector plate can be modulated due to i) modulation of the primary flux reaching the modulator grid and/or support ring, ii) modulation of the yield at the modulator grid and/or support ring, iii) modulation of the number of electrons getting by the shield ring, and iv) modulation of the yield at the suppressor grid. In regard to mechanism iii), some electrons may be stopped by the shield ring. An assessment of possible modulation due to the angular distribution of electrons emitted from the ring support combined with the potential distribution above the suppressor grid is beyond the scope of this study, however.

Figure 96 also shows possible trajectories of electrons produced by energetic primary electrons. Again, in this case it may be possible to produce a current on the collector plate which follows the yield curve for gold. This is apparently necessary to explain the "turn on" in the E2 plasma data observed in at least one of the "voids" observed by Voyager 2 near Ganymede.

The only source of readily available data on the relative amount of modulation in the secondary electron current for both normal and reversed suppressor configurations comes from early in the mission when both forward and reversed suppressor configurations were used in conjunction with DC return measurements. There are also a few places where both DC return and plasma data are available for the case of large secondary currents produced by energetic electrons. These cases occurred in the Jovian magnetosphere during the Voyager 1 pass. The "clean" data, i.e., those in which the fluxes are high enough to be over the DC threshold and positive ions are not flowing into the D cup, occurred outbound on day 65 of 1979.

First we consider spectra in the solar wind near the earth when the ambient electron population was relatively cold, i.e., no ambient electrons were energetic enough to produce a real signal in the E2 mode. The following table lists measured E2 currents as a function of channel number using the DN to DC return conversion of Table 1. All currents are in units of fA (10^{-15} amperes), and TH indicates a threshold current for the measurement in question. These spectra are plotted in Figures 97 through 100 along with neighboring E1 and L spectra (A and D cups). The format is the same as that used for Figures 55 through 69, with the currents from the plasma measurements plotted as positive for both ions and electrons. These figures also show the appearance of the solar wind in the A cup during the DC return measurements.

Voyager 2 1977				
Suppressor:	Normal		Reversed	
Time:	243:1856	238:2011	243:1954	242:2332
Channel	I_{DC}	I_{PLS}	I_{DC}	I_{PLS}
1	-1.00×10^5 = TH	8.475×10^2	-1.37×10^5	1.740×10^3
2	-1.00×10^5 = TH	9.787×10^2	-1.28×10^5	2.585×10^3
3	-6.20×10^5	1.353×10^2 = TH	-8.00×10^5	1.353×10^2 = TH
4	-3.20×10^6	1.353×10^2 = TH	-4.48×10^6	1.353×10^2 = TH
5	-5.44×10^6	1.052×10^5	-8.32×10^6	1.353×10^2 = TH
6	-5.92×10^6	1.353×10^2 = TH	-9.60×10^6	1.353×10^2 = TH
7	-6.40×10^6	1.353×10^2 = TH	-9.60×10^6	1.353×10^2 = TH
8	-6.40×10^6	1.353×10^2 = TH	-9.60×10^6	7.339×10^4
9	-6.40×10^6	1.355×10^2 = TH	-9.60×10^6	2.239×10^5
10	-6.40×10^6	1.172×10^5	-9.60×10^6	4.278×10^5
11	-6.40×10^6	2.494×10^5	-8.96×10^6	5.705×10^5
12	-5.92×10^6	2.160×10^5	-8.32×10^6	5.504×10^5
13	-5.92×10^6	1.305×10^5	-7.68×10^6	4.278×10^5
14	-5.92×10^6	4.597×10^4	-7.68×10^6	2.986×10^5
15	-5.92×10^6	1.353×10^2 = TH	-7.04×10^6	1.939×10^5
16	-5.44×10^6	1.353×10^2 = TH	-7.04×10^6	1.353×10^2 =TH

It is interesting to note that electrons produced at the modulator cannot reach the collector plate for the lowest 3 channels due to the suppressor potential. The currents measured in those channels could be due to feedthrough from higher energy electrons, but these are not present if "high energy" electrons are simply those photoelectrons ejected from the modulator grid. A constant current in the reversed mode would simply be due to photoelectrons produced at the suppressor grid, but here that grid is not illuminated. **At face value there seems to be no way of producing a negative current in these channels**; this is one mystery we return to later.

One final thought on this subject: the angle between the normal and the direction to the sun is 73.3°, as stated above. For sunlight not to be fully intercepted by the shield ring and the structure of the cup above it, an angle of less than 70.2° is required. Obviously, sunlight cannot be producing photoelectrons off of the suppressor grid, and these would not be modulated anyway. However, the solar wind is entering the cup at a large angle of incidence, and, as the modulator potential is increased, the protons are refracted more toward the center of the cup. This refraction effect may be just enough to illuminated the suppressor grid, produce secondary electrons via proton bombardment (more of this later), and produce a negative current from the secondaries. The protons themselves would have to miss the collector plate itself for the net current to be positive as the secondary yield is below unity for typical solar wind proton energies. In the corresponding positive ion mode, the DC return current in the side sensor is at positive threshold, while the measurements in the A cup suggest the solar wind current is $\sim 10^6$ fA. With all of the efficiency factors involved, this mechanism appears to be ruled out, as negative current approaching this in magnitude is measured in the D cup.

The solution to a complicated problem is always the obvious one! Recall from above that the measured suppressor potentials were -95.2 V in the normal mode and -85.9 V in the reversed mode. For channel 3, the modulator potential is oscillating between (nominal) potentials of 56.7 V and 92.3 V. Hence, we expect that a finite amount of secondary current can reach the collector in the reversed configuration. If the true modulator potential is off by as much as 3%, electrons would be just at the threshold for producing a current. Currents in the first two channels in the reversed configuration are still an embarrassment.

A source of negative current in the third channel of E2 is also present during the Cruise Science Maneuvers (normal suppressor configuration). A spot check of the DC return data shows positive currents in the first three channels of E2 when the solar wind is entering the D cup; channels 4 through 16 have negative currents due to the larger currents produced by photoelectrons. However, while the currents in the first two channels are the same, the current in channel 3 is consistently lower. For example, for Voyager 1 at 1978-258/0139: 8.237 the angle to the sun is 43.2° (the minimum reached). The previous L mode has a DN of 153 in channels 7 (solar wind + suppressor inefficiency + photoelectrons from suppressor grid). The E2 mode has DNs of 154 in channels 1 and 2, DN of 148 in channel 3, and DNs ranging between 0 and 34 (net negative current) in all the other channels. It is curious to note that the DNs in the previous E1 mode, all due to the solar wind plus photoelectrons, range from 165 to 174, i.e., much more positive current when the suppressor potential is lower Using the nominal values of Table 1, channels 1 and 2 of E2 show currents of 2.75×10^5 fA, while channel 3 has 2.17×10^5 fA, a change of 0.21. Given the relatively large suppressor grid transparency, this cannot be simply accounted for by secondary emission. Further study is required to pin down the source of negative current. Another possibility is leakage due to the grid plane not being an equipotential (A. J. Lazarus, private communication); it is possible that this is the source of the current (from electrons produced on the modulator at 92.3 volts). This mechanism cannot, of course, be the source of the negative current measured in the first two channels in the reversed suppressor configuration.

As noted above, the normal suppressor DC currents are, at most, one third of the current measured in the reversed suppressor mode. The normal plasma measurements are, at most, ~40% of the reversed suppressor plasma measurements, although this percentage is a fairly strong function of channel number.

One can also consider the fractional modulation by by taking the ratio of the plasma to DC return currents, keeping in mind the possible uncertainties in the DC currents due to temperature dependence and the quantization of the steps (~10% as compared to less than 1% for the plasma measurements). These ratios are shown in the following table for those channels not registering only threshold current; for the latter N/A (not available) is indicated.

Voyager 2 1977		
Suppressor:	Normal	Reversed
Time:	243:1856, 238:2011	243:1954, 242:2332
Channel	$-I_{PLS}/I_{DC}$	$-I_{PLS}/I_{DC}$
1	N/A	0.01270
2	N/A	0.0202
3	N/A	N/A
4	N/A	N/A
5	0.01934	N/A
6	N/A	N/A
7	N/A	N/A
8	N/A	0.00764
9	N/A	0.02332
10	0.01831	0.04456
11	0.03897	0.06367
12	0.03649	0.06615
13	0.02204	0.05570
14	0.00776	0.03888
15	N/A	0.02574
16	N/A	N/A

We estimate that $\Delta\delta \approx 0.1$ across one E2 channel near the peak plasma current, where $\Delta\delta$ is the variation in secondary yield (cf. eqn. (10)). If the yield variation were the only source of modulation for $\delta \approx 1$, we would obtain

$$I_{DC} \approx I_{inc} <\delta> \tag{29}$$

and

$$I_{PLS} \approx I_{inc}\, \Delta\delta\, [1 - (1 - \tfrac{1}{42})^2] \tag{30}$$

which yields a modulated fraction $I_{PLS}/I_{DC} \sim 5 \times 10^{-3}$, a smaller value than is actually measured in the spectra considered above. We have assumed that the conditions producing the spectra are constant and that eqn. (10) adequately represents the yield. These are probably not bad assumptions. It is also possible that the DC return currents are larger than assumed above, i.e., that the fractional modulation is smaller than indicated in the above tables. Given that table 1 is for low temperatures and the thermal dependence shown in Figure 9, this is likely to be part of the problem. More detailed calculations of secondary electron trajectories within the cup and/or actual measurements with the flight spare instrument will be required to resolve the apparent discrepancy.

As we have noted, a similar type of analysis is possible in the case that we know photoelectrons are not responsible by using data obtained during the Voyager 1 encounter with Jupiter. Currents and the modulation ratio from an example are listed in the following table (in the normal suppressor configuration).

The fractional modulation is apparently comparable to that obtained when photoelectrons are present. The variation with modulator potential is, of course, different in the two cases, and for both cases time aliasing, and the conversion of DC return DNs to current are possible sources of error. However, it appears that the resulting E2 spectra are qualitatively consistent.

Voyager 1 1979, Day 65			
Channel Number	DC Return Current (fA) 1122:55.416	Plasma Current (fA) 1121:27.560	Fractional Modulation
1	-1.09×10^5	1.647×10^2 - TH	N/A
2	-1.12×10^5	1.647×10^2 - TH	N/A
3	-1.20×10^5	1.647×10^2 - TH	N/A
4	-1.28×10^5	1.647×10^2 - TH	N/A
5	-1.40×10^5	1.647×10^2 - TH	N/A
6	-1.40×10^5	1.647×10^2 - TH	N/A
7	-1.40×10^5	1.647×10^2 - TH	N/A
8	-1.45×10^5	3.507×10^2	0.0024
9	-1.40×10^5	8.621×10^2	0.0062
10	-1.40×10^5	1.708×10^3	0.0122
11	-1.40×10^5	2.726×10^3	0.0195
12	-1.36×10^5	3.507×10^3	0.0258
13	-1.28×10^5	3.264×10^3	0.0255
14	-1.20×10^5	3.769×10^3	0.0314
15	-1.05×10^5	5.210×10^3	0.0496
16	-1.00×10^5 - TH	5.401×10^3	N/A

We have also examined the E1 spectra at this time. The DC return spectrum at 65/1123:43.416 exhibits a broad maximum from channel 4 through channel 8; the plasma measurement at 65/1122:15.560 shows occasional currents above the 0 DN level which have no organized structure, i.e., they are consistent with noise.

Given that there were no DC return measurements in the the Voyager 2 measurement sequence at Jupiter near the so-called voids, but there is also no indication of random noise in the lower channels, i.e., the lower channels appear to be "clamped" to threshold values, we con only conclude that those spectra are produced by a very hot primary population which produces significant numbers of secondary electrons within the instrument housing.

The E1 Spectra

We have not concentrated on the E1 spectra for because the physics of secondary emission is more complicated for impacting electrons at under 50 eV. In particular, it is difficult to differentiate between secondary electron, backscattered electrons, and reflected primaries at these low energies. It is clear from Figures 55 through 58, 97, and 99 that in the E1 spectra, the current at the collector increases for increasing potential for at least the first two, and sometimes, the first three channels (typically for the reversed suppressor configuration). This behavior covers the range from 10 to ~25 volts. However, from ~25 to ~ 140 volts, the measured current decreases with increasing modulator potential, i.e., the collected current does not simply follow the expected yield curve as occurs in the E2 mode measurements. This behavior is clear in the PLOMAN 2 spectrum from 1979-62/1832:31.471 as well (angle to the sun 43.7°). In the cruise science maneuvers, the signature is complicated by the solar wind at such small angles: the total current in the E1 spectra are positive in all channels but with variations due to the ambient electrons and photoelectrons also

present. In addition, the secondary yield is expected to be small; it is less than unity for less than 250 eV electrons bombarding tungsten [e.g., *McDaniel*, 1964].

The other fact of interest to note is that on the figures referred to immediately above, the E1 and E2 spectra do correspond. In the normal suppressor configuration, ~the same current is measured in the fourth channel of E2 and the top four channels of E1. In the reversed configuration, the current measured in E1 is always somewhat larger in magnitude. This variation between the two configurations suggests part of this behavior reflects the inefficiency of the suppressor in the normal configuration.

The decrease in measured current with increasing energy above 25 volts on the modulator must, therefore be related to the suppressor potential, by elimination. One possible way of decreasing the negative current would be by increasing the energy of the electrons liberated as secondaries from the collector plate as the primary energy increases. True secondaries have a common energy distribution independent of the energy of the incident primary. At 2.5 volts, a substantial fraction of secondaries from the collector can pass the suppressor to be absorbed at other grounded surfaces in the cup. The fraction lost is about 8% for the reversed suppressor and and 10% for the normal configuration (see Appendix B and Figure 15).

The energy of the secondaries is not a function of primary energy, but the energies of backscattered electrons are ([*Sternglass*, 1954] and references therein). Unfortunately, the literature on secondary and backscattered electrons at energies below 200 eV is limited and probably dated with respect to the measurement techniques employed. It is interesting to note that there are secondary maxima in the energy spectras of secondary electrons which are characteristic of the target material, although this seems to be related to the prior heating of the target [*Hachenberg and Brauer*, 1959]. *Rudberg* [1936] found such secondary maxima for a gold target at ~3 and ~24 eV. If such maxima are present in the secondaries emitted from the collector plate, then as the modulator potential (at which the photoelectrons are produced) exceeds 24 volts, electrons at this characteristic energy can be emitted; they would immediately be lost as they could not be stopped by the ~8 volts on the suppressor grid. If a larger fraction of the secondaries are emitted with this energy as the primary energy increases, this could account for the decrease in negative current at higher energies in the E1 mode. However, this does not appear to be easily reconciled with similar measured currents at similar accelerating potentials in the E2 mode; with a suppressor potential of -95 V, all the the higher energy secondaries should be stopped. This change in suppressor efficiency should be reflected in an abrupt increase in collector current magnitude. Such a change is, of course, not present.

A comparison of the E1 and E2 spectra does suggest that whatever mechanism is responsible for electrons to leak past the suppressor to the collector plate in the E2 mode is also responsible for them leaking past the suppressor in the E1 mode. This process must become independent of the suppressor potential once the primary energy has exceeded ~90 volts. Again, this could be due to the details of the secondary, reflected primary, and backscattered primary electrons at the energies where the distinction between these various populations becomes blurred.

A final consideration for interpreting E1 spectra is a problem with the amplitude in the E1 measurements (see section 3.1 of report by R. J. Butler, unpublished manuscript). The effect is present at some level in the first two channels and is due to transients from switching the suppressor potential just prior to the E1 measurements. Calibration curves exist which can be used to remove this problem in the analysis of the electron data.

Secondary Electrons Produced By Positive Ions

A subject not touched upon here, but of potential importance in the analysis of some of the magnetospheric data obtained by the Voyagers, is the production of secondary electrons by positive ions. Production of such electrons at the modulator grid was of concern in the analysis of IMP-2 and OGO 1 and 3 data obtained by M.I.T. Faraday cups in the Earth's magnetosphere [*Vasyliunas*, 1968; *Binsack*, 1967]. *Vasyliunas* [1966] noted that due to the energy dependence of the secondary yield with respect to ion energy, the current produced will be out of phase with respect to the synchronous detector (this effect has also been noted by *Sittler* [1983]). As the yield is an increasing function of proton energy, more negative modulator potentials, should lead to larger yields of electron currents. Evidence that this was indeed occurring came in the form of electron data from OGO 1 in which the telemetered signal was clamped to the instrument zero level, below the noise level [*Binsack*, 1967]. These measurements occurred in the plasmapause where all of the cold, high density protons appeared within a given energy window, exceeding the nominal electron flux in that window by some two orders of magnitude.

The behavior of the measurements, i.e., a "clamping" at the zero DN level, is exactly the phenomenon found in the E2 measurements discussed above. In that case, the electrons have to simply be "hot", i.e., mostly in an energy range over which the secondary yield coefficient exceeds unity.

The yield coefficient for O^+ incident on tungsten exceeds unity around a few keV [*Large*, 1963]. It is almost certainly the case that that the 0 DN values in the upper channels of the E2 spectra in the warm Io torus (1979, day 64 for Voyager 1) are produced by this effect, i.e., the positive ions are accelerated to ~5 keV by the negative modulator potential, and hit the modulator grid yielding secondary electrons. This current would be out of phase with that due to the primary electron population, and, if of sufficiently large magnitude, can produce the observed effect [see also *Sittler and Strobel*, 1987]. A more complex version of this effect, including yield curve modulation of the daughter secondaries, is almost certainly responsible for the bizarre E2 spectra recorded in the cold Io torus when large fluxes of positive ions could reach the (negative) modulator support ring but not the collector plate itself (due to the geometry of the flow).

Comparison with Other Instrumentation

The problem of secondary electron contamination in plasma experiment observations in space is not limited to modulated

grid Faraday cups. Difficulties associated with secondaries in RPAs due to large positive ion fluxes [*Knudsen and Harris*, 1973] as well as in electrostatic analyzers due to large electron fluxes [*Zwickl et al.*, 1987] have been reported. In both cases, the problem was only recognized when trying to explain unexpected observations. This is also true of the motivation for this report; however, our investigations indicate that the effects of secondaries can be present at other times as well and not be noticeable due to the "masking" effect of expected observations. Such behavior is, in principle, possible in RPAs and electrostatic analyzers as well, especially in exotic environments for which only limited data sets are available. Hence, one is left **with the caveat that significant corrections for spurious secondary electrons may be required to characterize the local plasma environment around a spacecraft, but the need to make such corrections may not be obvious in the data.**

Remaining Questions

Quantitative Modeling

The central question is whether a quantitative model of these secondary emission effects can be made which will allow us to simulate the data to a high degree of accuracy (~1% level). Such simulations are possible with the positive ion data in all four Faraday cups under conditions of negligible charging in the Jovian magnetosphere even when the ions are hot (see, e.g., [*Barnett*, 1986]. To accomplish this task the cascading or "feedthrough" of higher energy ions into lower energy measurement channels must be effectively taken into account. The feedthrough of electrons into the positive ion mode and of positive ions into the electron mode, both of which have been known of for some time [*Vasyliunas*, 1971], have been incorporated into the simulation code PMODEL (written by V. M. Vasyliunas, with documentation and corrections by J. W. Belcher). As noted above, PMODEL has been modified (with the efforts of G. S. Gordon, Jr.) to include the effect of suppressor inefficiency in simulating electron spectra. The additional current source provided by secondary electrons created at the modulator grid/support assembly and the suppressor grid have not as yet been included.

The possibility of feedthrough from higher to lower energies was also recognized by *Vasyliunas* [1971] but was dismissed as a "higher order correction". The latter is certainly the case for measurements of the supersonic solar wind, the task for which the PLS experiment was primarily designed [*Bridge et al.*, 1977], but is a crucial effect to model in interpreting plasma data returned from the magnetospheres of the outer planets. Such a feedthrough effect is also present in electron data but is not modeled in the current analysis scheme (details of the analysis are given by *Sittler* [1983]). As more superthermal electrons are added this effect becomes more important; it accounts for ~10% corrections to the relatively well-behaved electron data acquired during the Uranus encounter of Voyager 2 (see Voyager Memorandum 136). A recent analysis of the electron data from the Io torus by *Sittler and Strobel* [1987] showed that ion feedthrough provides a substantial contribution to the high energy electron channels. The calculation was made with the unmodified PMODEL code, i.e., suppressor inefficiency not taken into account, and was based upon the thermal ions; the feedthrough effect is actually larger as there are significant fluxes of non-Maxwellian ions in this region [*Bagenal*, 1987].

The other effects of secondaries with which we are concerned have been recognized in a qualitative way for some time as "extraneous effects" characteristic of the modulated-grid Faraday cup scheme [*Vasyliunas*, 1971]. These effects include the modulated signal produced when sunlight illuminates the interior of the cup, which was not well understood at the time but thought to be related to yield of secondaries produced at the suppressor by photoelectrons produced at the modulator grid; this mechanism appears to be solidly supported by the Voyager data. They also include the out of phase signal resulting from secondaries produced by ion impact on the modulator grid (in the electron mode), and the enhancement of electron current due to secondaries produced at the modulator and suppressor grids in the electron mode. That the latter effect can also produce out of phase signals was not noted or, more likely, not considered, before as a very hot primary electron population is required to produce this effect. Such a situation has been encountered in the magnetospheres of Jupiter and Uranus (see below), and the study of these bizarre plasma conditions provided the impetus for this in depth study.

The modeling problem is also complicated by having no a priori information as to the functional form of the distribution function to be used. The current state of affairs is illustrated in Figure 101. We show E1 and E2 spectra taken in the Jovian magnetosphere at the top. Note the 0 DN levels in channel 1 of E1 and channel 3 of E2. Both of these features, as well as potentially low values of current in channels 2 and 3 of E1 and 4 of E2 are due to out-of-phase signals produced by internal secondary emission due to the electrons present in the non-Maxwellian tail. The second two plots (from the top) show a best simulation from the unmodified PMODEL code. Note that there can be no direct current in the first 3 channels of E2 due to the suppressor potential; the currents there are entirely due to feedthrough from higher energy electrons. Note also that the simulated and measured currents in the first two channels of E2 show a rather good match. This simulation assumed a κ distribution (see , e.g., [*Vasyliunas*, 1971] and references therein), with $\kappa = 1.5$. The next two rows of plots show, respectively, a simulation with $\kappa = 5.5$ and $\kappa \rightarrow \infty$, i.e., a Maxwellian, both with only somewhat higher most probable speeds. Finally, the fourth row shows the simulated two Maxwellian fit from the NSSDC. Although, the E1 currents match fairly well, the match to the high energy tail is not good. This latter discrepancy has been alleviated to some extent by the use of four Maxwellians to fit the data (E. C. Sittler, Jr., private communication). Note that none of these simulations include effects due to secondaries or ion feedthrough. Note also that the effects in the first few channels of the E1 spectrum introduce difficulties in the determination of an electron "temperature" (or most probable speed). This problem systematically occurs when the apparent electron temperature exceeds a few tens of volts (E. C. Sittler, Jr., private communication).

Other Qualitative Problems

There is a great deal of data, especially from the Voyager encounters with Jupiter, which has not been analyzed because we have not understood how to do the analysis. The example of the "voids" near Ganymede during the Voyager 2 encounter is one, but not the only, example. The positive ion data acquired during the times in which 0 DN levels are recorded in the E2 data have been mystifying as well. The Voyager 2 encounter with Uranus may have provided the Rosetta stone with which these data may be understood, at least qualitatively.

Spacecraft Charging at Uranus. Figure 102 shows positive ion and electron data (long and short integration times) from the Uranus encounter during that time that a large (~ -400 V) potential on the spacecraft is inferred [*McNutt et al.*, 1987]. It is important to note that the low energy tail is not "real", i.e., the ions are all accelerated to a potential consistent with the peak location in the ion spectra; the "tail" is purely a feed through effect due to these ions down to lower channels. The plot format is described in Voyager Memorandum 122 and is a modification of the "1800" plots produced during the other encounters (refer to Voyager Memorandum 79) to incorporate all of the GS-5 mode data. The charging signature is readily apparent in the D cup in all of the L and M mode spectra. Similar signatures can be seen in the A, B, and C cups. It should also be noted that the E2 spectra exhibit the "turn on" signature characteristic of secondary electron production. In other words, **if the ambient electrons are hot enough to produce secondary electrons which contaminate the E2 spectra, then the ambient electron flux is large enough to charge the spacecraft to negative potentials of several hundred volts.** The transition to clear signatures in E2 occur as the ion spectra show an average acceleration through ~250 eV. The channel corresponding to the turn on is about one channel lower than that containing the the peak in the L mode. This is the qualitative behavior expected: the spacecraft charges to a potential corresponding to the peak location in the electron flux, and, if the latter is below the maximum in the secondary yield curve, the secondaries produced will provide a large out of phase signal in lower channels. Further quantitative analysis of these features may be possible; however, such an effort is hampered by the relatively small signal-to-noise ratio and additional noise produced by the LECP stepping motor.

Inferred Charging at Jupiter. Figures 103 and 104 show ~45 minutes of data from the PLS experiment on Voyager 2 as it was outbound from Jupiter. The spacecraft is ~21 R_J from the center of the planet, the D cup should show some response to corotating flow of plasma ions, and the main sensor cups none at all. The obvious question is what is the origin of the currents in the positive ion measurements? The E2 spectra suggest an answer, in light of the Uranus charging data. In all of the E2 spectra, channels 2 through 7 are clamped to 0 DN; in addition, the turn on occurs slowly with channel number suggesting the gradual reduction of an out-of-phase signal. Such electron spectra can only be produced if the ambient electrons are hot. The Uranus spectra suggest that electrons which are that hot provide fluxes sufficient to charge the spacecraft negative. Given the similarity of the ion spectra with those at Uranus, it is probable that the spacecraft is charged to a large negative potential, and most of the ion currents are the feedthrough signatures of the positive ions (of several different plasma species) which are being accelerated into the four cups of the PLS instrument. The occurrence of a peak in the ion spectra in channels 14, 15, or 16 implies that the potential is at least -2500 volts. There is roughly a 24 hour period during which these charging levels were maintained. If this interpretation is correct, it may be possible to extract positive ion densities which can be checked against the cut off frequency observed in the Plasma Wave (PWS) data [*Scarf et al.*, 1981].

Figures 105 and 106 show a similar set of spectra which include the last of the plasma depletions observed during the Voyager 2 inbound pass [*McNutt et al.*, 1987]. The E2 spectra show the same qualitative behavior but are clamped to 0 DN up to a larger channel number. Most of the positive ion spectra peak in channel 16 or higher (with the two obvious exceptions). Both of the features are consistent with a hotter ambient electron population and, as a consequence, more negative spacecraft potential. Such behavior is observed in all of the depletions. In all qualitative respects, the data obtained within the depletions is consistent with that obtained for more extended periods outbound illustrated in Figures 103 and 104.

Similar data were obtained by Voyager 1 outbound from Jupiter. Figure 107 shows data obtained ~22 R_J from Jupiter by the PLS instrument on Voyager 1. At the top of the figure and just past the center are E2 spectra similar to those of Figure 104. The corresponding L mode spectra also show the characteristic rise with channel number which would be associated with ions accelerated into the various Faraday cups. t the center of the figure are two sets of DC return spectra acquired ~1120. One of these was used in the analysis of the fractional modulation due to secondaries given in tabular form above. It is readily apparent from the E2 spectra in Figure 107 that the turn on in the plasma spectrum is associated with the location of the peak in the DC return E2 spectra.

Puzzling Features in the Ion Spectra. The lower part of Figure 107 shows a feature which is not so readily understood. The E2 and E1 spectra indicate relatively cooler electron temperatures, and the lower channels in the ion spectra have apparently been filled in with direct signals. However, Channel 16 in the main sensor cups remains at a relatively low level. Figure 108 shows similar behavior a few hours earlier on day 65, along with some bizarre jumps in the data in the D cup (the glitches in the M mode spectra are from LECP 6 second stepping). Figures 109 and 110 show similar behavior from the inbound pass of Voyager 1 on day 63 of 1979. In this latter case, azimuthally flowing ions are apparent in the D cup.

Similar E2 and L spectra were also acquired for a limited region during the Voyager 1 outbound pass at Saturn. The signatures are not as clear due to the signal to noise ratio.

The ion spectra in Figure 110 are particularly puzzling in that there is a drop to the 0 DN level in high channels of the C cup for both the L and M modes, without corresponding behavior in the A or B cups. The 16th channel of E2 also seems to be adversely affected. These spectra are not easily understood. If the signals in the upper channels of the A, B, and C cups in the L mode were due entirely to the ambient plasma population, the

ions producing the signature would be hot, and the signature should be the same in all of the cups. Large anisotropies can also be ruled out if the anisotropy is gyrotropic. Similarly, if the measured currents were due to energetic electrons, a similar signature should be present in all the cups of the main sensor, which it clearly is not. In addition, the affected cup is not always C, i.e., the cup showing 0 DN in channel 16 changes, so an electronics failure can be ruled out.

The 0 DN levels certainly suggest an out-of-phase signal which must somehow be associated with the direction of positive ion flow. We come to this latter conclusion as there is no other phenomenon to distinguish between cups at the highest energies. Unfortunately, there are no DC return measurements for which the downturn is seen in the A cup plasma measurements and the fluxes are sufficiently above the photoelectron current (from suppressor leakage) for the change in net phase to be directly measurable.

An out of phase signal is not readily produced in the positive ion measurements. As the modulator has a positive potential, secondary electrons can only be produced at the negative suppressor grid. For such a current to be modulated, the rate must be varied via the refraction modulation of the particles reaching the suppressor grid [*Vasyliunas*, 1971]. To produce an out-of-phase current, the net (positive) current must increase with increasing (positive) modulator potential. Either, more positive ions must reach the collector plate or less electrons. Neither of these options has an obvious mechanism. The out-of-phase signal does seem to occur in the cups furthest away from the ion flow. As secondary electrons can escape only from grids charged to negative potentials, and the energies are two low to produce ions from either electron or ion impact, it would appear that the effect must be related to the collection of fewer secondary electrons with increasing modulator potential. Further study will require a full accounting of all feedthrough and secondary production corrections.

Figures 111 and 112 show a sequence from Voyager 1 inbound as the spacecraft neared the warm Io torus. Toward the end of the sequence, there is a component of convective flow into the B, C, and D cups. Up until ~0135, there is a relatively high energy background signal in all cups in the positive ion modes. At this time the superthermal electrons disappear and both the electron and ion spectra change qualitatively. The signals in the high energy ion channels drop, indicating that these signals were probably feedthrough from the hot electrons (those with energies greater than 95 volts which could reach the collector in spite of the suppressor potential). After this time much of the electron currents may be due to ion feedthrough in the upper channels; the 0 DN level in channel 16 is almost certainly due to secondary electrons produced by the ions at the modulator grid. This effect must also have been present in previously but masked by the hot ambient electrons. Such a combination of effects would explain the somewhat depressed electron current in channel 16 of the E2 spectra in Figures 103 through 106 and 109 through 111. In some of these figures, the ions producing the secondaries must have been accelerated by the spacecraft potential in the first place where the latter was caused by the hot electron flux; such synergistic effects apparently result in the complexities found in attempting to explain many of the ion and electron spectra.

Other strange features are found in spectra obtained with the Voyager 1 instrument within the Io torus itself. Figures 113 and 114 shown data from ~9 R_J and ~6 R_J from Jupiter, respectively. In Figure 113, out-of-phase currents contribute to the low energy channels in the A and B cups in the L mode but not the M mode. In Figure 114, intermediate channels of the L mode spectra from the B and C cup exhibit large subtracting currents never seen again in the mission. This behavior could be related to the saturation of the amplifiers in the L mode, as there is no analogous affect in the M mode spectra and the L mode measurements are highest in the B and C cups of the M mode. More thought should be given to this possibility.

The Oscillator Effect. Figures 115 and 116 show the best example of the most bizarre effect to appear in the data. For this particular period, the E2 spectra are relatively unaffected, although there are counterexamples. The E1, L, and, especially, M mode spectra exhibit oscillations with respect to channel number. In the M mode, the oscillation period is clearly resolved, with the telemetered currents reaching down to the 0 DN level between peaks. This behavior is presumably to be interpreted as indicating an out-of-phase signal in these regions; if DC return measurements were available (and none seem to be) they would apparently show a current varying sinusoidally with respect to the channel number. It is worth noting that the widths of the zero DN regions are less than half the widths of the nonzero DN regions. In other words, a the sinusoidal variation appears to be superimposed on top of an in-phase modulated current, shifting the oscillation point upward from the zero level. That this is likely the case is more evident in the bottom of Figure 116. The oscillation frequency appears to reach a minimum ~192/0815, and a similar minimum occurred ~192/0515. Plate 1 of *Scarf et al.* [1981] suggests that these times may be associated with rapidly changing plasma densities. During these times, the plasma frequency was rapidly swept through 2.4 kHz, which is the frequency of the square wave power supplied to the PLS experiment; the plasma frequency apparently remained above 1 kHz throughout this region. The square wave applied to the modulator grids has a frequency of 400 Hz, so it is not obvious why an effect is seen. Presumably, the oscillations in the measured current are a beat phenomenon occurring at the difference between the local plasma frequency and some reference frequency produced by the PLS experiment. The 400 Hz square wave on the modulator grid will also produce odd harmonics, so the relevant frequency provided by the instrument may be 1.2 or 2.0 kHz (3rd or 5th harmonic, J. H. Binsack, private communication). Only narrow band data from the PWS experiment is available at this time, so the error bars on the density determined from the cutoff of the continuum radiation are rather large. Further, more detailed comparisons are required to determine the exact limits which can be put on the density.

A better determination of the relevant spacecraft frequency may be obtainable from Voyager 2 data in the solar wind just prior to its encounter with Saturn. Here the solar wind is clearly visible in the M mode spectra, as are the oscillations. A fit to the solar wind proton peak at 1981-236/1300:58 (J. D. Richardson, private communication) yields a proton density of

0.0475 cm^{-3}. The oscillation envelope occupies ~10 M mode channels, or ~2.4 seconds. The corresponding electron plasma (from charge neutrality, neglecting the α particles) and difference frequencies would then be 1960 Hz and 0.42 Hz. This is suspiciously close to the 5th harmonic. The 3rd harmonic corresponds to an electron density of 0.018 cm^{-3}. Such low density regions have been sampled, and there is, presumably, more power in the third harmonic than the 5th. It is possible that such lower densities do not provide enough electrons to yield a signal above the noise level. It is also possible that the spectra of Figures 116 and 117 correspond to such lower densities. Again, careful comparisons are needed to further pin down this effect. We note that a plasma frequency of 400 Hz corresponds to a density of 0.00198 cm^{-3}. Rather large speeds would be required to produce a measurable flux.

For the solar wind spectrum considered above, the amplitude corresponds to a flux of $\sim 2 \times 10^5$ cm^{-2} s^{-1}. For the density quoted above, the speed is 4.2×10^6 cm s^{-1}. This does not seem to relate to much of anything but is based on the assumption that the oscillating charges are spread out uniformly on the collector. If the area of the collector impacted were smaller, the corresponding particle speeds would be larger.

Obviously, this phenomenon is not understood. Other complications include the exact mechanism of setting up current oscillations at the collector plate and to what extent, if any, Doppler shifts in the plasma frequency affect the exact resonance conditions. The reason for selecting a 400 Hz frequency for the modulator was a concern about resonance effects (A. J. Lazarus and J. H. Binsack, private communication). The alternating changes in the modulator potential are certainly suspect for establishing charge density oscillations, but no detailed studies of mechanisms were ever conducted. Another possible clue is the fact that the PWS experiment "sees" the PLS experiment when the modulator is on; presumably this is due to waves excited in the ambient plasma (H. S. Bridge, private communication).

Implications

There several implications which follow from this study, one being major. The major result is that the energetic electron spectra, i.e., those obtained in the E2 mode cannot be taken at face value. We have also noted that corrections to the E1 spectra can be important if the electron temperature is high enough. Even in those cases where there is no obvious out-of-phase current, the electron current below channel 8 will be decreased and above channel 8 increased over the fluxes present in the parent population outside the instrument housing. Obviously, the extent of the corrections are a function of the electron distribution function which cannot be simply read off of the measured currents due to the electron cascade-type of feedthrough effect. Further complications arise due to feedthrough from the ions, which can be affected by feedthrough from the electrons, and spacecraft charging. These effects, and the resulting corrections to the analysis, are certainly minimal in the solar wind or cold Io torus. In other locales they may also be unimportant to some level, e.g., 1% or 10% say, but this must be judged on a case by case basis. These complications may (or may not) have a major effect on the electron impact ionization rates for multiply charged ions in the warm Io torus as calculated by *Sittler and Strobel* [1987]. Their rates are probably within a factor of 3 or so of the true rates, but a more detailed study is necessary to confirm or reject such a number. Given that the ionization cross sections typically peak around 100 eV and secondaries apparently cause an out-of-phase signal up to ~750 eV, the published rates are almost certainly low. Their other conclusions based upon details of variations in the hot electron component, rather than those based upon gross morphological characteristics, are also called into question by these results and should be reexamined.

Consequences for positive ion results tend to be less dramatic, as a ready source of modulated secondaries within the instrument is no longer available. The major source of "contamination" is expected to be simple electron feedthrough, which may explain currents in the main sensor in the upper channels, such as depicted in the top of Figure 111. The feedthrough contribution should be relatively flat (based on some simulations), and certain features remain unexplained, notably the downturn in the highest energy channels, present in the C cup in Figure 110. As a matter of course, we have refrained from publishing these data or any analysis based upon them because we could not duplicate them from our knowledge of the instrument response. This "policy" has, perhaps been overdone. A search for a qualitative mechanism for producing an out-of-phase signal in the ion measurements is required and, can perhaps lead to new physical insights concerning the characteristics of the ambient plasma.

A final major consequence is that many of the spectra from the various planetary encounters can be understood in terms of a very hot electron environment and a negative charging of the Voyager spacecraft. The work of *Khurana et al.* [1987] not withstanding, the spacecraft potential never seems to have exceeded significantly a few kV. Some of the spectra shown in Figure 105 appear at first sight to be difficult to reconcile with this solution, as a turnover in channel 16 alone must be viewed with suspicion. On the other hand, for the apparent feedthrough signals to be the amplitude they are with the corresponding spectral shape, the ion energy cannot appreciably exceed 5 kV. Some preliminary work suggests 7 kV is a hard upper limit unless appreciable plasma injection (factors of 10) is occurring simultaneously with the charging process. The latter can be ruled out as it would give rise to a corresponding discharge current to the spacecraft, lowering the potential, and contradicting the observations. The charging levels found in the Voyager data should prove useful in the interpretation of plasma data returned from the Jovian magnetosphere from the Galileo orbiter, as such charging levels had not previously been inferred from Voyager and Pioneer data sets (F. L. Scarf seems to be vindicated on this point!).

Finally, we note in passing that the DC return measurements have been crucial in sorting out these various phenomena. At the same time, they are difficult to work with due to the (presumed) thermal dependence of the DN to current conversion. Examination of data during the thermal cycling of the Voyager 1 instrument seems to preclude as strong a dependence as inferred from the pre-flight calibrations, however

(see Voyager Memorandum #158). The DC return measurements are typically difficult to interpret due to the the presence of the suppressor grid and the combined effects of ion, electron, and secondary electron currents. The PLS experiment is fundamentally different from an RPA (retarding potential analyzer) due to the grounded aperture grid, i.e., the instrument potentials do not, except to low order, intrude into the local plasma (this may be a bit misleading: using the formulas of *Morse and Feshbach* [1953], I estimate about a 4% "leakage" in the ion modes, or about 100 V for a modulator potential of 2500 V). As a result, the floating potential of the spacecraft cannot be determined, and, at zero modulator potential, there should be a net zero current to the collector plate. That this does not happen in the Jovian and Saturnian magnetospheres can usually be traced to i) directional effects due to supersonic ion flow, ii) photoelectron production and suppressor leakage, iii) changing electron temperature with respect to the suppressor potentials used for E1, E2, and ion measurements, and iv) secondary electron production at the skin of the spacecraft itself. Effect ii) accounts for the difference in the A and D cup currents in Figures 55 through 59. Effect i) accounts for the differences between the currents in the A and D cups in Figures 61, 64, 65, and 66. Effects iii) and iv) apparently account for the zero in the current (with respect to modulator potential) in Figures 67, 68, and 71. It may be possible to understand the some aspects of the secondary emission characteristics of the spacecraft from these data, but it will not be an easy undertaking. Note that due to effect iii) the measured DC return current is almost always positive; in the E2, L, and M modes, the suppressor potential is -95.2 volts, and current carrying electrons with energies less than this cannot reach the collector plate to cancel the positive current carried by the ions. This also explains why the D cup, L mode and E2 traces are usually continuous as the average modulator potential changes sign. The spectra in Figure 61 are the exception; in this case most of the electron current is carried by hot electrons.

Summary and Conclusions

We have completed an extensive survey of PLS data from the two Voyager spacecraft in an attempt to understand certain anomalous spectra obtained within the magnetospheres of the outer planets. The study of the plasma voids on the Voyager 2 pass and the ensuing argument over charging levels with investigators studying LECP data motivated this study. In attempting to explain these spectra we have developed a much improved understanding of how modulated-grid Faraday cups actually respond to the often bizarre plasma environments encountered in deep space. This has included an understanding of the generation of photo- and secondary electrons within the cup housing, and how these populations affect the currents actually measured by the instrument and telemetered to Earth. Some of this understanding is quantitative while much is not. Due to the various synergistic effects, such quantitative study will require the use of the flight spare in laboratory tests coupled with further numerical modeling. We have also found regions in these magnetospheres where the spacecraft was apparently charged negatively to kilovolt potentials. This may well open up possibilities for further analysis of PLS data. Finally, we have made the first systematic study of the DC return spectra from then PLS instrument, used them in interpreting some of the strange plasma data, and identified the difficulties and potential uses of this data set.

Acknowledgements. The preparation of this document has benefited greatly from discussions with H.S. Bridge, who still knows more about the PLS instrument than he sometimes realizes; this includes facts known to no one else which are also not written down anywhere in recognizable form. Other "culprits" whose memories and help have been invaluable are J. H. Binsack, R. J. Butler, A. J. Lazarus, and S. Olbert, all associated in the present, past, or both with M.I.T. and O. Divers of JPL. G. S. Gordon, Jr. of M.I.T. was essential in the development and implementation of the algorithm for computing the positive current caused by the loss of secondary electrons by the suppressor grids and for the fringing field calculation near the modulator grid support. E. C. Sittler, Jr. of Goddard Space Flight Center is thanked for copies of notes from his early investigations of secondary electrons within the instrument as well as for his stimulating comments and accompanying discussions. R. S. Selesnick was responsible for pulling together information on DC return measurements as a function of heliocentric distance. P. Milligan and J. Quigley were indispensable in locating dusty tapes to which no one has wanted access in 10 years and managing to use them to produce readable data files. Without their efforts, use of the Cruise Science Maneuver data sets would have been impossible. Finally, J. Quigley is thanked again for her valiant efforts in locating EDRs stored in building N52 and thermally cycled every summer for about the last 5 years; without these tapes the temperature values needed to decipher the DC return DN values would not have been accessible. C. K. Clark is thanked for producing the plots of the equipotential surfaces in the vicinity of the modulator grid support. This work was supported under NASA contract 957781 from the Jet Propulsion Laboratory and NASA grant NGL 22-009-015.

References

Bagenal, F., Torus-magnetosphere coupling, *Proceedings of the International Jupiter Watch Workshop on Time-Variable Phenomena in the Jovian System*, Flagstaff, AZ, 1987.

Barnett, A., The response function of the Voyager plasma science experiment, M. I. T. Center for Space Research *Technical Report CSR-TR-84-1*, Cambridge, MA, 1984.

Barnett, A., In situ measurements of the plasma bulk velocity near the Io flux tube, *J. Geophys. Res., 91*, 3011–3019, 1986.

Barnett, A., and S. Olbert, The response function of modulator grid Faraday cup plasma instruments, *Rev. Sci. Instrum., 57*, 2432-2440, 1986.

Binsack, J. H., Plasmapause observations with the M.I.T. experiment on IMP 2, *J. Geophys. Res., 72*, 5231-5237, 1967.

Bridge, H. S., J. W. Belcher, R. J. Butler, A. J. Lazarus, A. M. Mavretic, J. D. Sullivan, G. L. Siscoe, and V. M. Vasyliunas, The plasma experiment on the 1977 Voyager mission, *Space Sci. Rev., 21*, 259-287, 1977.

Chung, M. S. and T. E. Everhart, Simple calculation of energy distribution of low-energy secondary electrons emitted from metals under electron bombardment, *J. App. Phys., 45*, 707-709, 1973.

Dekker, A. J., Secondary electron emission, Chap. 17 of *Solid State Physics*, Prentice-Hall, Inc., Englewood Cliffs, N. J., 1957.

Garrett, H. B., The charging of spacecraft surfaces, *Rev. Geophys. Space Phys., 19*, 577-616, 1981.

Gazis, P.R., Observations of plasma bulk parameters and the energy balance of the solar wind between 1 and 10 AU, *J. Geophys. Res., 89*, 775-785, 1984.

Gradshteyn, I. S. and I. M. Ryzhik, *Table of Integrals, Series, and Products*, Academic Press, Inc,, New York, 1980.

Grard, R. J. L., Properties of the satellite photoelectron sheath derived from photoemission laboratory measurements, *J. Geophys. Res., 78*, 2885-2906, 1973.

Hachenberg, O. and W. Brauer, Secondary electron emission from solids, pp. 413-499 in *Advances in Electronics and Electron Physics*, Vol. XI, ed. L. Marton, Academic Press, New York, 1959.

Khurana, K.K., M.G. Kivelson, T.P. Armstrong, and R.J. Walker, Voids in the Jovian magnetosphere revisited: Evidence of spacecraft charging, *J. Geophys. Res., 92*, 13399-13408, 1987.

Knudsen, W. C., and K. K. Harris, Ion-impact-produced secondary electron emission and its effect on space instrumentation, *J. Geophys. Res., 78*, 1145-1152, 1973.

Kober, H., *Dictionary of Conformal Representations*, Dover Publications, Inc., 1957.

Kollath, R., Zur Energieverteilung der Secundarelektronen, II. Meβergebnisse und Diskussion, *Ann. Phys., 6*, 357-380, 1947.

Kollath, R., Sekundarelektronen-Emission fester Korper bei Bestrahlung mit Elektronen, *Hand. d. Phys., 21*, 232- , 1956.

Koller, L. R., *Ultraviolet Radiation*, John Wiley & Sons, Inc., New York, 1965.

Large, L. N., Secondary electron emission from a clean tungsten surface bombarded by various positive ions, *Proc. Phys. Soc., 81*, 1101-1103, 1963.

Lazarus, A. J. and R. L. McNutt, Jr., Low Energy Plasma Ion Observations in Saturn's Magnetosphere, *J. Geophys. Res., 88*, 8831, 1983.

Leung, P., A. C. Whittlesey, H. B. Garrett, and P. A. Robinson, Jr., Environment-induced electrostatic discharges as the cause of Voyager 1 power-on resets, *J. Spacecraft, 23*, 323-330, 1986.

McDaniel, E. W., *Collision Phenomena in Ionized Gases*, § 13-3, John Wiley & Sons, Inc., New York, 1964.

McNutt, Ralph L. Jr., Paolo S. Coppi, Richard S. Selesnick, and Bruno Coppi, Plasma Depletions in the Jovian Magnetosphere: Evidence of Transport and Solar Wind Interaction, *J. Geophys. Res., 92*, 4377-4398, 1987.

McNutt, R. L., Jr., R. S. Selesnick, and J. D. Richardson, Low Energy Plasma Observations in the Magnetosphere of Uranus, *J. Geophys. Res., 92*, 4399-4410, 1987.

Rudberg, E., Inelastic scattering of electrons from solids, *Phys. Rev., 50*, 138-150, 1936.

Sands, M. R. , and R. L. McNutt, Jr., Plasma flow in Jupiter's dayside middle magnetosphere, *J. Geophys. Res., 93*, 8502-8518, 1988.

Scarf, F. L., D. A. Gurnett, and W. S. Kurth, Measurements of plasma wave spectra in Jupiter's magnetosphere, *J. Geophys. Res., 86*, 8181-8198, 1981.

Selesnick, R. S., and R. L. McNutt, Jr., Voyager 2 Plasma Ion Observations in the Magnetosphere of Uranus, *J. Geophys. Res., 92*, 15,249-15,262, 1987.

Schultz, A. A., and M. A. Pomerantz, Secondary electron emission produced by relativistic primary electrons, *Phys. Rev., 130*, 2135, 1963.

Sittler, E. C., Jr., Plasma electron analysis: Voyager plasma science experiment, *NASA Tech. Memo., 85037*, 1983.

Sittler, E. C., and D. F. Strobel, Io plasma torus electrons: Voyager 1, *J. Geophys. Res., 92*, 5741-5762, 1987.

Sternglass, E. J., Backscattering of kilovolt electrons from solids, *Phys. Rev., 95*, 345-358, 1954.

Vasyliunas, V. M., Observations of low energy electrons with the OGO-A satellite, Ph.D. Thesis, Massachusetts Institute of Technology, Cambridge, MA, 1966.

Vasyliunas, V. M., Deep space plasma measurements, in *Methods of Experimental Physics*, R. H. Lovbergs, ed., *Methods of Experimental Physics, 9B*, 49-88, 1971.

Vasyliunas, V. M., A survey of low-energy electrons in the evening sector of the magnetosphere with OGO 1 and OGO 3, *J. Geophys. Res., 73*, 2839-2884, 1968.

Whipple, E. C., Jr. and L. W. Parker, Effects of secondary electron emission on electron trap measurements in the magnetosphere and solar wind, *J. Geophys. Res., 74*, 5763-5774, 1969.

Whipple, E. C., Potentials of surfaces in space, *Rep. Prog. Phys., 44*, 1197-1250, 1981.

Zwickl, R. D., S. J. Bame, J. L. Goetzinger, J. T. Gosling, M. F. Thomsen, and D. T. Young, The low energy intermediate electron population observed in hot dense plasmas by ISEE-3, *EOS, 68*, 1417, 1987.

DC RETURN CURRENTS - FROM PLCONS

-1.000E+05	-1.050E+05	-1.090E+05	-1.120E+05	-1.160E+05	-1.200E+05	-1.240E+05	-1.280E+05	-1.320E+05	-1.360E+05
-1.400E+05	-1.450E+05	-1.500E+05	-1.550E+05	-1.600E+05	-1.650E+05	-1.700E+05	-1.750E+05	-1.800E+06	-1.850E+05
-1.900E+05	-1.970E+05	-2.040E+05	-2.110E+05	-2.180E+05	-2.250E+05	-2.360E+05	-2.470E+05	-2.580E+05	-2.690E+05
-2.800E+05	-2.960E+05	-3.120E+05	-3.280E+05	-3.440E+05	-3.600E+05	-3.800E+05	-4.000E+05	-4.200E+05	-4.400E+05
-4.600E+05	-4.840E+05	-5.080E+05	-5.320E+05	-5.560E+05	-5.800E+05	-6.000E+05	-6.200E+05	-6.400E+05	-6.600E+05
-6.800E+05	-7.040E+05	-7.280E+05	-7.520E+05	-7.760E+05	-8.000E+05	-8.280E+05	-8.560E+05	-8.840E+05	-9.120E+05
-9.400E+05	-1.150E+06	-1.360E+06	-1.580E+06	-1.790E+06	-2.000E+06	-2.400E+06	-2.800E+06	-3.200E+06	-3.600E+06
-4.000E+06	-4.480E+06	-4.960E+06	-5.440E+06	-5.920E+06	-6.400E+06	-7.040E+06	-7.680E+06	-8.320E+06	-8.960E+06
-9.600E+06	-1.050E+07	-1.140E+07	-1.220E+07	-1.310E+07	-1.400E+07	-1.510E+07	-1.620E+07	-1.730E+07	-1.840E+07
-1.950E+07	-2.060E+07	-2.170E+07	-2.280E+07	-2.390E+07	-2.500E+07	-2.640E+07	-2.780E+07	-2.920E+07	-3.060E+07
-3.200E+07	-3.340E+07	-3.480E+07	-3.620E+07	-3.760E+07	-3.900E+07	-4.100E+07	-4.300E+07	-4.500E+07	-4.700E+07
-4.900E+07	-5.120E+07	-5.340E+07	-5.560E+07	-5.780E+07	-6.000E+07	-6.280E+07	-6.560E+07	-6.840E+07	-7.120E+07
-7.400E+07	-7.760E+07	-8.120E+07	-8.480E+07	-8.840E+07	-9.200E+07	-9.600E+07	-1.000E+08	7.500E+04	8.750E+04
1.000E+05	1.050E+05	1.100E+05	1.150E+05	1.200E+05	1.250E+05	1.310E+05	1.370E+05	1.430E+05	1.490E+05
1.550E+05	1.620E+05	1.690E+05	1.760E+05	1.830E+05	1.900E+05	1.990E+05	2.080E+05	2.170E+05	2.260E+05
2.350E+05	2.450E+05	2.550E+05	2.650E+05	2.750E+05	2.850E+05	2.980E+05	3.110E+05	3.240E+05	3.370E+05
3.500E+05	3.660E+05	3.820E+05	3.980E+05	4.140E+05	4.300E+05	4.480E+05	4.660E+05	4.840E+05	5.020E+05
5.200E+05	5.400E+05	5.600E+05	5.600E+05	6.000E+05	6.200E+05	6.440E+05	6.680E+05	6.920E+05	7.160E+05
7.400E+05	7.600E+05	7.800E+05	8.000E+05	8.200E+05	8.400E+05	8.820E+05	9.240E+05	9.660E+05	1.010E+06
1.050E+06	1.380E+06	1.710E+06	2.040E+06	2.370E+06	2.700E+06	3.160E+06	3.620E+06	4.080E+06	4.540E+06
5.000E+06	5.520E+06	6.040E+06	6.560E+06	7.080E+06	7.600E+06	8.280E+06	8.960E+06	9.640E+06	1.030E+07
1.100E+07	1.190E+07	1.280E+07	1.370E+07	1.460E+07	1.550E+07	1.660E+07	1.770E+07	1.880E+07	1.990E+07
2.100E+07	2.240E+07	2.380E+07	2.520E+07	2.660E+07	2.800E+07	2.930E+07	3.060E+07	3.200E+07	3.350E+07
3.500E+07	3.660E+07	3.840E+07	4.020E+07	4.200E+07	4.400E+07	4.600E+07	4.800E+07	5.000E+07	5.200E+07
5.400E+07	5.640E+07	5.880E+07	6.120E+07	6.360E+07	6.600E+07	6.920E+07	7.240E+07	7.560E+07	7.880E+07
8.200E+07	8.560E+07	8.920E+07	9.280E+07	9.640E+07	1.000E+08				

TABLE 1

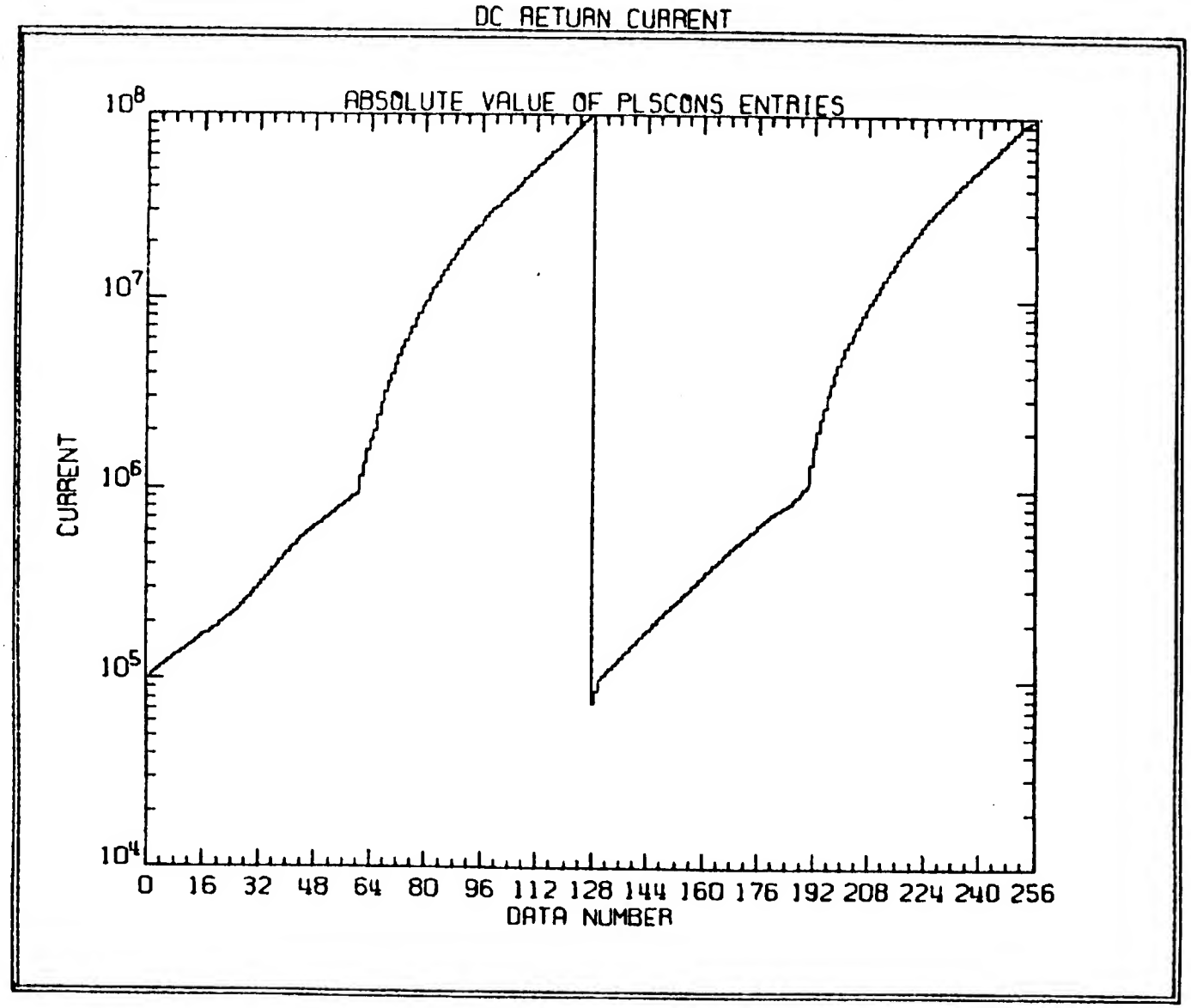
DC RETURN CURRENT
ABSOLUTE VALUE OF PLSCONS ENTRIES
10^8
10^7
10^6
10^5
10^4
CURRENT
0 16 32 48 64 80 96 112 128 144 160 176 192 208 224 240 256
DATA NUMBER

FIGURE 1

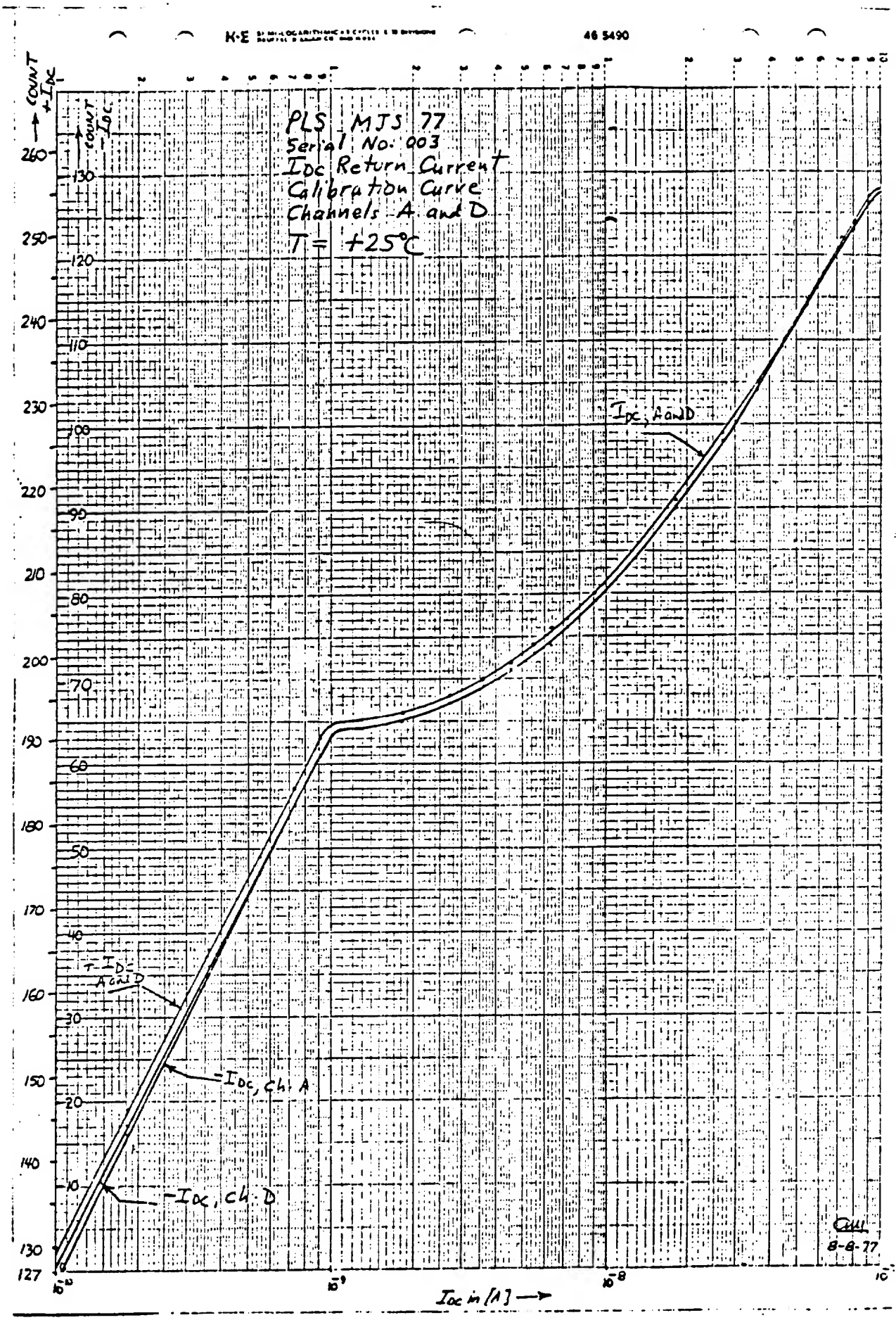

ORIGINAL PAGE IS
OF POOR QUALITY

FIGURE 2

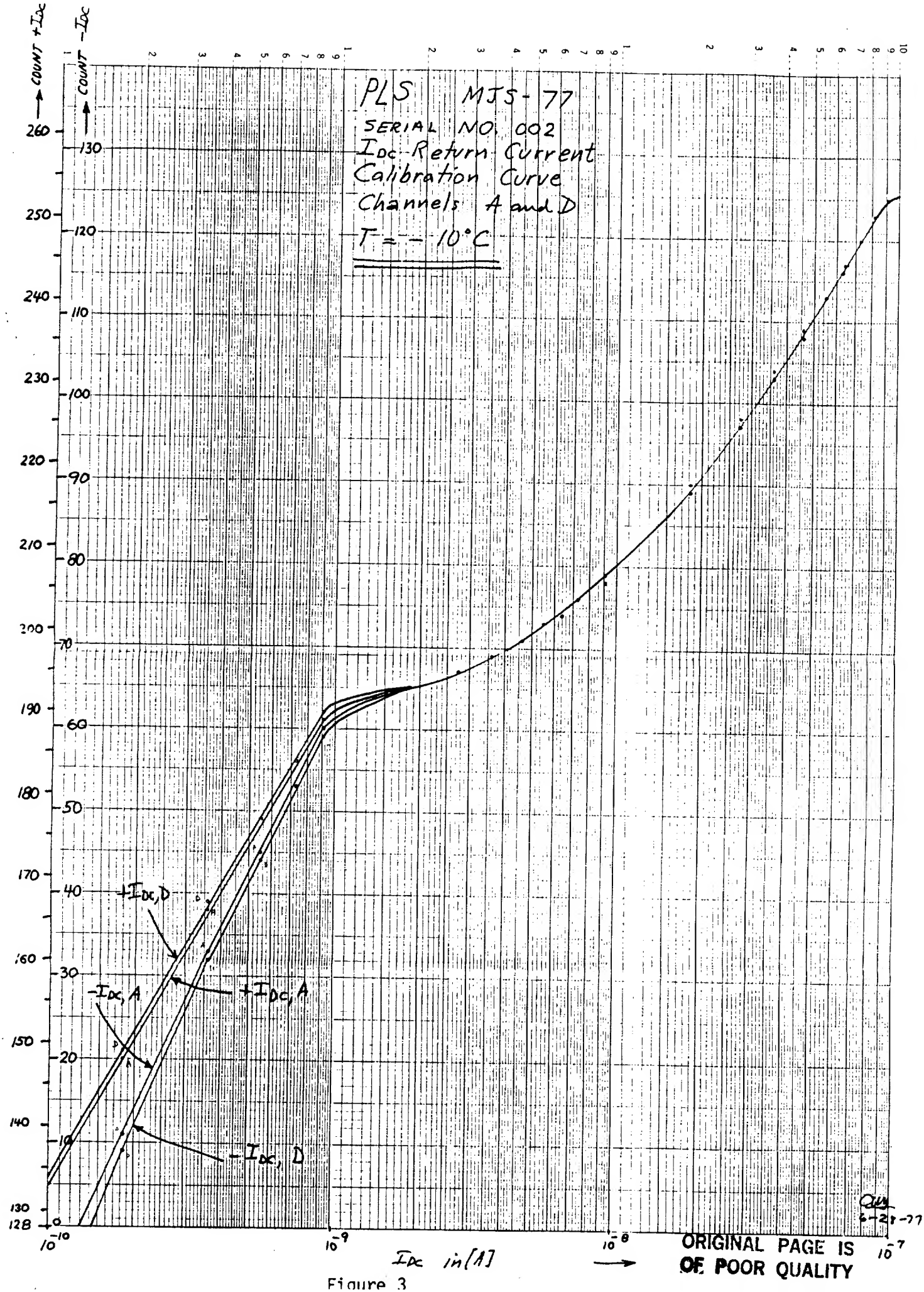
PLS MJS-77
SERIAL NO. 002
I_{DC} Return Current
Calibration Curve
Channels A and D
T = -10°C
COUNT +I_{DC}
COUNT -I_{DC}
260
130
250
120
240
110
230
100
220
90
210
80
200
70
190
60
180
50
170
40
160
30
150
20
140
10
130
128
0
$+I_{DC,D}$
$-I_{DC,A}$
$+I_{DC,A}$
$-I_{DC,D}$
10^{-10}
10^{-9}
10^{-8}
10^{-7}
I_{DC} in [A]
6-21-77
ORIGINAL PAGE IS
OF POOR QUALITY

Figure 3

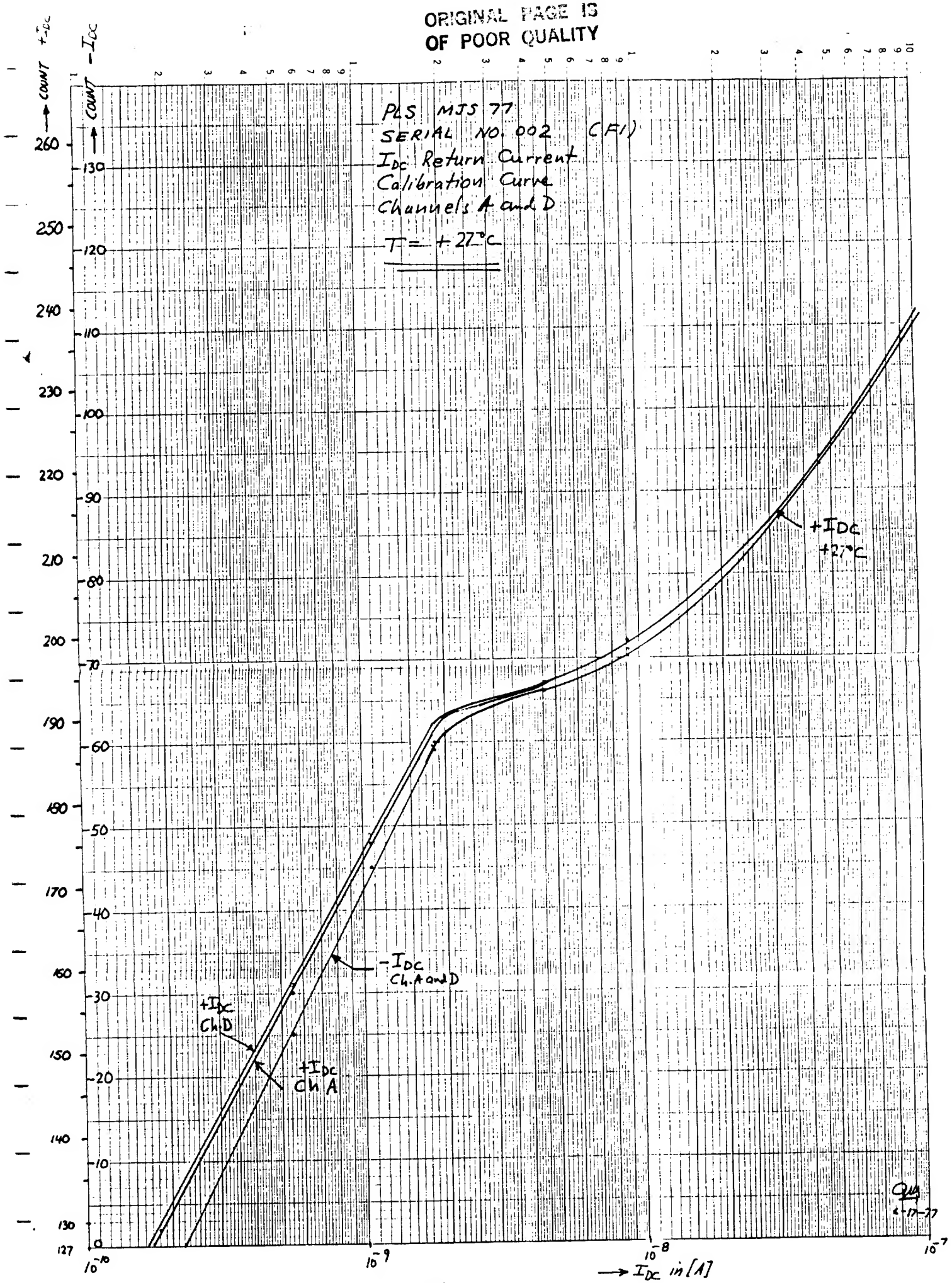

Figure 4

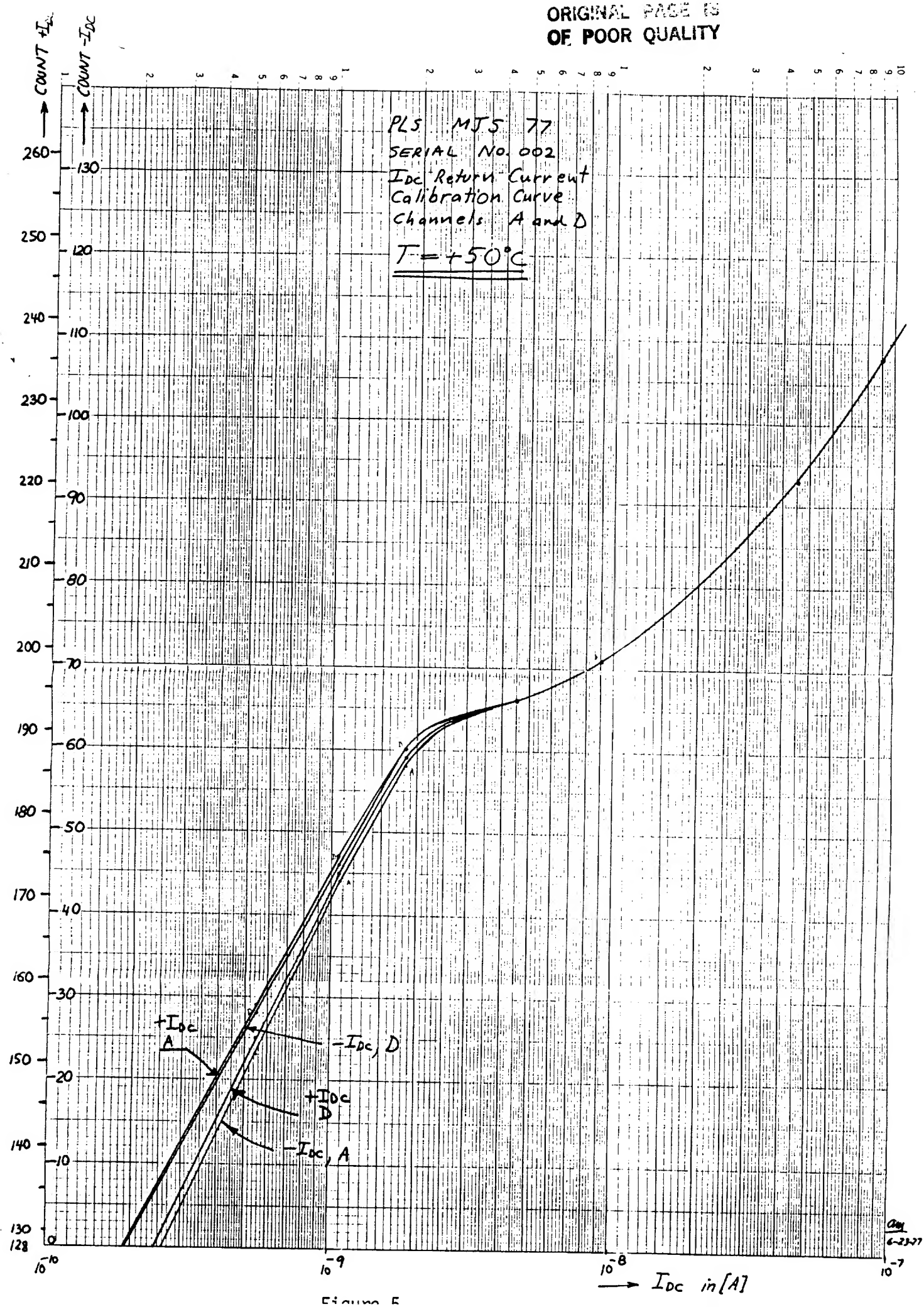

Figure 5

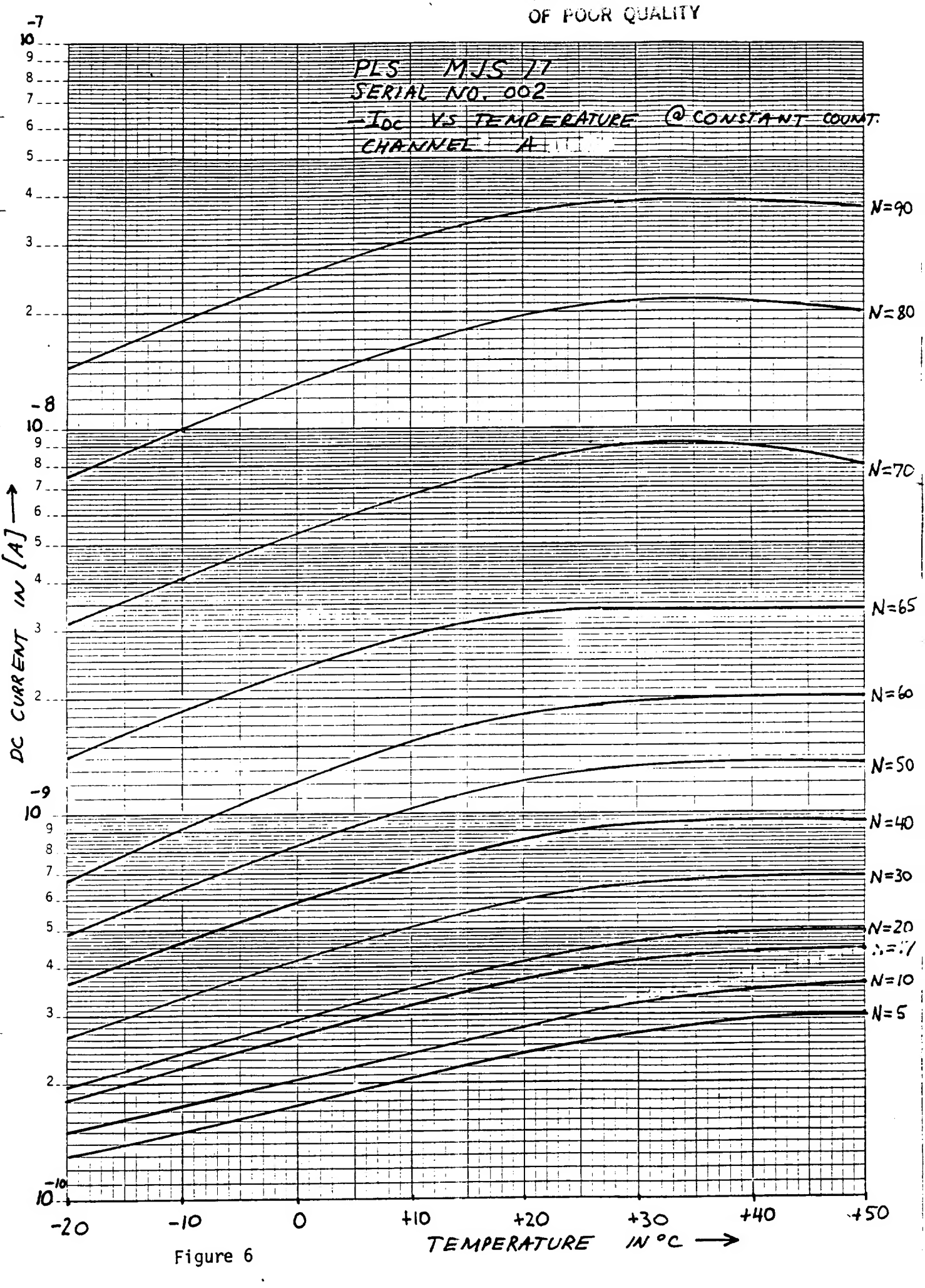

Figure 6

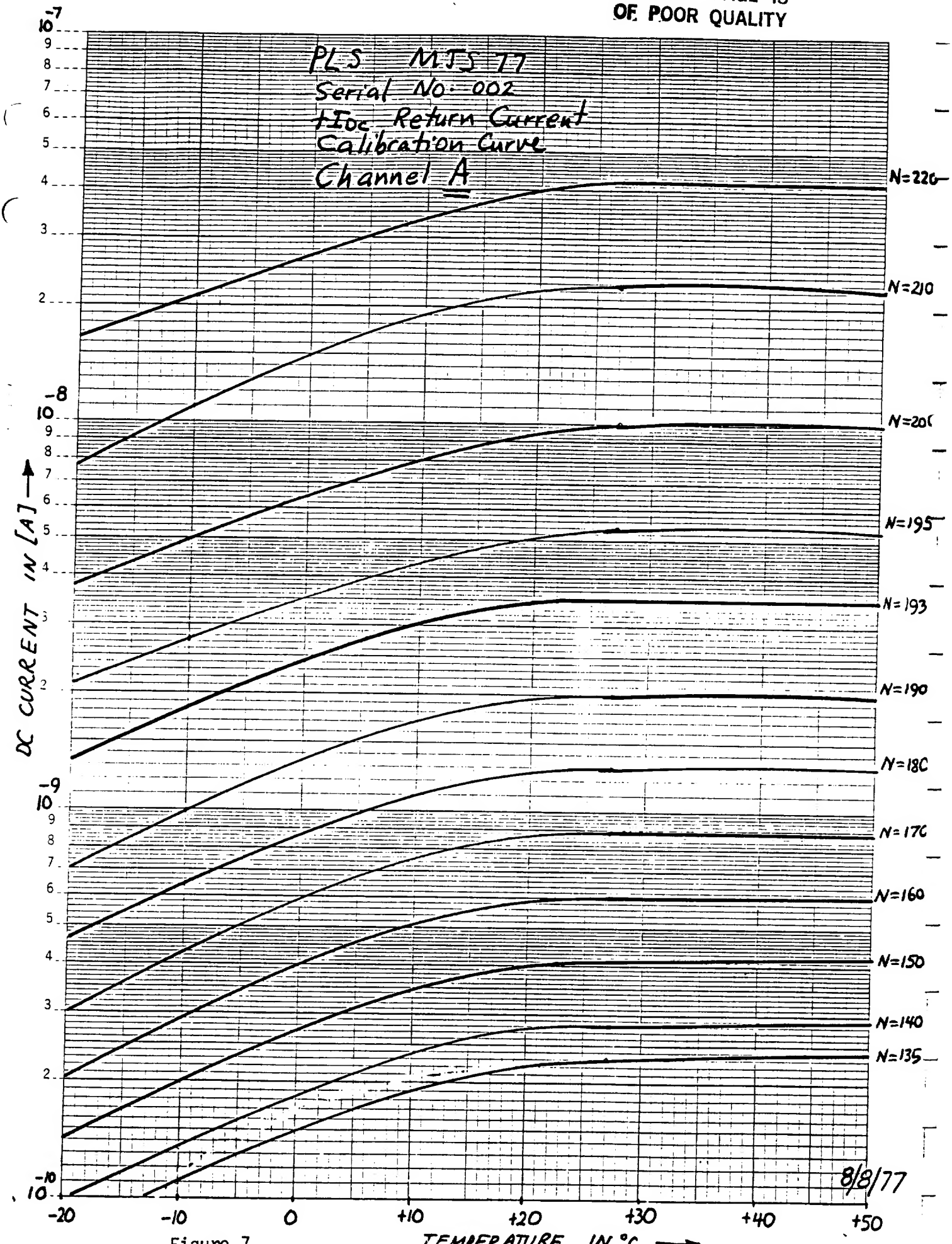

Figure 7

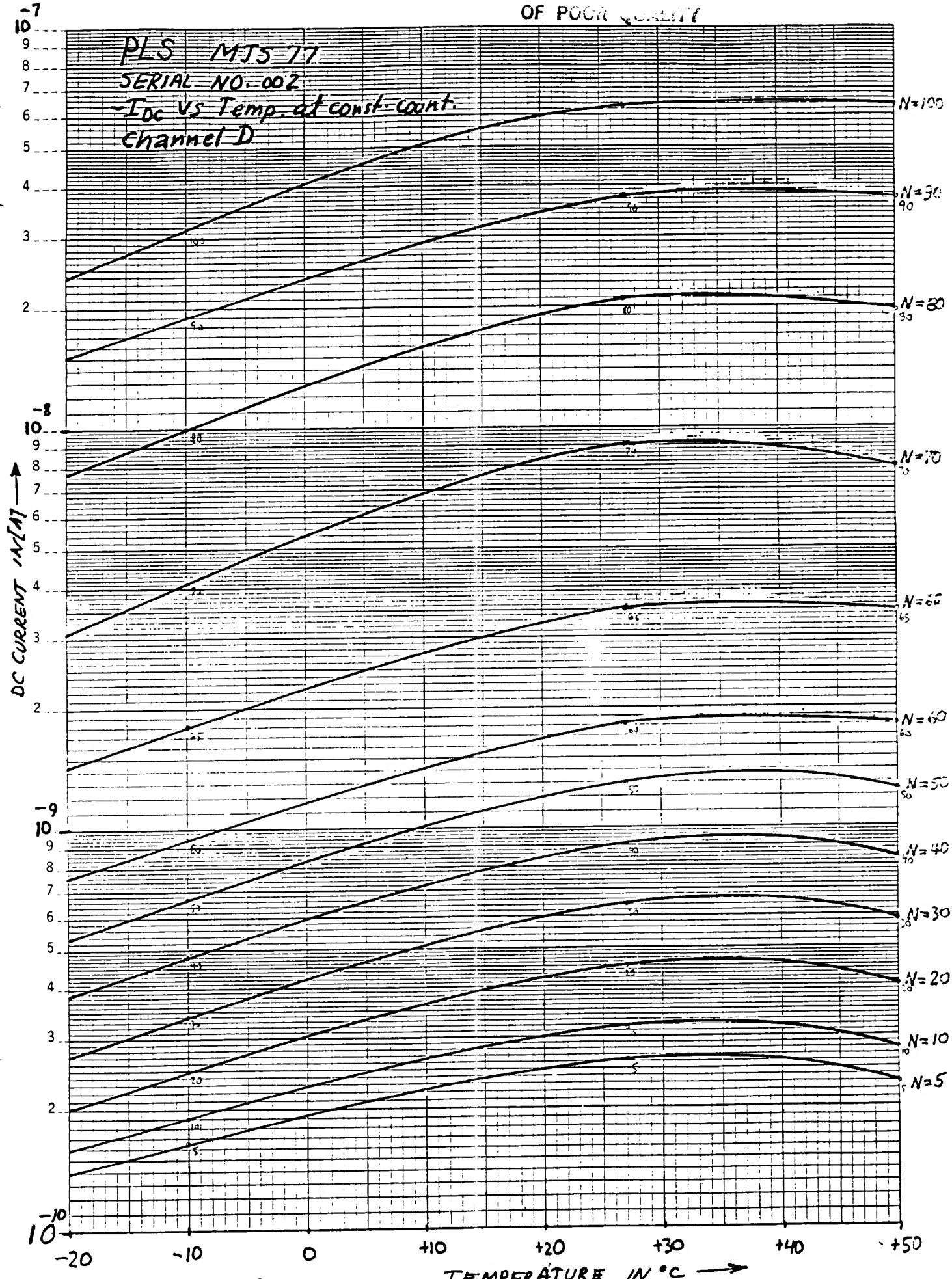

Figure 8

ORIGINAL PAGE IS
OF POOR QUALITY

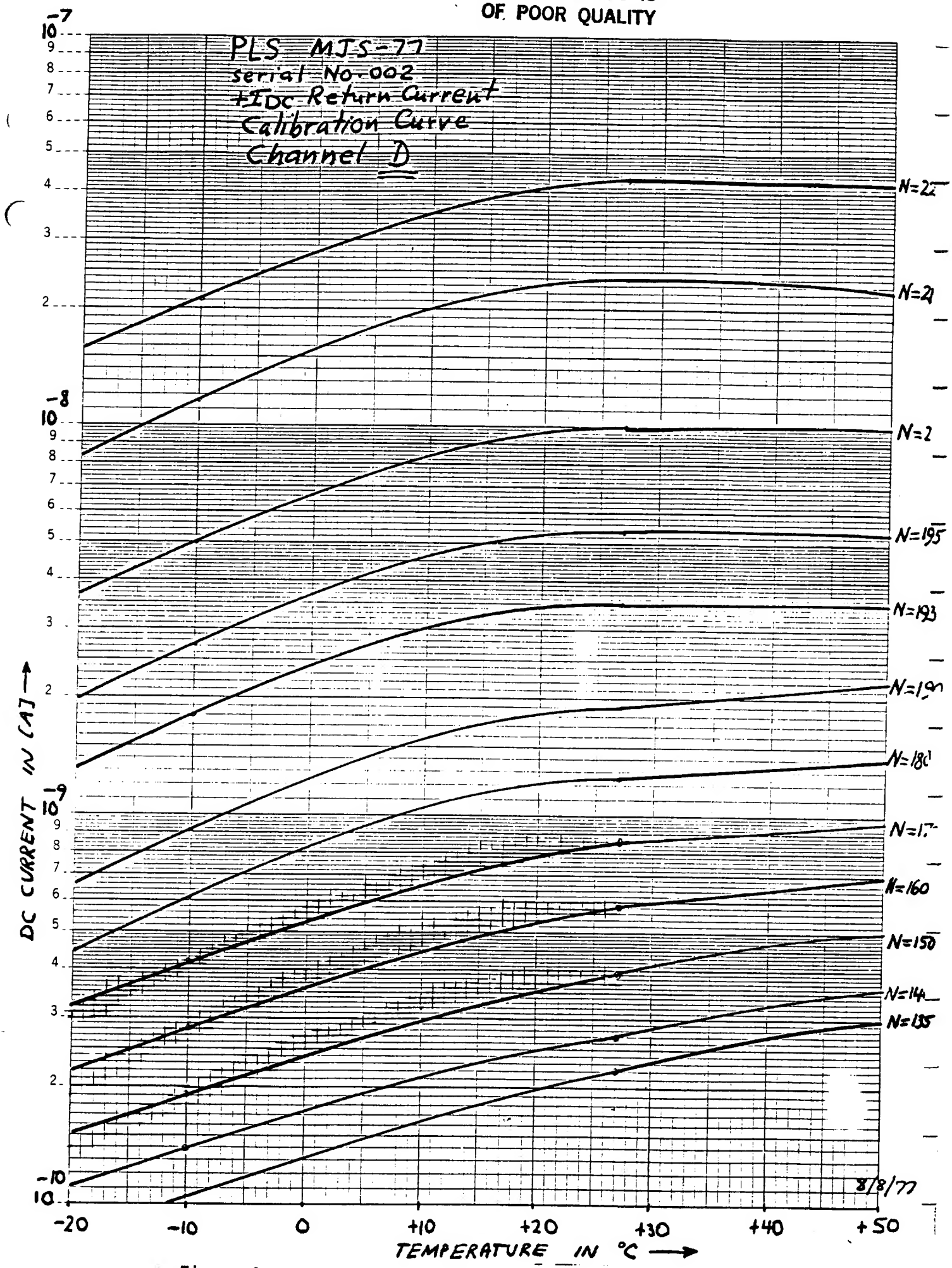

Figure 9

DC RETURN CURRENT VERSUS HELIOCENTRIC DISTANCE

ORIGINAL PAGE IS
OF POOR QUALITY

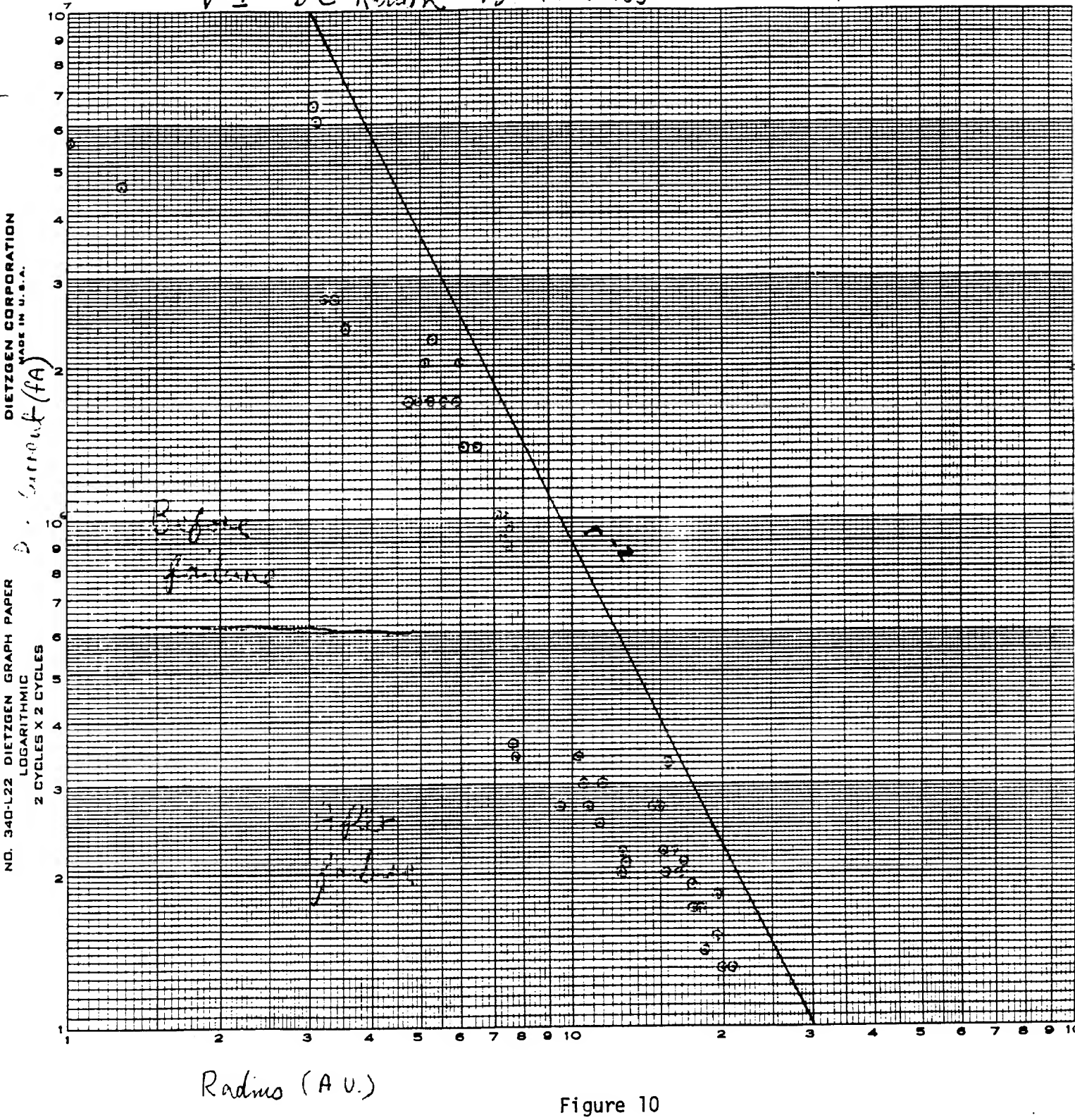

Figure 10

DC RETURN CURRENT VERSUS HELIOCENTRIC DISTANCE

V2 DC Return vs. Radius

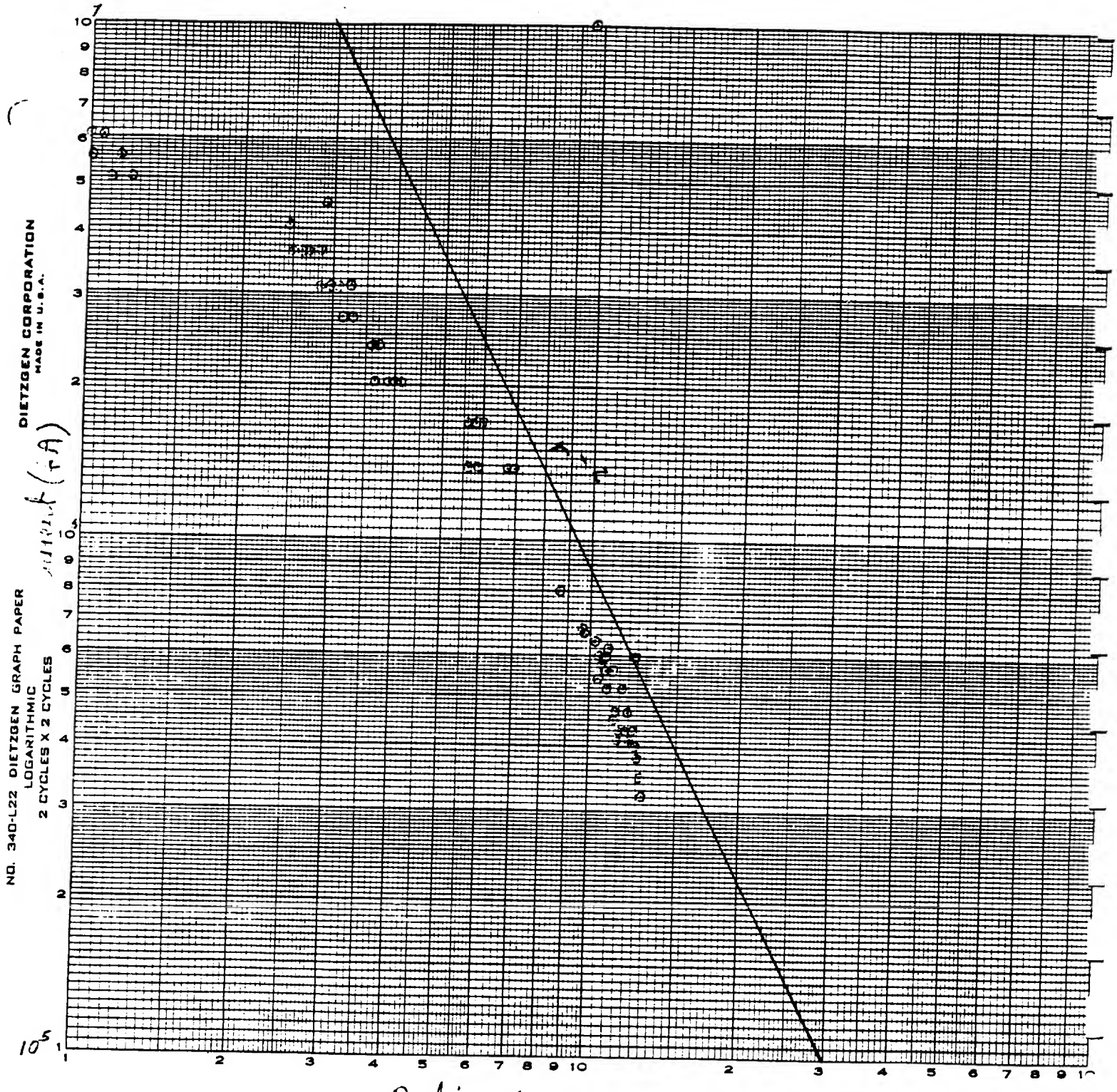

Figure 11

Section B

Fig. 1

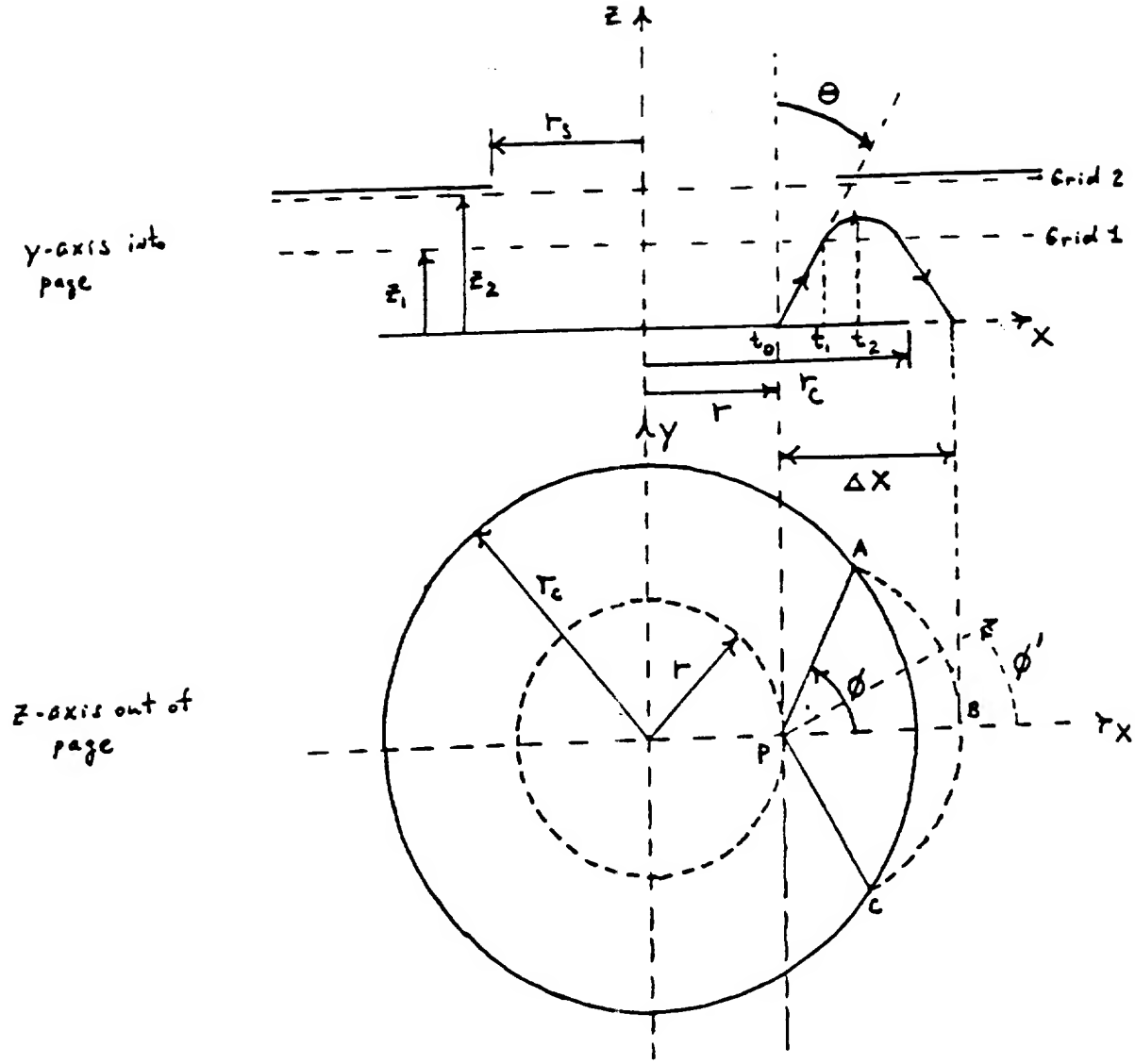

Figure 12

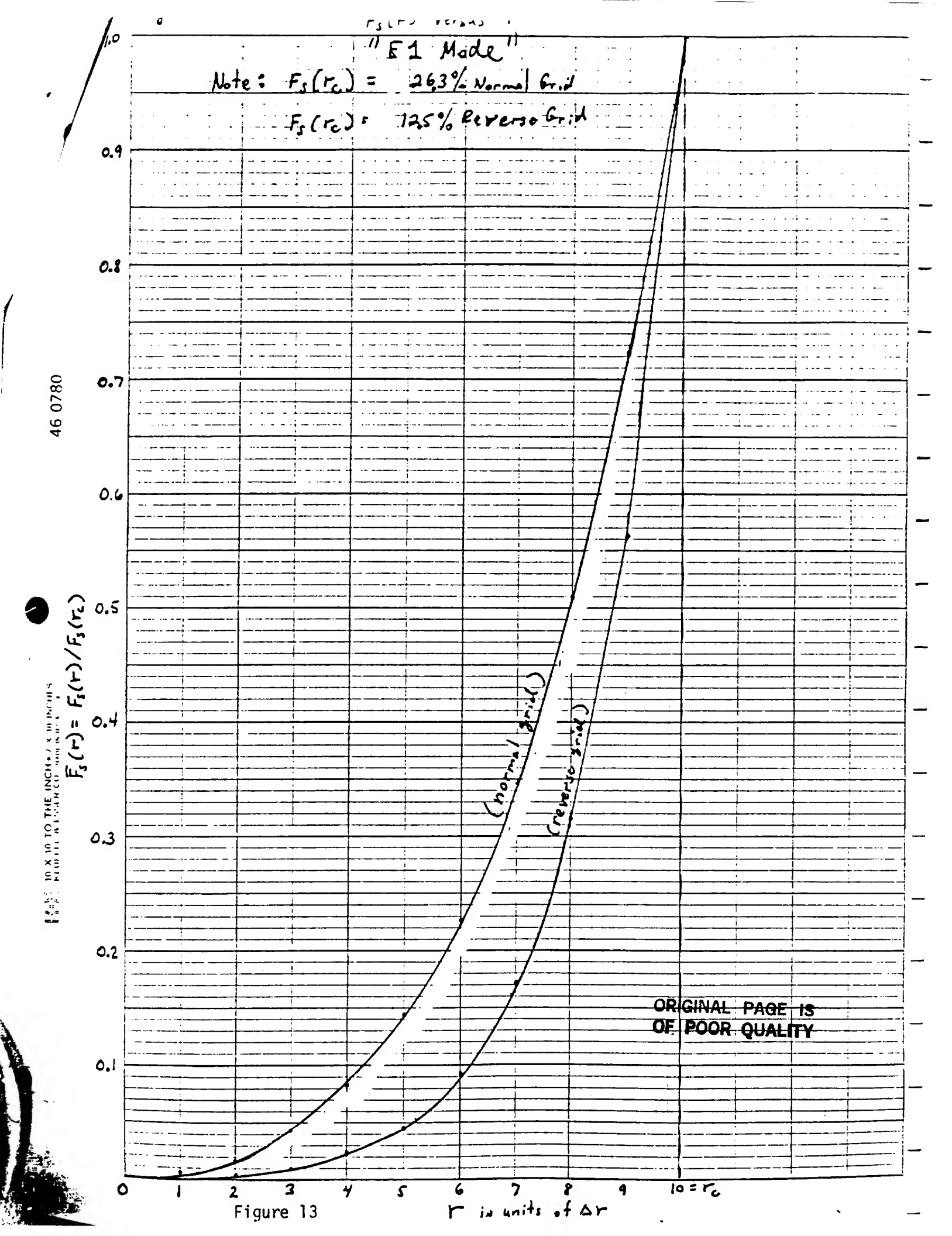
"E1 Mode"
Note: $F_s(r_c)$ = 263% Normal Grid
$F_s(r_c)$ = 125% Reverse Grid
$F_s(r) = F_s(r)/F_s(r_c)$
(normal grid)
(reverse grid)
1.0
0.9
0.8
0.7
0.6
0.5
0.4
0.3
0.2
0.1
0
1
2
3
4
5
6
7
8
9
10 = r_c
r in units of Δr
46 0780
10 X 10 TO THE INCH • 7 X 10 INCHES
ORIGINAL PAGE IS
OF POOR QUALITY

Figure 13

Figure 6 F_s vs. r 2/21/79

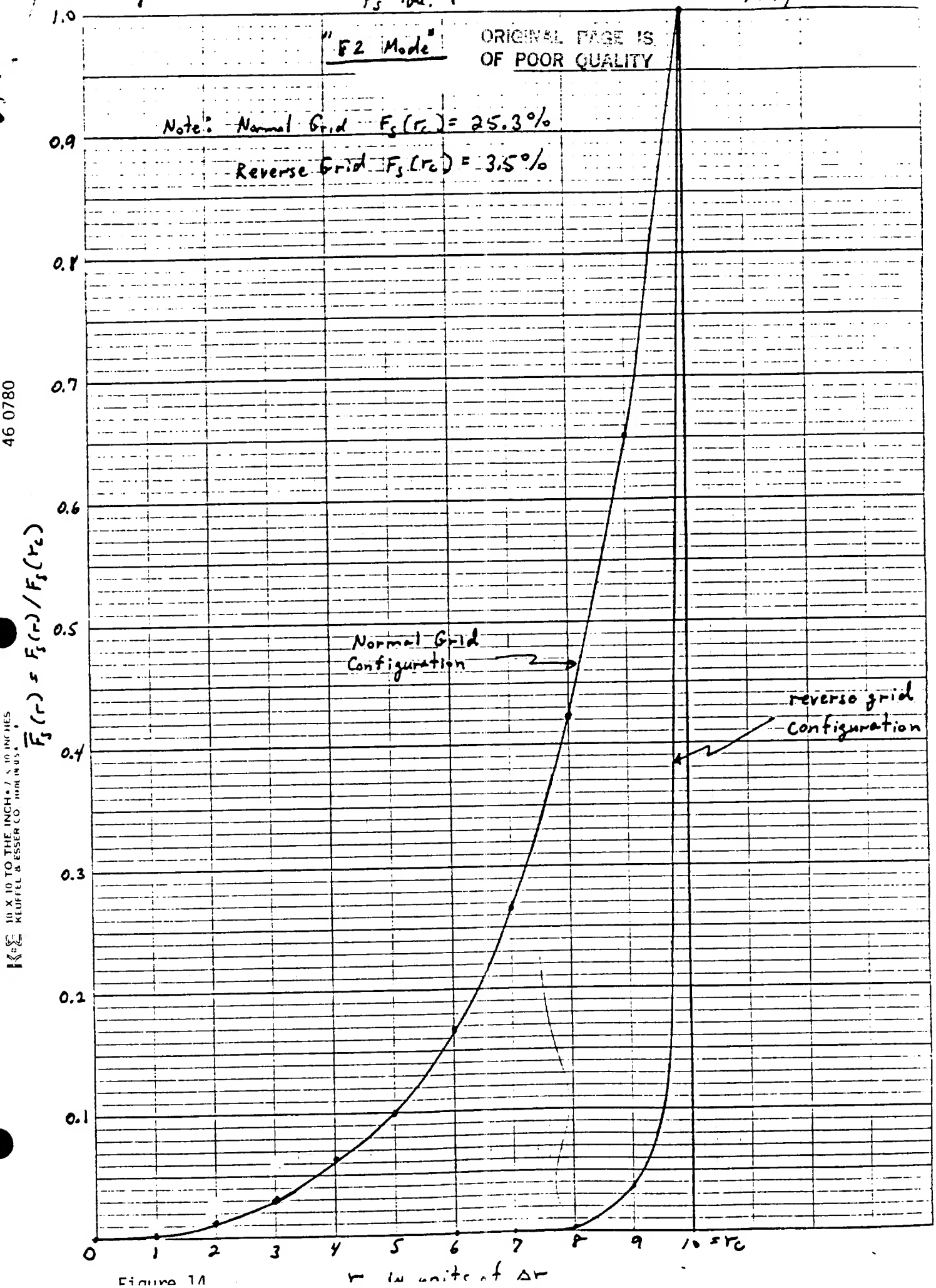

46 0780

10 X 10 TO THE INCH • 5 X 10 INCHES
KEUFFEL & ESSER CO. MADE IN U.S.A.

Figure 14

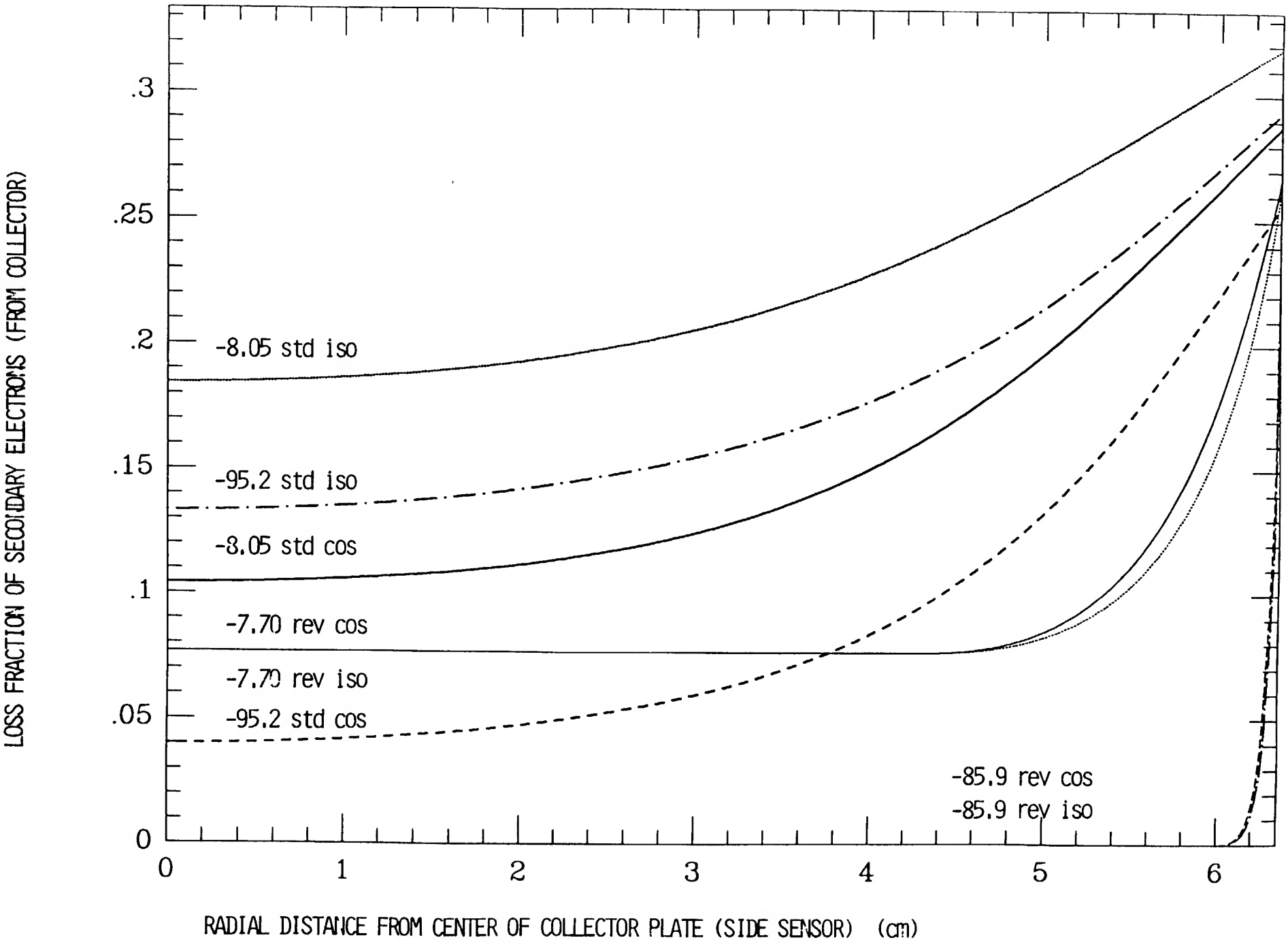
LOSS FRACTION OF SECONDARY ELECTRONS (FROM COLLECTOR)
.3
.25
.2
.15
.1
.05
0
-8.05 std iso
-95.2 std iso
-8.05 std cos
-7.70 rev cos
-7.70 rev iso
-95.2 std cos
-85.9 rev cos
-85.9 rev iso
0
1
2
3
4
5
6
RADIAL DISTANCE FROM CENTER OF COLLECTOR PLATE (SIDE SENSOR) (cm)

Figure 15

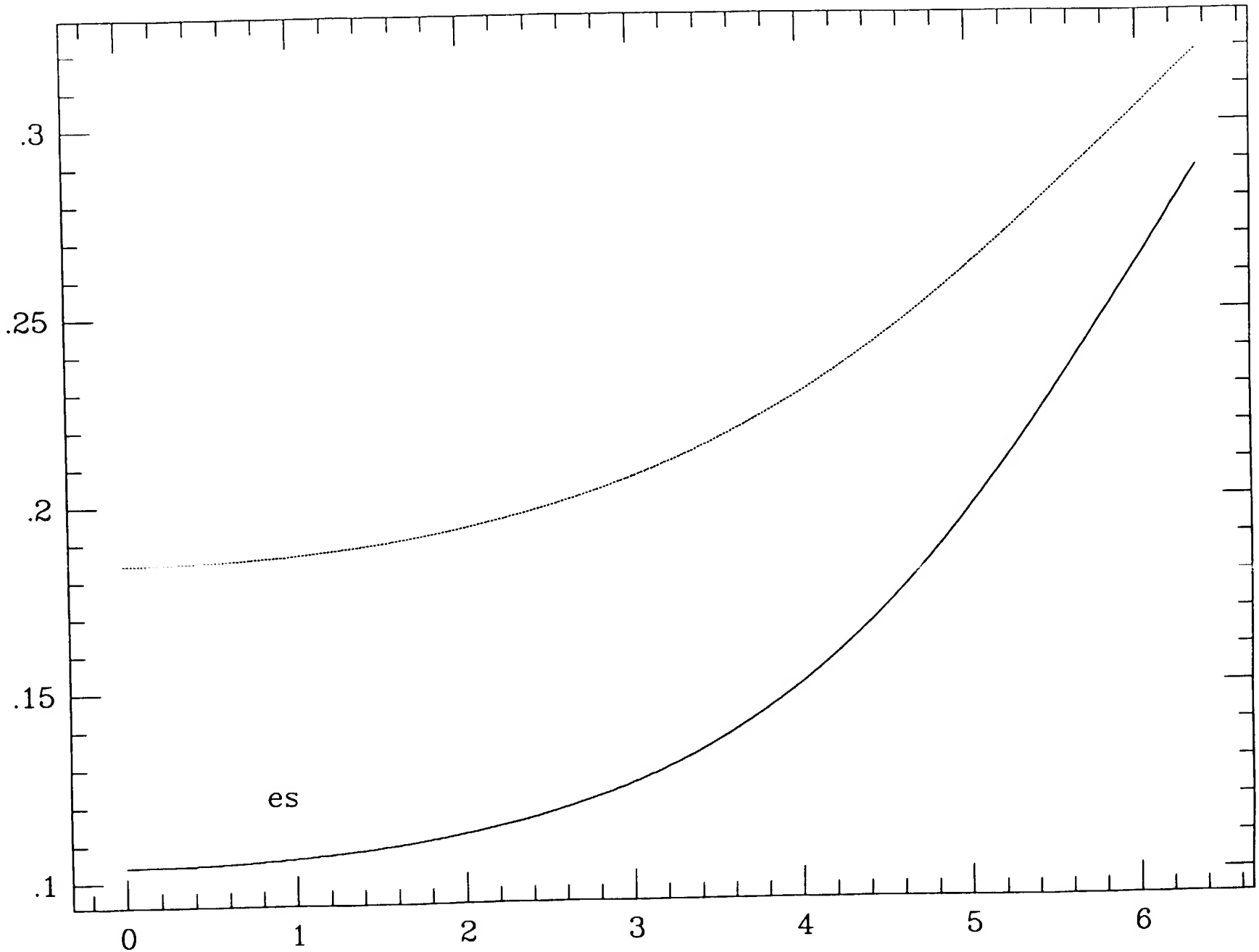

Figure 16

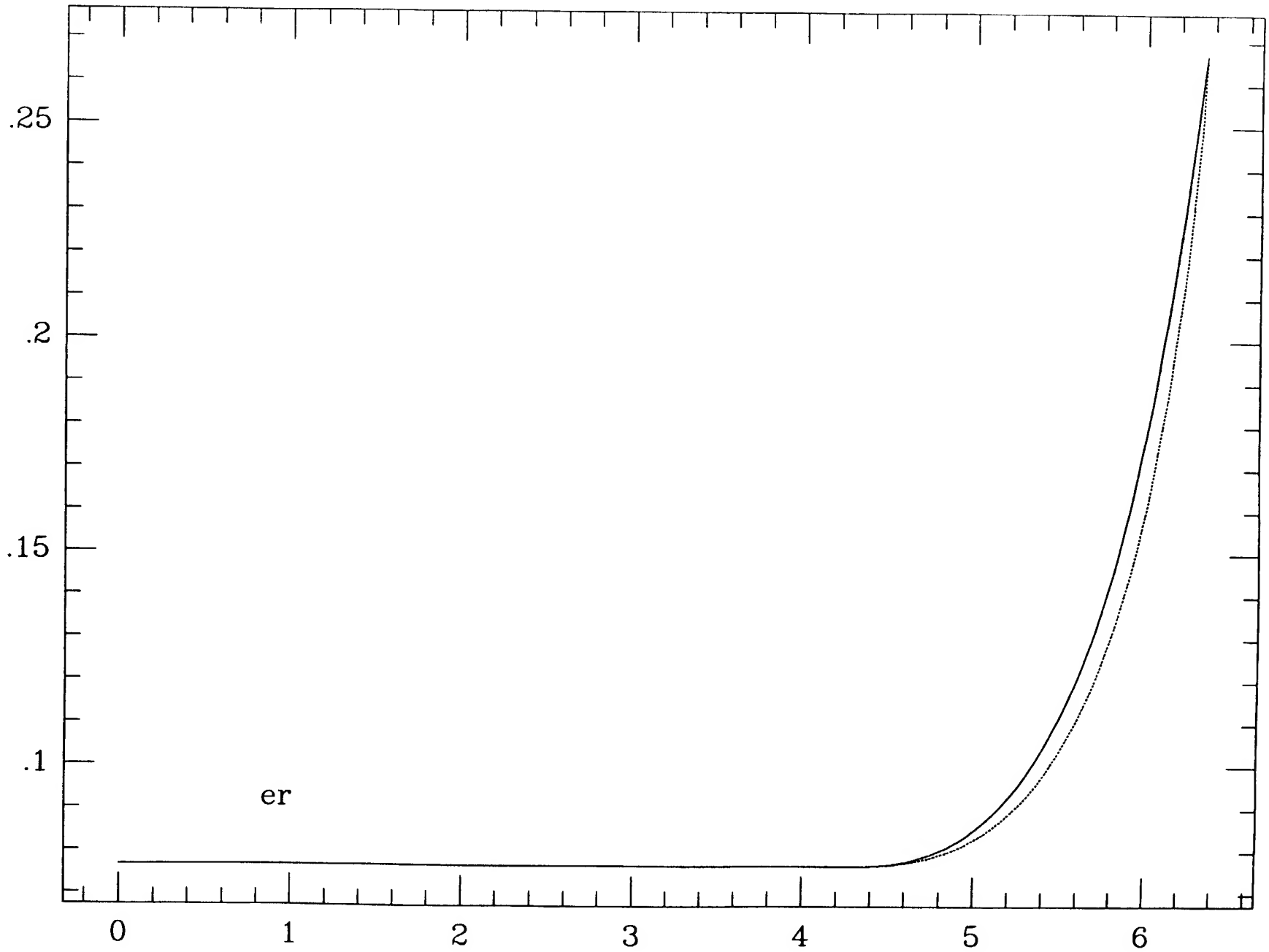

Figure 17

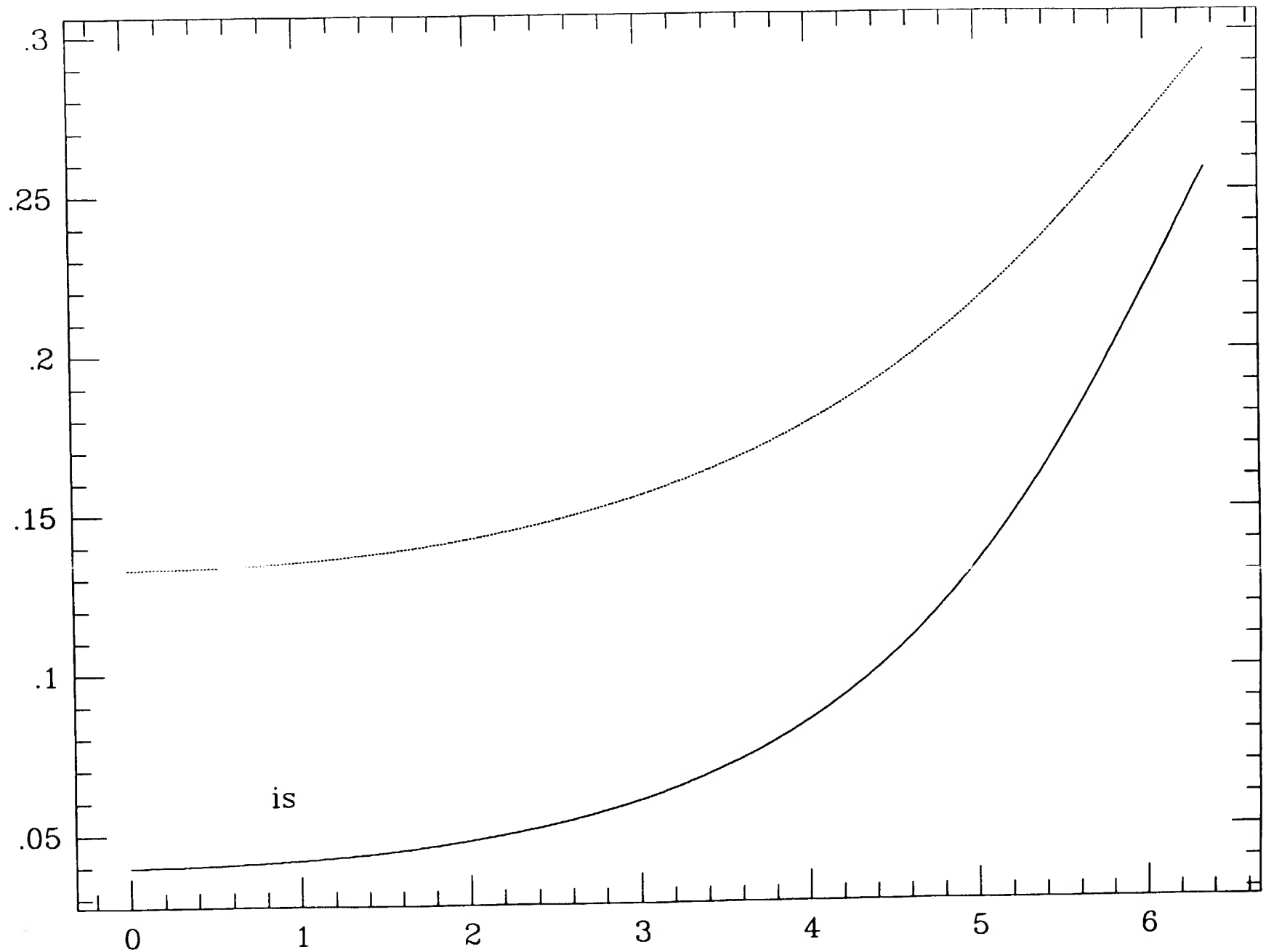

Figure 18

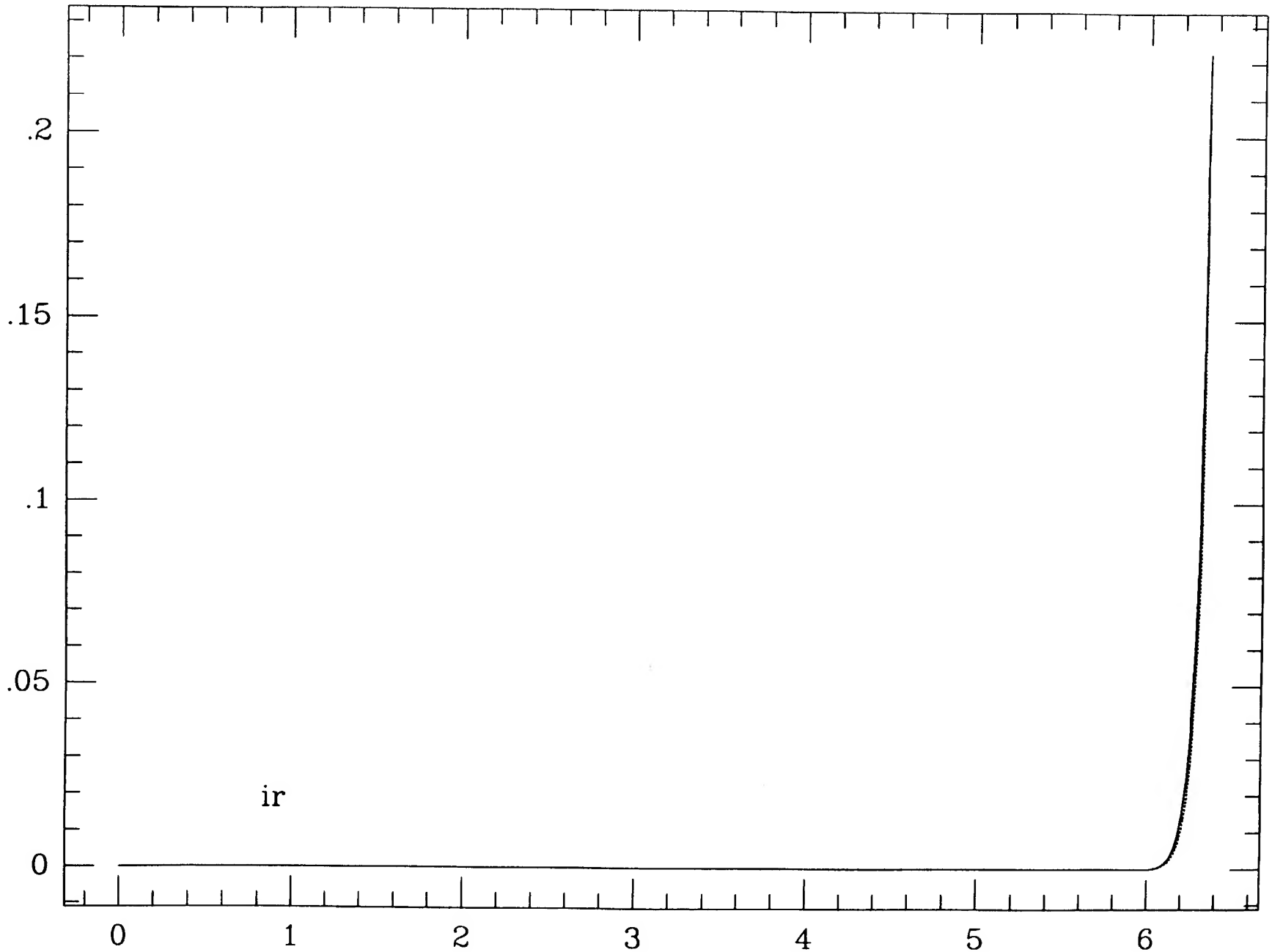

Figure 19

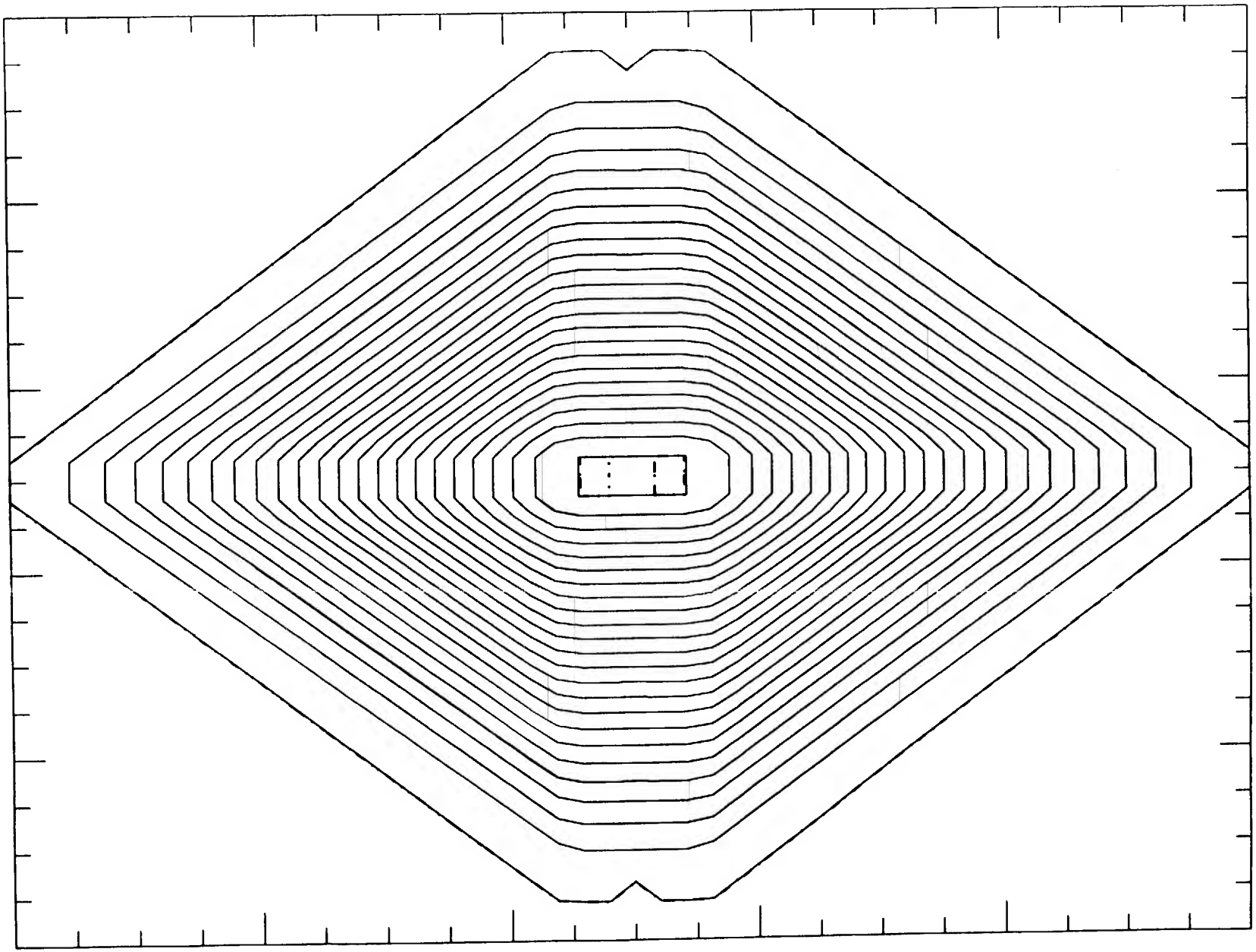

Figure 20

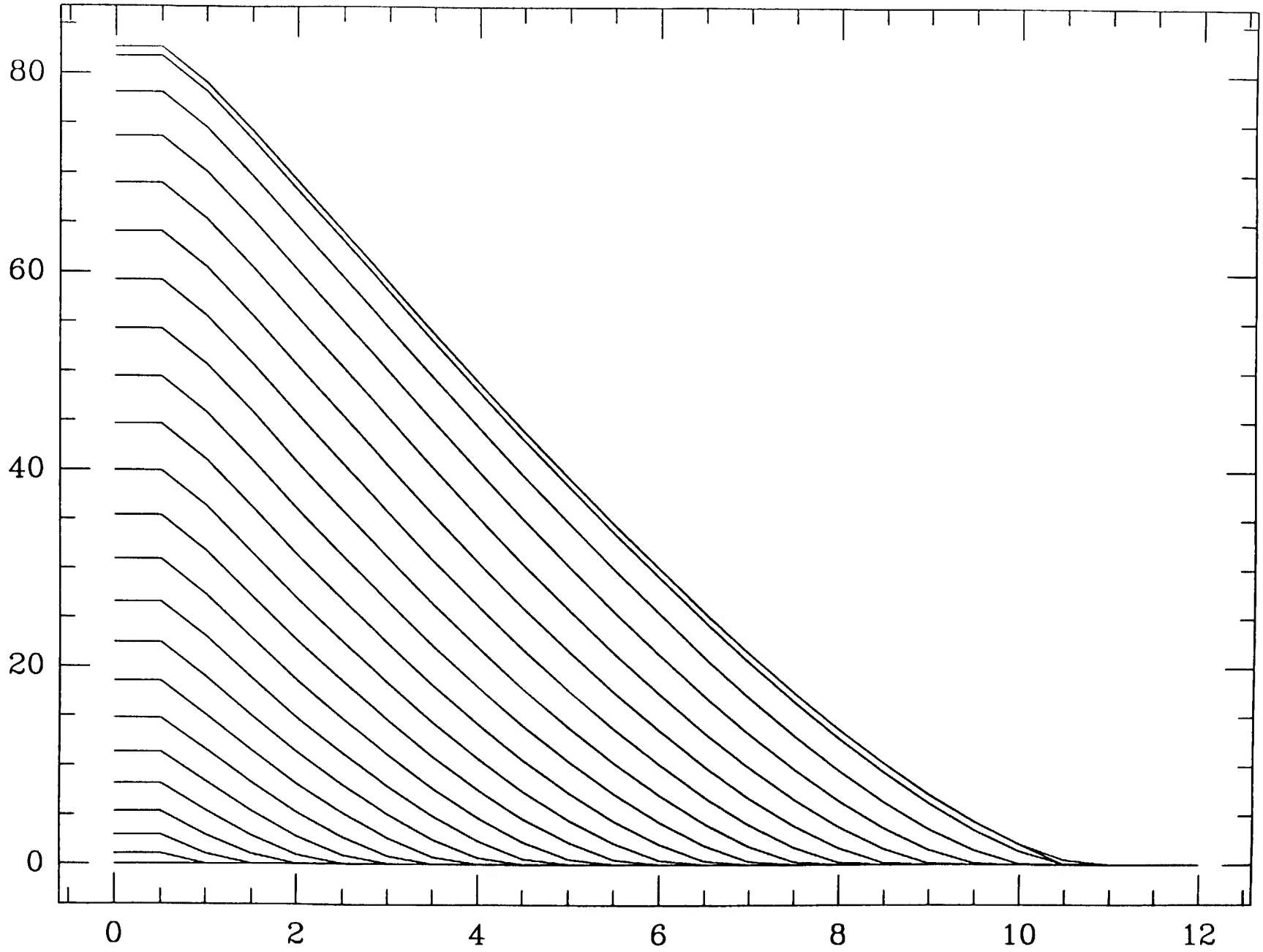

ar1

Figure 21

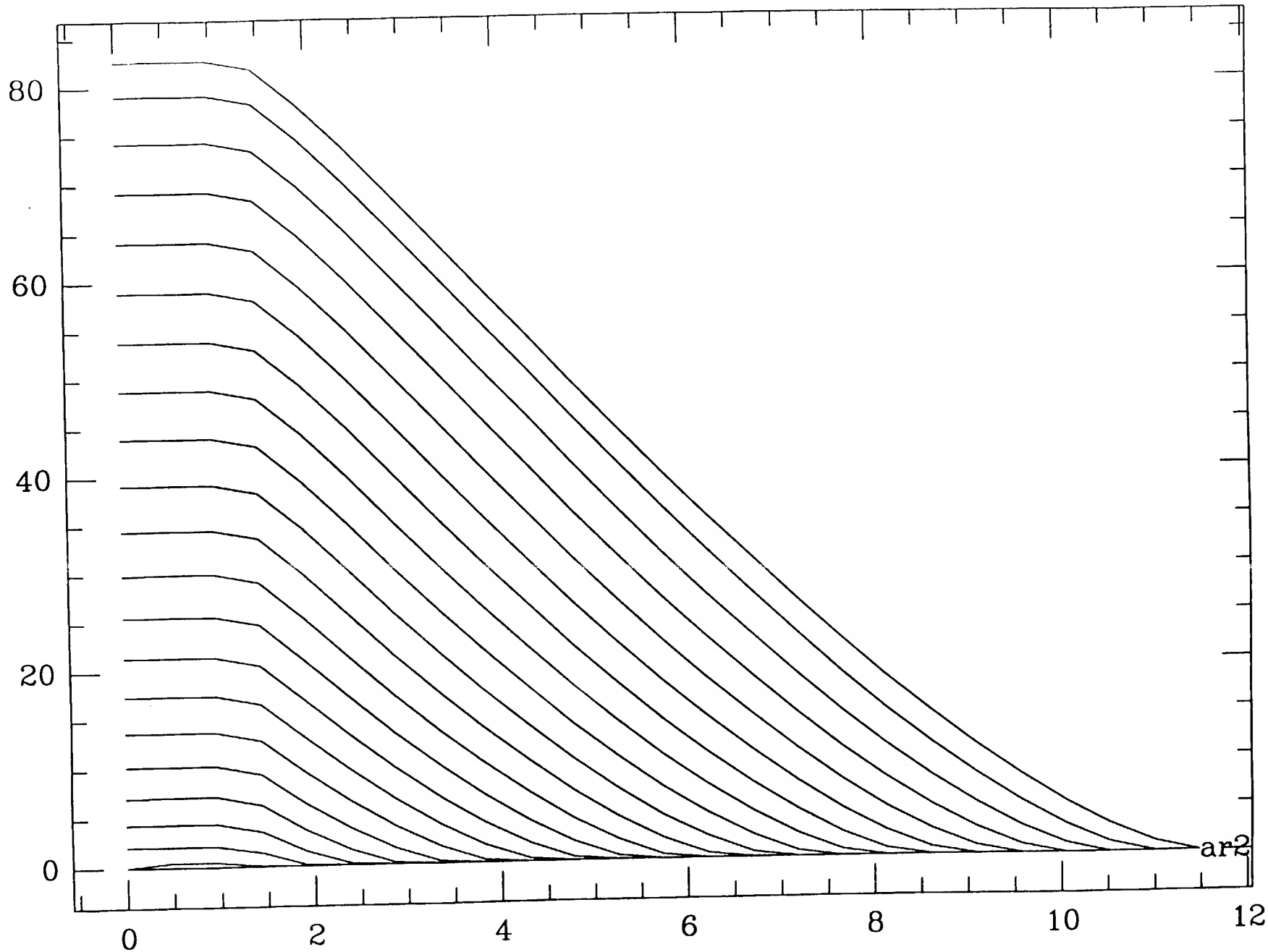

Figure 22

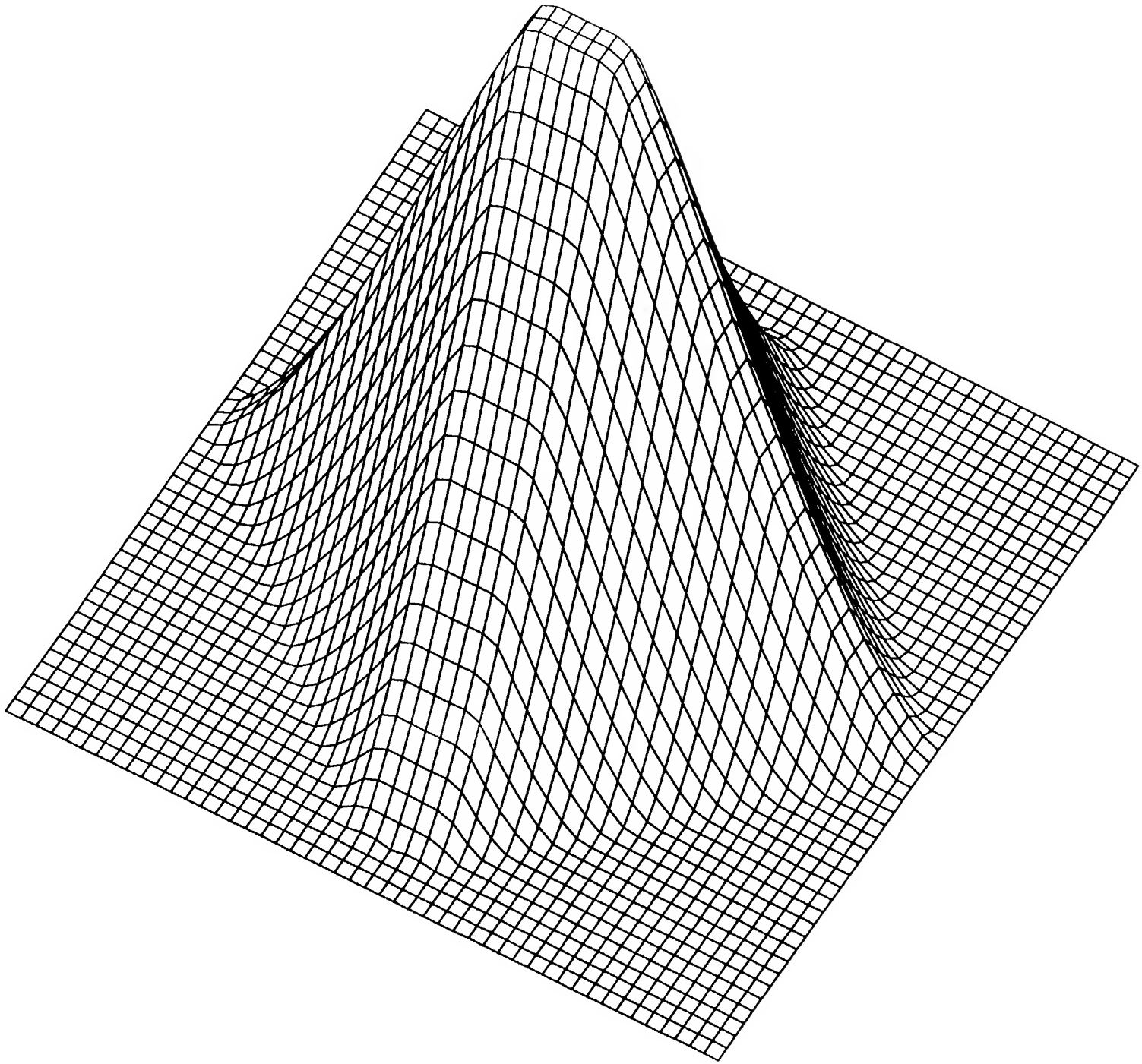

arc
0.05 -8 55 60

Figure 23

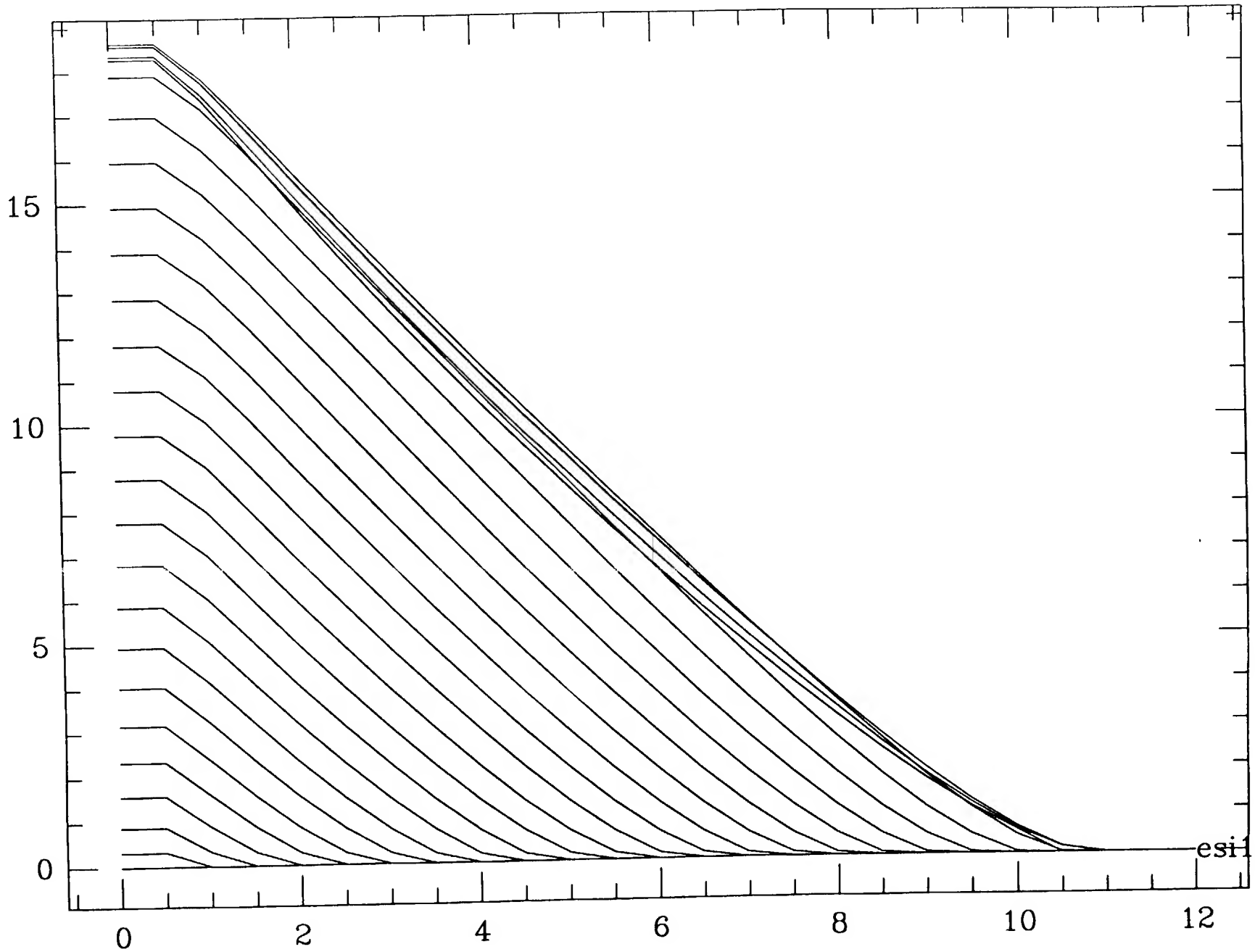

Figure 24

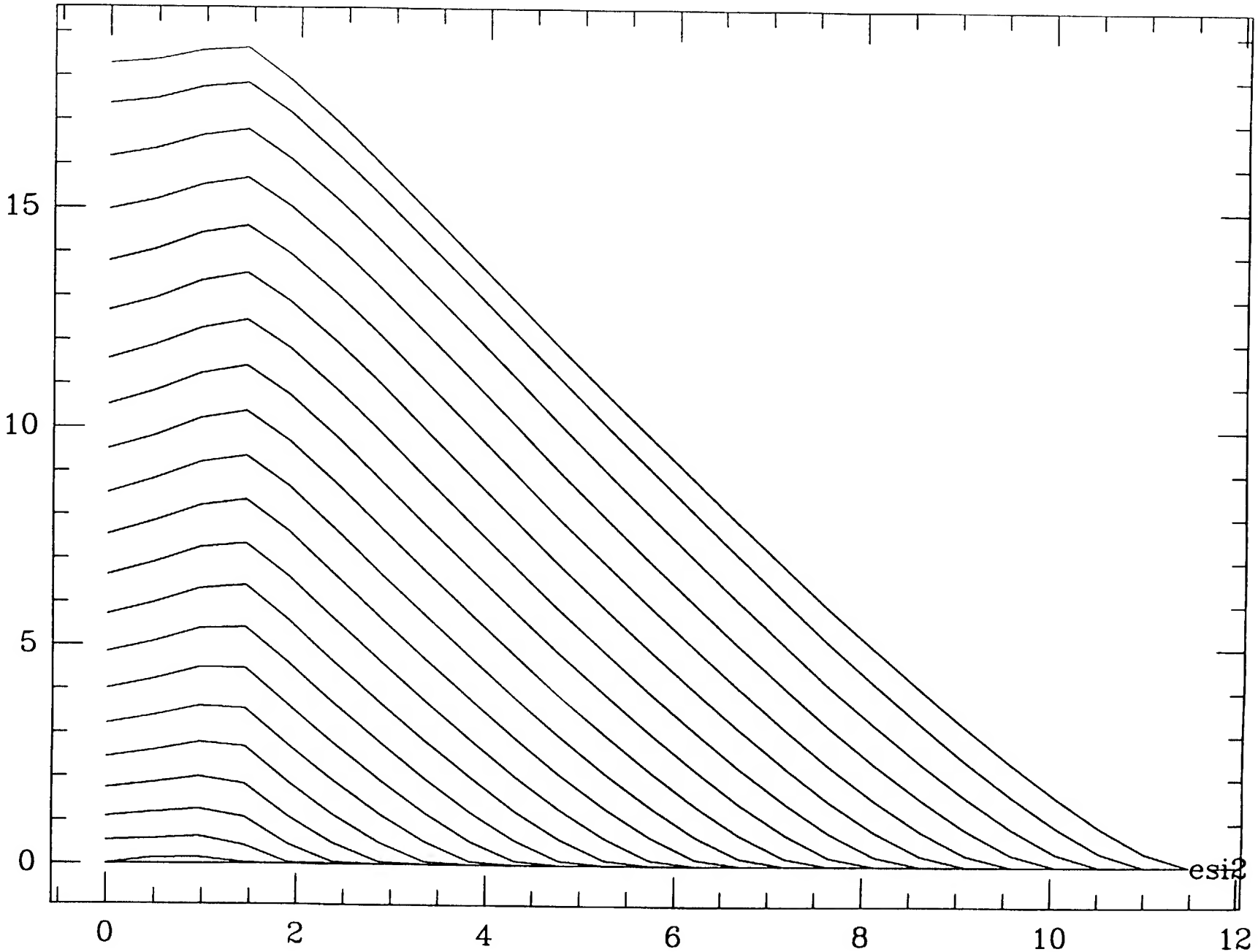

Figure 25

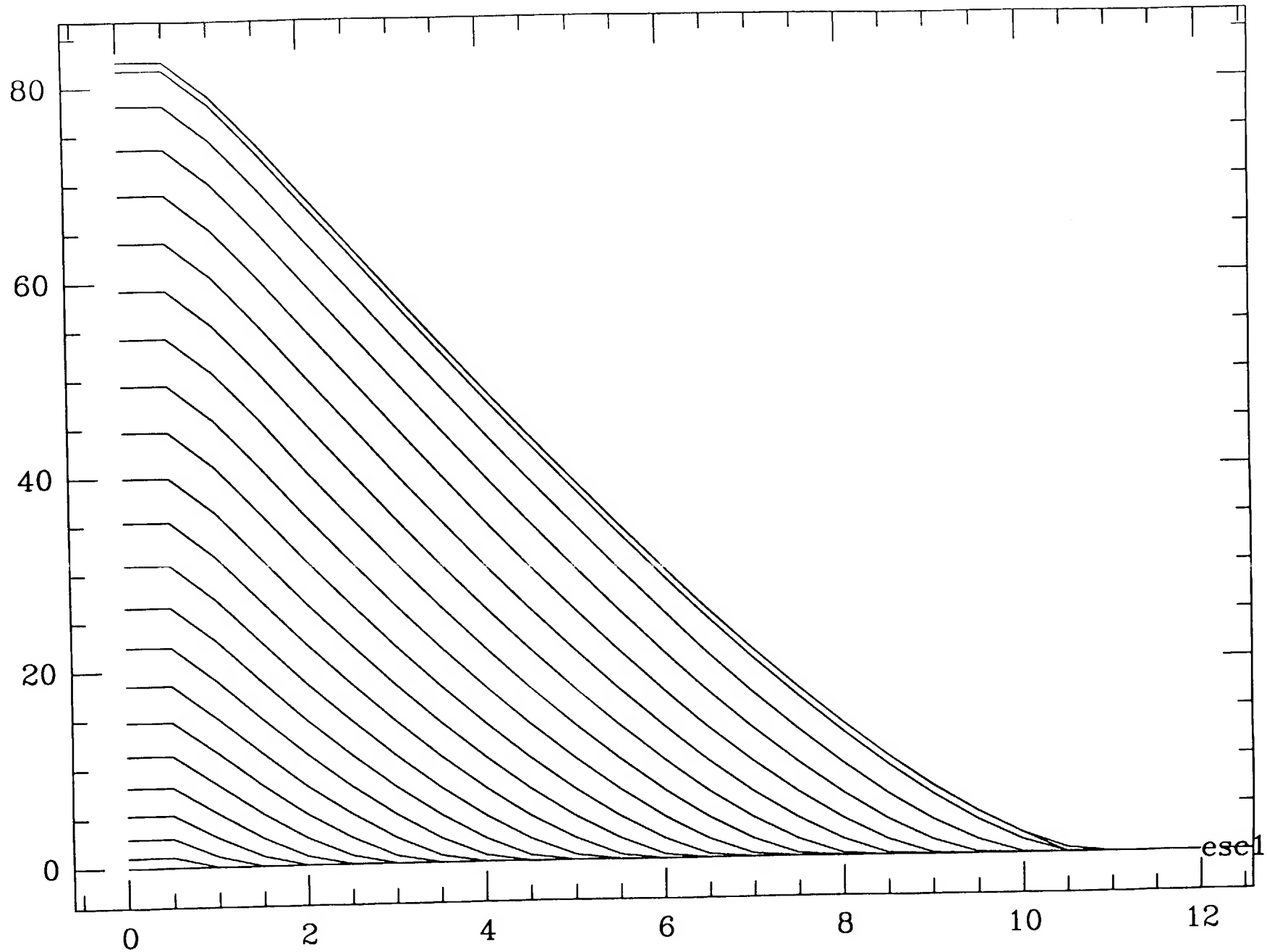

Figure 26

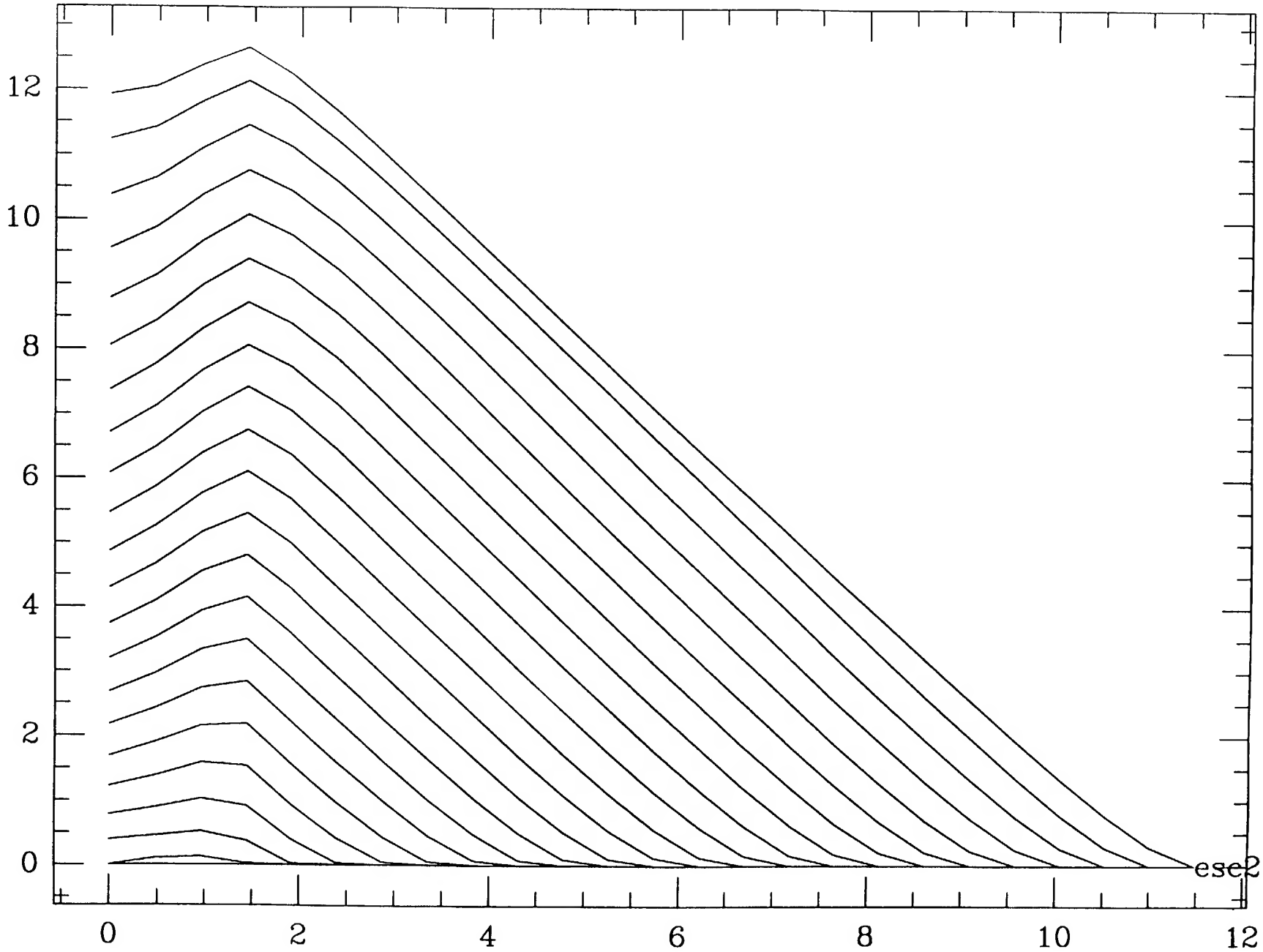

Figure 27

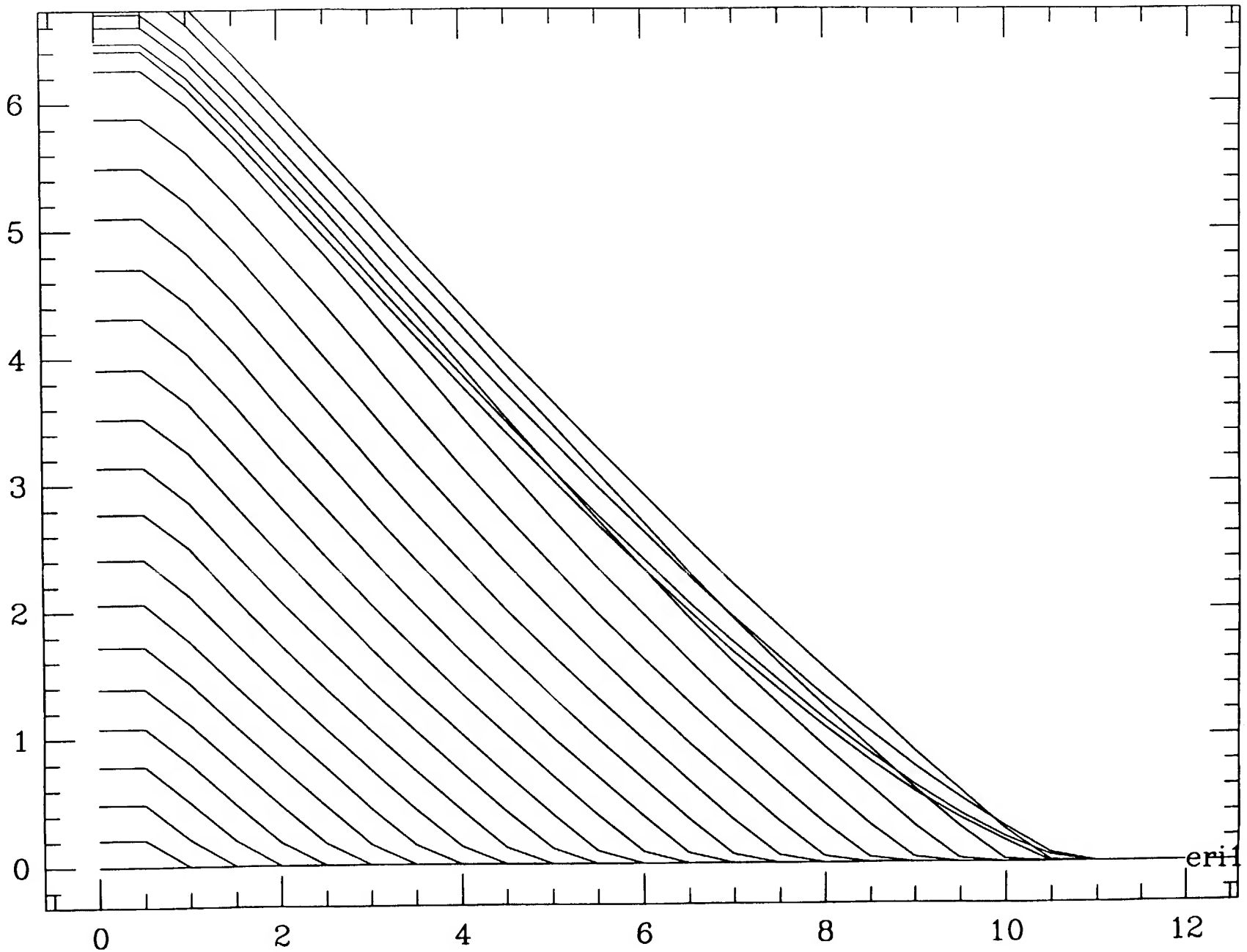

Figure 28

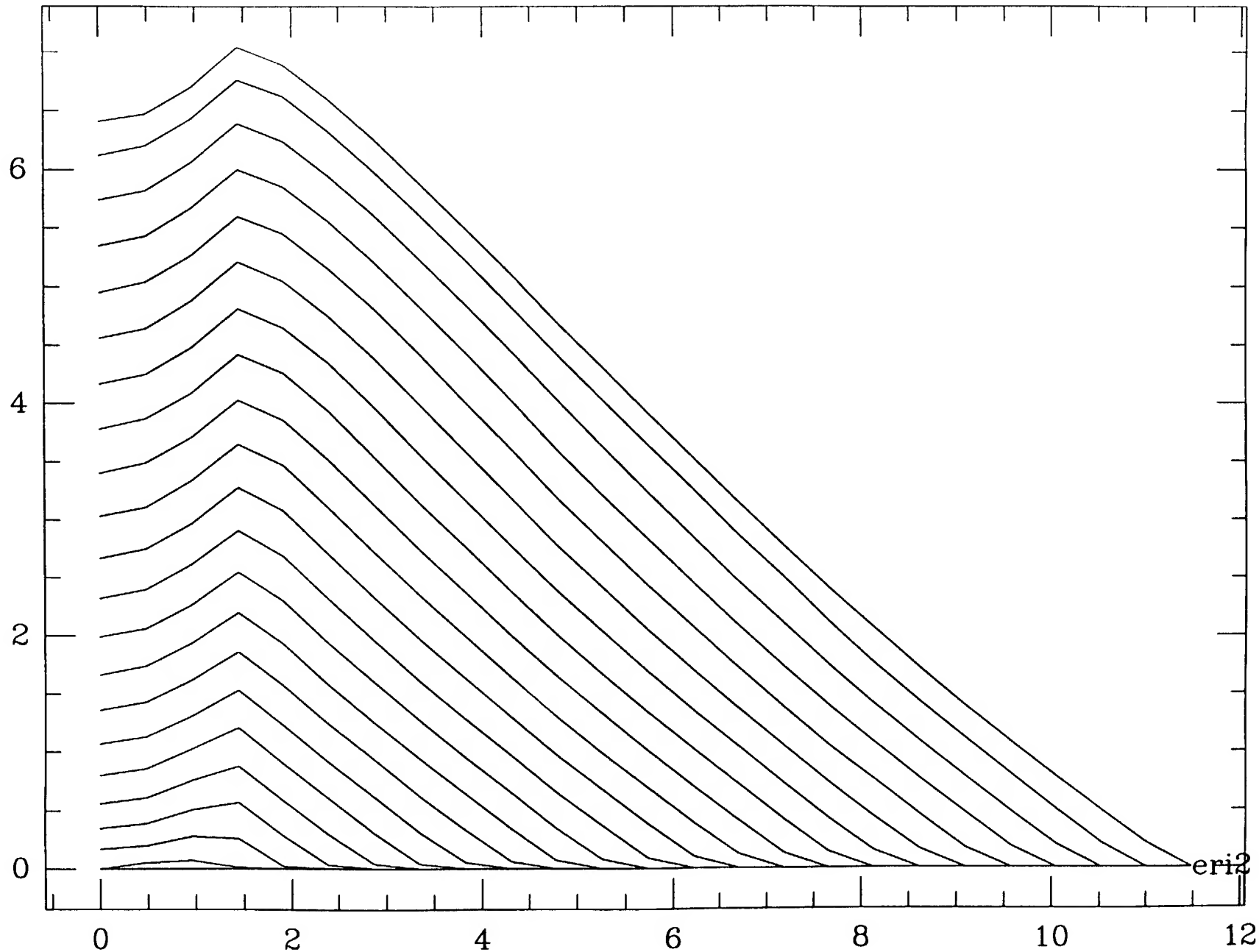

Figure 29

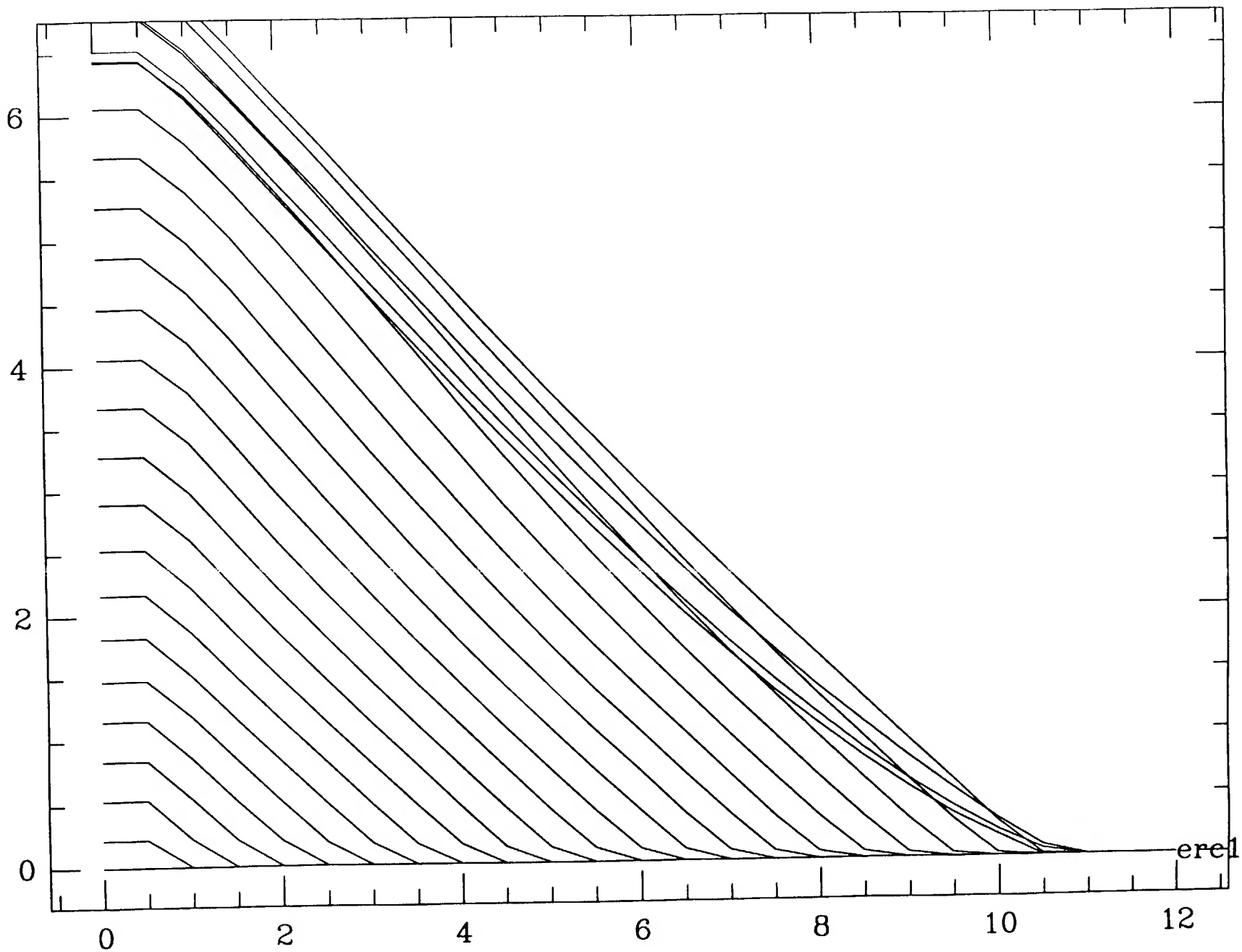

Figure 30

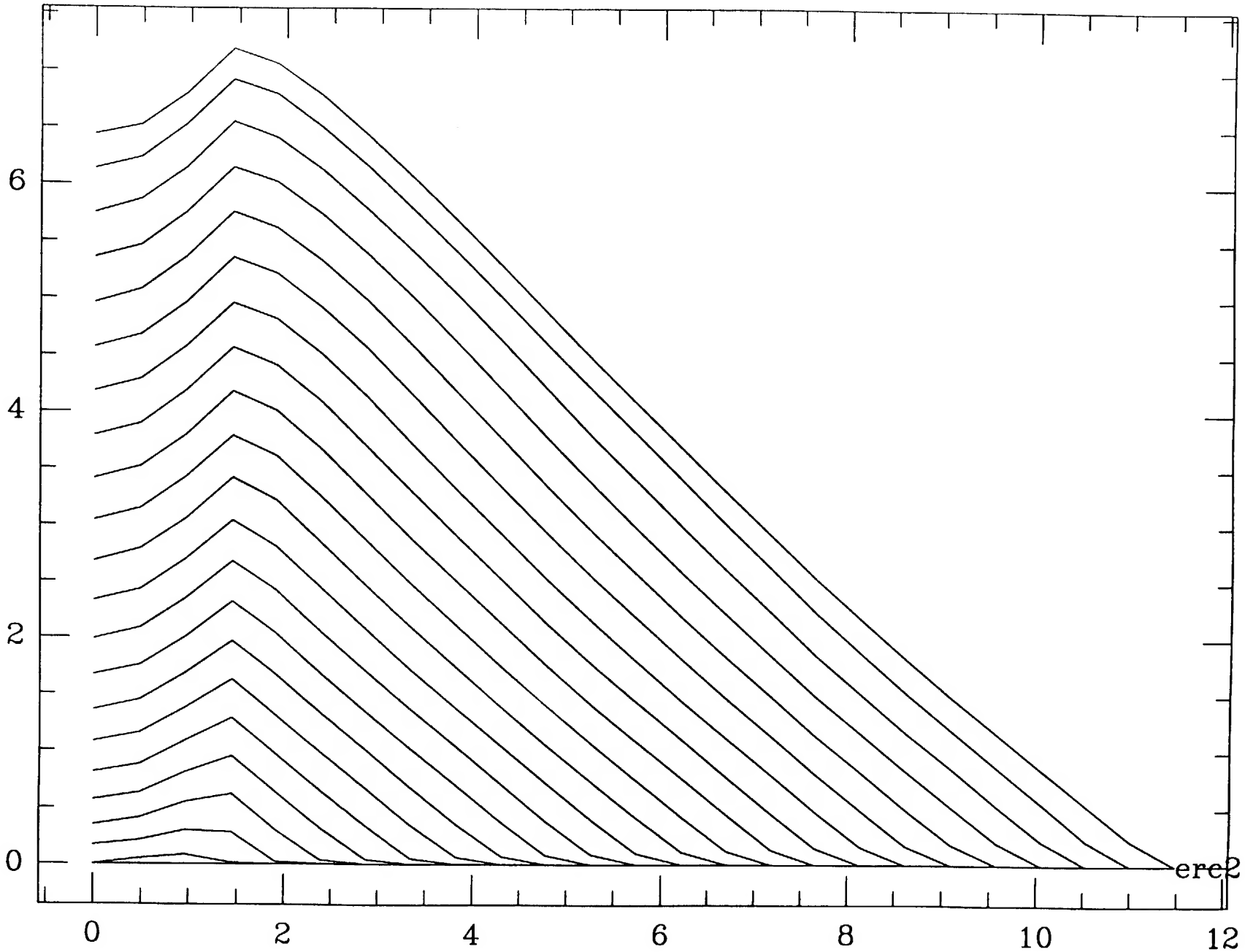

Figure 31

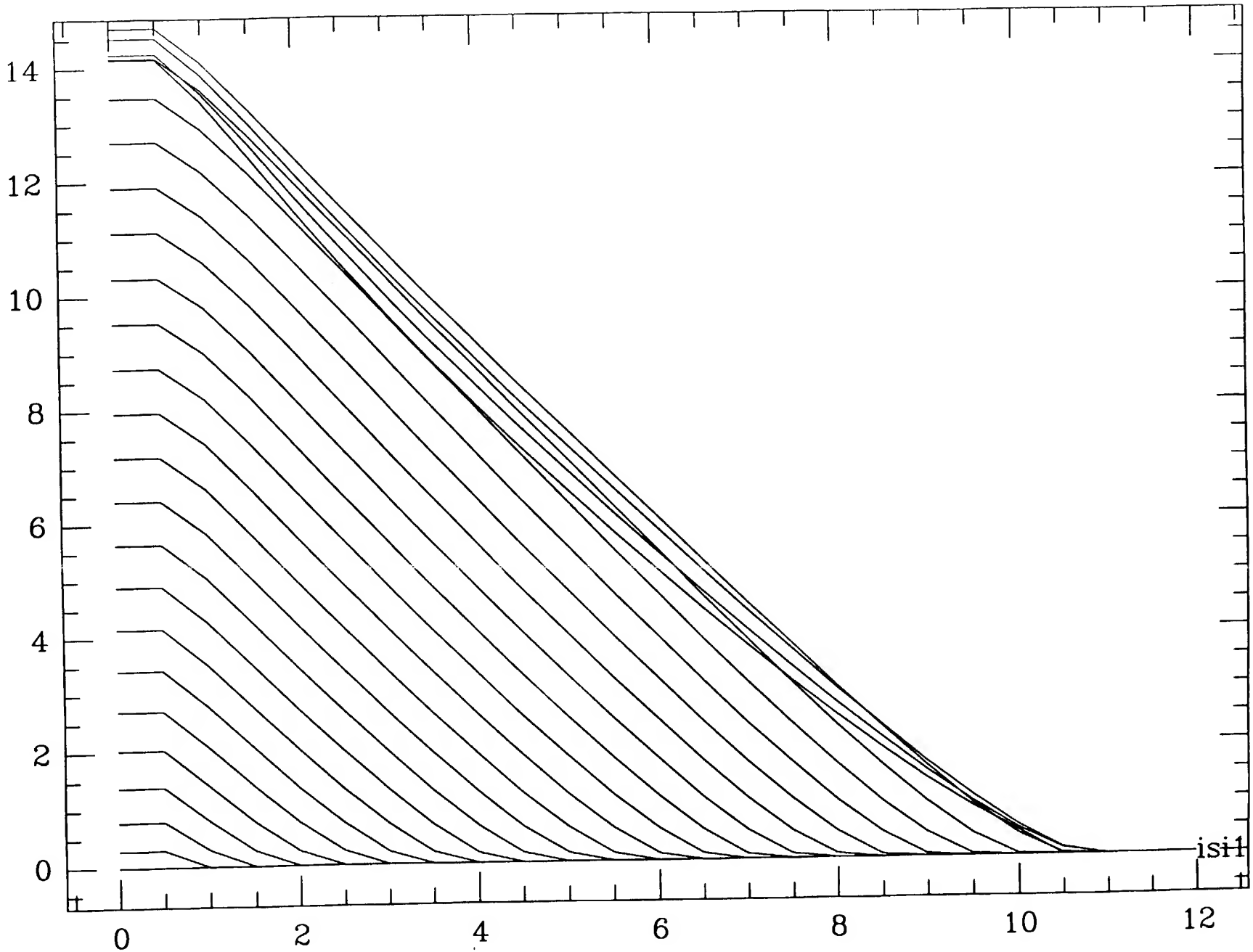

Figure 32

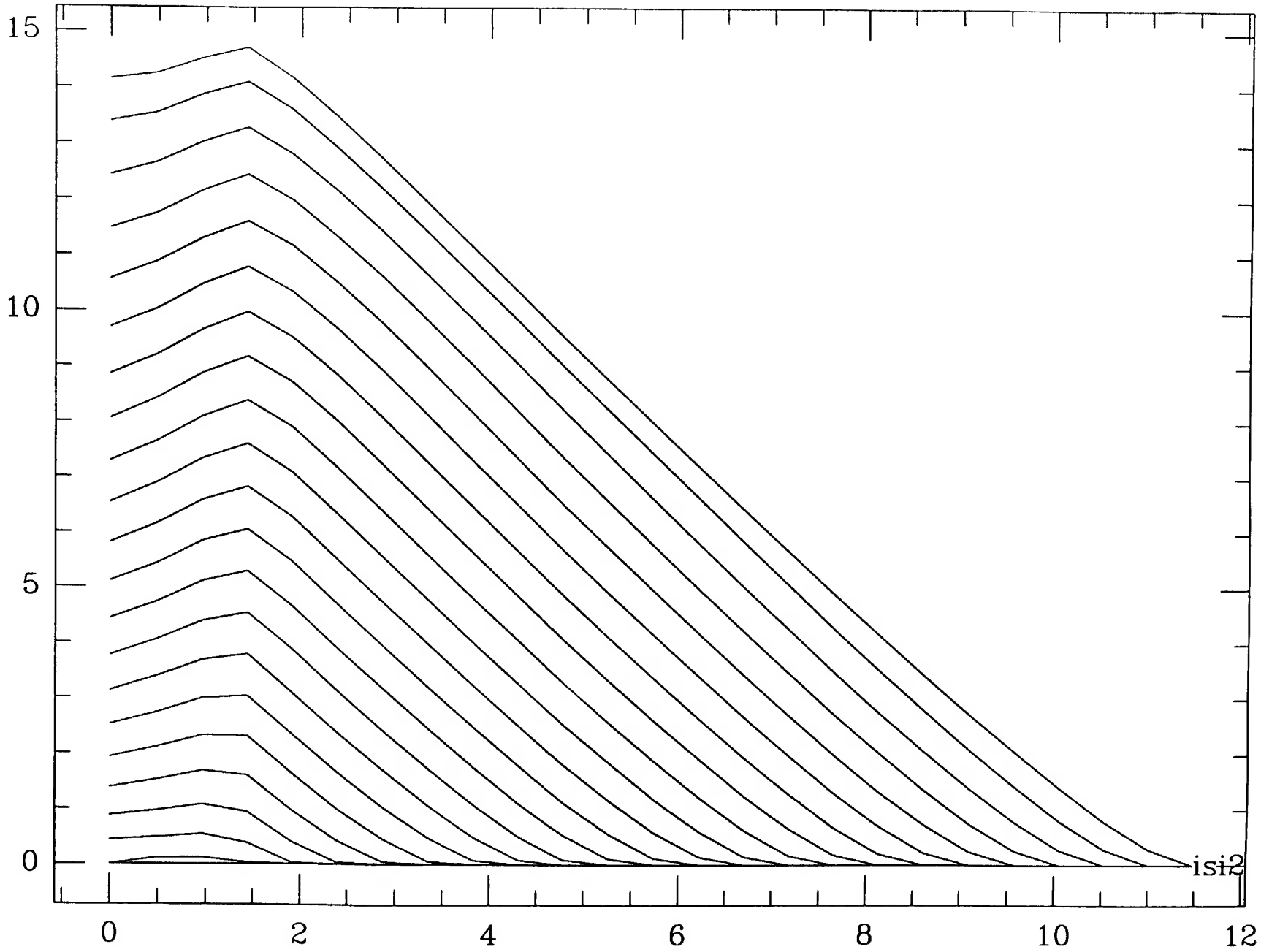

Figure 33

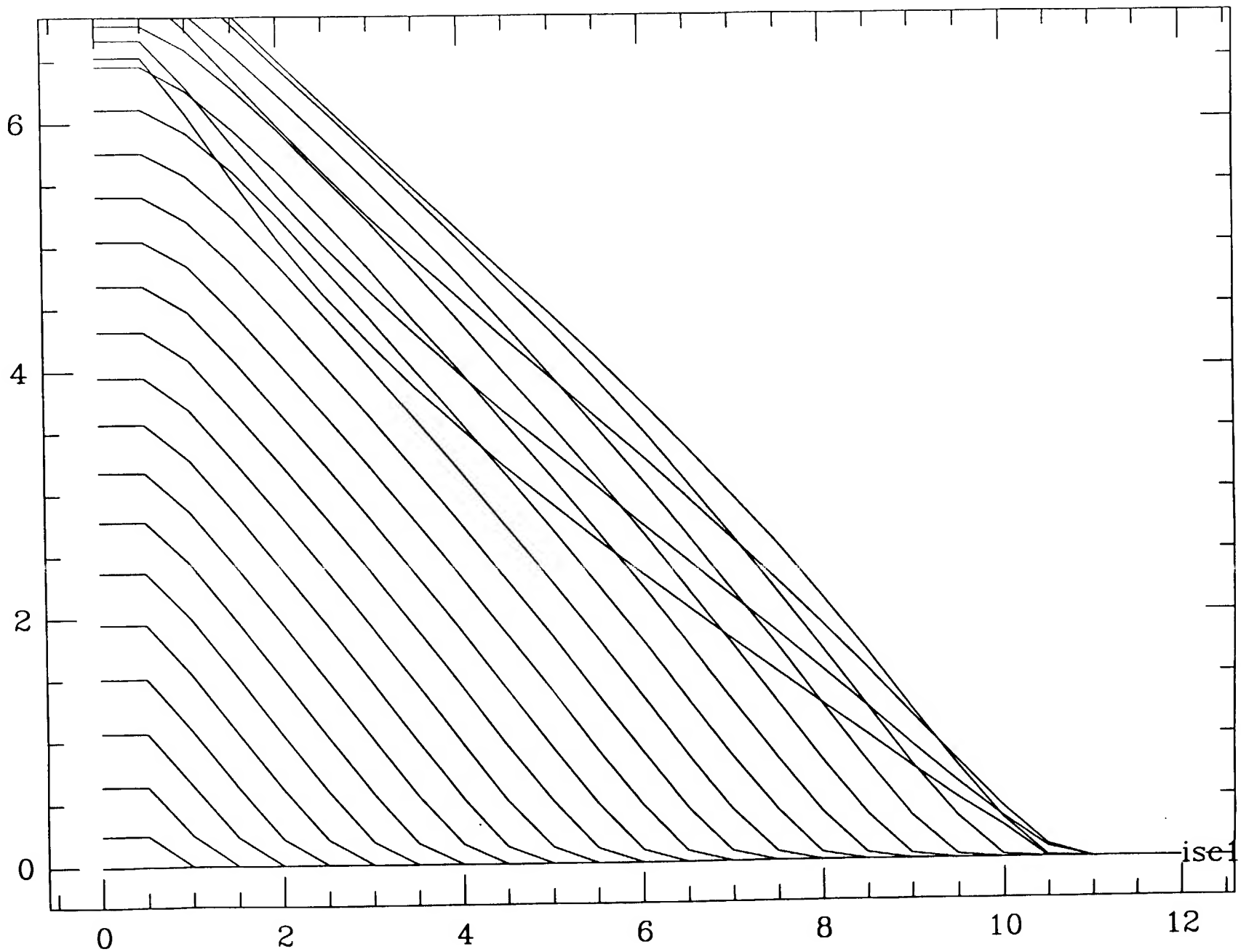

Figure 34

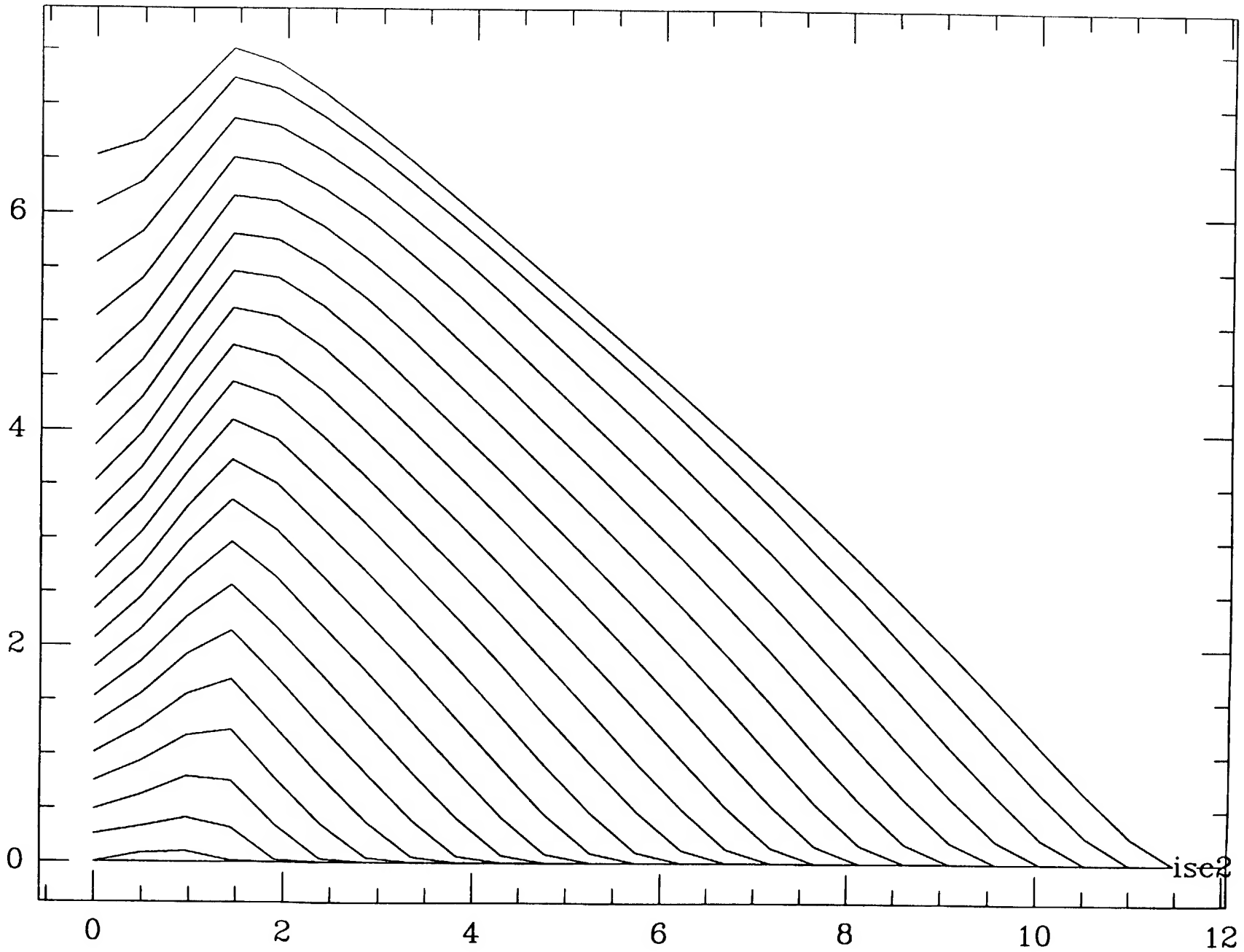

Figure 35

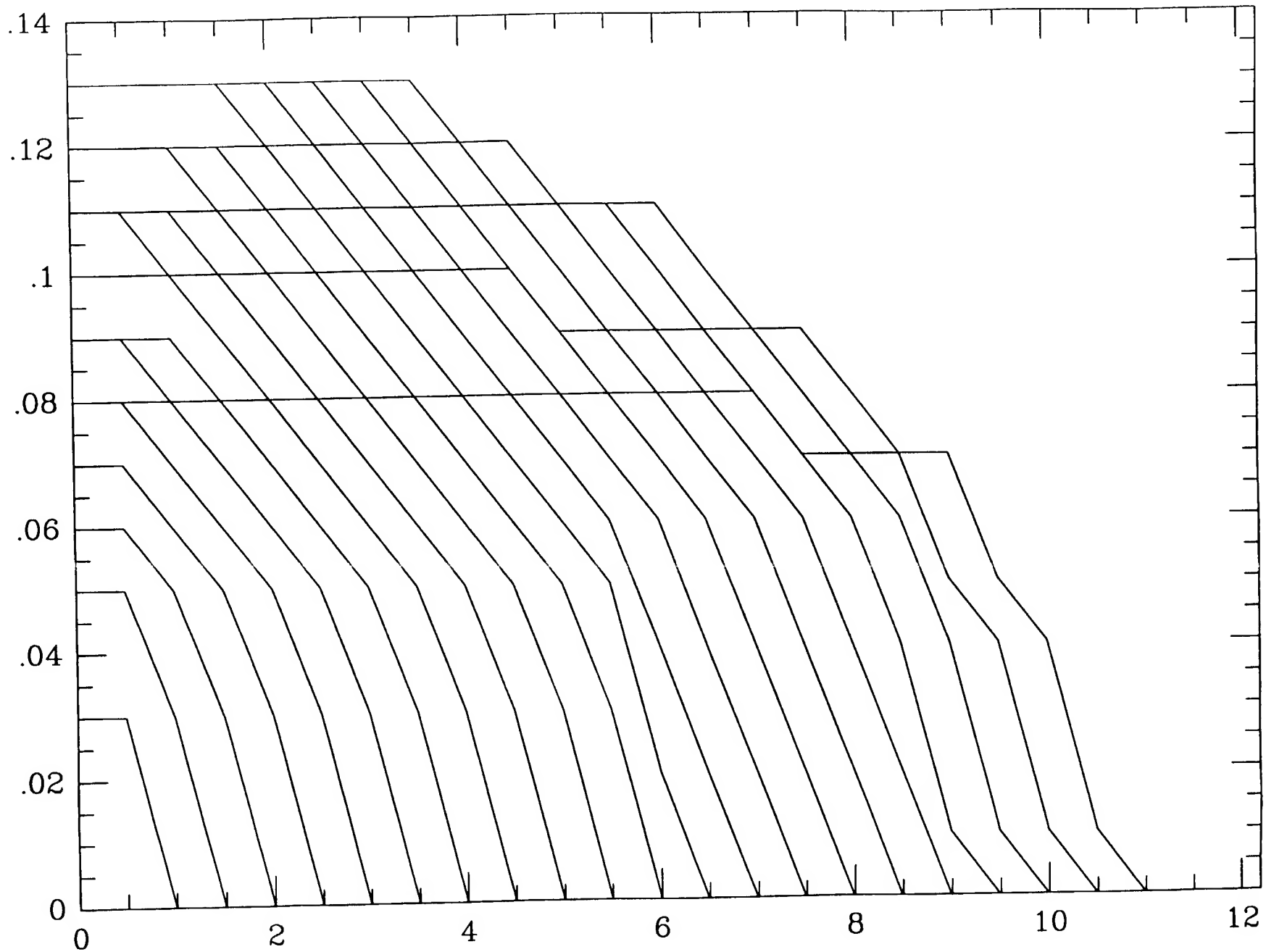

Figure 36

iri1

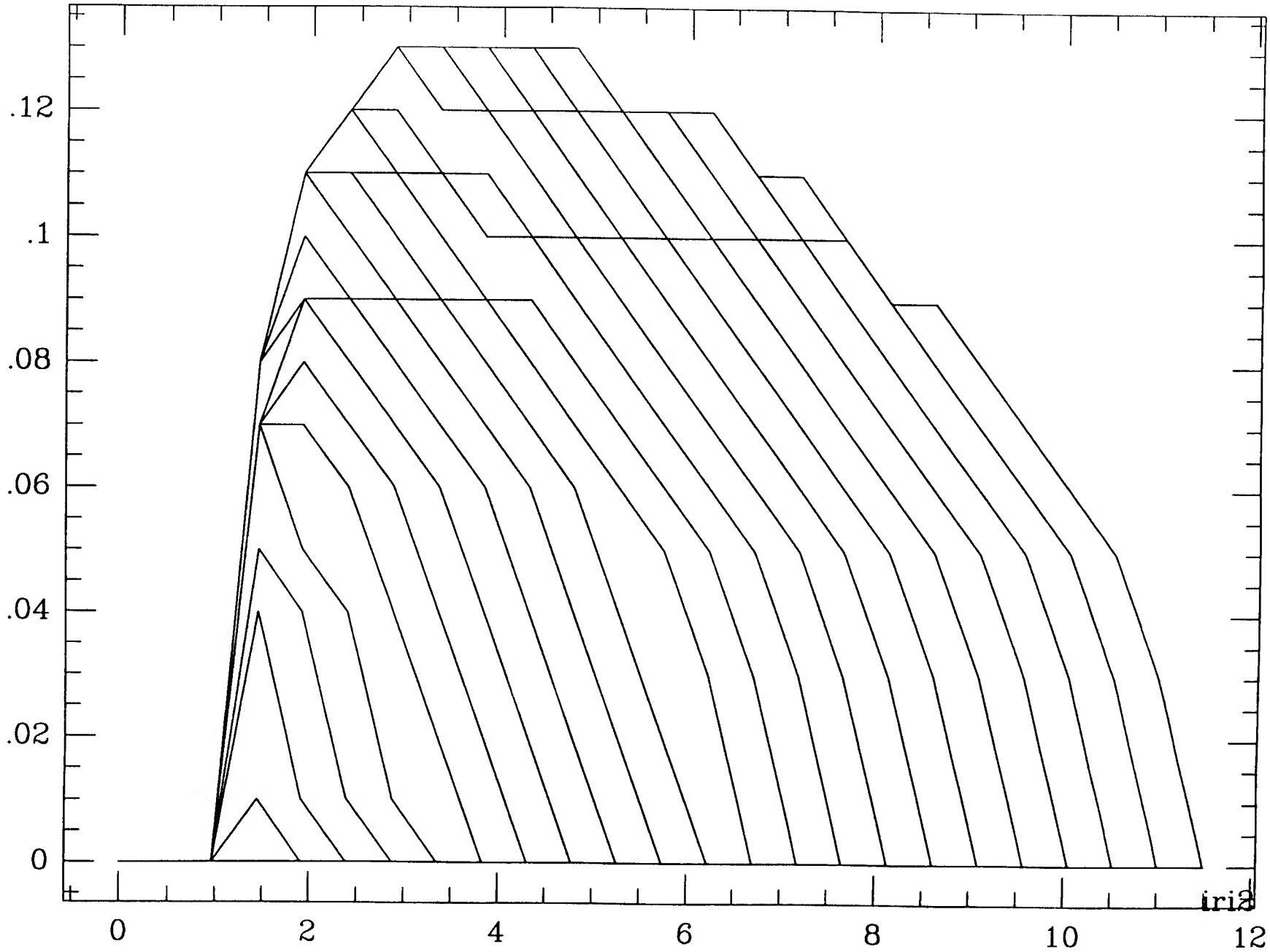

Figure 37

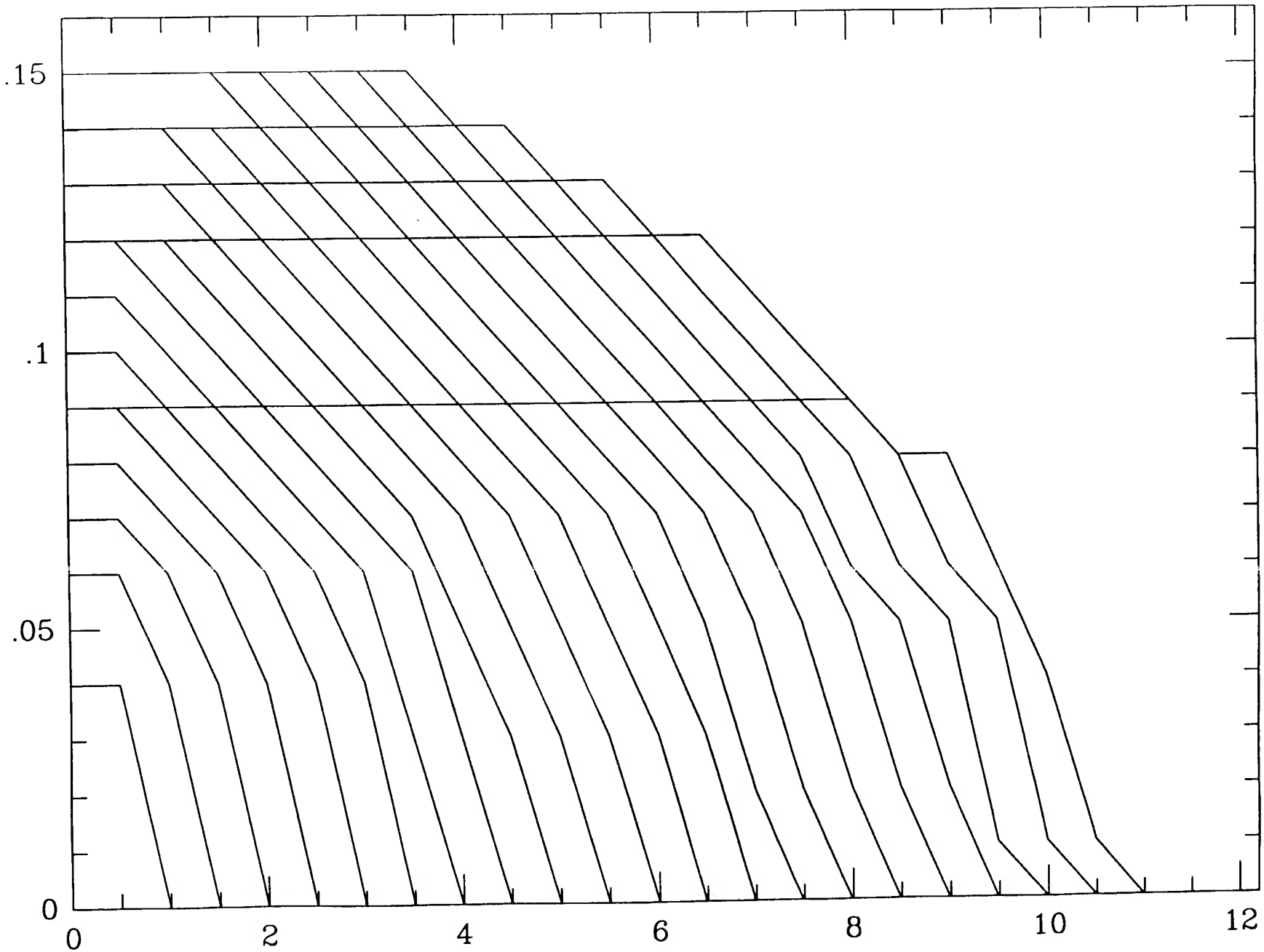

Figure 38

irc1

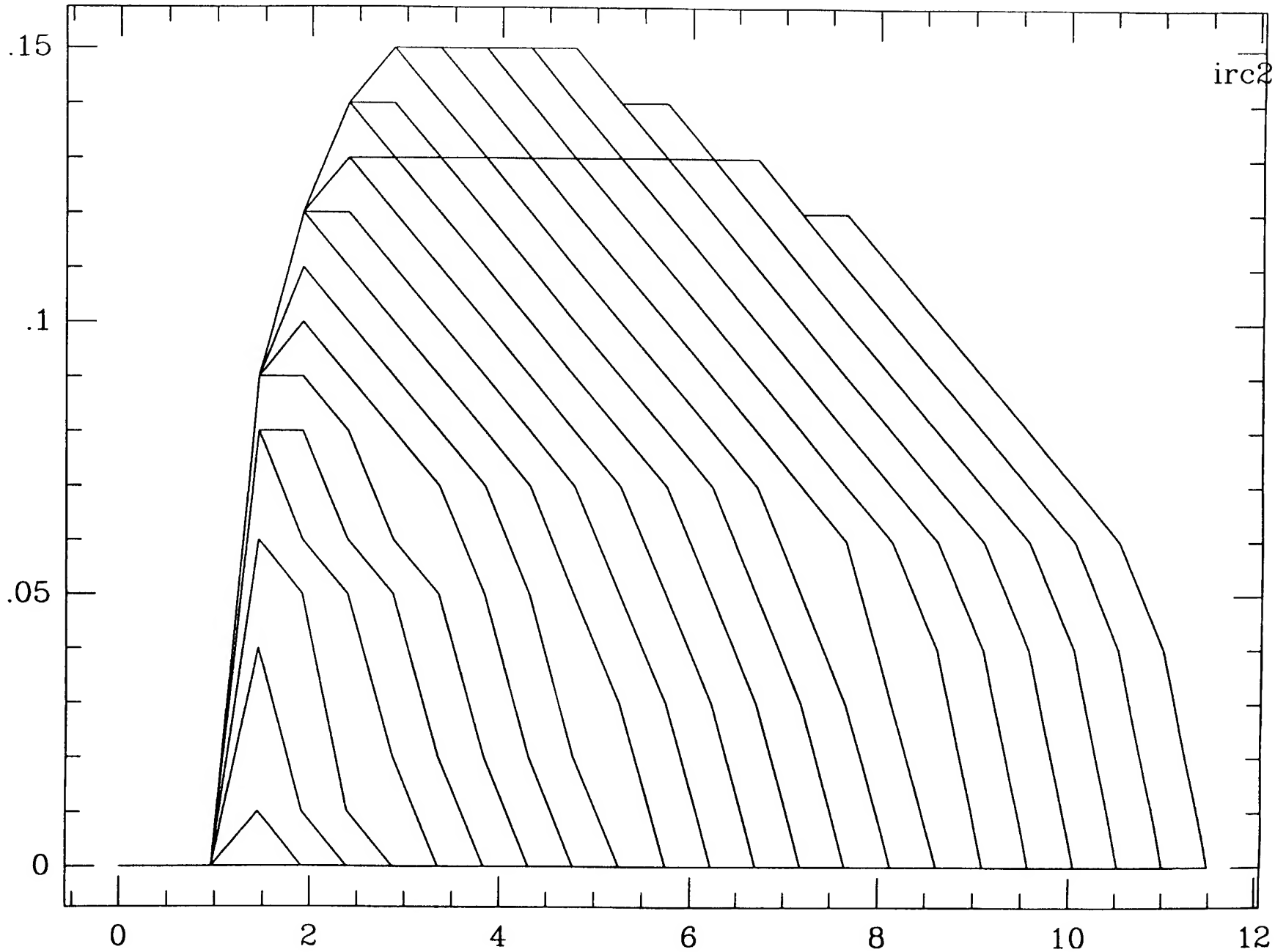

Figure 39

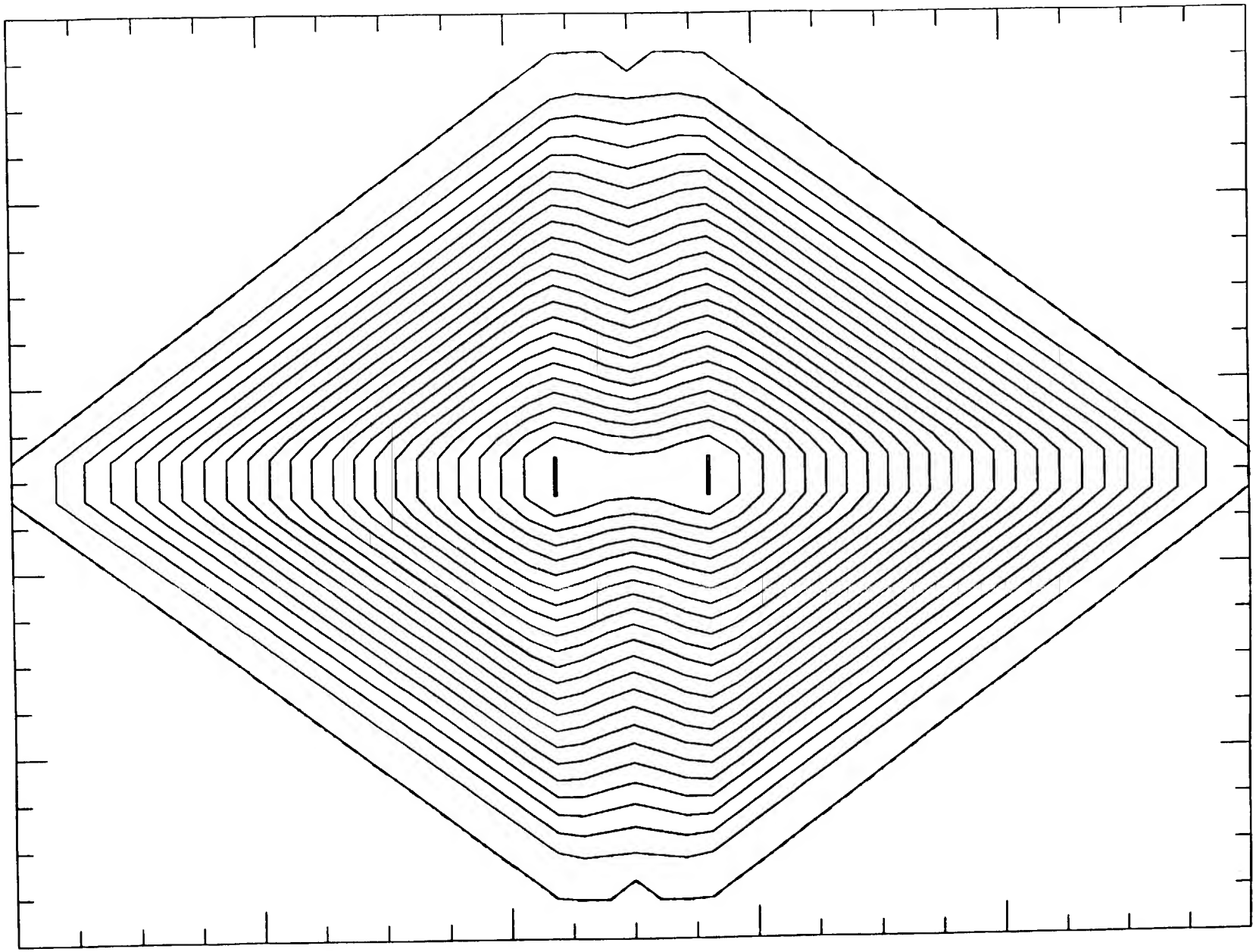

Figure 40

I S I 2

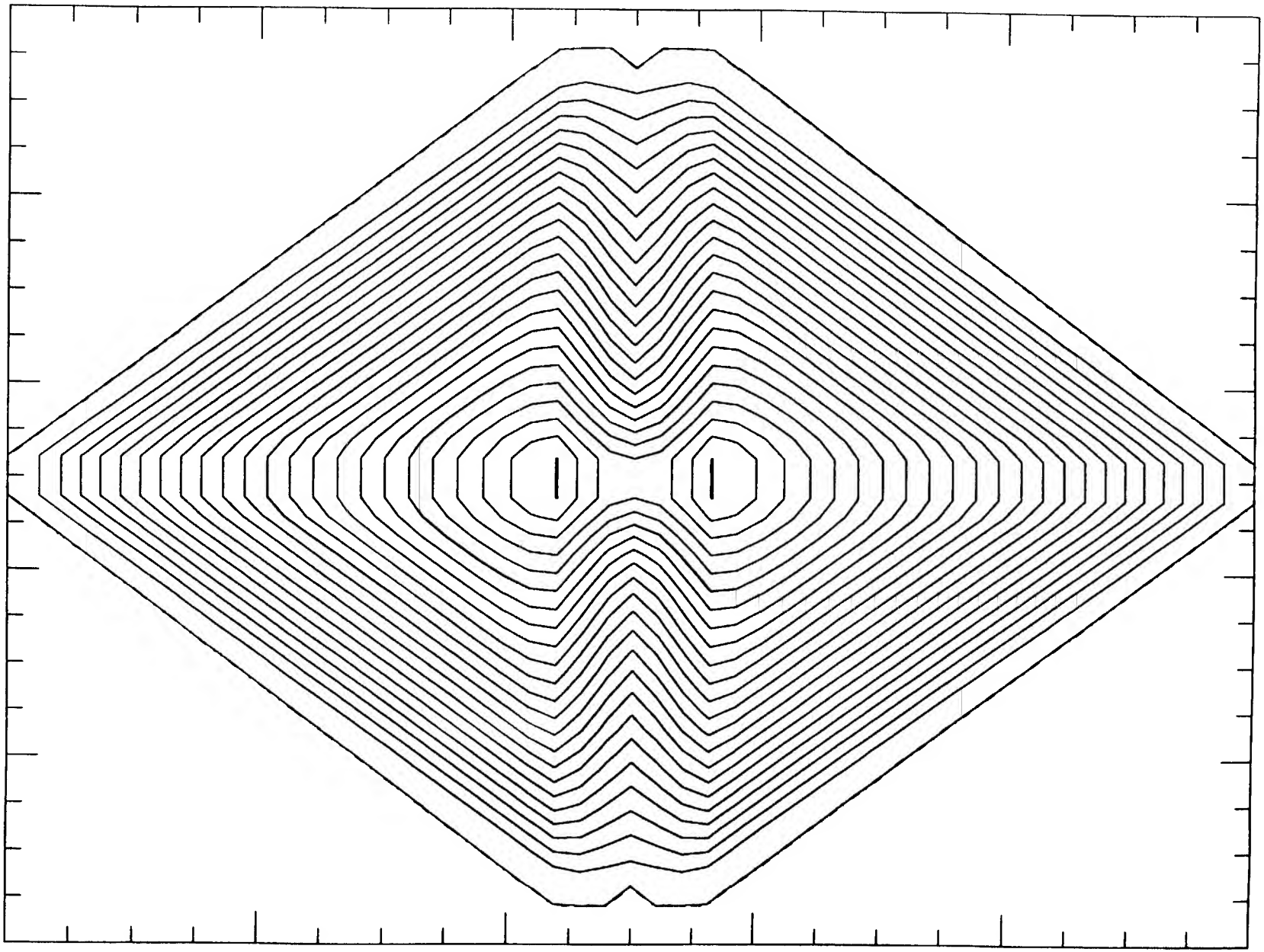

Figure 41

DSC 2

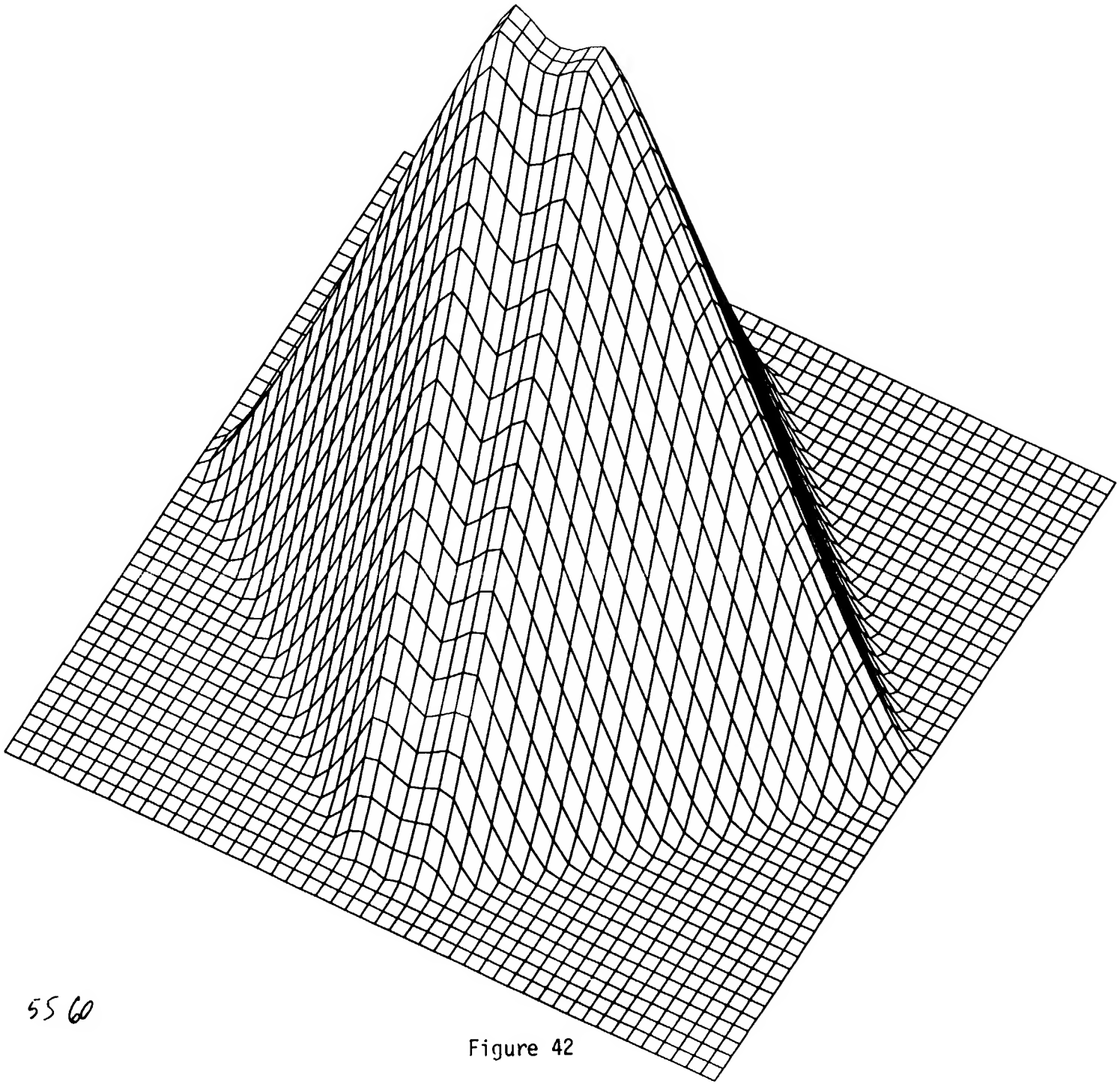

Figure 42

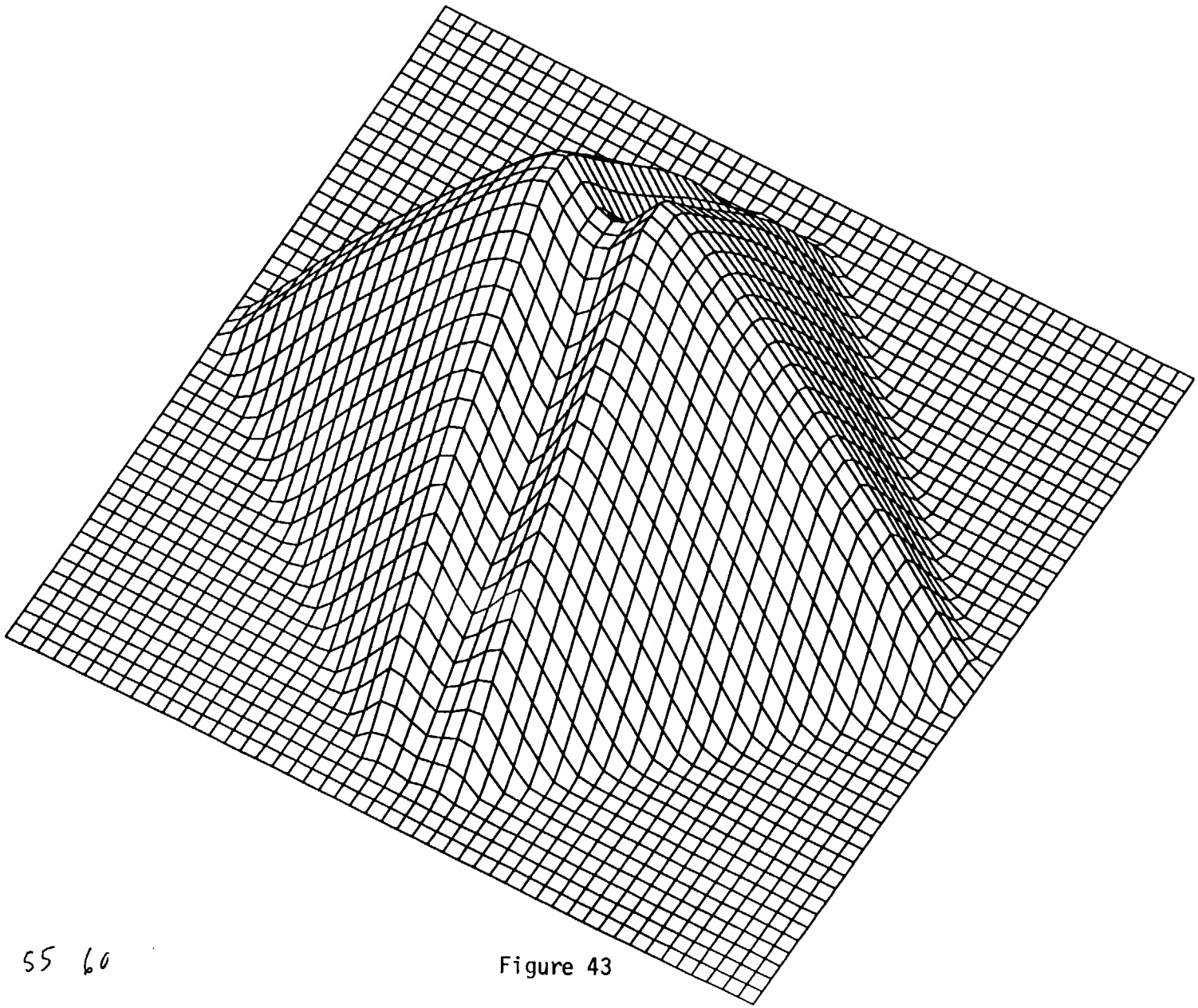

ISC2 0,3 -2 55 60

Figure 43

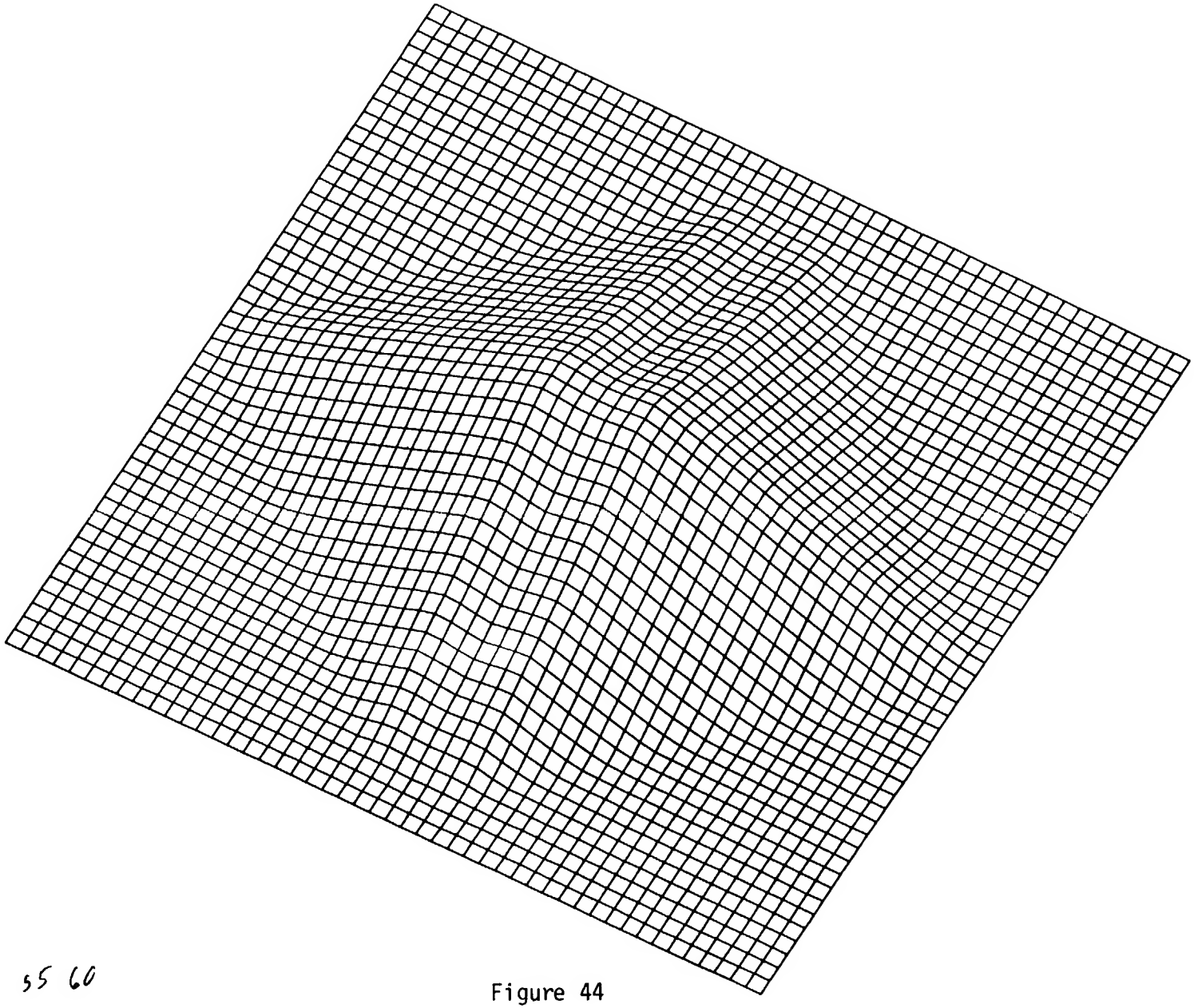

ISEZ 0.05 -8 55 60

Figure 44

```
0 VOYAGER DATA  -   CURRENTS (FA)    J=  3

 0.000e+00 0.000e+00 0.000e+00 0.000e+00 0.000e+00 0.000e+00 0.000e+00 0.000e+00
 0.000e+00 0.000e+00 0.000e+00 0.000e+00 0.000e+00 0.000e+00 0.000e+00 0.000e+00

0 VOYAGER DATA  -   CURRENTS (FA)    J=  4

 4.210e+01 6.382e+01 1.110e+02 4.570e+02 6.945e+02 8.442e+02 1.058e+03 1.178e+03
 1.080e+03 8.548e+02 5.786e+02 2.710e+02 1.050e+02 2.499e+01 2.670e+00 1.882e-01

TYPE 1 TO CONTINUE
```

```
$0.78
CONNECT= 00:
LOGOFF AT 00
VM/370 ONLIN
[Back at Loc
C-Kermit>q
Retain log?
gsg@space[8]
gsg@space[8]
4.9u 9.5s 2:
gsg logged o
Connection c
win3 gsg[9]$
aeb      spa
dje      pla
dje      spa
dumpster spa
gsg      spa
gsg      sta
gsg      sta
gsg      sta
gsg      sta
gsg      sta
gsg      sta
gsg      sta
jwb      spa
jwb      spa
jwb      spa
jwb      spa
jwb      spa
jwb      spa
jwb      spa
win3 gsg[10]
USER       F
gsg      117
gsg      117
gsg      117
win3 gsg[11]
win3 gsg[12]
win3 gsg[13]
win3 gsg[14]
win3 gsg[15]
win3 gsg[15]
lp is ready
Rank   Owner
active gsg
1st    gsg
win3 gsg[16]
win3 gsg[17]
```

```
TYPE 1 TO CONTINUE
1
0PLOT SIMULATED DATA? 1=YES, 0=NO
1
 THE SCALE STARTS AT 1.00e+01 FEMTOAMPS AND GOES UP 3 DECADES
0CHANGE CURRENT SCALE FROM CURRENT VALUE? 1=YES, 0=NO
0

 Plot option [cefghnqw]: g
```

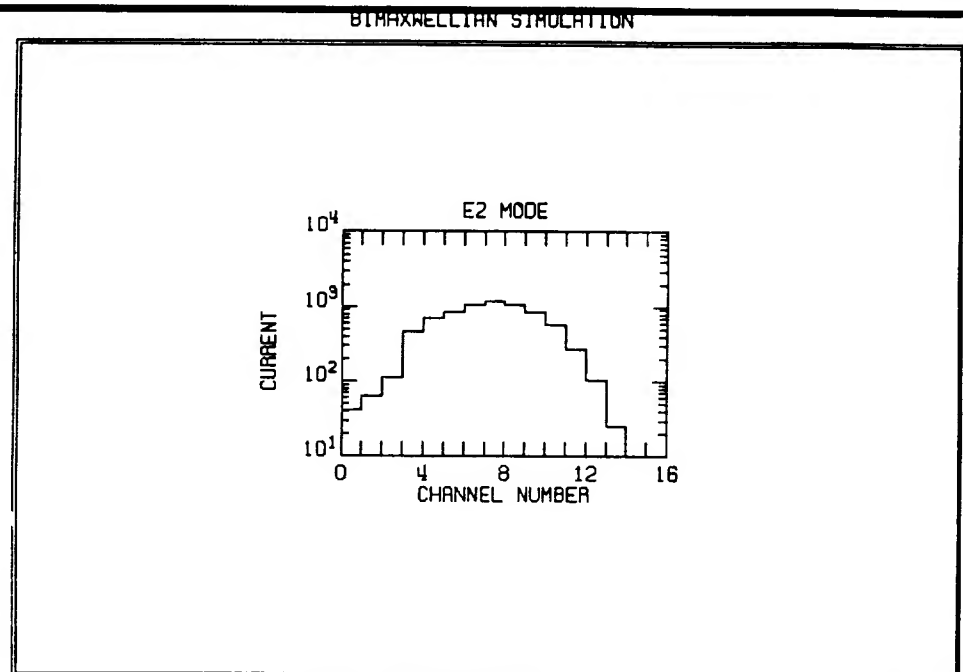

Figure 45

ORIGINAL PAGE IS
OF POOR QUALITY

```
0 VOYAGER DATA  -   CURRENTS (FA)    J=  3

  0.000e+00 0.000e+00 0.000e+00 0.000e+00 0.000e+00 0.000e+00 0.000e+00 0.000e+00
  0.000e+00 0.000e+00 0.000e+00 0.000e+00 0.000e+00 0.000e+00 0.000e+00 0.000e+00

0 VOYAGER DATA  -   CURRENTS (FA)    J=  4

  3.858e+01 4.667e+01 8.244e+01 3.588e+02 5.368e+02 6.264e+02 7.687e+02 8.357e+02
  7.666e+02 6.216e+02 4.336e+02 2.186e+02 8.377e+01 2.047e+01 2.239e+00 1.585e-01

 TYPE 1 TO CONTINUE
```

```
CONNECT= 00:
LOGOFF AT 08
VM/370 ONLIN
[Back at Loc
C-Kermit>q

Retain log?
gsg@space[8]
gsg@space[8]
4.9u 4.5e 2:
gsg logged o
Connection c
win3 gsg[9]%
aeb      spa
dje      pla
dje      spa
dumpster spa
gsg      spa
gsg      sta
gsg      sta
gsg      sta
gsg      sta
gsg      sta
gsg      sta
gsg      sta
jwb      spa
jwb      spa
jwb      spa
jwb      spa
jwb      spa
jwb      spa
jwb      spa
win3 gsg[10]
USER       P
gsg      117
gsg      117
gsg      117
win3 gsg[11]
win3 gsg[12]
win3 gsg[13]
win3 gsg[14]
win3 gsg[15]
win3 gsg[15]
lp is ready
Rank   Owner
active gsg
1st    gsg
win3 gsg[16]
win3 gsg[17]
win3 gsg[18]
win3 gsg[19]
```

```
 TYPE 1 TO CONTINUE
1
0PLOT SIMULATED DATA? 1=YES, 0=NO
1
 THE SCALE STARTS AT 1.00e+01 FEMTOAMPS AND GOES UP 3 DECADES
0CHANGE CURRENT SCALE FROM CURRENT VALUE? 1=YES, 0=NO
0


 Plot option [cefghnqw]: g
```

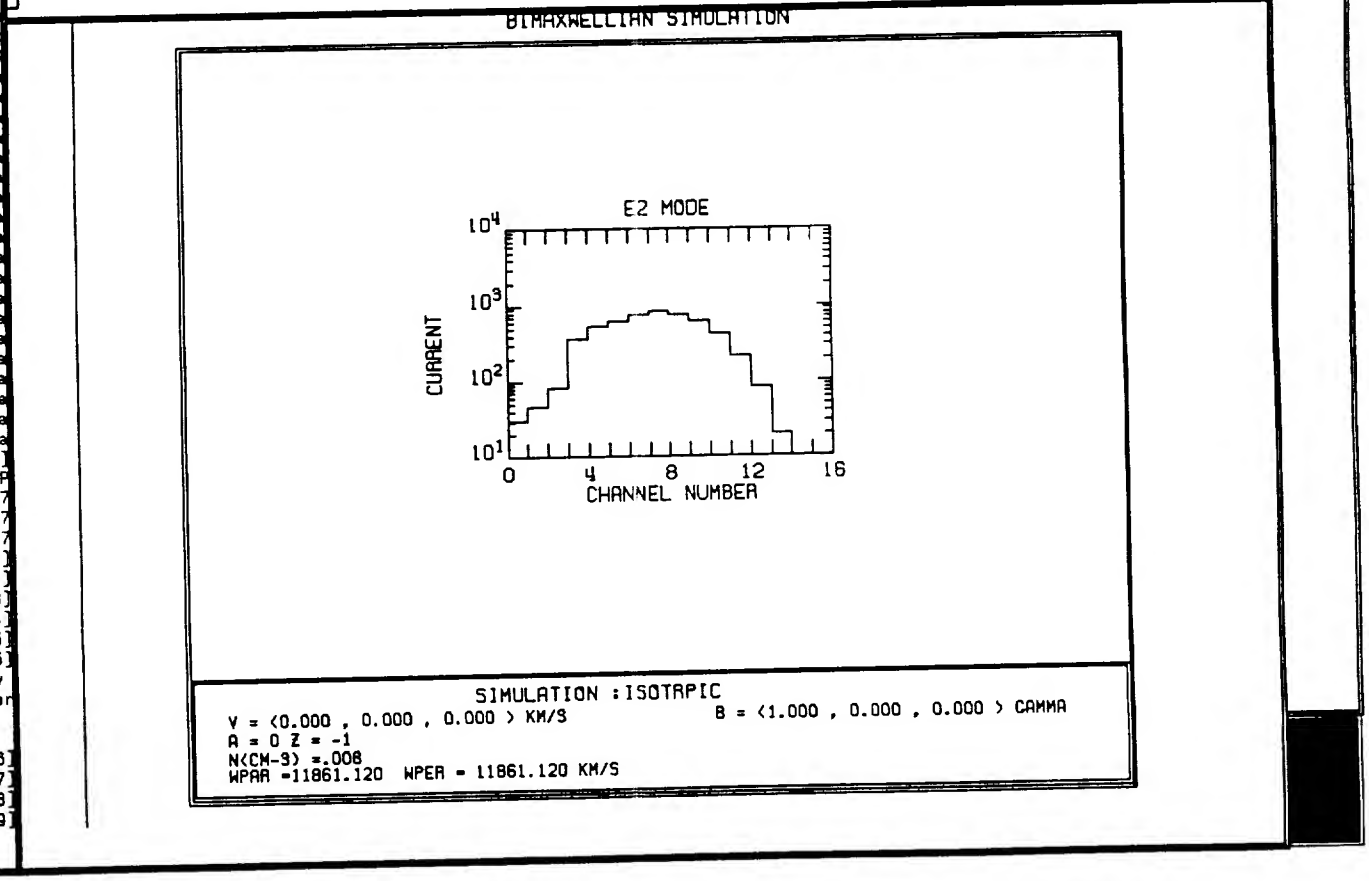

Figure 46

```
0 VOYAGER DATA  -   CURRENTS (FA)    J=  3

  0.000e+00 0.000e+00 0.000e+00 0.000e+00 0.000e+00 0.000e+00 0.000e+00 0.000e+00
  0.000e+00 0.000e+00 0.000e+00 0.000e+00 0.000e+00 0.000e+00 0.000e+00 0.000e+00

0 VOYAGER DATA  -   CURRENTS (FA)    J=  4

  3.598e+01 5.466e+01 9.549e+01 4.074e+02 6.059e+02 7.246e+02 8.976e+02 9.985e+02
  9.193e+02 7.388e+02 5.077e+02 2.424e+02 9.497e+01 2.288e+01 2.473e+00 1.735e-01

 TYPE 1 TO CONTINUE
```

```
 TYPE 1 TO CONTINUE
1
0PLOT SIMULATED DATA? 1=YES, 0=NO
1
 THE SCALE STARTS AT 1.00e+01 FEMTOAMPS AND GOES UP 3 DECADES
0CHANGE CURRENT SCALE FROM CURRENT VALUE? 1=YES, 0=NO
0


 Plot option [cefghnqw]: g
```

```
VM/370 ONLIN
[Back at Loc
C-Kermit>q
Retain log?
gsg@space[8]
gsg@space[8]
4.9u 0.5s 2:
gsg logged o
Connection c
win3 gsg[9]$
aeb       spa
dje       pla
dje       spa
dumpster spa
gsg       spa
gsg       sta
gsg       sta
gsg       sta
gsg       sta
gsg       sta
gsg       sta
gsg       sta
jwb       spa
jwb       spa
jwb       spa
jwb       spa
jwb       spa
jwb       spa
jwb       spa
win3 gsg[10]
USER        R
gsg       117
gsg       117
gsg       117
win3 gsg[11]
win3 gsg[12]
win3 gsg[13]
win3 gsg[14]
win3 gsg[15]
win3 gsg[15]
lp is ready
Rank   Owner
active gsg
1st    gsg
win3 gsg[16]
win3 gsg[17]
win3 gsg[18]
win3 gsg[19]
win3 gsg[20]
win3 gsg[21]
```

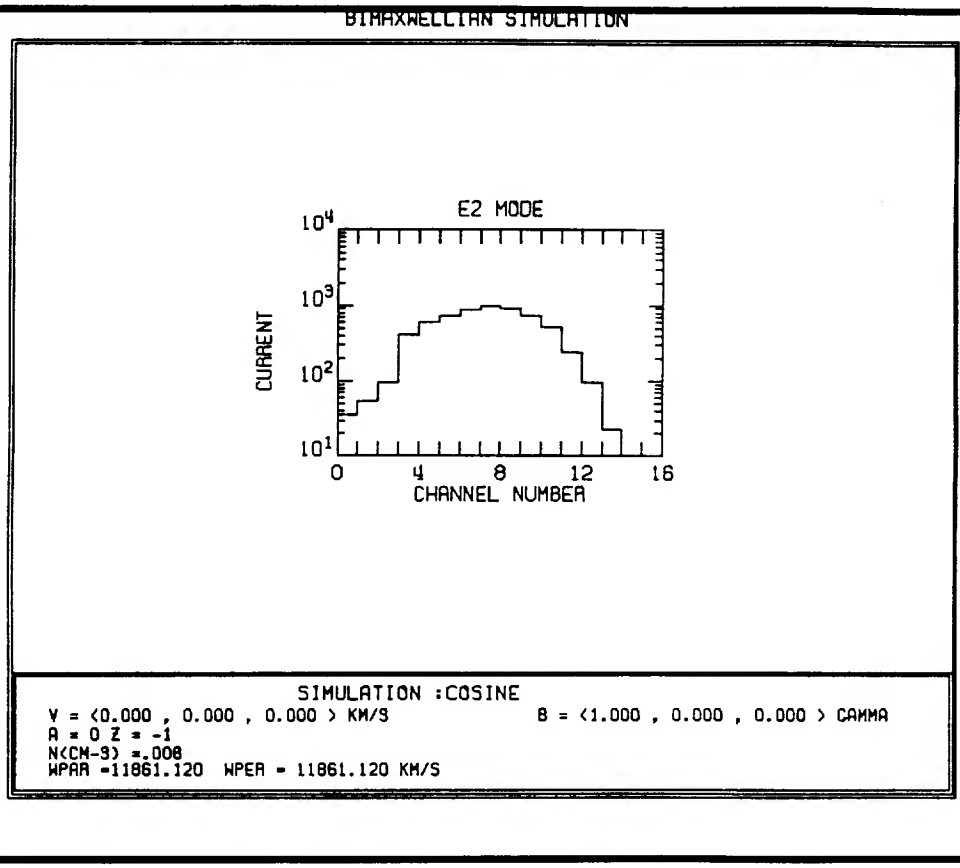

Figure 47

DSTEP = 1.0
~25 CPU MIN


```
0 VOYAGER DATA  -   CURRENTS (FA)    J=  3

 0.000e+00 0.000e+00 0.000e+00 0.000e+00 0.000e+00 0.000e+00 0.000e+00 0.000e+00
 0.000e+00 0.000e+00 0.000e+00 0.000e+00 0.000e+00 0.000e+00 0.000e+00 0.000e+00

0 VOYAGER DATA  -   CURRENTS (FA)    J=  4

 4.481e+02 7.197e+02 1.457e+03 1.349e+04 1.108e+04 9.847e+03 7.483e+03 6.282e+03
 5.321e+03 4.462e+03 3.824e+03 3.175e+03 2.584e+03 1.918e+03 1.854e+03 1.858e+02

TYPE 1 TO CONTINUE
```

```
\s+2\fBWAYNE
.sp
.nf
.ta 5.0i
        7 Co
        Lexi
        (617
.sp
.fi
.nf
.ta 0.5iC 1.
\fBObjective

\fBEducation
        1983
,

80,68000)

        1979
      to 1983

\fBProjects\

lice

"res.n" 64 1
|wlg@plas2[1
ptroff res.n
wlg@plas2[18
```

```
TYPE 1 TO CONTINUE
1
0PLOT SIMULATED DATA? 1=YES, 0=NO
1
 THE SCALE STARTS AT 1.00e+01 FEMTOAMPS AND GOES UP 4 DECADES
0CHANGE CURRENT SCALE FROM CURRENT VALUE? 1=YES, 0=NO
0


 Plot option [cefghnqw]: g
```

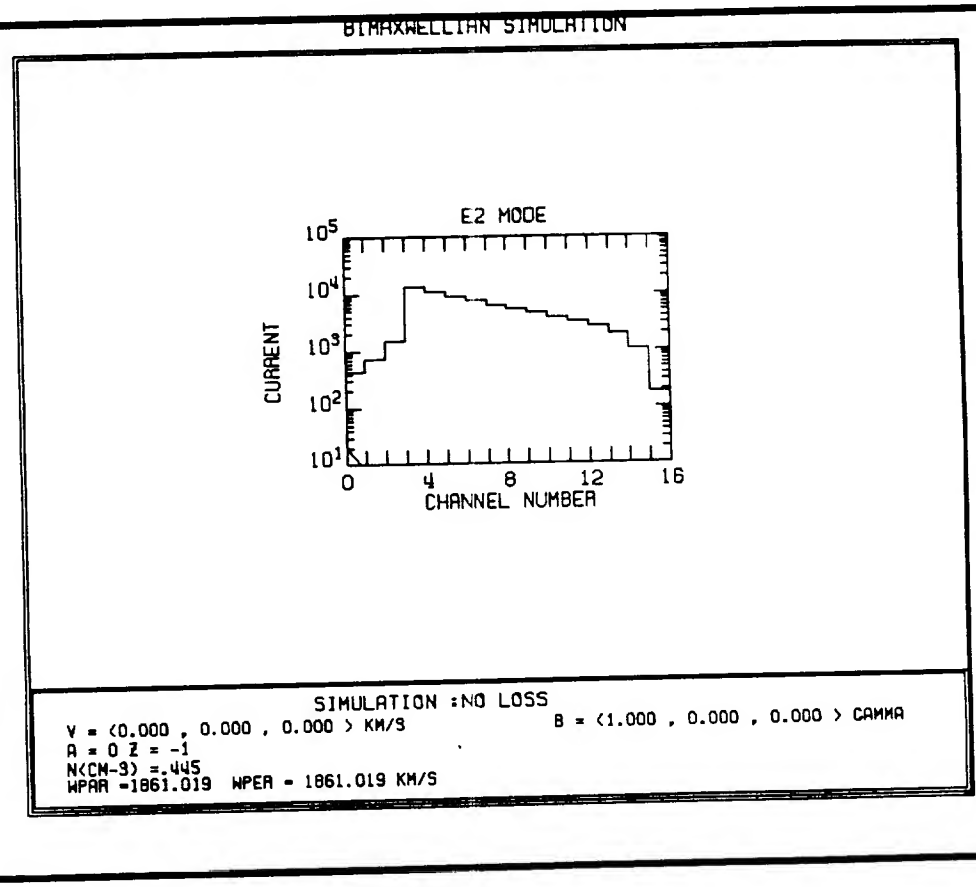


```
D
gsg/11
R
D
gsg/11
R
D
gsg/11
R
R
D
R
D
R
```

Figure 48

RSTEP=1.0
~45 CPU MIN

```
0 VOYAGER DATA  -   CURRENTS (FA)    J=  3

  0.000e+00 0.000e+00 0.000e+00 0.000e+00 0.000e+00 0.000e+00 0.000e+00 0.000e+00
  0.000e+00 0.000e+00 0.000e+00 0.000e+00 0.000e+00 0.000e+00 0.000e+00 0.000e+00

0 VOYAGER DATA  -   CURRENTS (FA)    J=  4

  3.503e+02 5.673e+02 1.173e+03 1.186e+04 9.096e+03 7.038e+03 5.544e+03 4.492e+03
  3.788e+03 3.217e+03 2.832e+03 2.429e+03 2.043e+03 1.555e+03 8.827e+02 1.588e+02

 TYPE 1 TO CONTINUE
1
```

```
C       TYPE 1 TO CONTINUE
      FUNCTI1
      COMMON0PLOT SIMULATED DATA? 1=YES, 0=NO
      REAL*81
      DATA A  THE SCALE STARTS AT 1.00e+01 FEMTOAMPS AND GOES UP 4 DECADES
      XMAX=00CHANGE CURRENT SCALE FROM CURRENT VALUE? 1=YES, 0=NO
C     0
C FUNCTION I
C FAC AND WT
C AKAP IS KA  Plot option [cefghnqw]: g
C     IF(W/W
C     WRITE
C 998 FORMAT
      W2=W**W
C     ZZZ=-W
C     IF (ZZ
      IF ( W
C
C FOR E1 MOD
C
C     IF (W
C
C CALCULATE
C
      ZZZ=WZ
      ARG1=A
C
C AG1 = GAMM
C
      AG1=DG
      ARG2=A
C
C AG2 = GAMM
C
      AG2=DG
      AFAC=F
      XMAX=A
C     WRITE
C 999 FORMAT
   15 RETURN
      END
C        01
C BIMAXWELLI
C
      FUNCTI
c      REAL*
c     | '
      COMMON
      XMAX=0
      IF(W/W
"xx.f" 62 1
win3 gsg[21]
win3 gsg[22]
```

BIMAXWELLIAN SIMULATION

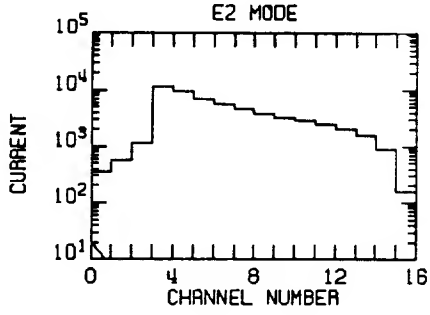

SIMULATION : isotropic Ross
V = (0.000 , 0.000 , 0.000) KM/S B = (1.000 , 0.000 , 0.000) GAMMA
A = 0 Z = -1
N(CM-3) =.445
WPAR =1861.019 WPER = 1861.019 KM/S

Figure 49

ORIGINAL PAGE IS OF POOR QUALITY

```
@ VOYAGER DATA  -   CURRENTS (FA)    J=  3

  0.000e+00 0.000e+00 0.000e+00 0.000e+00 0.000e+00 0.000e+00 0.000e+00 0.000e+00
  0.000e+00 0.000e+00 0.000e+00 0.000e+00 0.000e+00 0.000e+00 0.000e+00 0.000e+00

@ VOYAGER DATA  -   CURRENTS (FA)    J=  4

  9.778e+01 1.524e+02 2.839e+02 1.830e+03 1.980e+03 2.009e+03 1.939e+03 1.778e+03
  1.542e+03 1.245e+03 9.919e+02 7.455e+02 5.414e+02 3.554e+02 1.716e+02 2.781e+01

 TYPE 1 TO CONTINUE
```

```
1
@PLOT SIMULATED DATA? 1=YES, 0=NO
1
 THE SCALE STARTS AT 1.00e+01 FEMTOAMPS AND GOES UP 4 DECADES
@CHANGE CURRENT SCALE FROM CURRENT VALUE? 1=YES, 0=NO

@


 Plot option [cefghnqw]: g
```

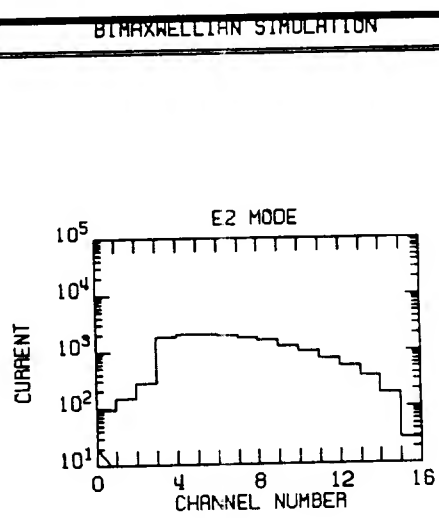

Figure 50

SPACE CRAFT SHOWN IN 0° ROLL ORIENTATION
ROLL ANGLE IS COUNTERCLOCKWISE ABOUT SPACECRAFT -Z AXIS

NOTE THAT ROL
DIRECTIONS
ARE SPACE FI
WHILE CLOCK
DIRECTIONS A
SPACECRAFT F

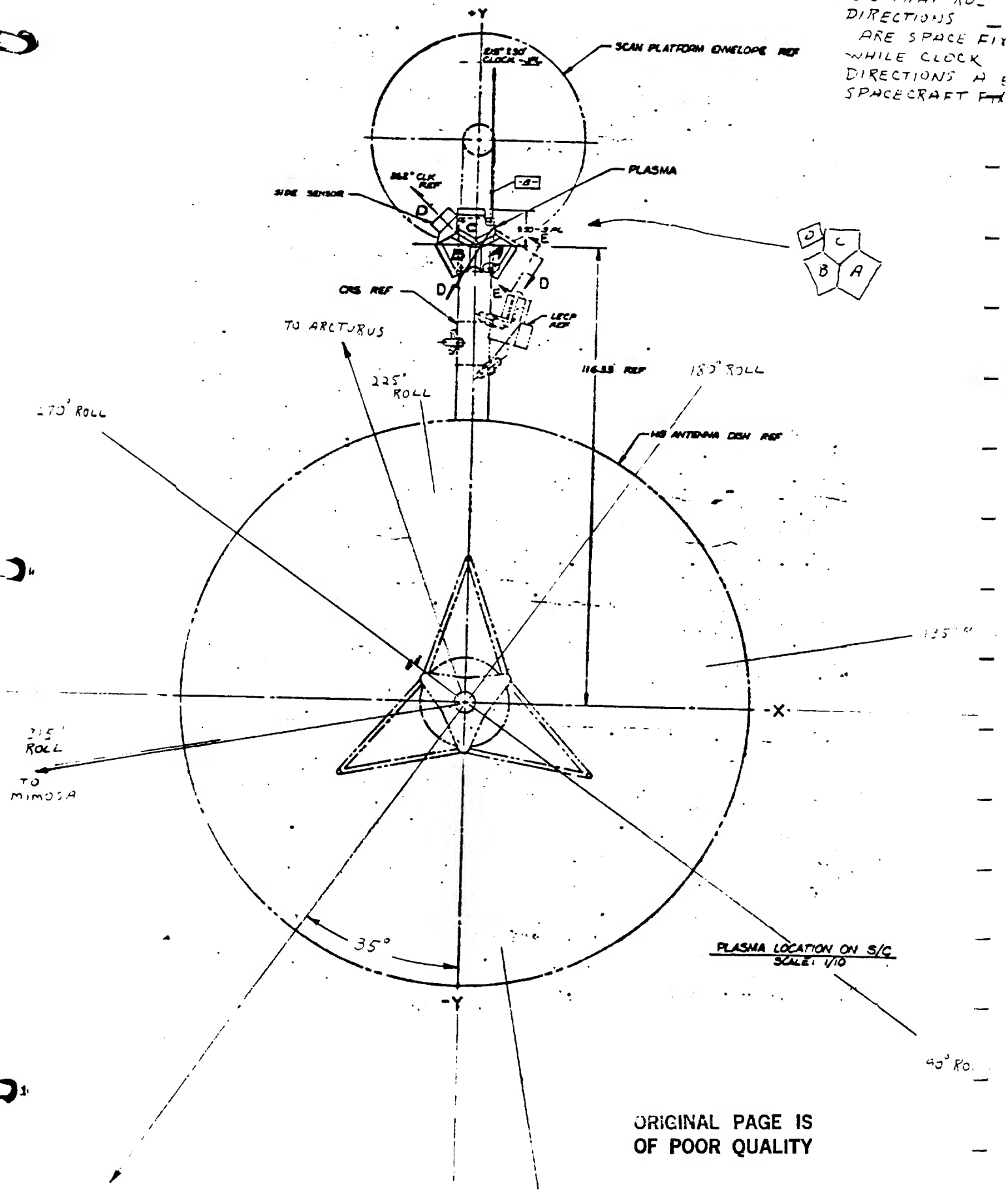

Figure 51

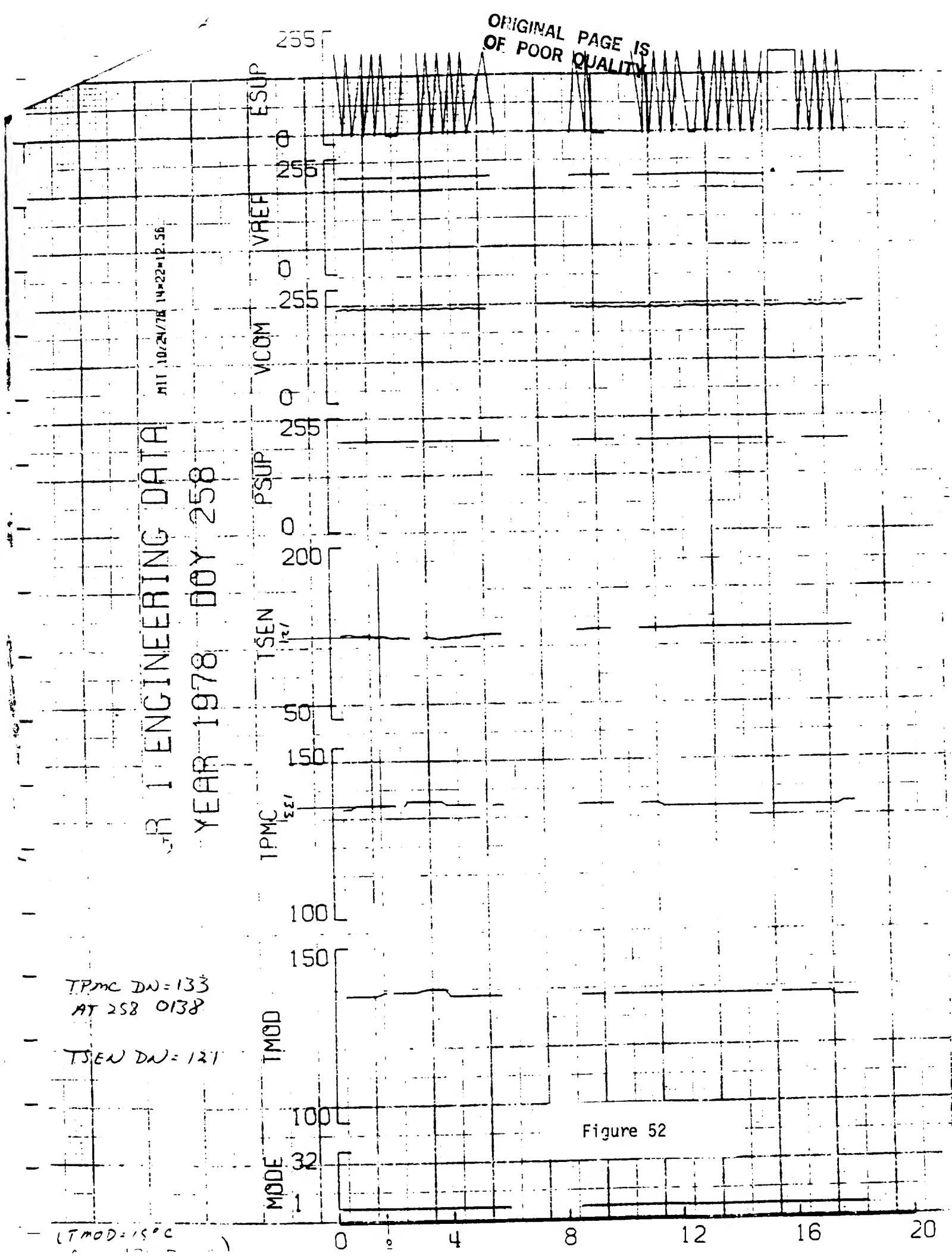

Figure 52

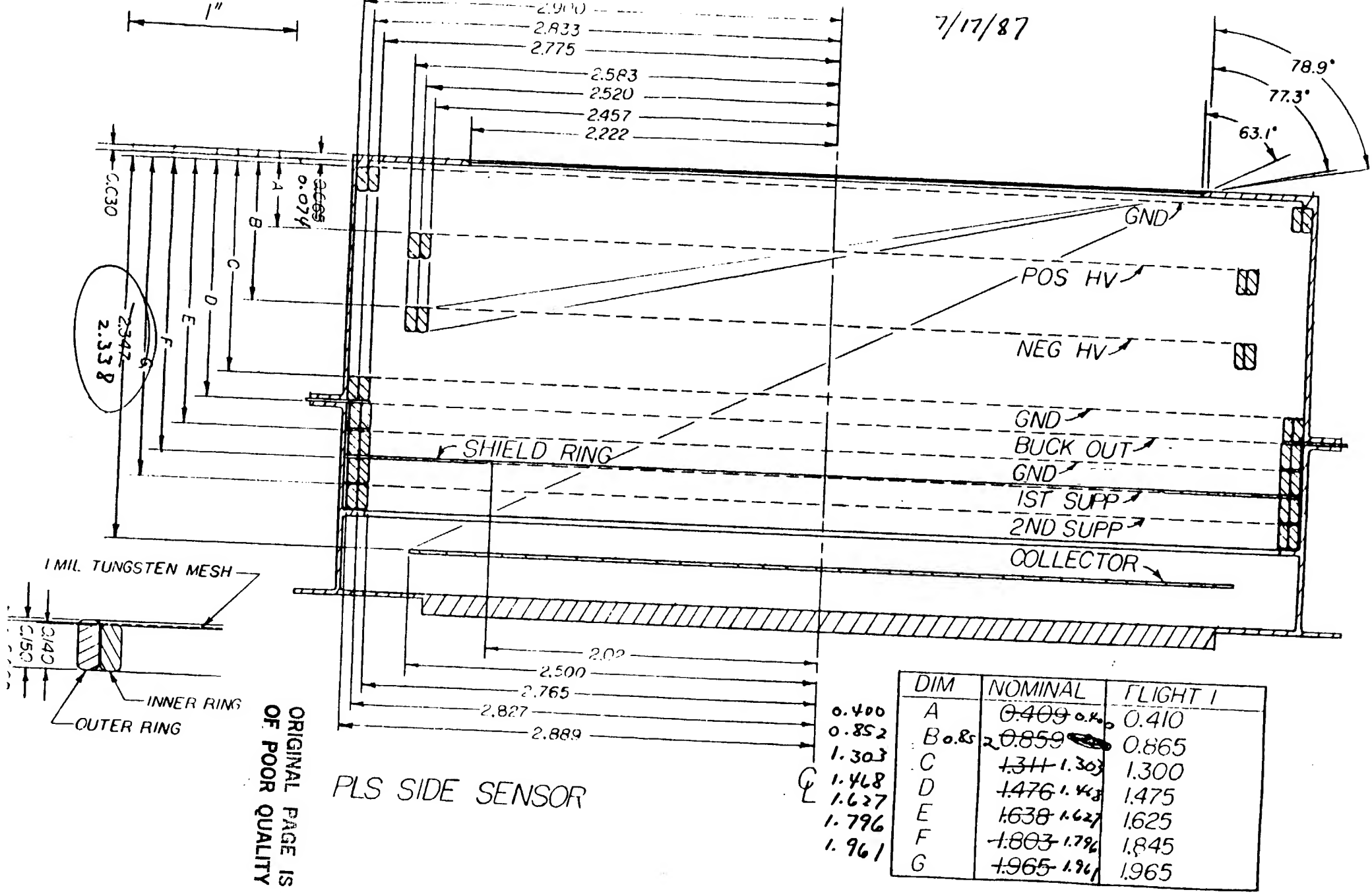

DIM	NOMINAL	FLIGHT 1
A	~~0.409~~ 0.400	0.410
B	0.85 ~~0.859~~	0.865
C	~~1.311~~ 1.303	1.300
D	~~1.476~~ 1.468	1.475
E	~~1.638~~ 1.627	1.625
F	~~1.803~~ 1.796	1.845
G	~~1.965~~ 1.961	1.965

ORIGINAL PAGE IS OF POOR QUALITY

Remains made on engine
7/21/87

Figure 53

Side Sensor - Vertical cut

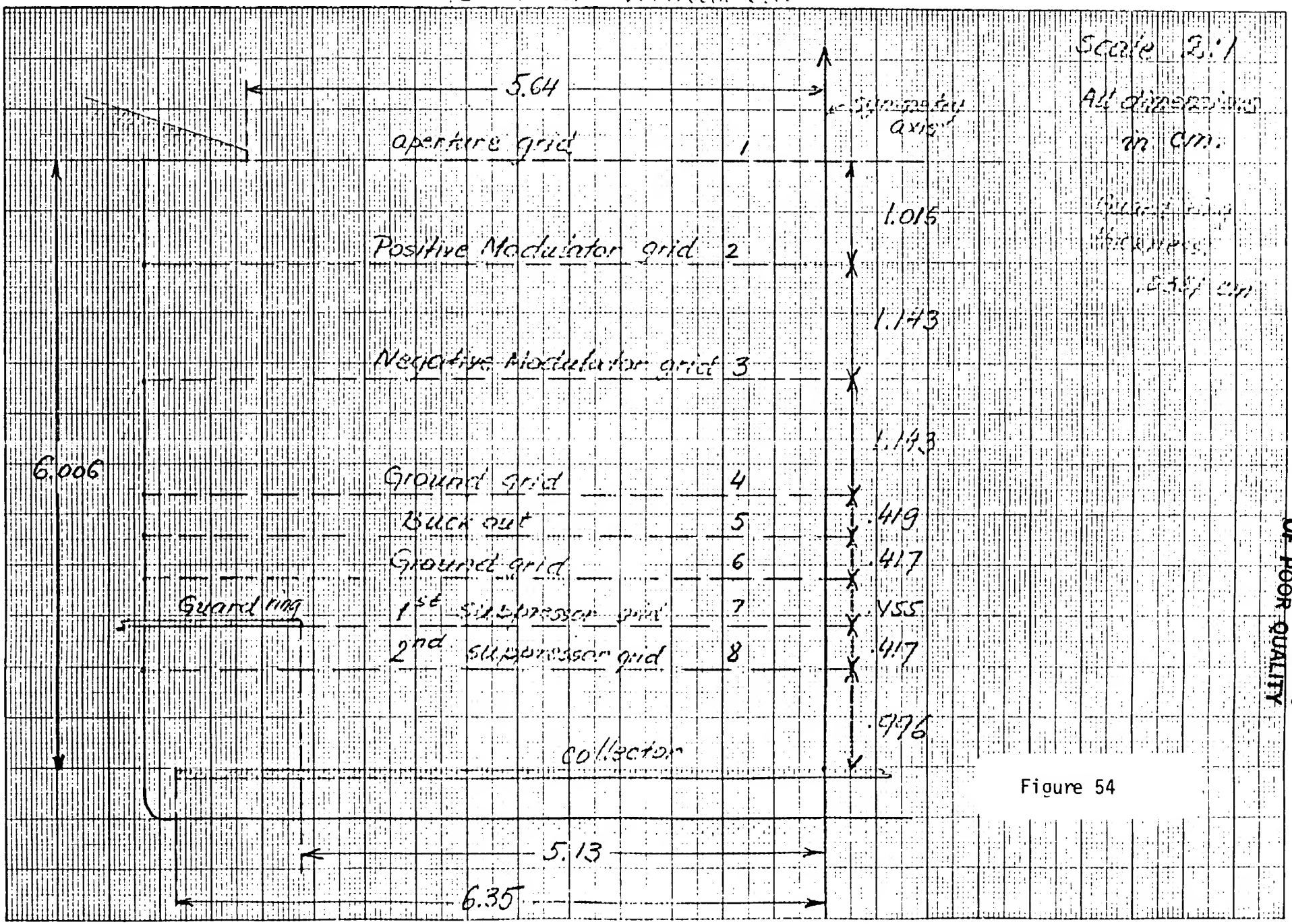

Figure 54

MOD ON NORMAL IDC

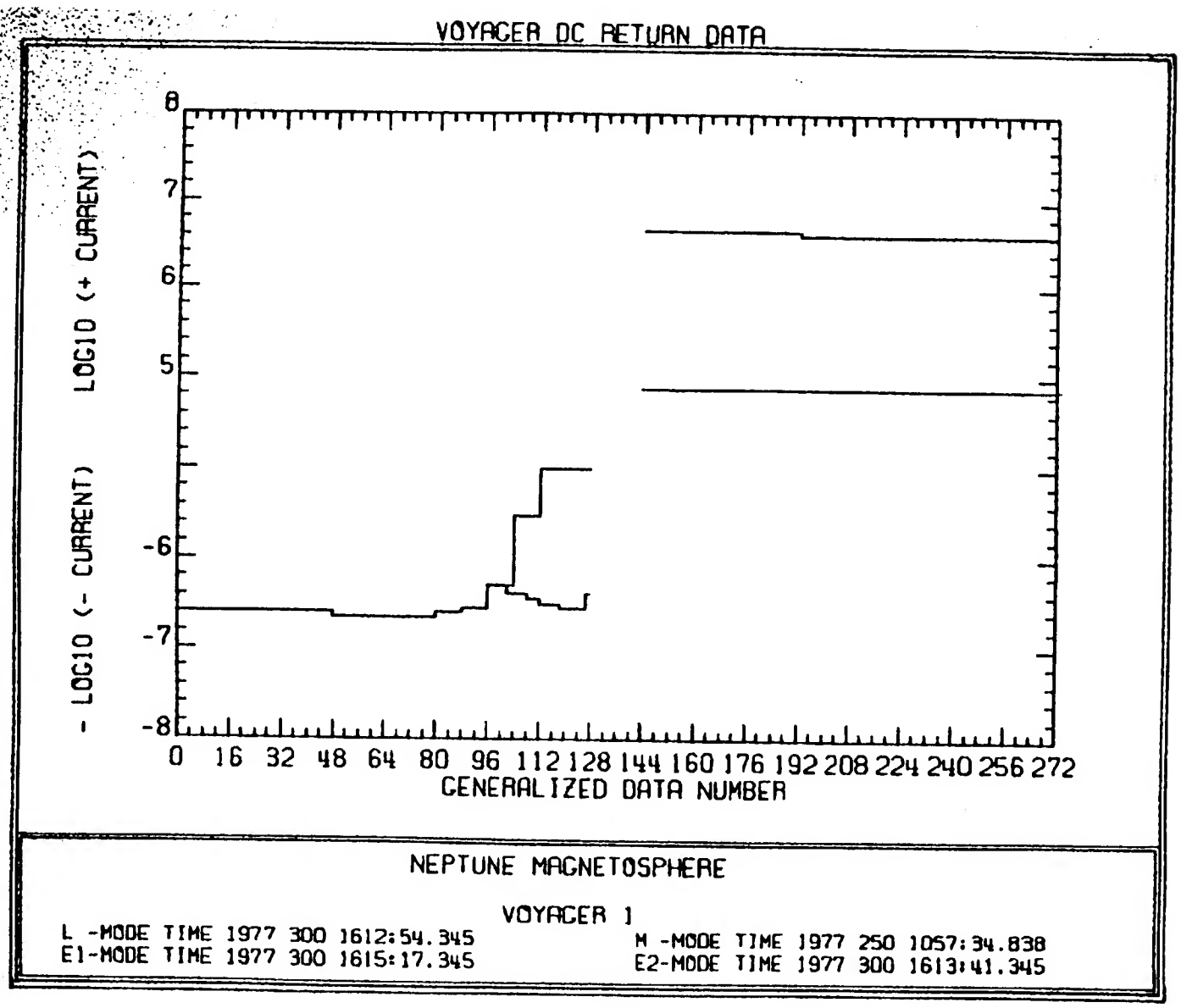

Figure 55

DC RET MOD ON
NORMAL

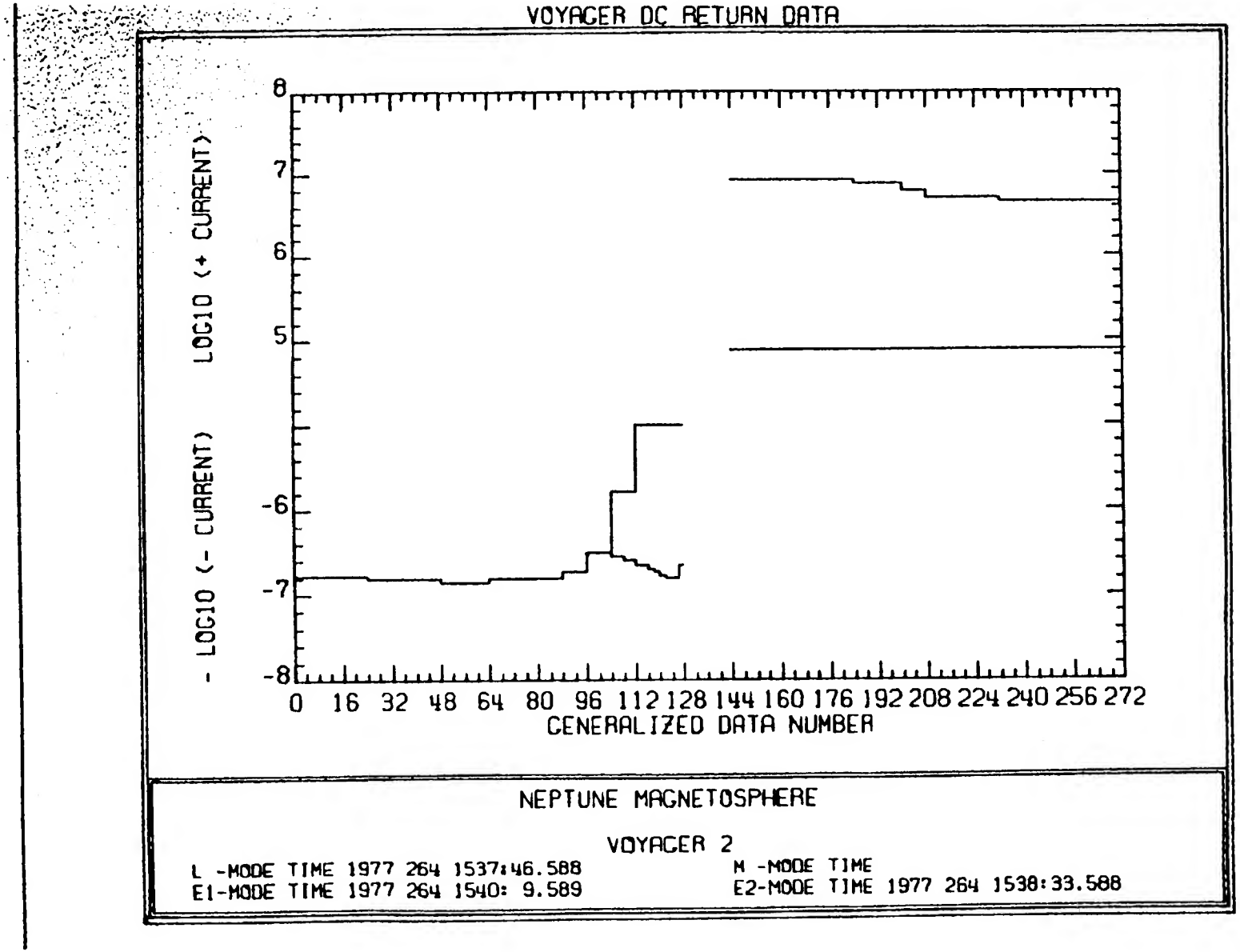

Figure 56

MOD ON - REV - IDC

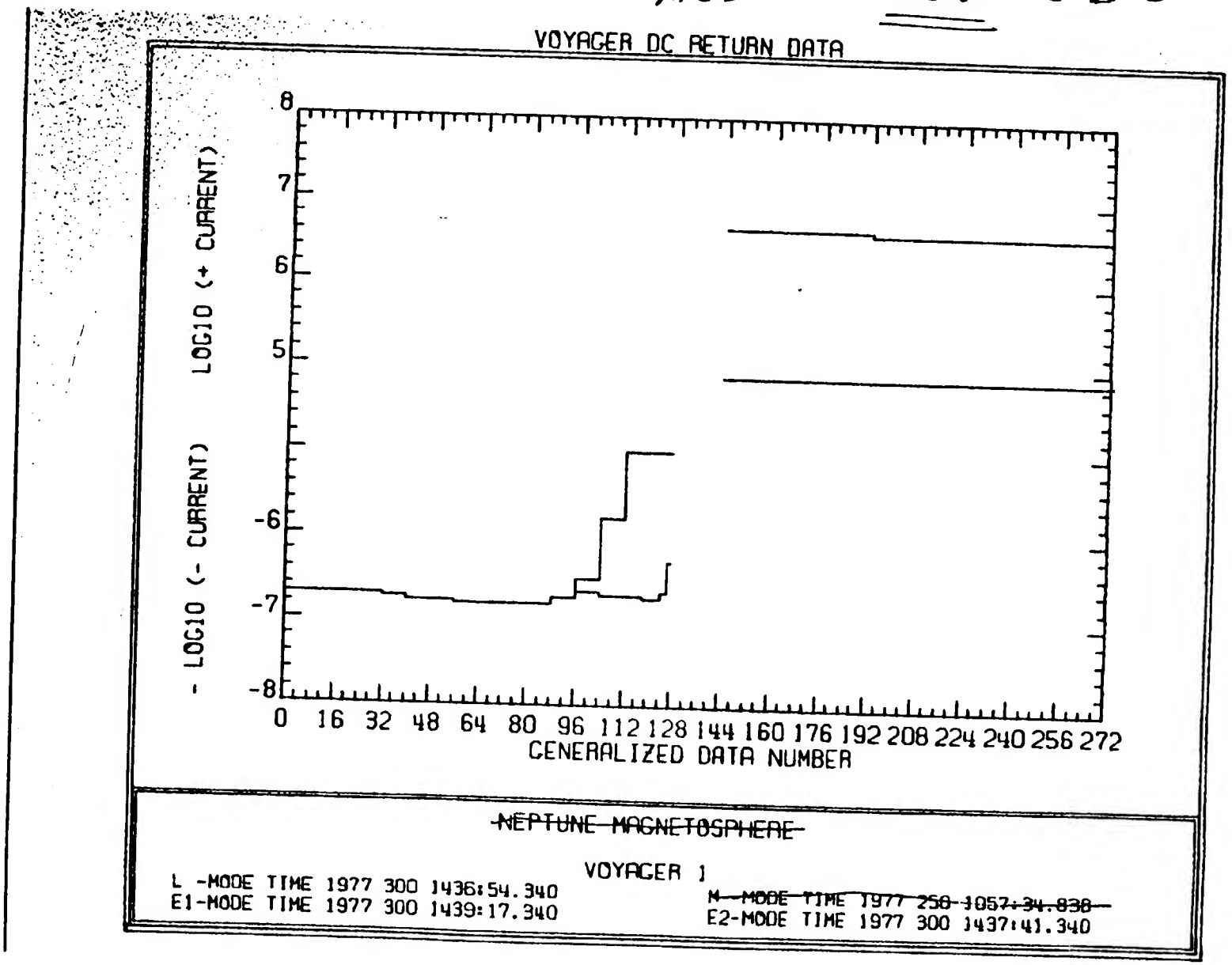

Figure 57

DC RET
MODON REV

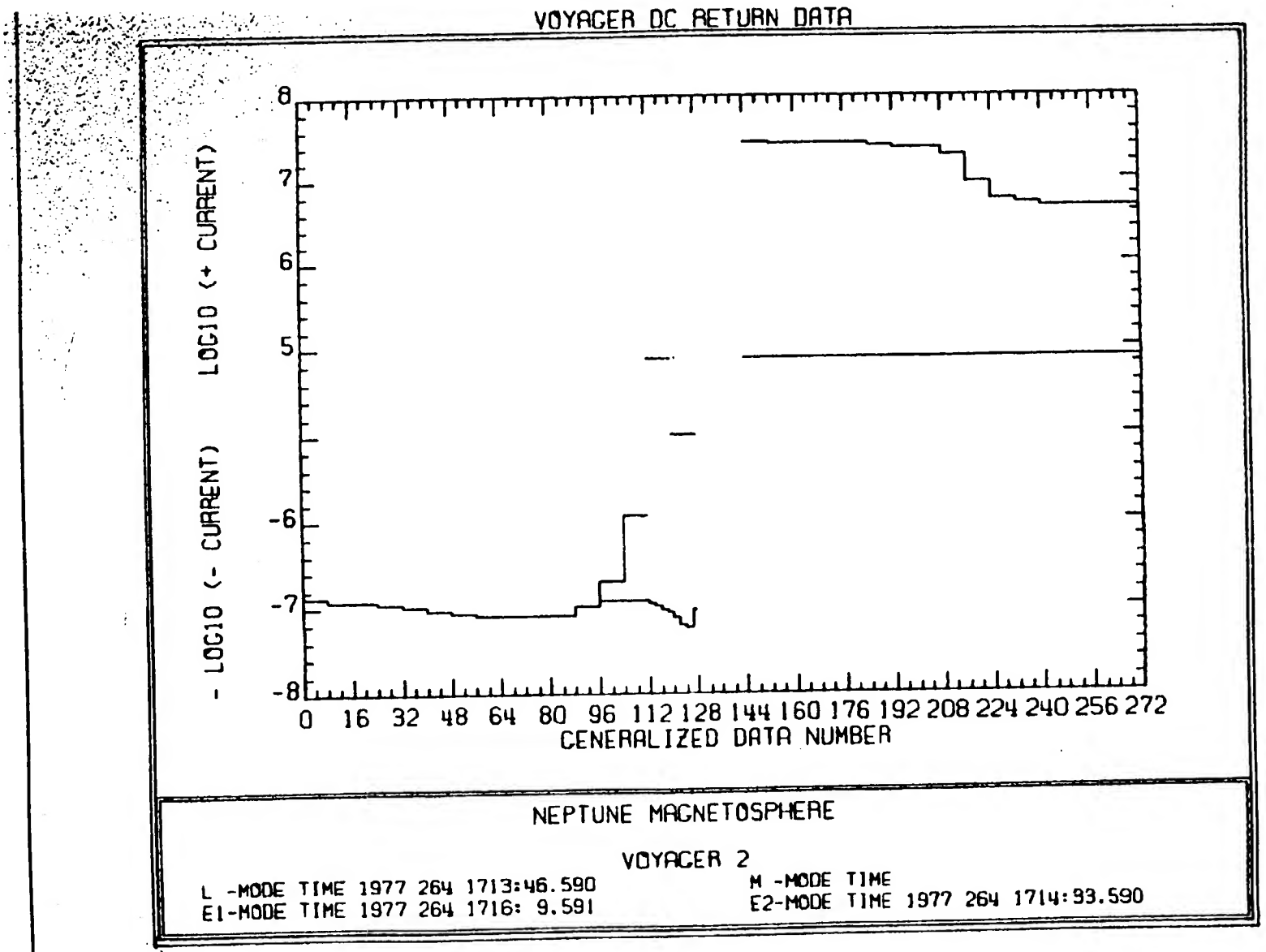

Figure 58

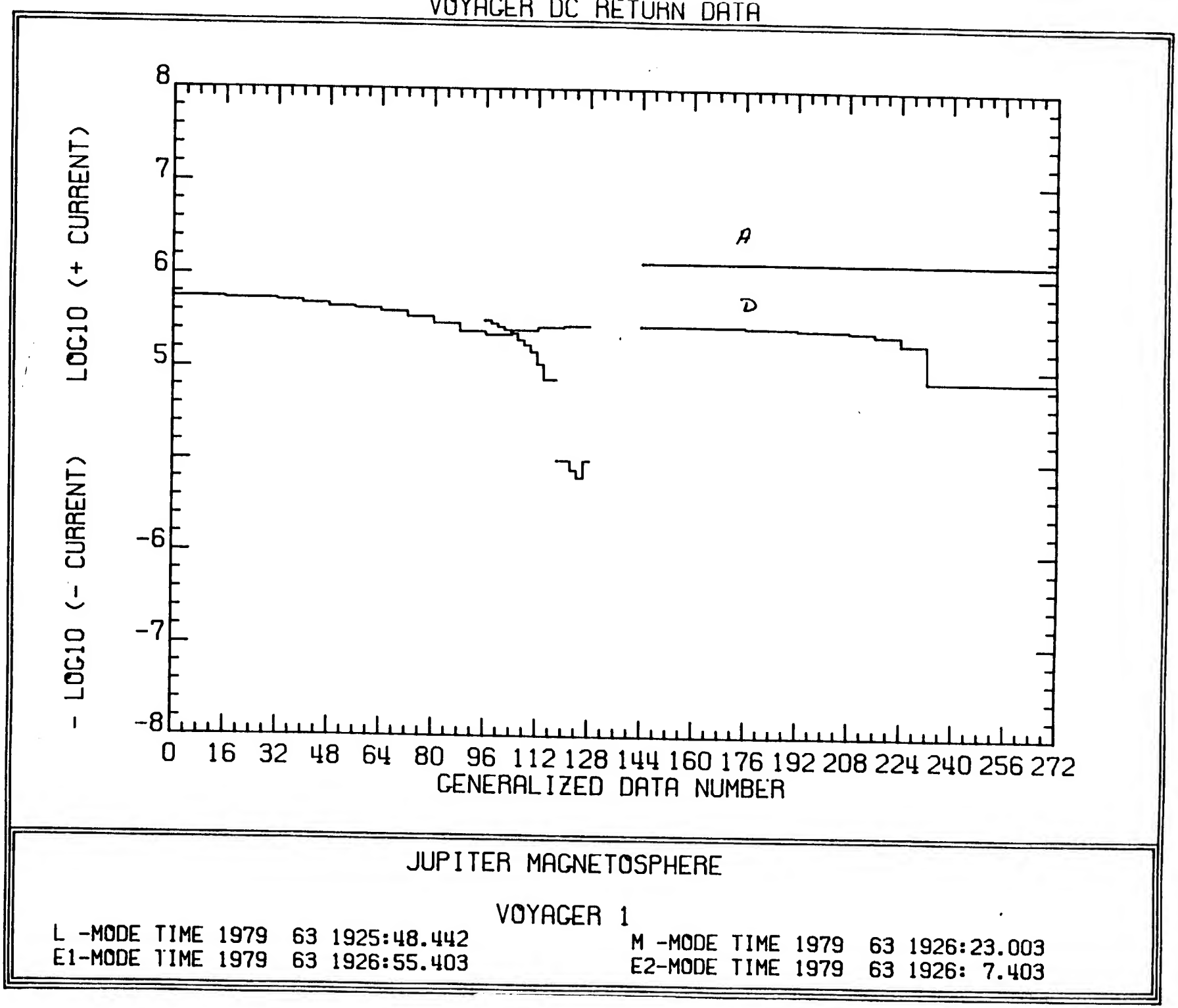
VOYAGER DC RETURN DATA
8
7
6
5
-6
-7
-8
LOG10 (+ CURRENT)
- LOG10 (- CURRENT)
A
D
0 16 32 48 64 80 96 112 128 144 160 176 192 208 224 240 256 272
GENERALIZED DATA NUMBER
JUPITER MAGNETOSPHERE
VOYAGER 1
L -MODE TIME 1979 63 1925:48.442
E1-MODE TIME 1979 63 1926:55.403
M -MODE TIME 1979 63 1926:23.003
E2-MODE TIME 1979 63 1926: 7.403

Figure 59

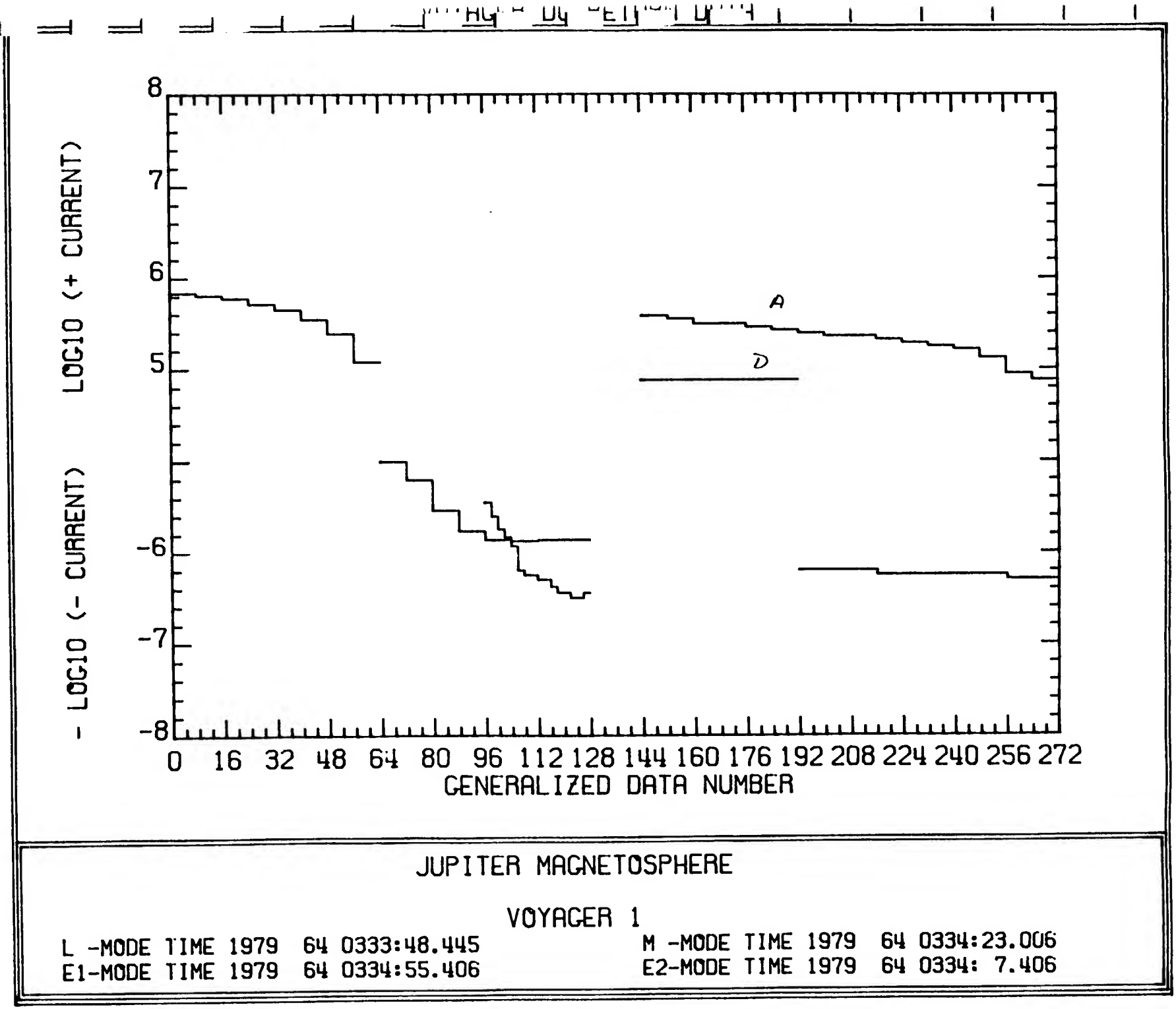
8
7
6
5
-6
-7
-8
LOG10 (+ CURRENT)
- LOG10 (- CURRENT)
A
D
0 16 32 48 64 80 96 112 128 144 160 176 192 208 224 240 256 272
GENERALIZED DATA NUMBER
JUPITER MAGNETOSPHERE
VOYAGER 1
L -MODE TIME 1979 64 0333:48.445
M -MODE TIME 1979 64 0334:23.006
E1-MODE TIME 1979 64 0334:55.406
E2-MODE TIME 1979 64 0334: 7.406

Figure 60

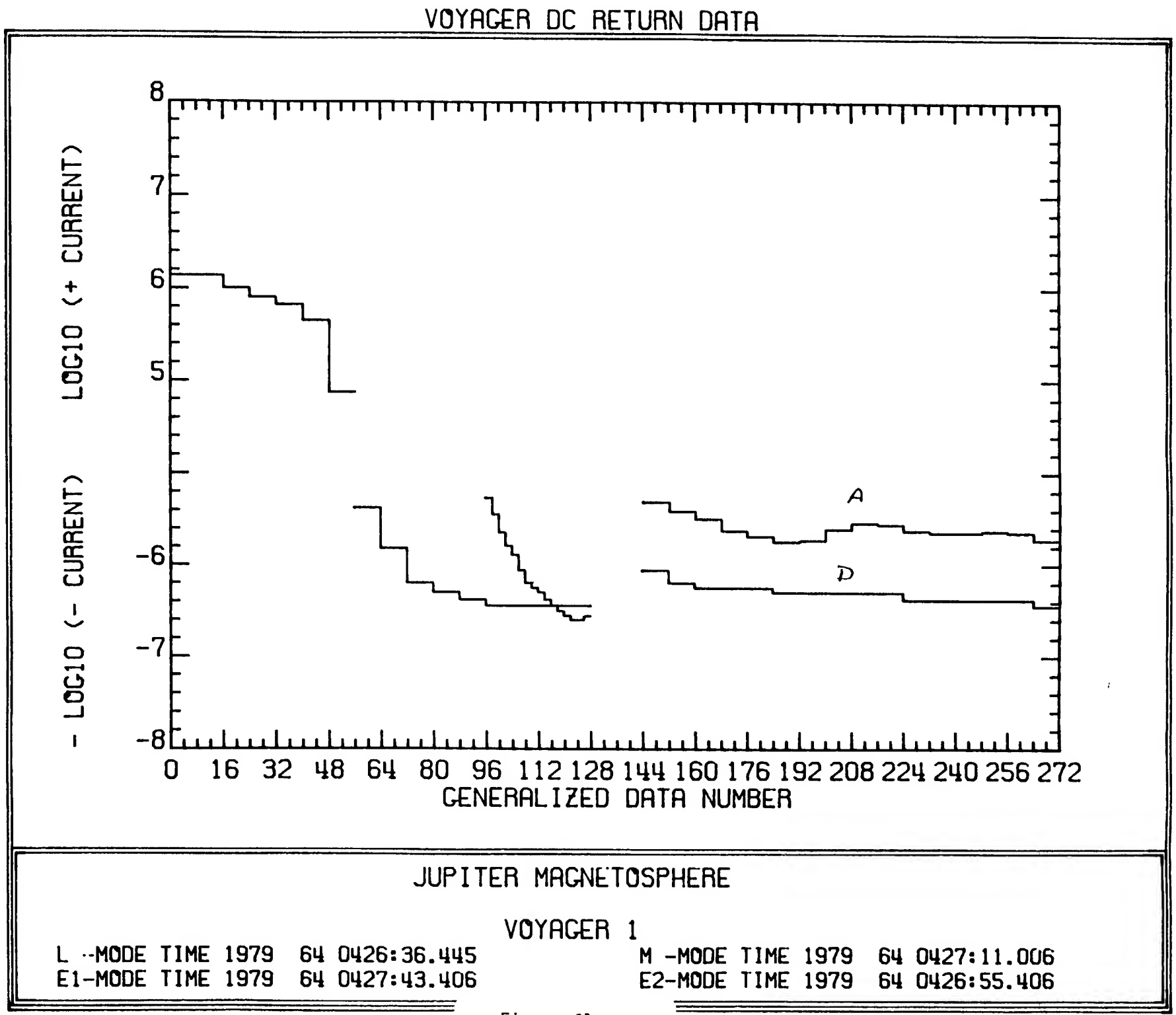

Figure 61

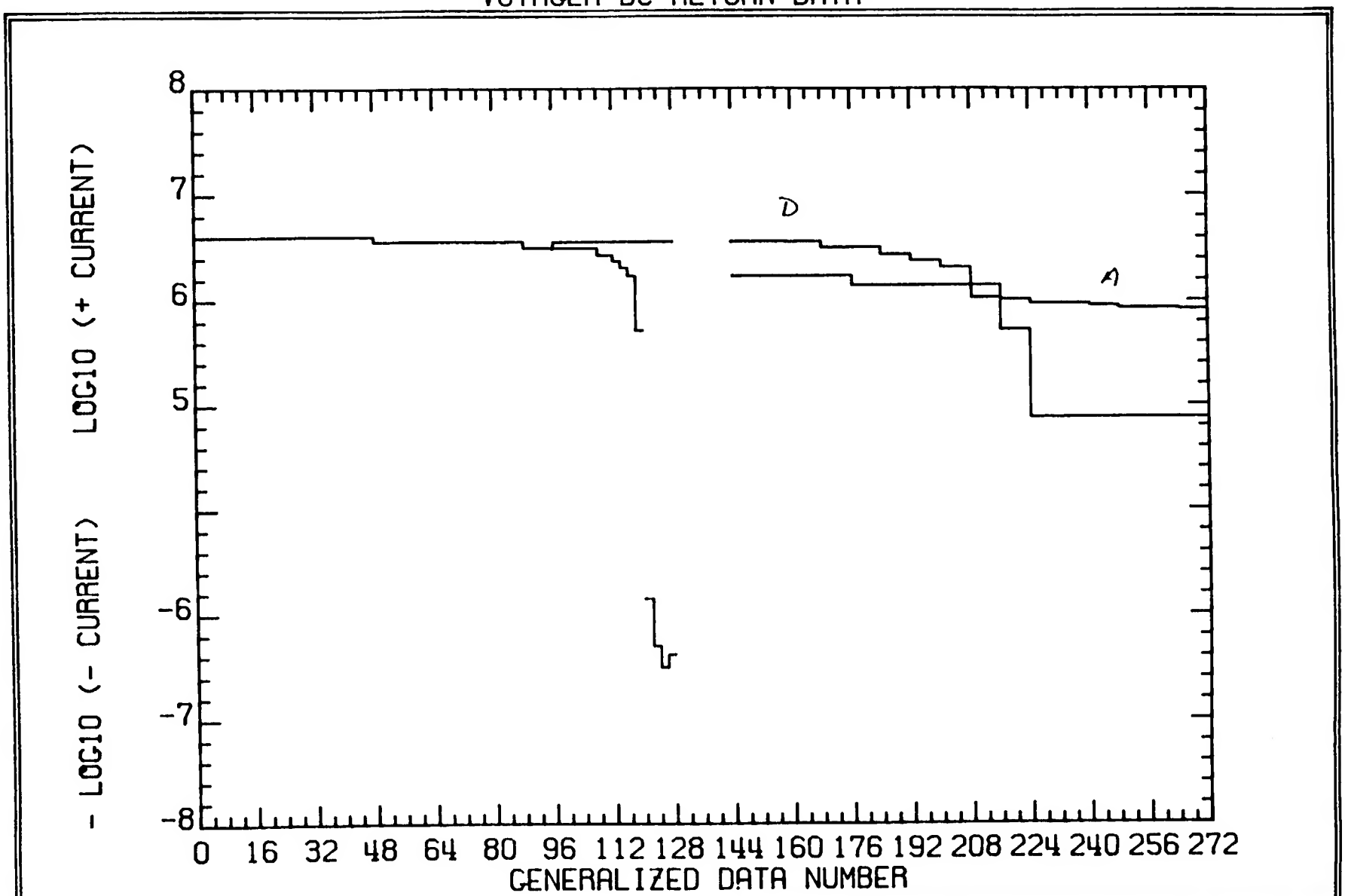

JUPITER MAGNETOSPHERE

VOYAGER 1

L -MODE TIME 1979 64 0503:24.446
E1--MODE TIME 1979 64 0504:31.407
M -MODE TIME 1979 64 0503:59.007
E2-MODE TIME 1979 64 0503:43.407

Figure 62

VOYAGER DC RETURN DATA
LOG10 (+ CURRENT)
- LOG10 (- CURRENT)
8
7
6
5
-6
-7
-8
0 16 32 48 64 80 96 112 128 144 160 176 192 208 224 240 256 272
GENERALIZED DATA NUMBER
A
D
JUPITER MAGNETOSPHERE
VOYAGER 1
L -MODE TIME 1979 64 0737: 0.445
E1-MODE TIME 1979 64 0738: 7.406
M -MODE TIME 1979 64 0737:35.006
E2-MODE TIME 1979 64 0737:19.406

Figure 63

VOYAGER DC RETURN DATA
LOG10 (+ CURRENT)
- LOG10 (- CURRENT)
8
7
6
5
-6
-7
-8
0 16 32 48 64 80 96 112 128 144 160 176 192 208 224 240 256 272
GENERALIZED DATA NUMBER
A
P
JUPITER MAGNETOSPHERE
VOYAGER 1
L -MODE TIME 1979 64 0921: 0.447
E1-MODE TIME 1979 64 0922: 7.408
M -MODE TIME 1979 64 0921:35.008
E2-MODE TIME 1979 64 0921:19.408

Figure 64

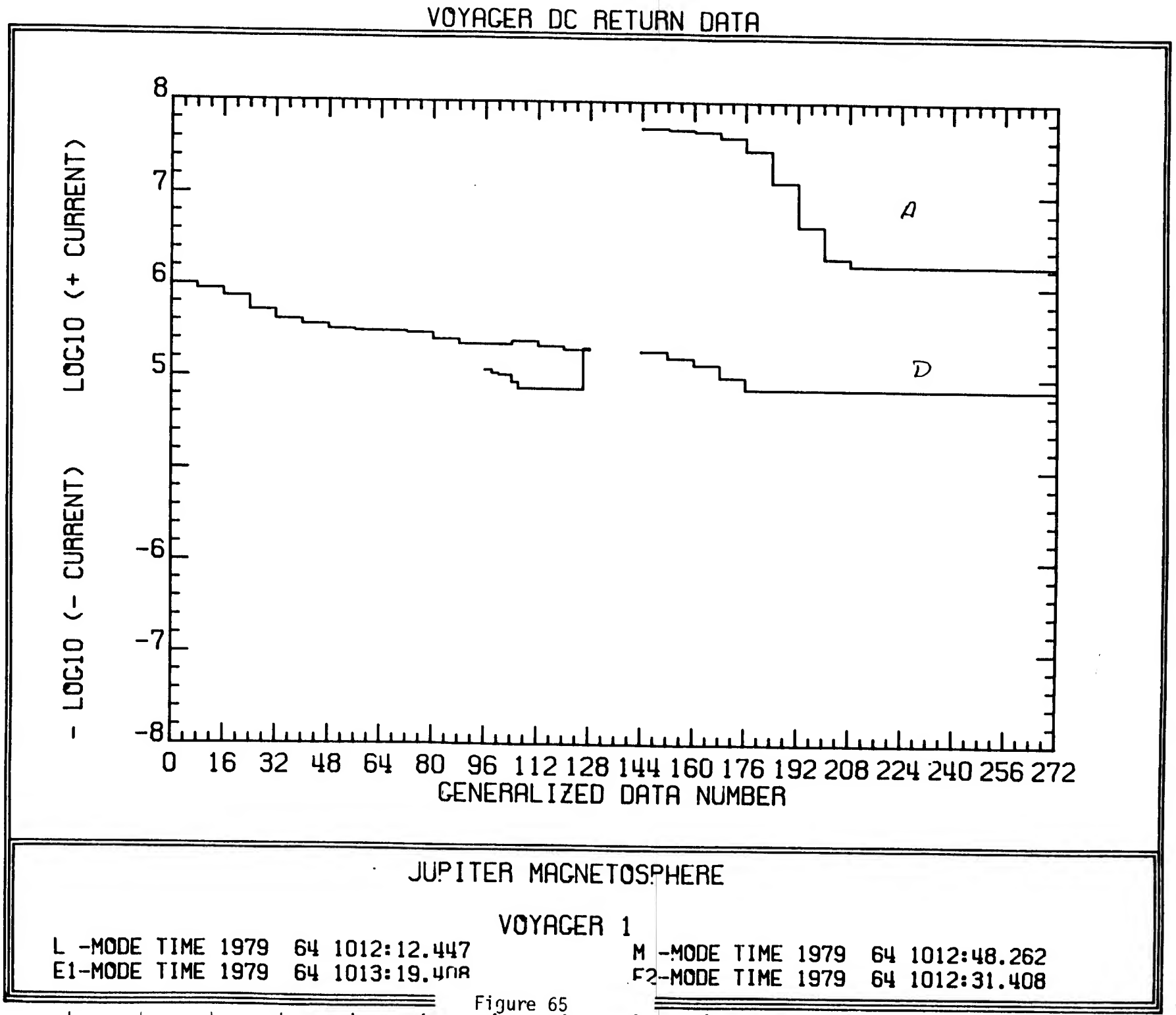

Figure 65

VOYAGER DC RETURN DATA
LOG10 (+ CURRENT)
- LOG10 (- CURRENT)
8
7
6
5
-6
-7
-8
A
D
0 16 32 48 64 80 96 112 128 144 160 176 192 208 224 240 256 272
GENERALIZED DATA NUMBER
JUPITER MAGNETOSPHERE
VOYAGER 1
L -MODE TIME 1979 64 1426:41.626
E1-MODE TIME 1979 64 1427:48.597
M -MODE TIME 1979 64 1427:16.192
DE TIME 1979 64 1427: 0.587

Figure 66

VOYAGER DC RETURN DATA

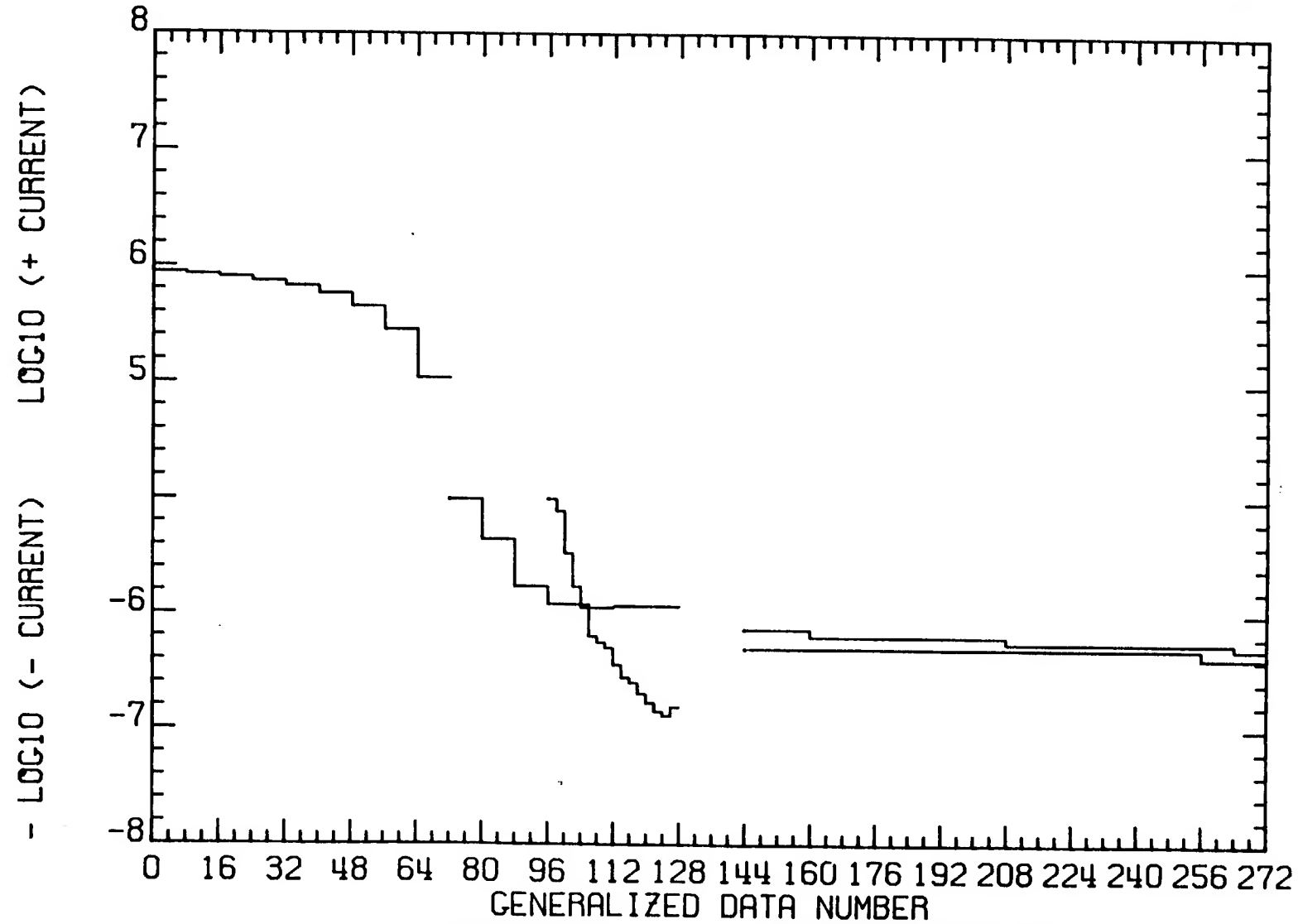

JUPITER MAGNETOSPHERE

VOYAGER 1

L -MODE TIME 1979 64 1829:55.382
E1-MODE TIME 1979 64 1831: 2.353
M -MODE TIME 1979 64 1830:29.948
E2-MODE TIME 1979 64 1830:14.343

Figure 67

R. L. MCNUTT, JR M I T

VOYAGER DC RETURN DATA
LOG10 (+ CURRENT)
- LOG10 (- CURRENT)
8
7
6
5
-6
-7
-8
0 16 32 48 64 80 96 112 128 144 160 176 192 208 224 240 256 272
GENERALIZED DATA NUMBER
A
JUPITER MAGNETOSPHERE
VOYAGER 1
L -MODE TIME 1979 64 1921: 7.711
E1-MODE TIME 1979 64 1922:14.682
M -MODE TIME 1979 64 1921:42.277
E2-MODE TIME 1979 64 1921:26.672

Figure 68

VOYAGER DC RETURN DATA
LOG10 (+ CURRENT)
- LOG10 (- CURRENT)
8
7
6
5
-6
-7
-8
0 16 32 48 64 80 96 112 128 144 160 176 192 208 224 240 256 272
GENERALIZED DATA NUMBER
SATURN MAGNETOSPHERE
VOYAGER 1
L -MODE TIME 1980 318 0343:23.564
E1-MODE TIME 1980 318 0344:30.525
M -MODE TIME 1980 318 0343:58.125
E2-MODE TIME 1980 318 0343:42.525

Figure 69

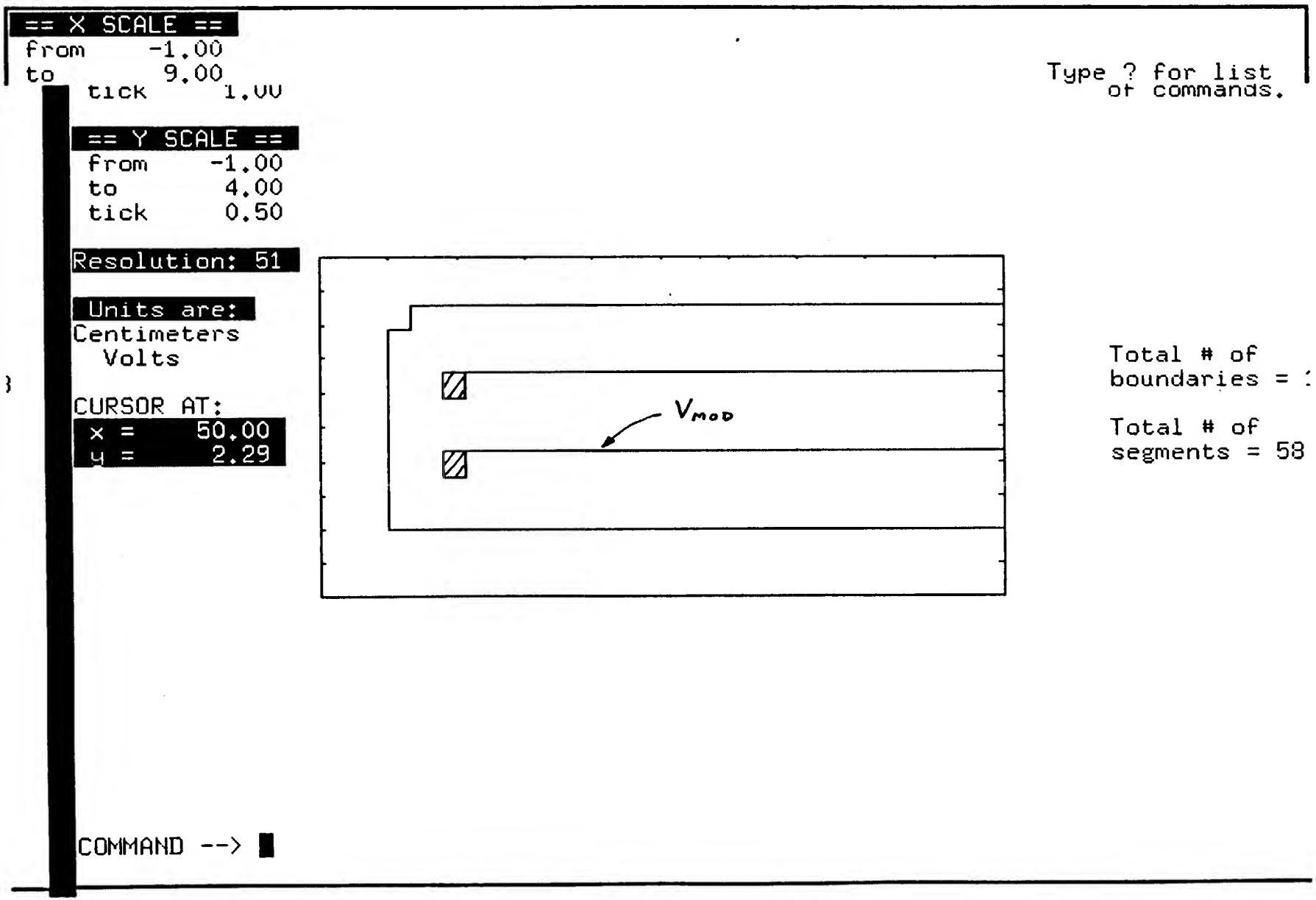
== X SCALE ==
from -1.00
to 9.00
tick 1.00
== Y SCALE ==
from -1.00
to 4.00
tick 0.50
Resolution: 51
Units are:
Centimeters
Volts
CURSOR AT:
x = 50.00
y = 2.29
Type ? for list
of commands.
V_{MOD}
Total # of
boundaries = 1
Total # of
segments = 58
COMMAND -->

Figure 70

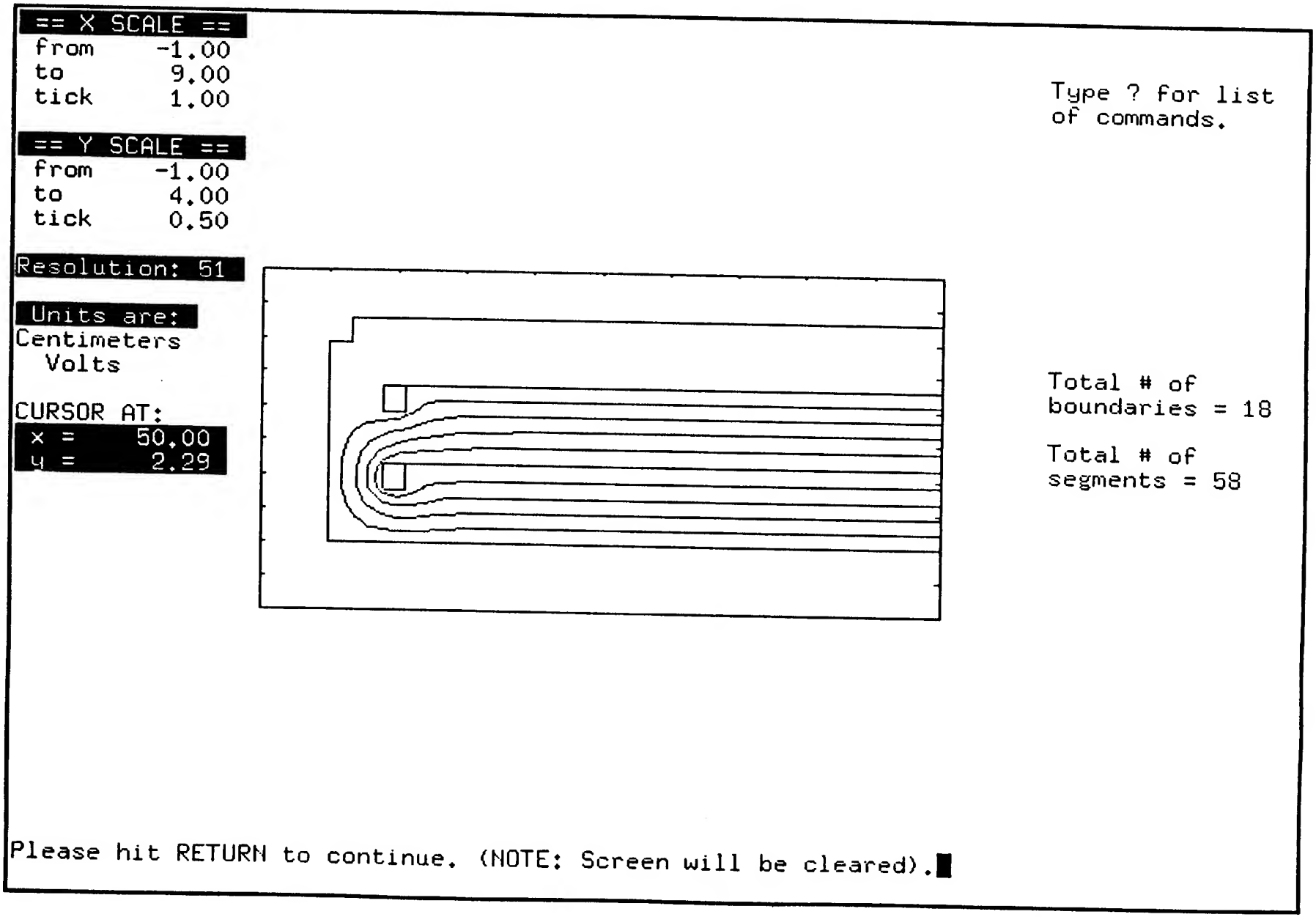
== X SCALE ==
from -1.00
to 9.00
tick 1.00
== Y SCALE ==
from -1.00
to 4.00
tick 0.50
Resolution: 51
Units are:
Centimeters
Volts
CURSOR AT:
x = 50.00
y = 2.29
Type ? for list of commands.
Total # of boundaries = 18
Total # of segments = 58
Please hit RETURN to continue. (NOTE: Screen will be cleared).

Figure 71

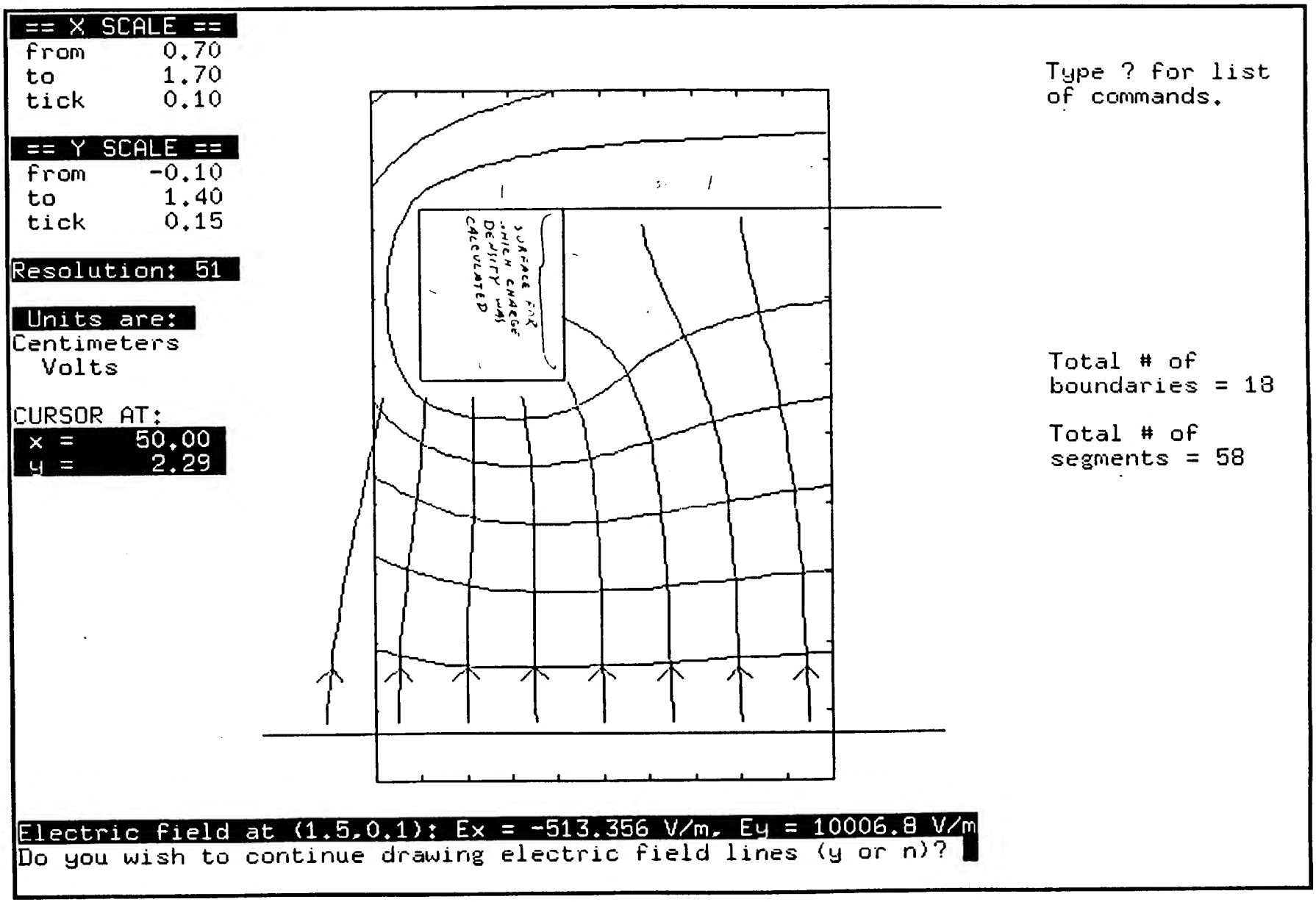
== X SCALE ==
from 0.70
to 1.70
tick 0.10
== Y SCALE ==
from -0.10
to 1.40
tick 0.15
Resolution: 51
Units are:
Centimeters
Volts
CURSOR AT:
x = 50.00
y = 2.29
Type ? for list of commands.
Total # of boundaries = 18
Total # of segments = 58
Electric field at (1.5,0.1): Ex = -513.356 V/m, Ey = 10006.8 V/m
Do you wish to continue drawing electric field lines (y or n)?

Figure 72

$$\frac{dz}{dw} = -\frac{\sqrt{(w^2-a^2)}}{w^2-1}, \quad 0 < a < 1.$$

$$z = \frac{i\pi}{2} - \cosh^{-1}\frac{w}{a} + \frac{(1-a^2)^{1/2}}{2}\cosh^{-1}\frac{w^2(2-a^2)-a^2}{a^2(w^2-1)}.$$

z - plane | w - plane

points $z = 0;\ -ih;\ ih$ | points $w = 0;\ -a;\ a$

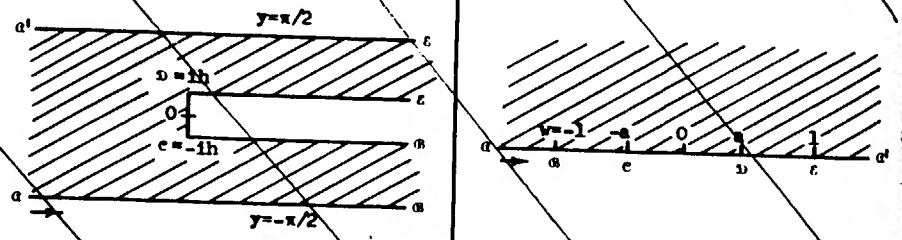

$$a = \frac{2}{\pi}\sqrt{(\pi h - h^2)}, \quad 0 < h = \frac{1}{2}\pi - \frac{1}{2}\pi\sqrt{(1-a^2)} < \frac{1}{2}\pi$$

12.8 Further transformations.

$$\frac{dz}{dw} = -\frac{w}{(w+1)^\beta}, \quad 0 < \beta < 1; \quad z = -\frac{1}{2-\beta}(w+1)^{2-\beta} + \frac{1}{1-\beta}(w+1)^{1-\beta}.$$

z - plane | w - plane

points $z = 0;\ \{(1-\beta)(2-\beta)\}^{-1} = z_0$ | points $w = -1;\ 0$

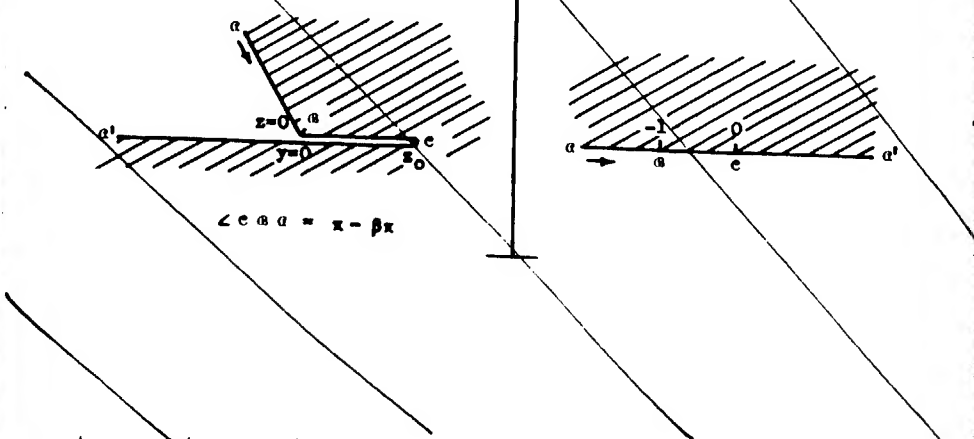

$$\angle e\,\beta\,\alpha = \pi - \beta\pi$$

$$\frac{dz}{dw} = \frac{k(w-1)^{1/2}}{\pi w(w-c)^{1/2}}, \quad c > 1; \quad k > 0, \ kc^{-1/2} = h$$

$$z = \frac{k}{\pi}\cosh^{-1}\left(\frac{2w-c-1}{c-1}\right) - \frac{k}{\pi\sqrt{c}}\cosh^{-1}\left(\frac{(c+1)w-2c}{(c-1)w}\right)$$

z - plane | w - plane

points $i(k-h) = z_1;\ 0$ | points $w = 1;\ c$

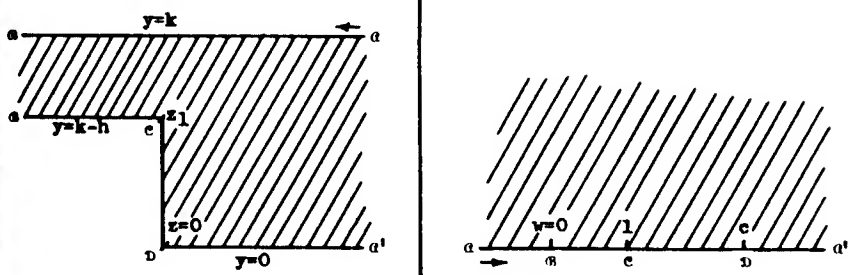

$$\frac{dz}{dw} = \left(\frac{w+1}{w-1}\right)^\beta, \quad 0 < \beta < 1.$$

Representable in terms of elementary functions, if $\beta = p/q$ (p, q integers):

$$z = 2q\int_\zeta^\infty t^{p+q-1}(t^q-1)^{-2}\,dt, \text{ where } \zeta = (w+1)^{1/q}(w-1)^{-1/q}.$$

z - plane | w - plane

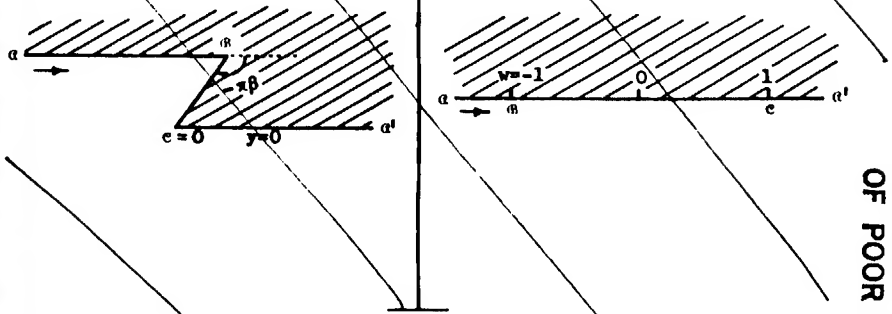

Figure 73

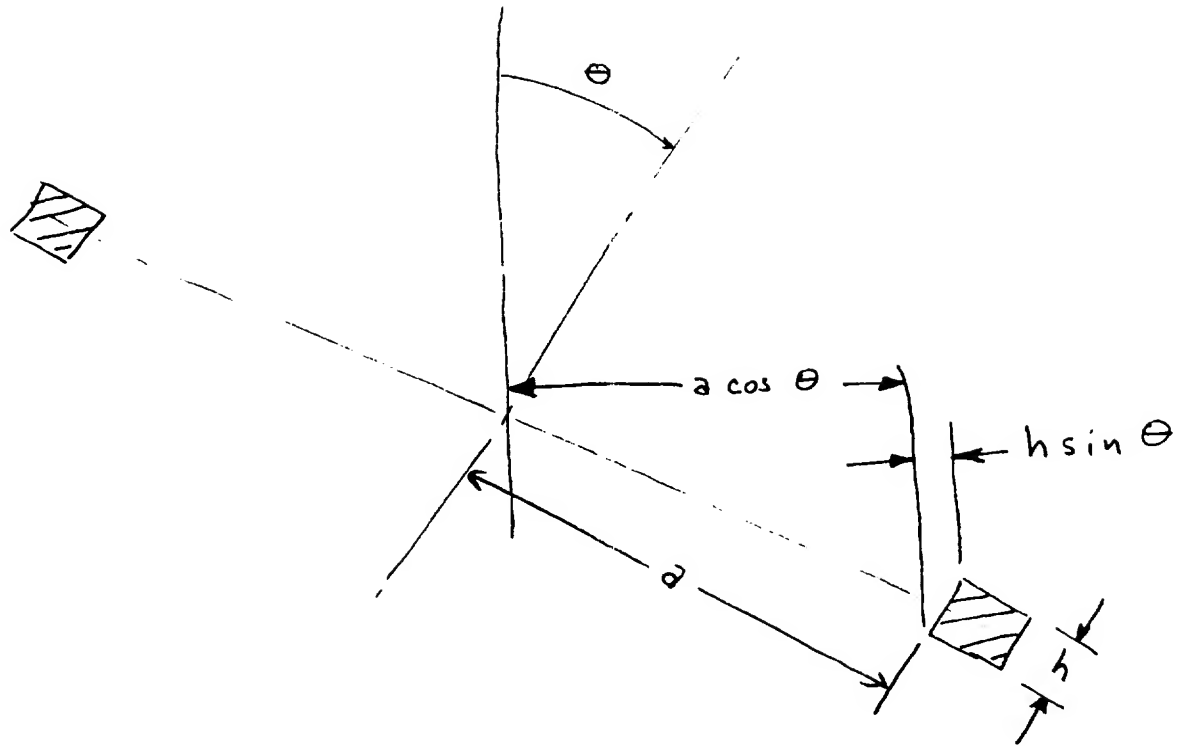

SIDE VIEW

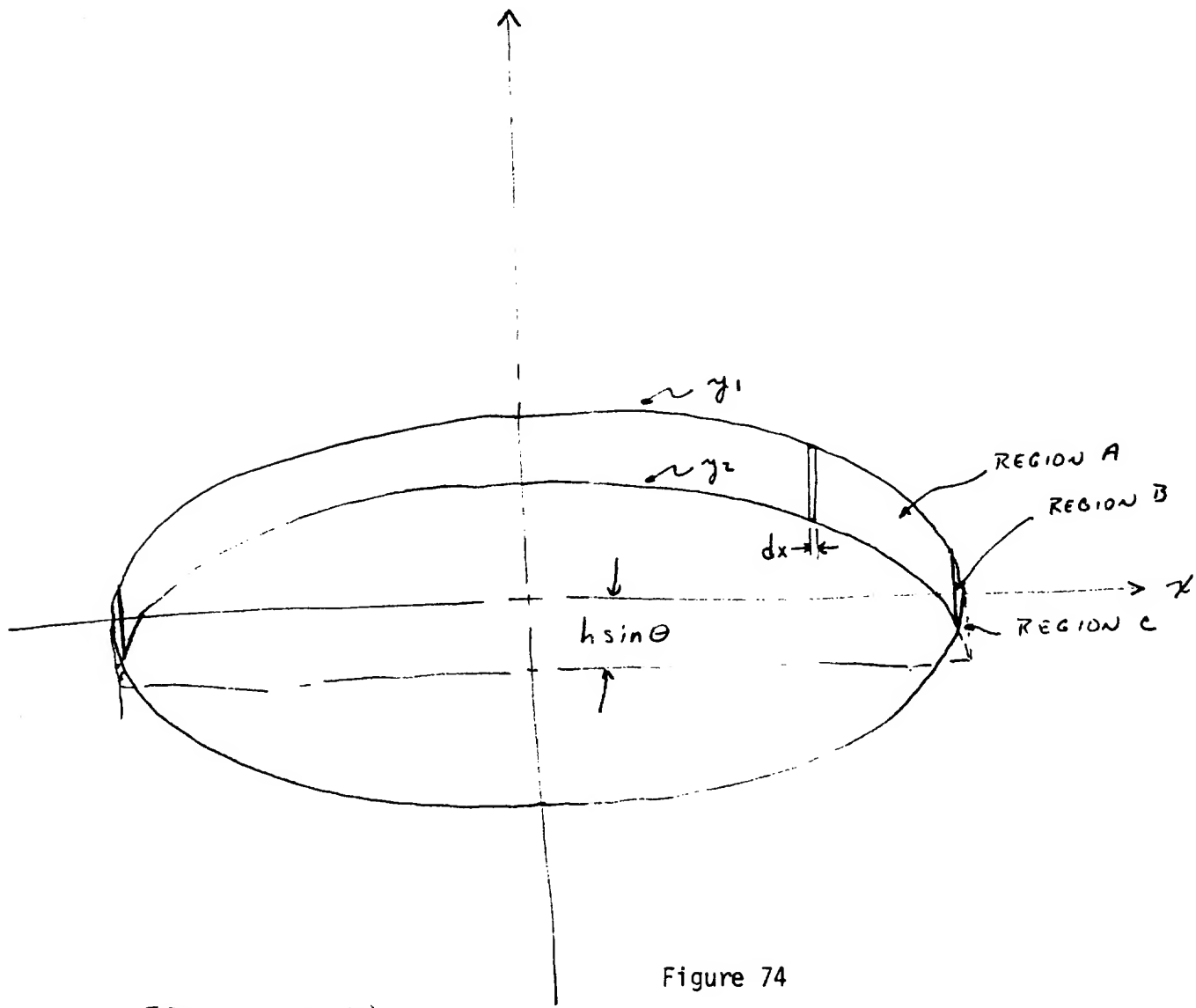

FRONT VIEW

Figure 74

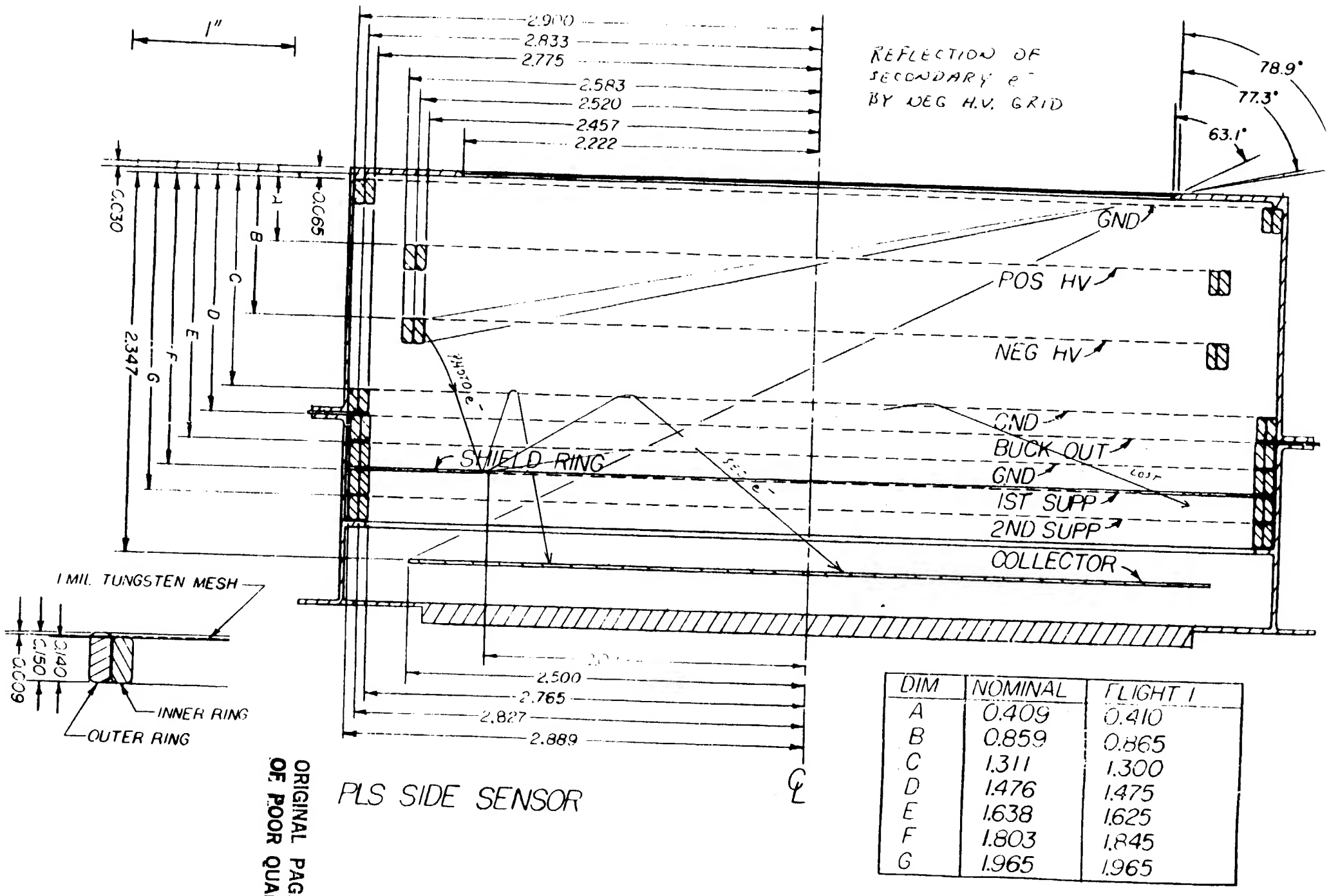

DIM	NOMINAL	FLIGHT 1
A	0.409	0.410
B	0.859	0.865
C	1.311	1.300
D	1.476	1.475
E	1.638	1.625
F	1.803	1.845
G	1.965	1.965

Figure 75

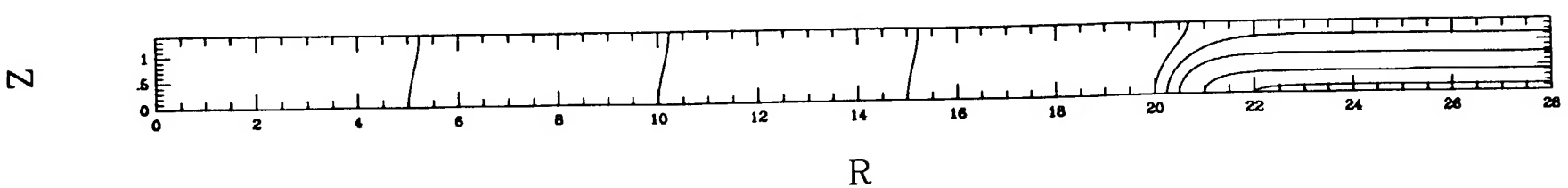

Figure 76

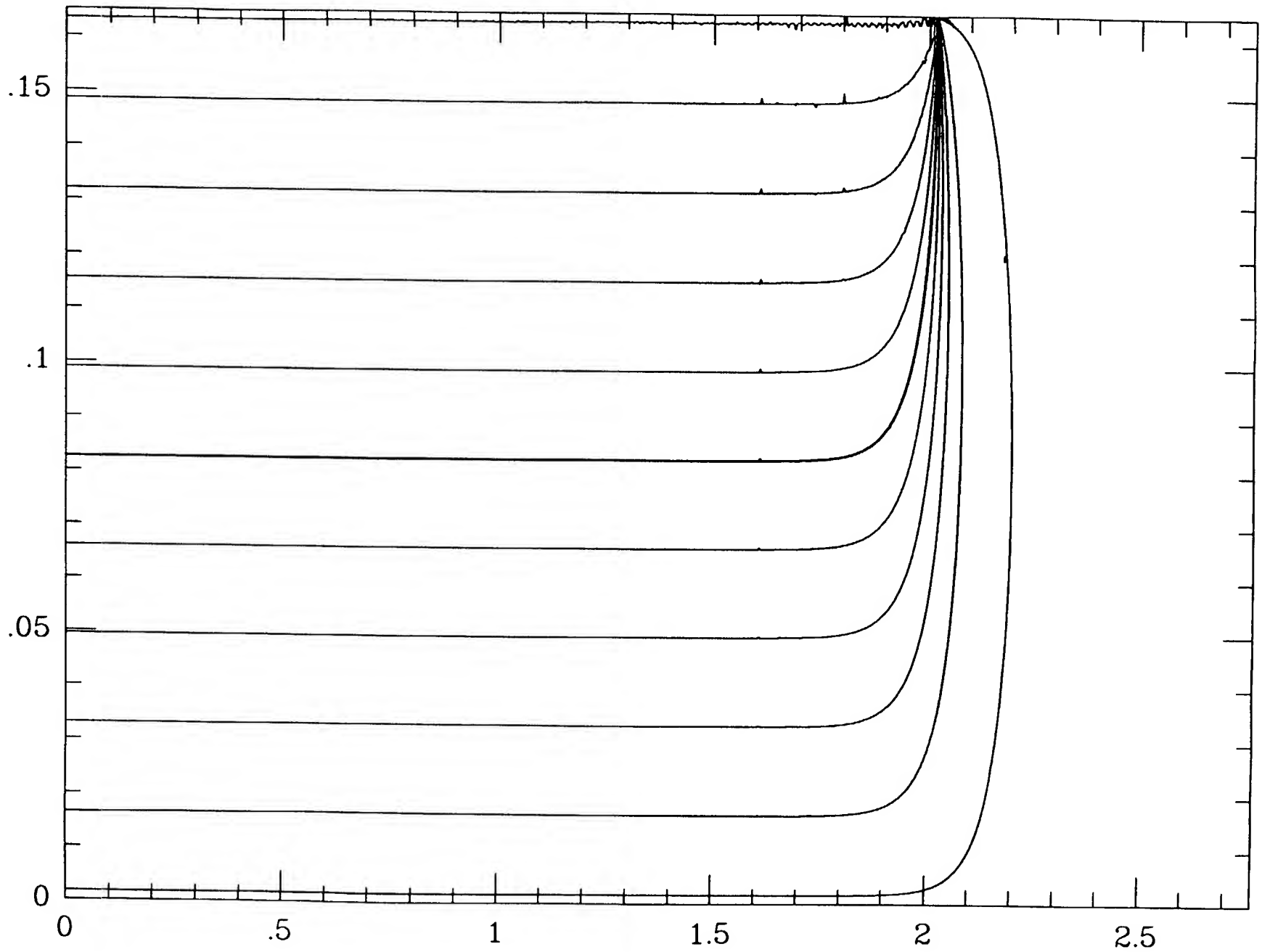

Figure 77

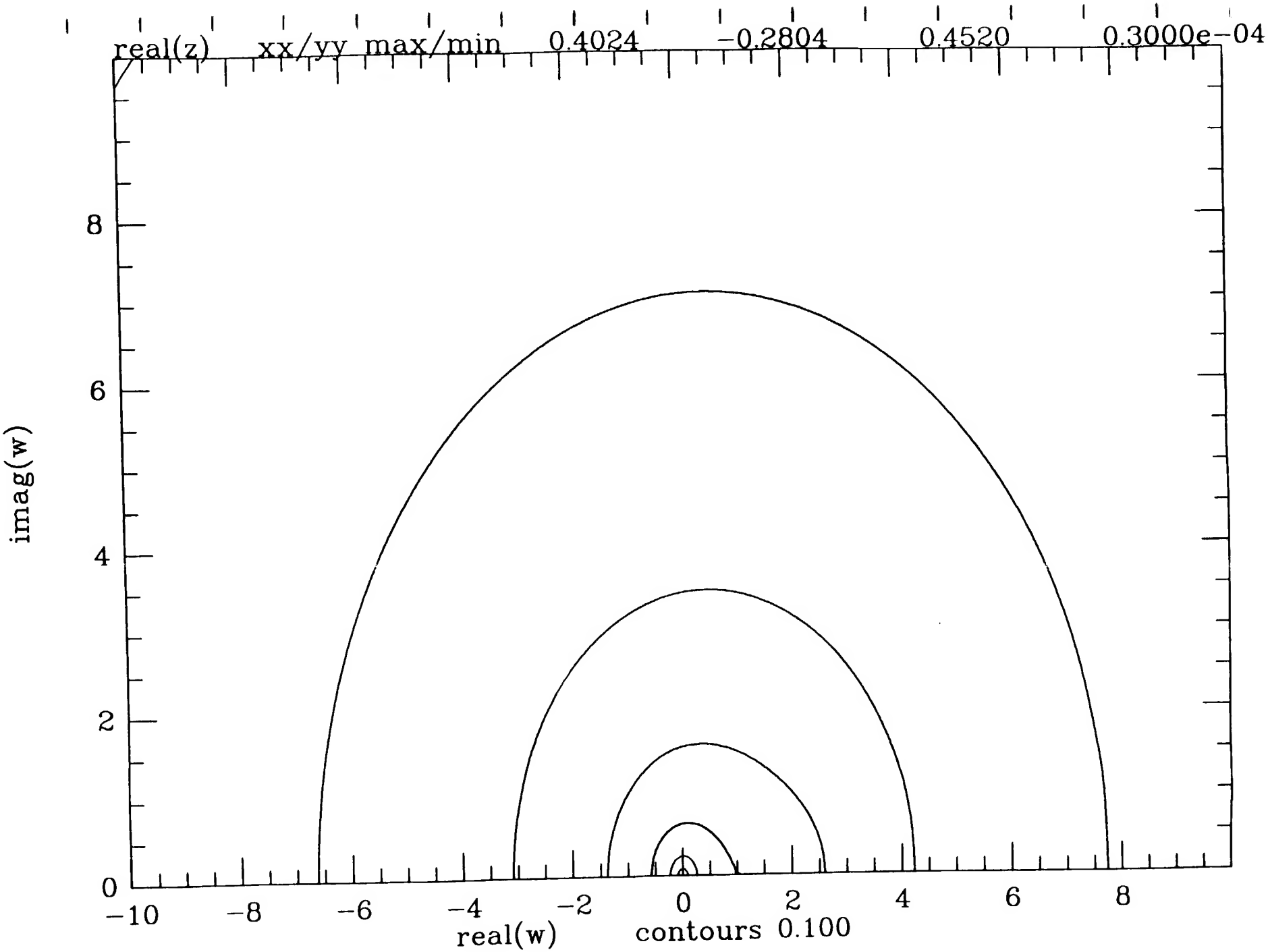
real(z) xx/yy max/min 0.4024 -0.2804 0.4520 0.3000e-04
imag(w)
real(w)
contours 0.100
8
6
4
2
0
-10
-8
-6
-4
-2
0
2
4
6
8

Figure 78

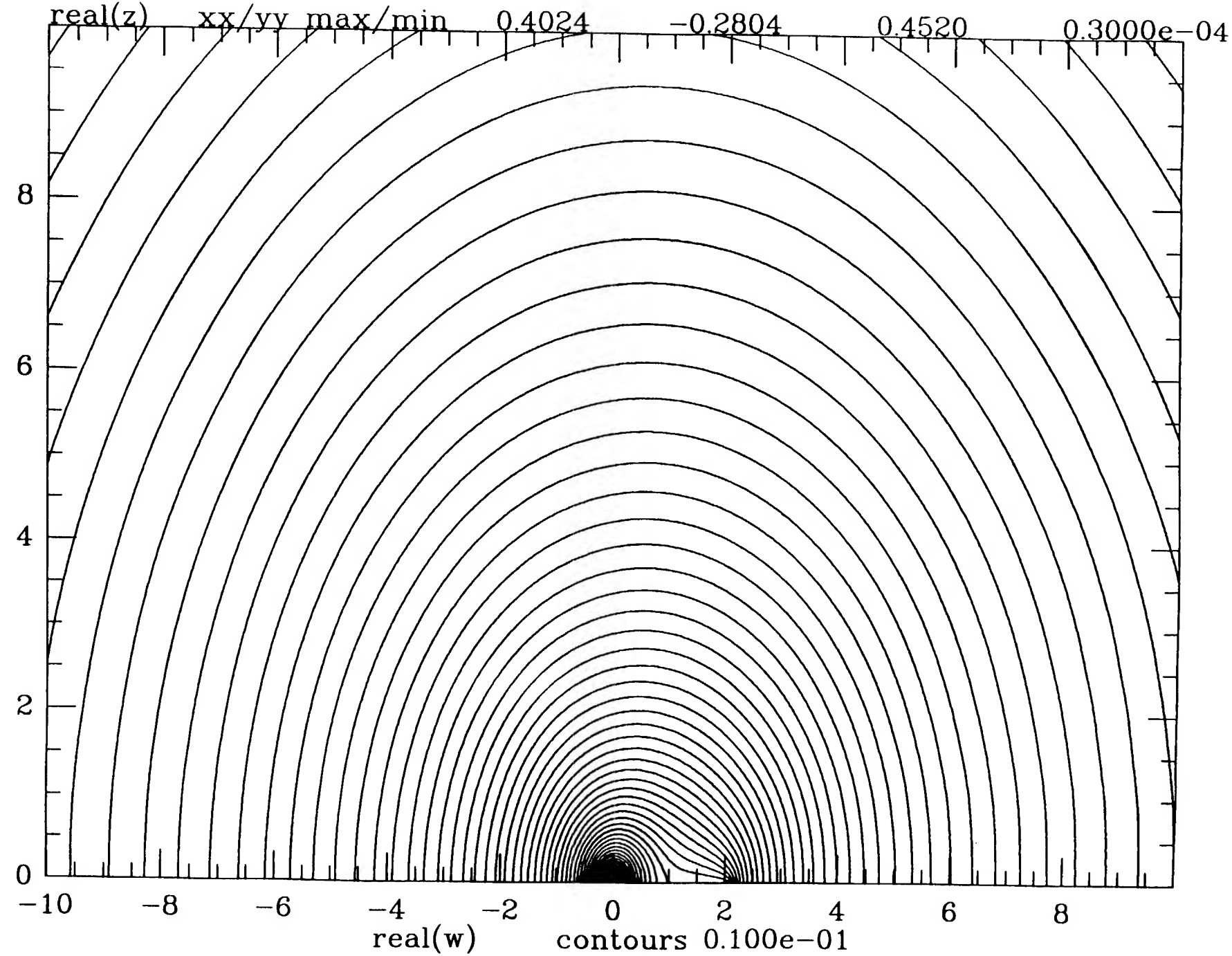

Figure 79

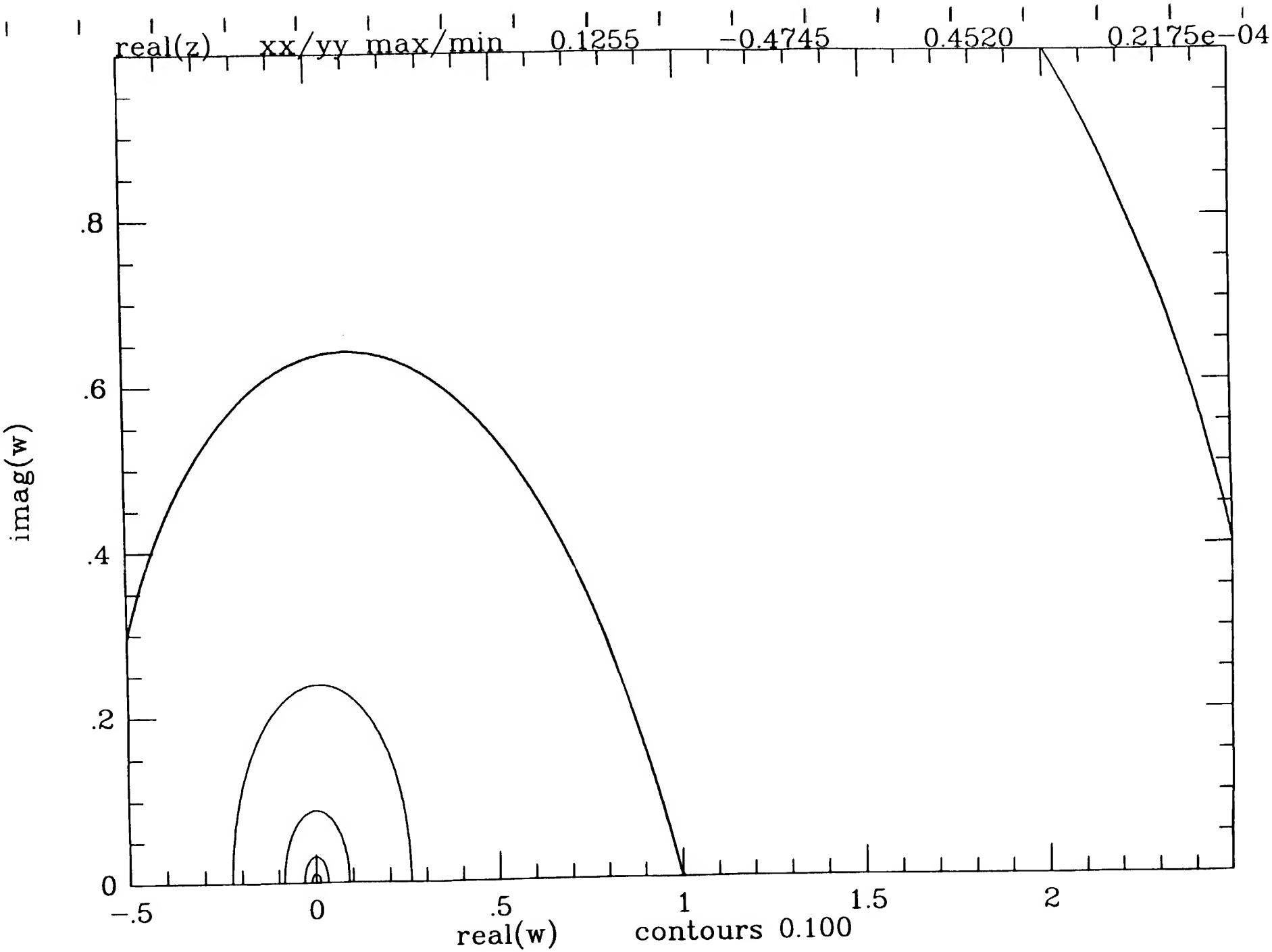
real(z) xx/yy max/min 0.1255 −0.4745 0.4520 0.2175e−04
.8
.6
.4
.2
0
imag(w)
−.5
0
.5
1
1.5
2
real(w)
contours 0.100

Figure 80

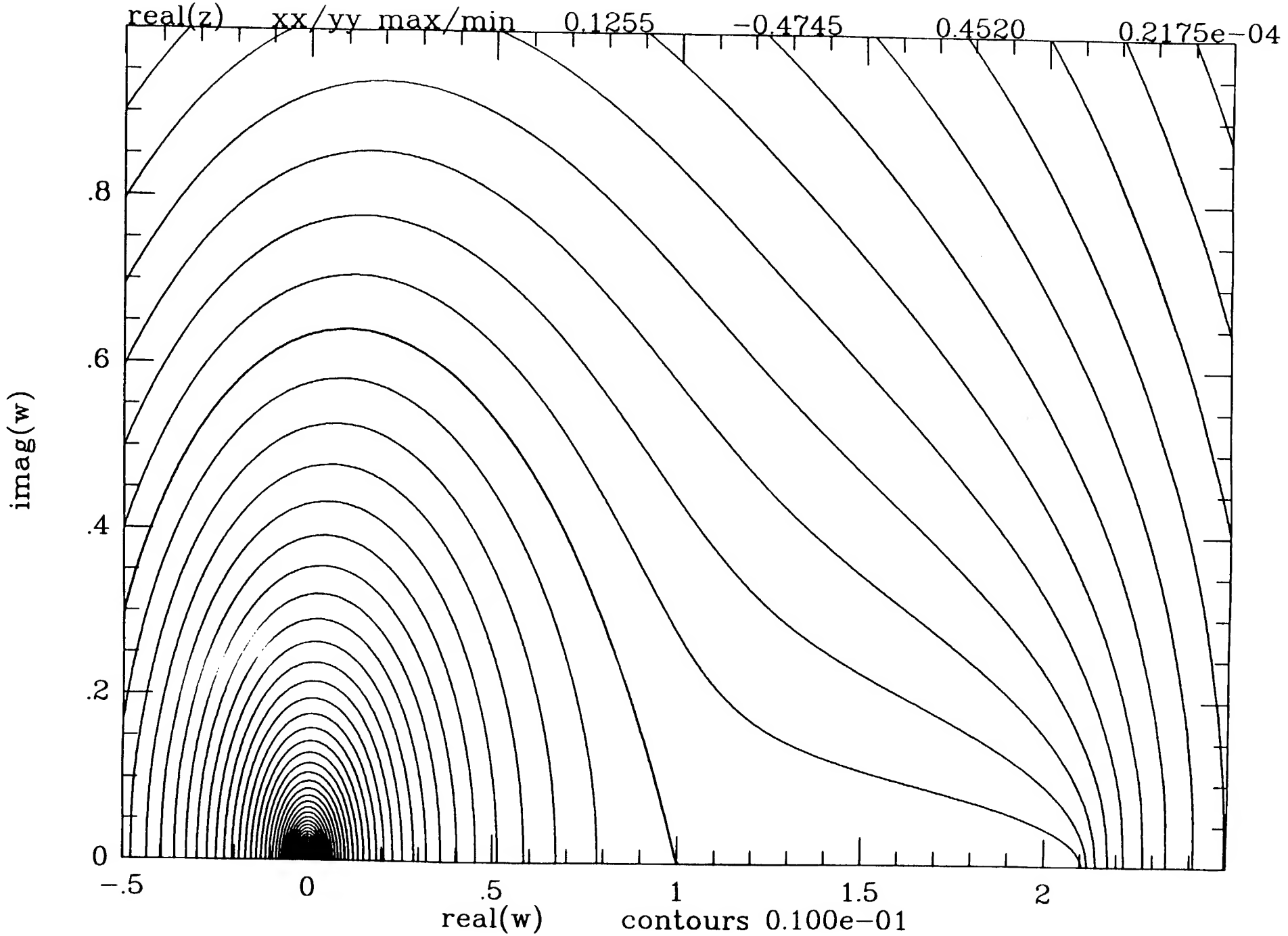
real(z) xx/yy max/min 0.1255 -0.4745 0.4520 0.2175e-04
imag(w)
.8
.6
.4
.2
0
-.5
0
.5
1
1.5
2
real(w)
contours 0.100e-01

Figure 81

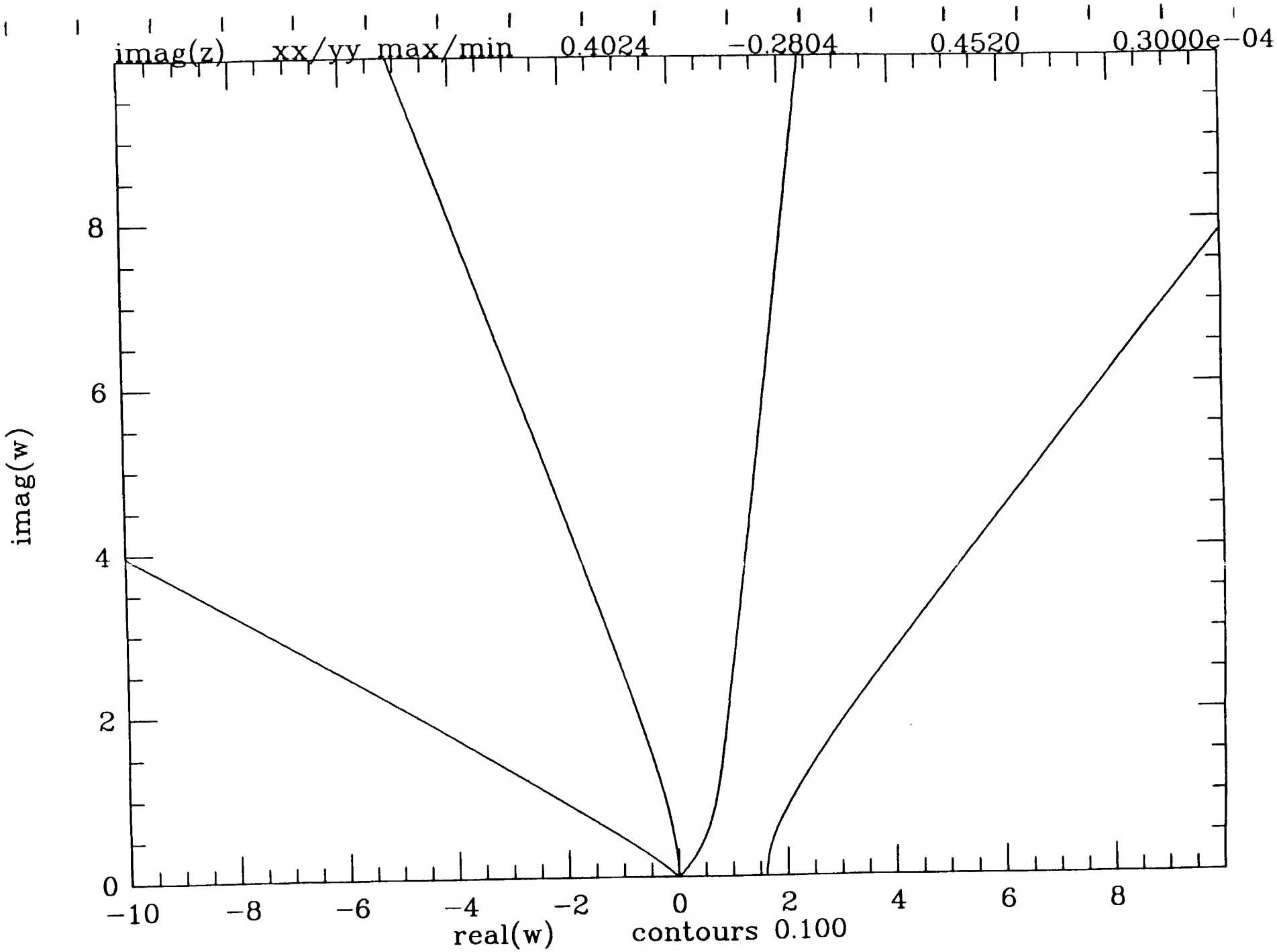
imag(z) xx/yy max/min 0.4024 -0.2804 0.4520 0.3000e-04
imag(w)
real(w)
contours 0.100
0
2
4
6
8
-10
-8
-6
-4
-2
0
2
4
6
8

Figure 82

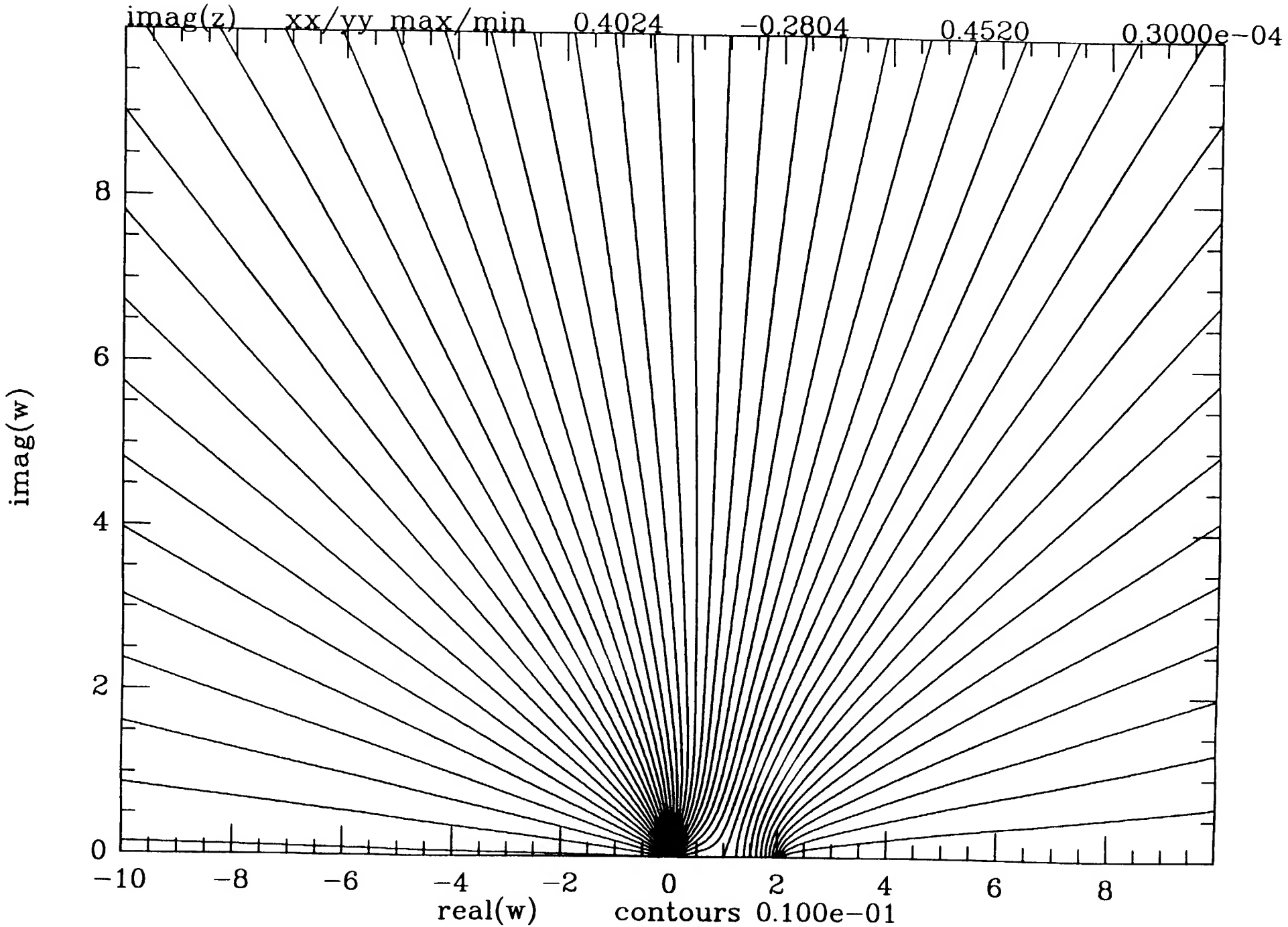
imag(z) xx/yy max/min 0.4024 −0.2804 0.4520 0.3000e−04
imag(w)
8
6
4
2
0
−10 −8 −6 −4 −2 0 2 4 6 8
real(w) contours 0.100e−01

Figure 83

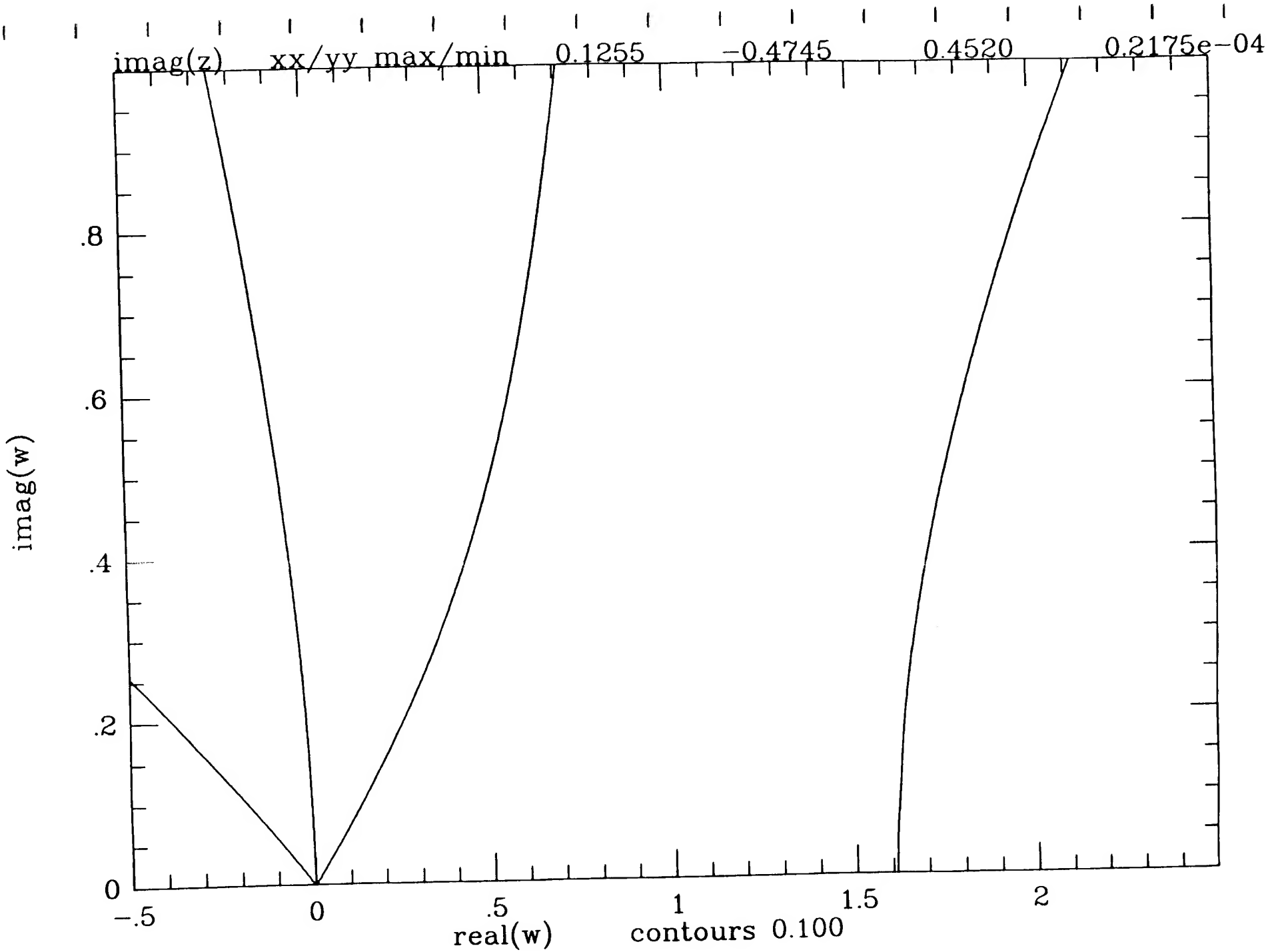
imag(z) xx/yy max/min 0.1255 −0.4745 0.4520 0.2175e−04
.8
.6
.4
.2
0
imag(w)
−.5
0
.5
1
1.5
2
real(w)
contours 0.100

Figure 84

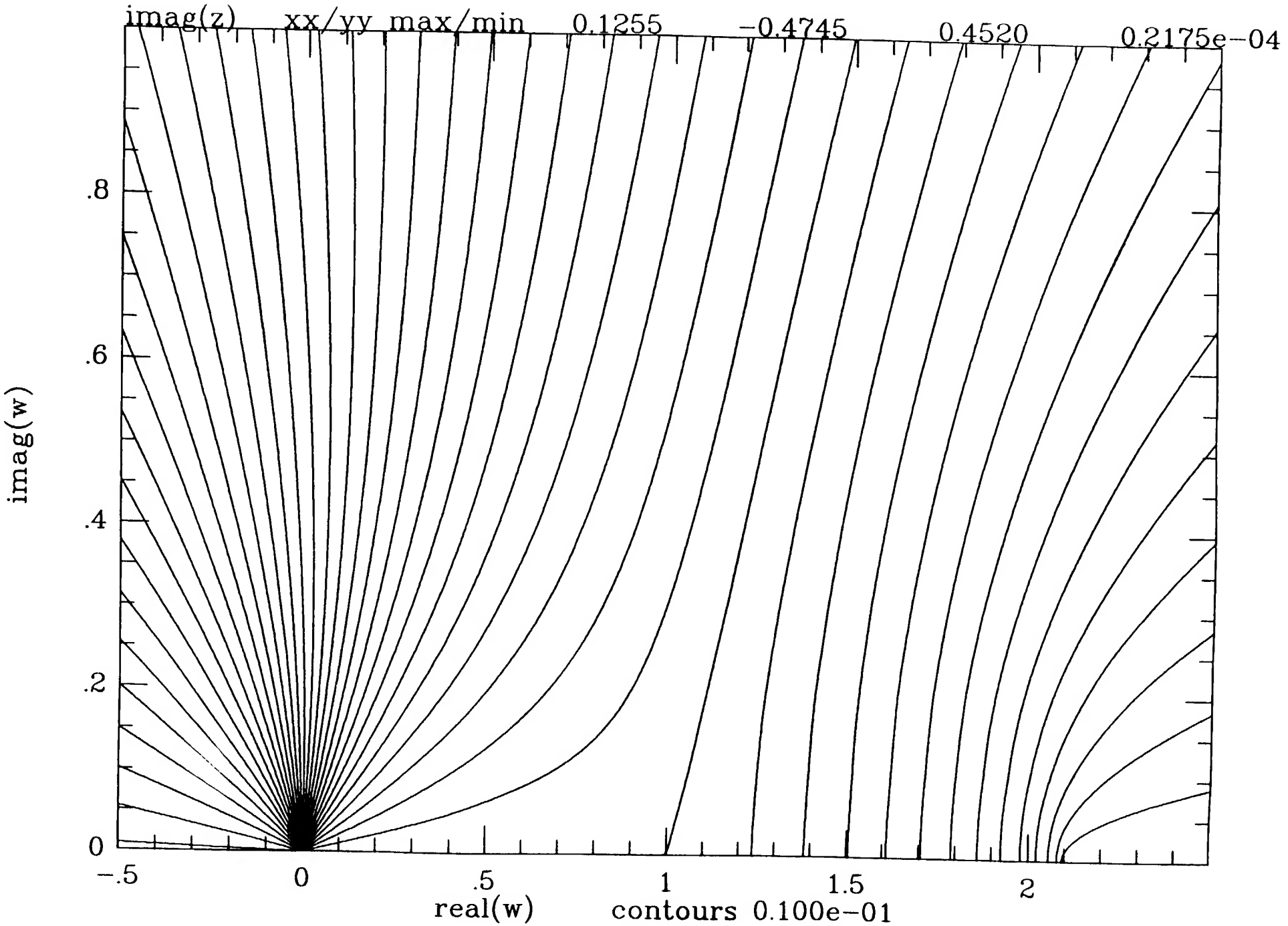
imag(z) xx/yy max/min 0.1255 −0.4745 0.4520 0.2175e−04
.8
.6
.4
.2
0
imag(w)
−.5
0
.5
1
1.5
2
real(w)
contours 0.100e−01

Figure 85

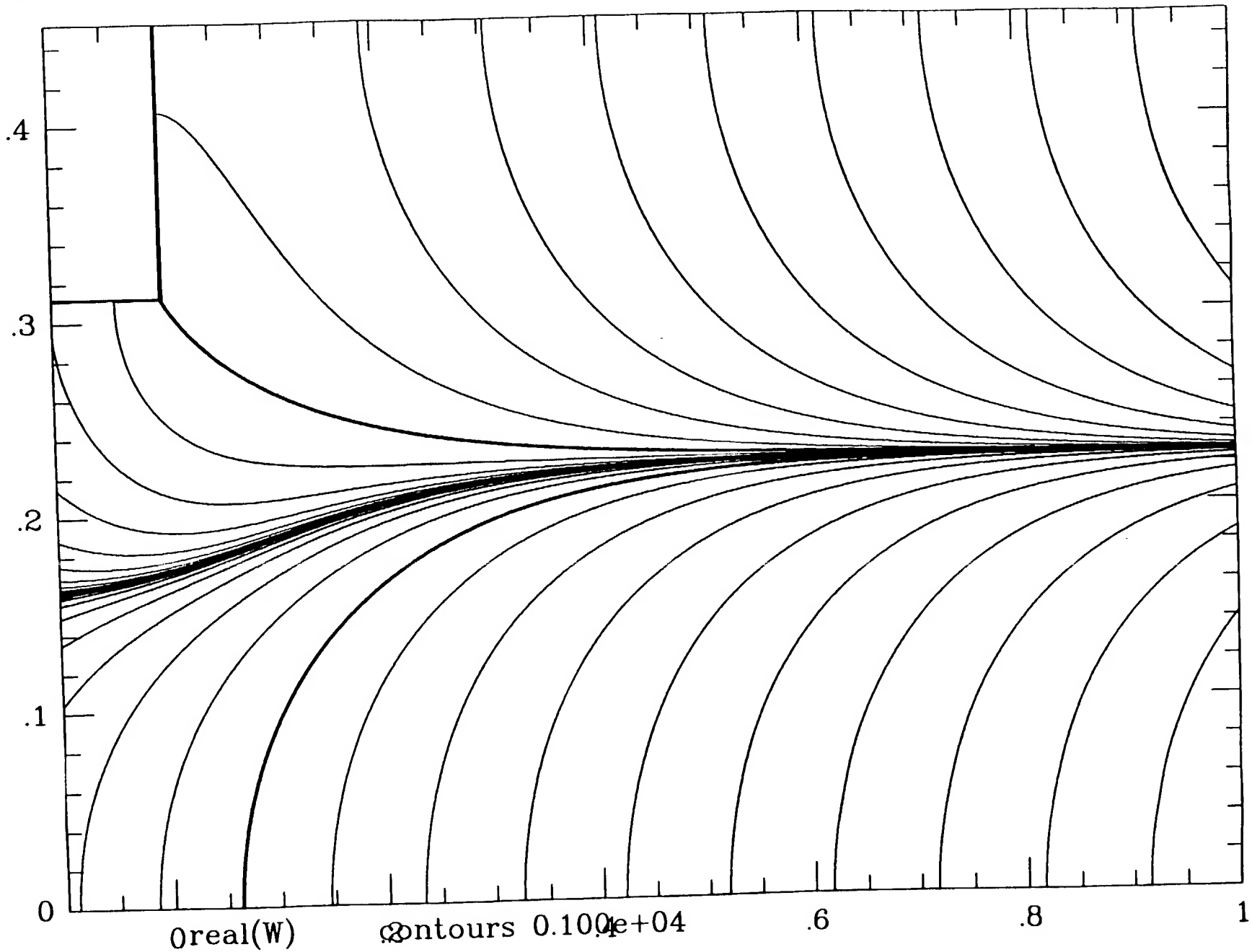

N 200 2

Figure 86

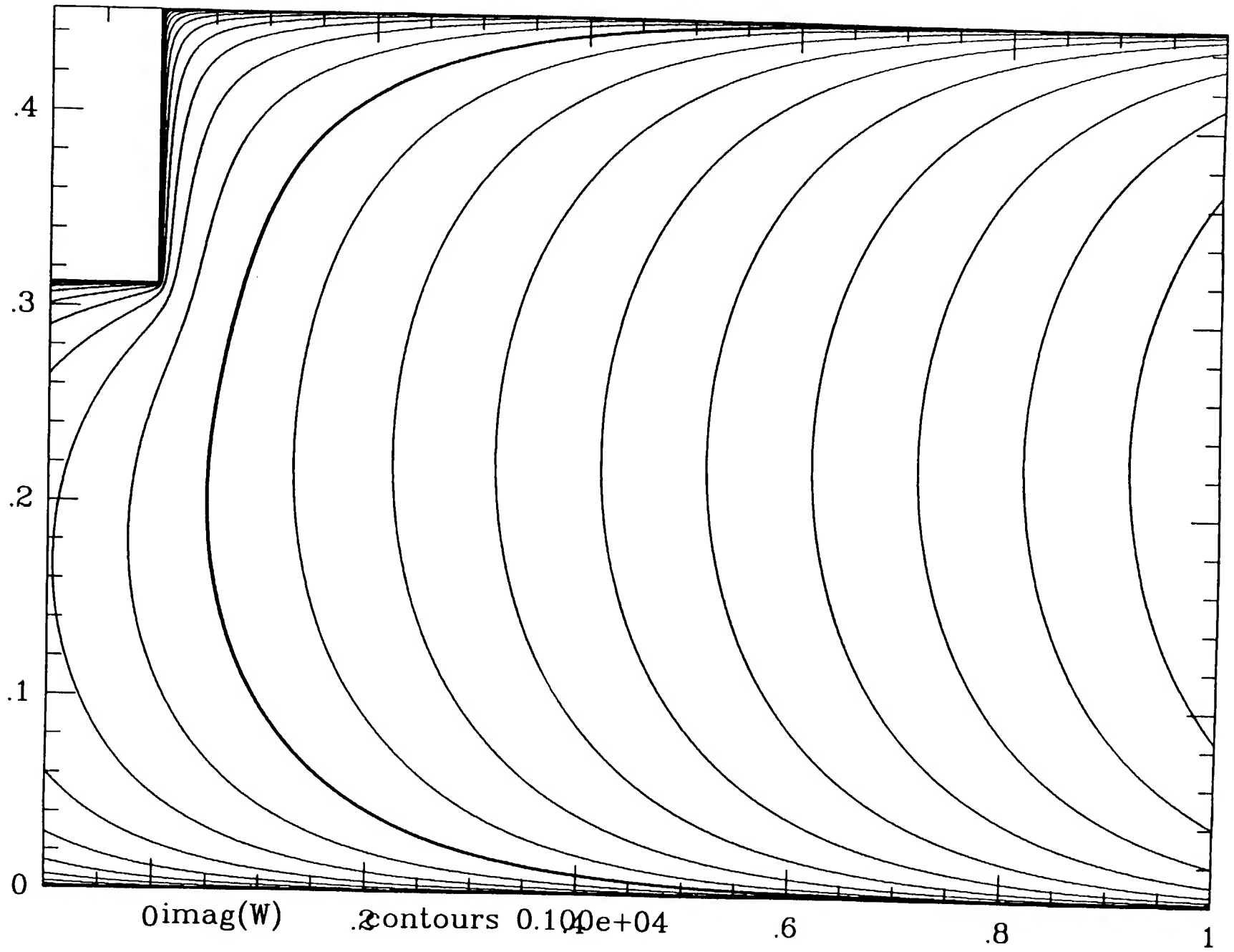

Figure 87

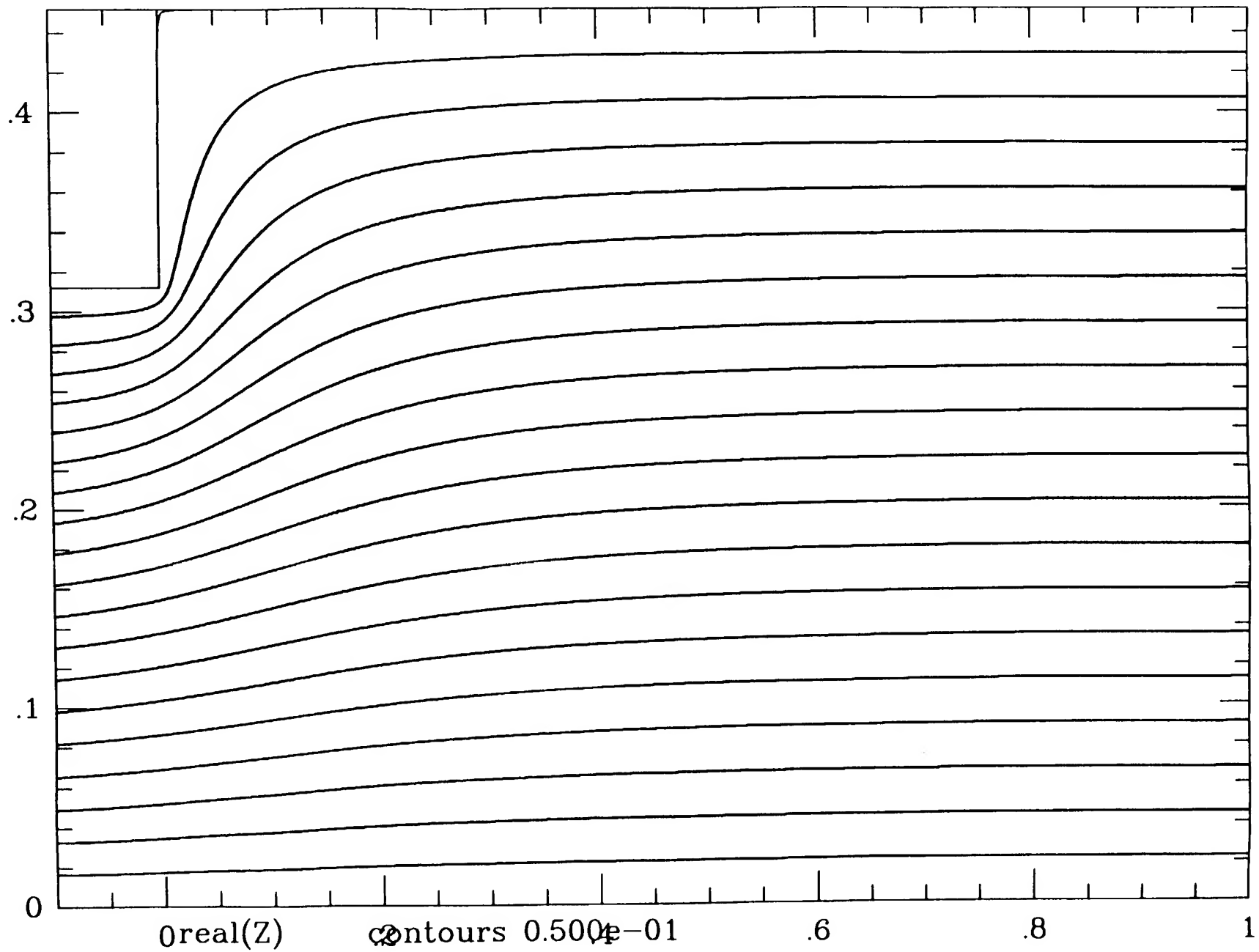

Figure 88

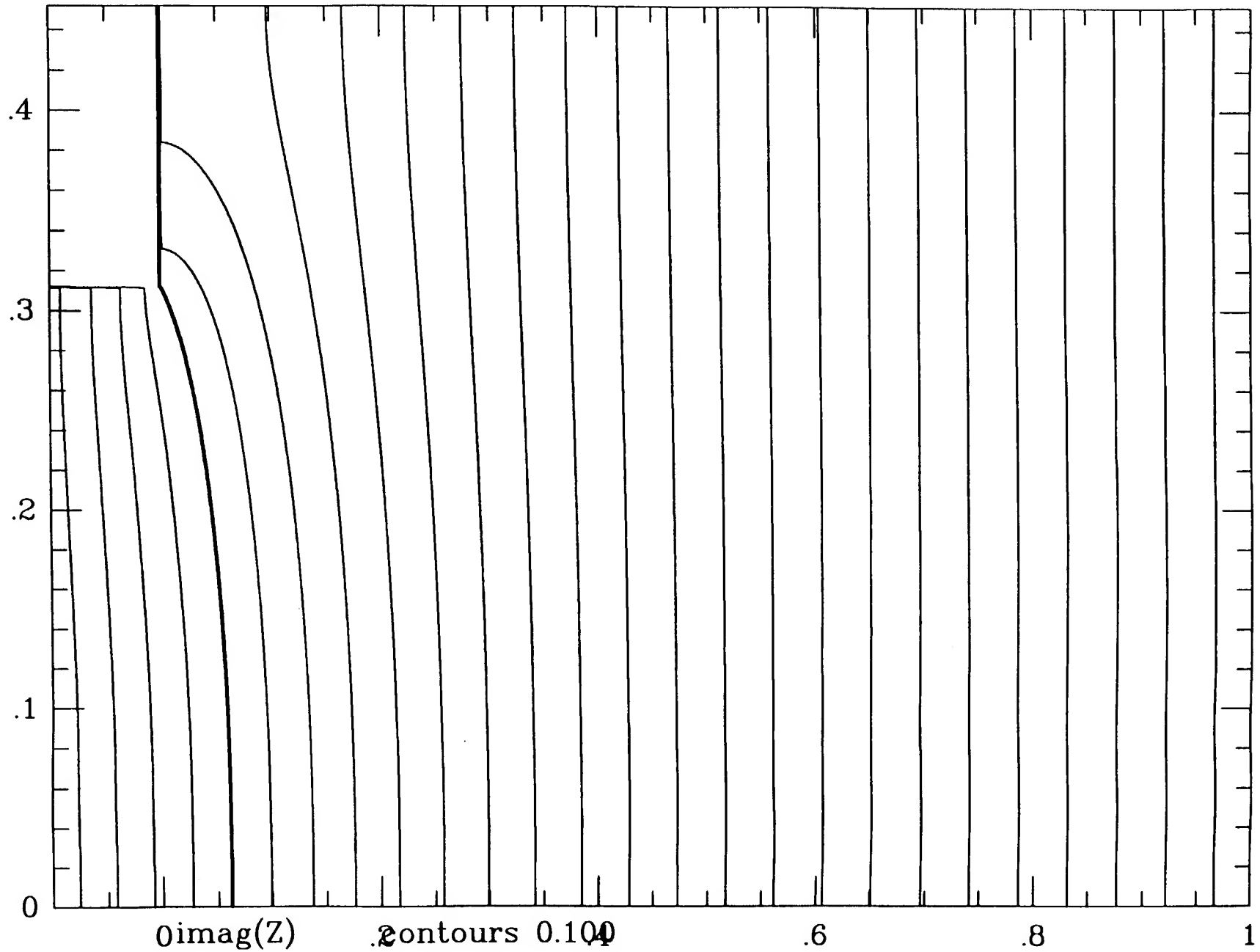

Figure 89

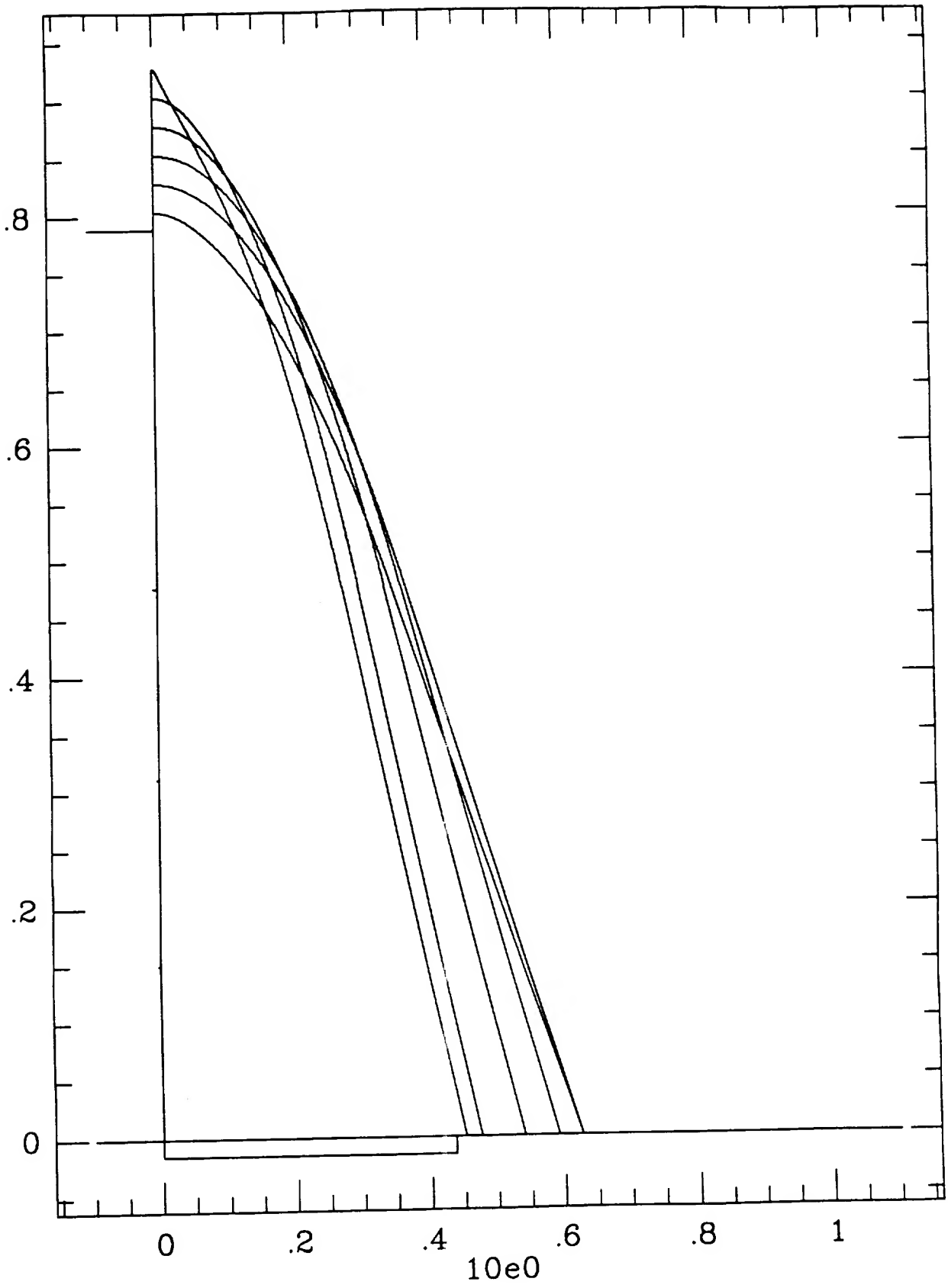

Figure 90

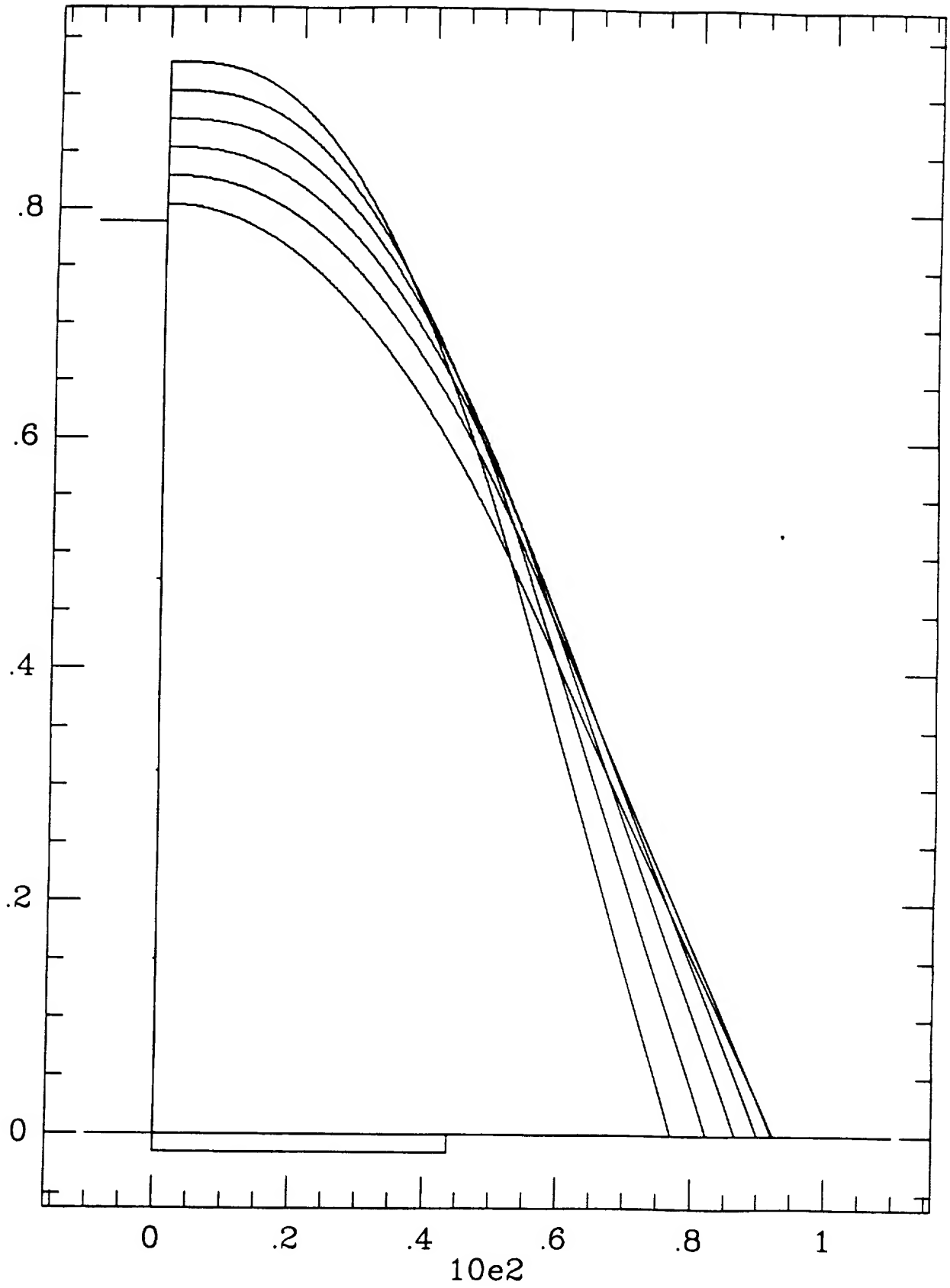

Figure 91

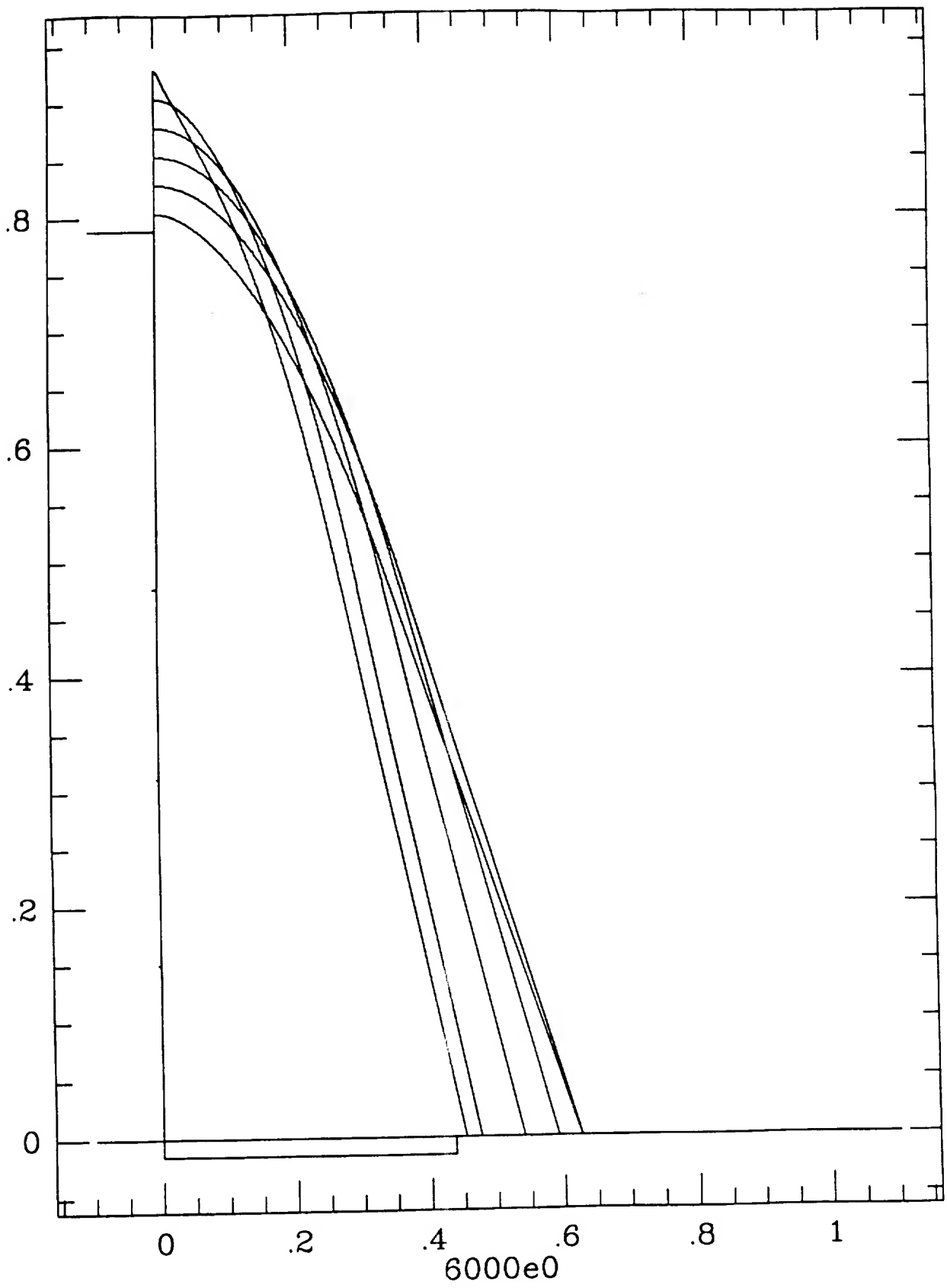

Figure 92

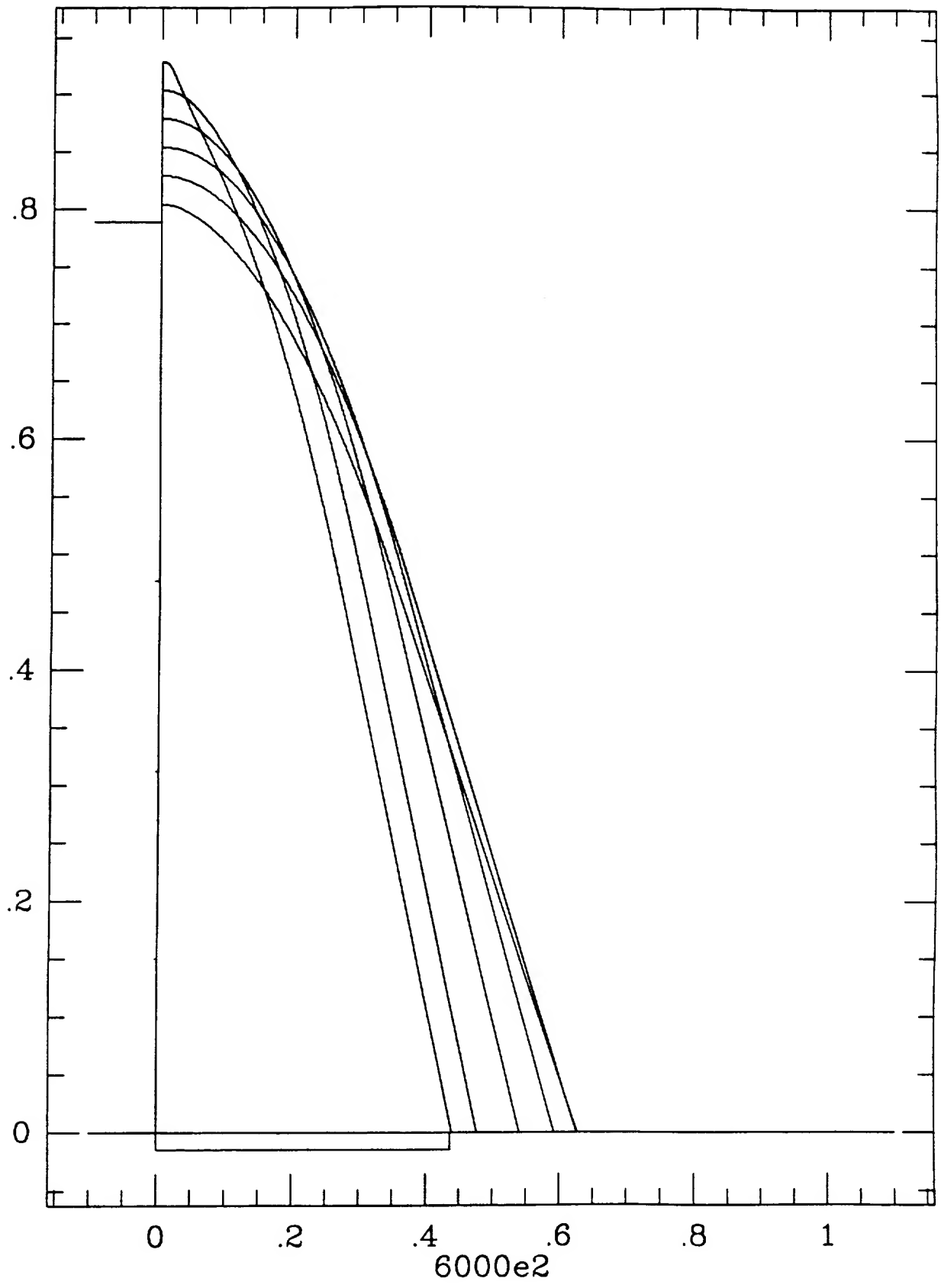

Figure 93

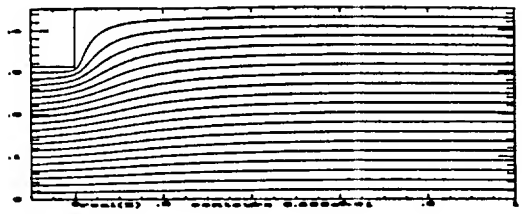

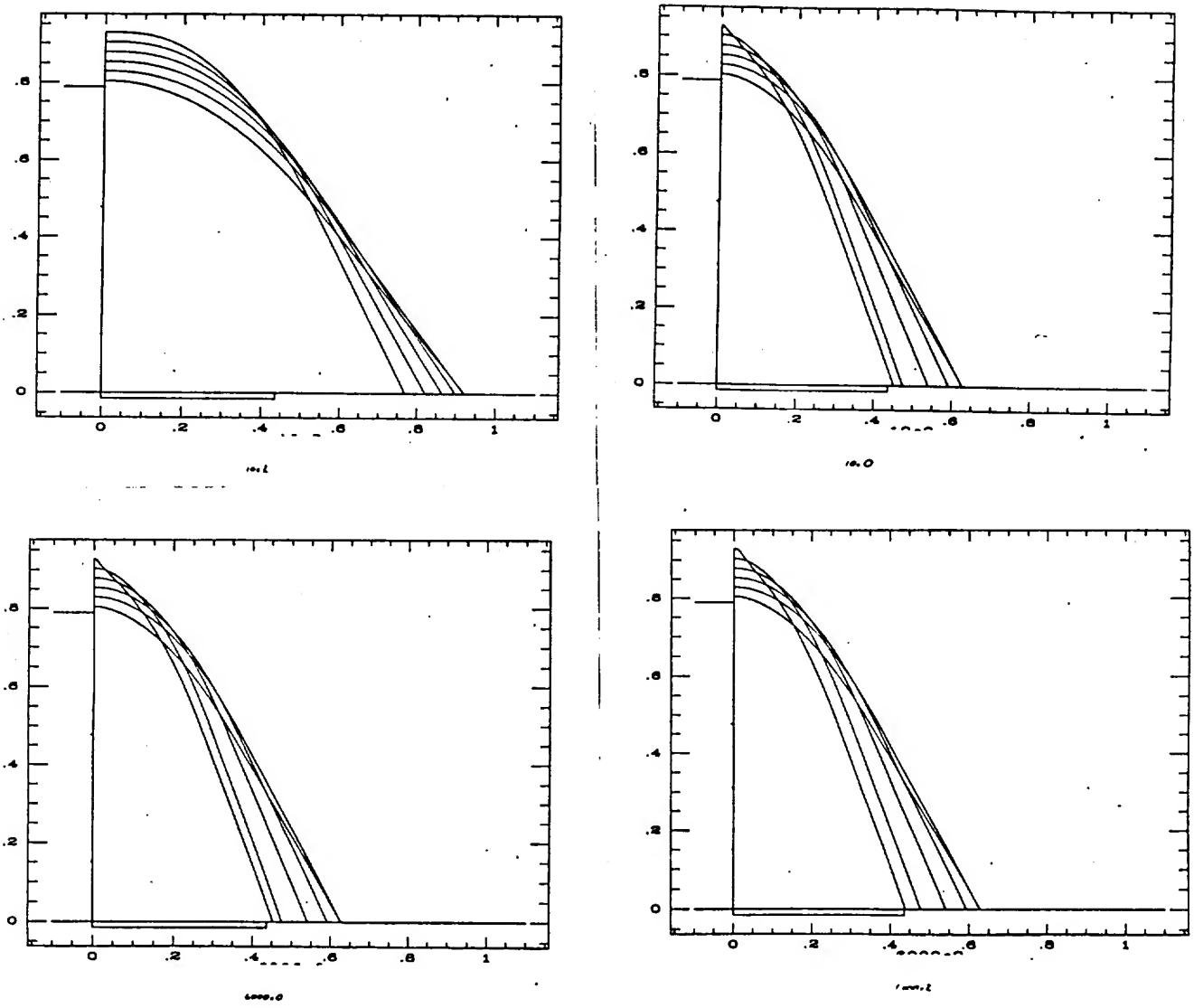

Figure 94

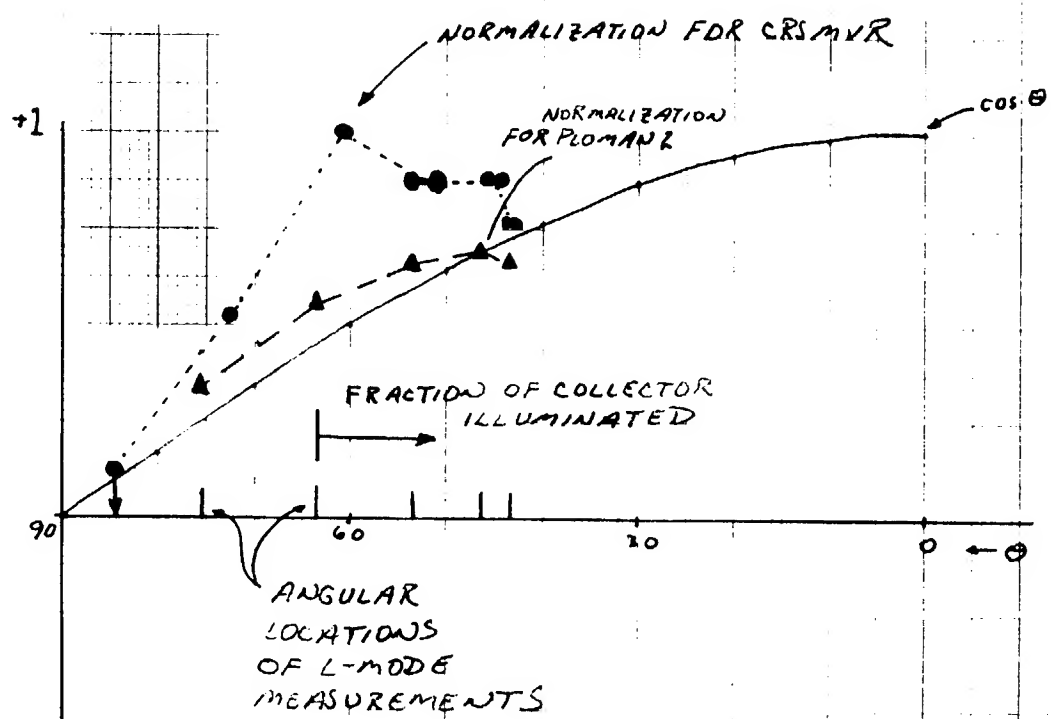

▲ NORMALIZED PEAK CURRENT FROM PLOMAN 2 (MODULATED)

● DC COMPONENT FROM CRSMVR ON V1: 1978-258 E2 ONLY

●●● E2-L

Figure 95

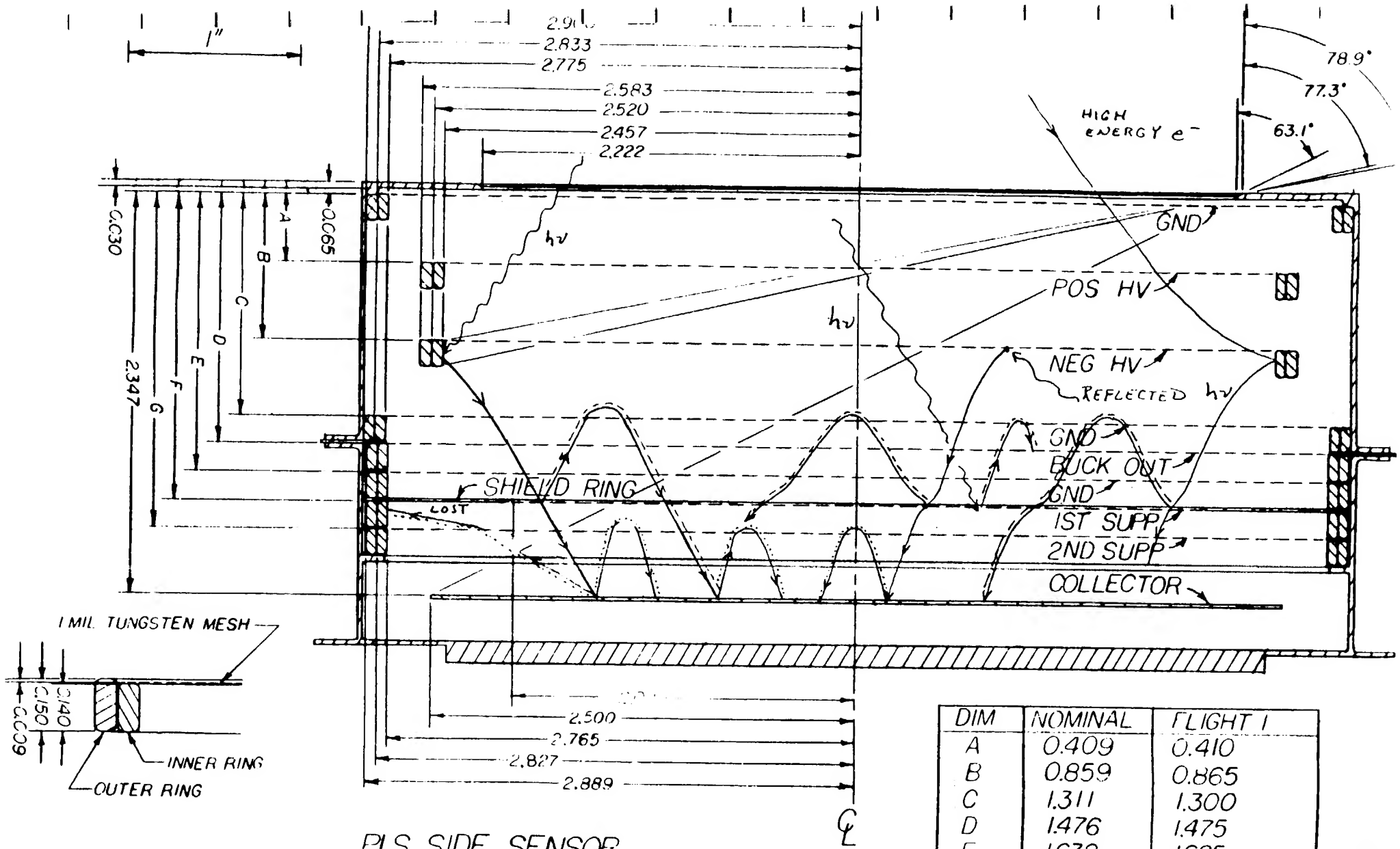

PLS SIDE SENSOR

DIM	NOMINAL	FLIGHT I
A	0.409	0.410
B	0.859	0.865
C	1.311	1.300
D	1.476	1.475
E	1.638	1.625
F	1.803	1.845
G	1.965	1.965

---→ SECONDARY ELECTRONS PRODUCED AT SUPPRESSOR GRID

·····→ SECONDARY ELECTRONS PRODUCED AT COLLECTOR PLATE

Figure 96

DC RET MOD ON
NORMAL

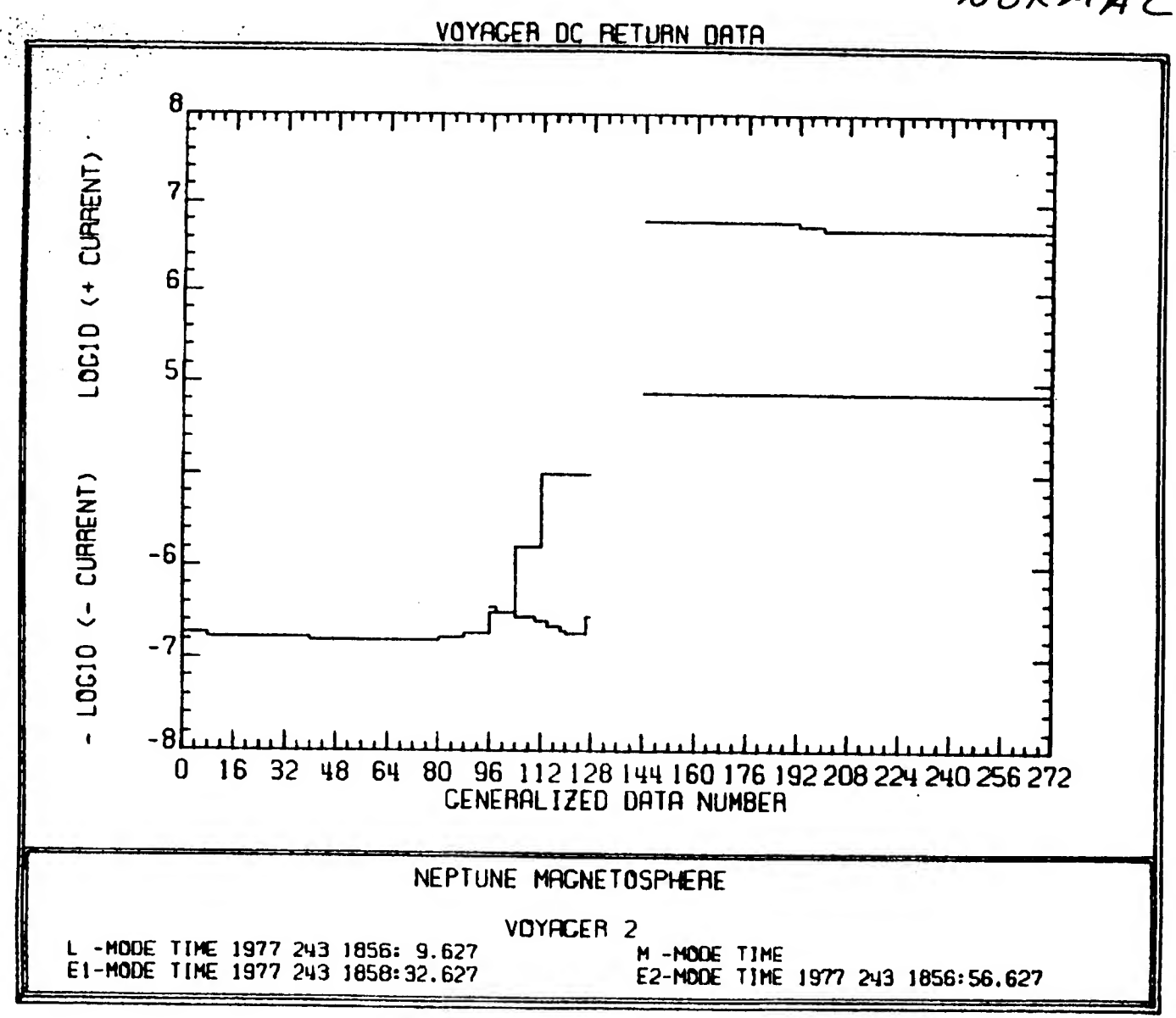

Figure 97

PCJ MOD ON

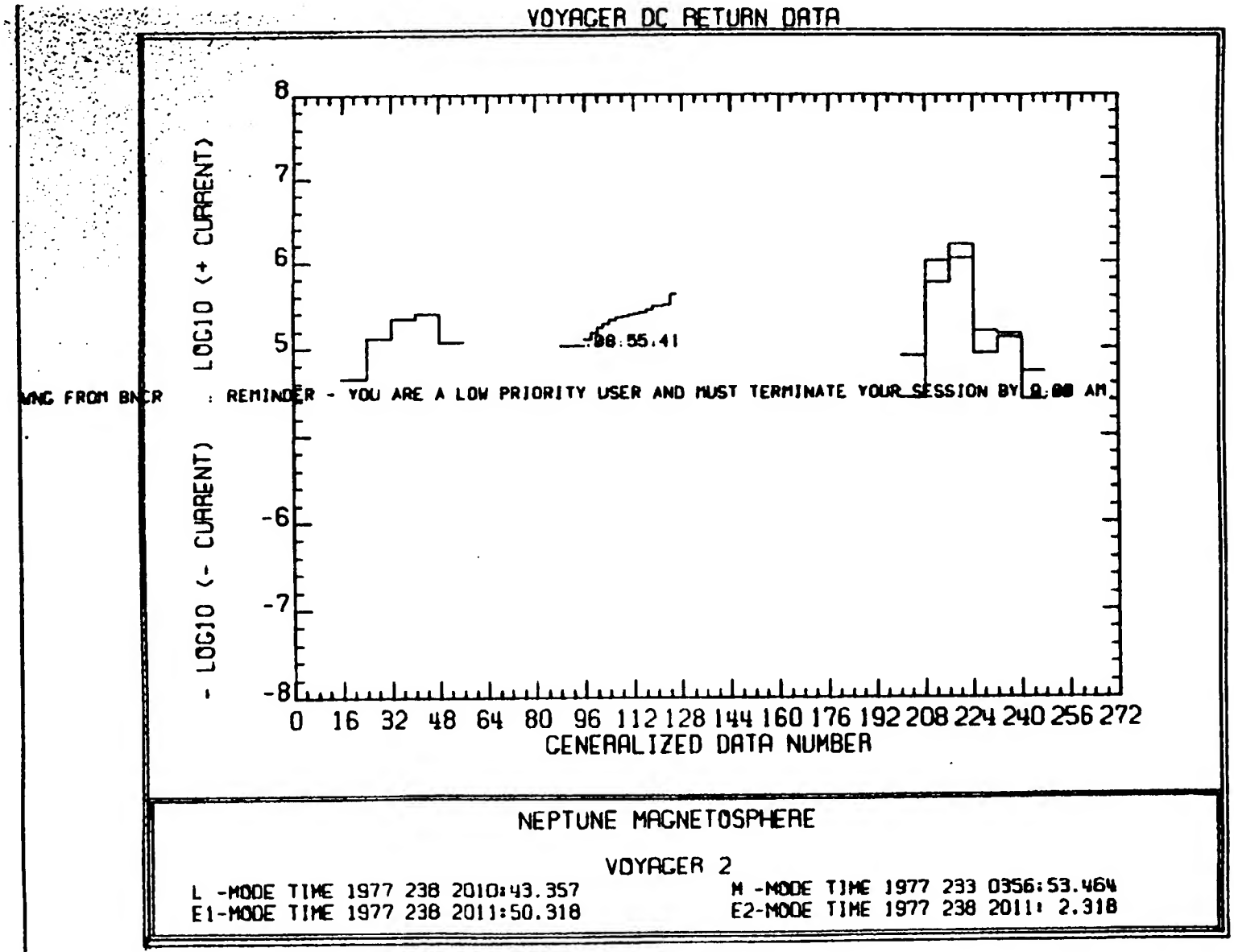

Figure 98

DC RET
REV MOD ON

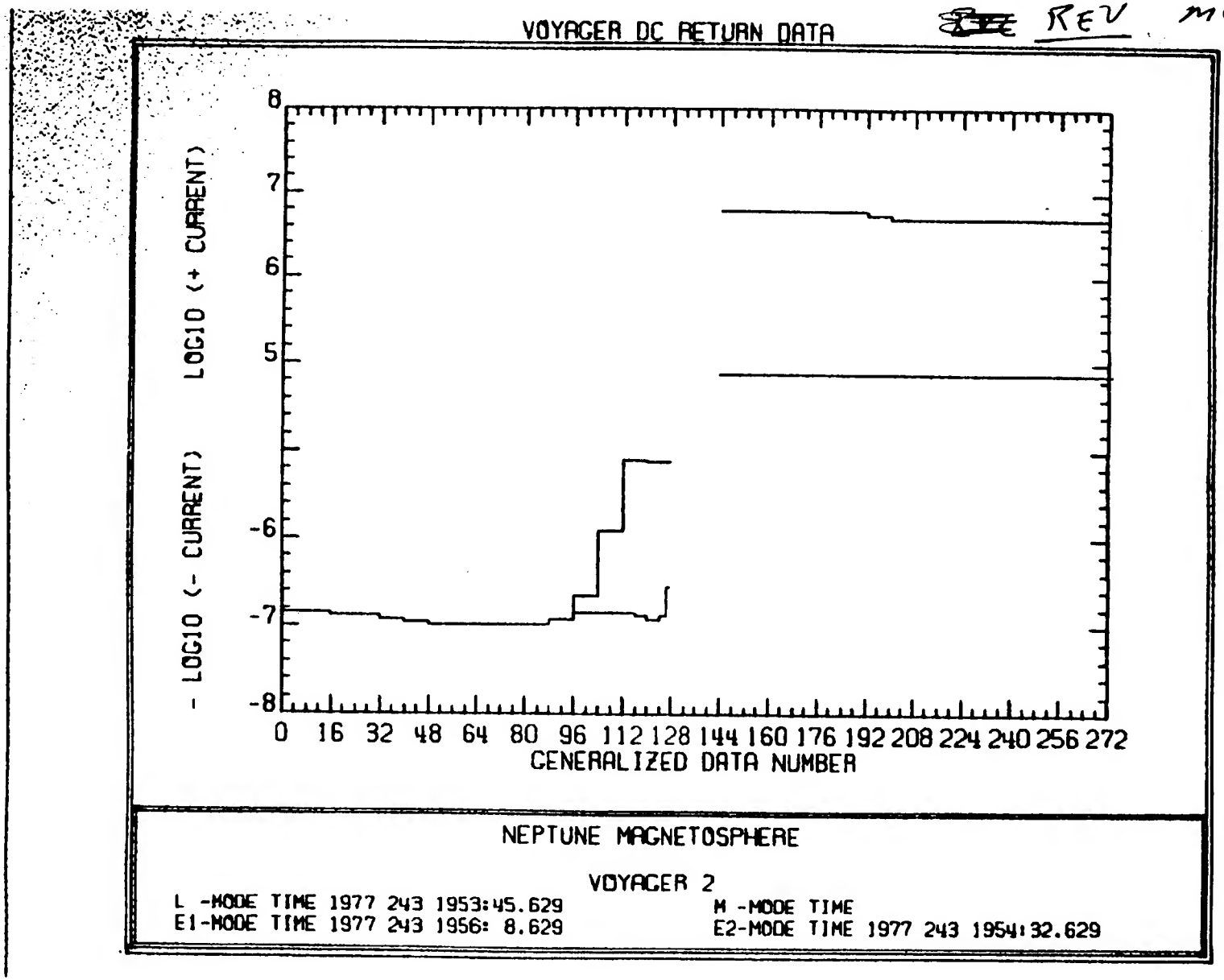

Figure 99

PLS MOD ON REV

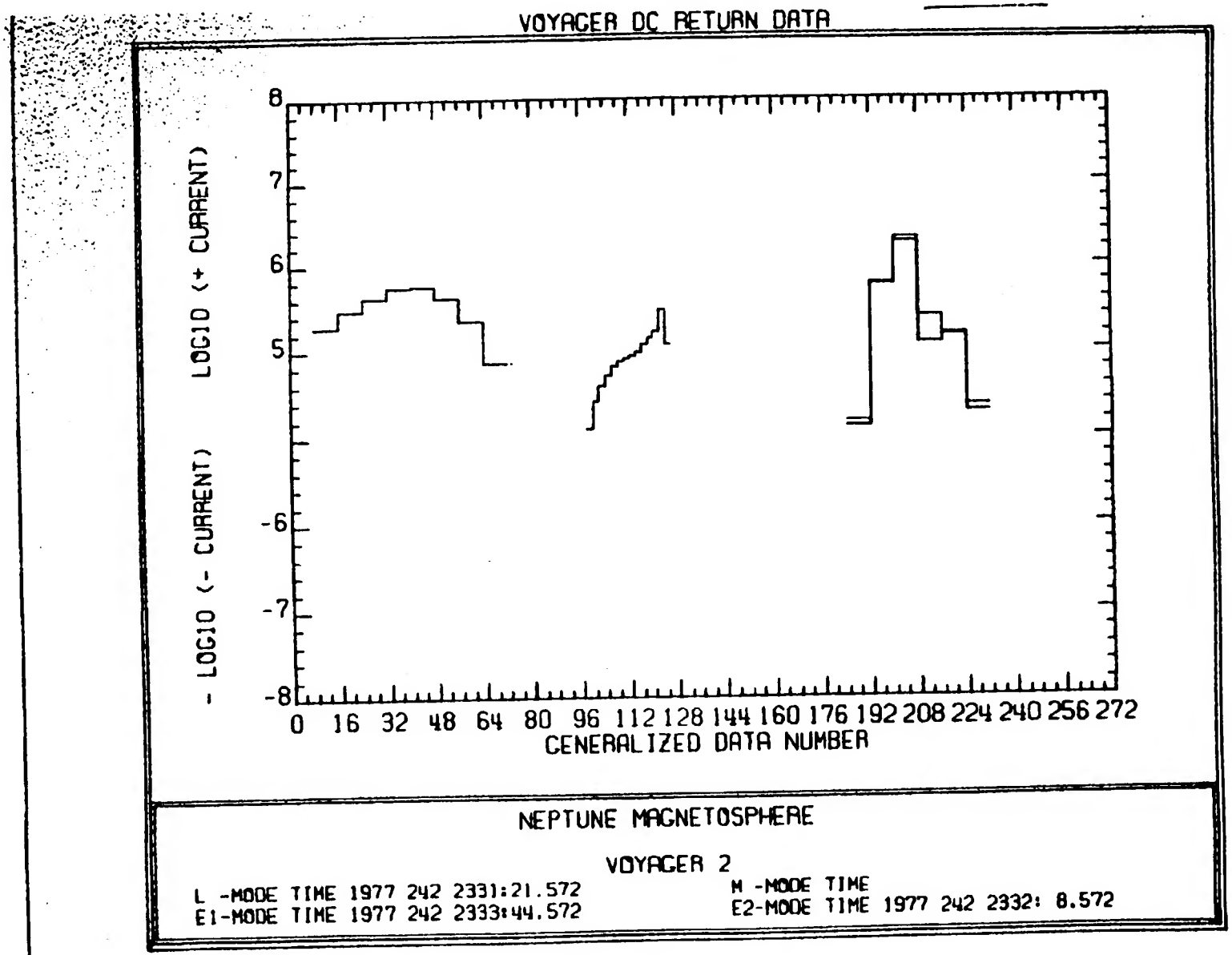

Figure 100

Figure 101

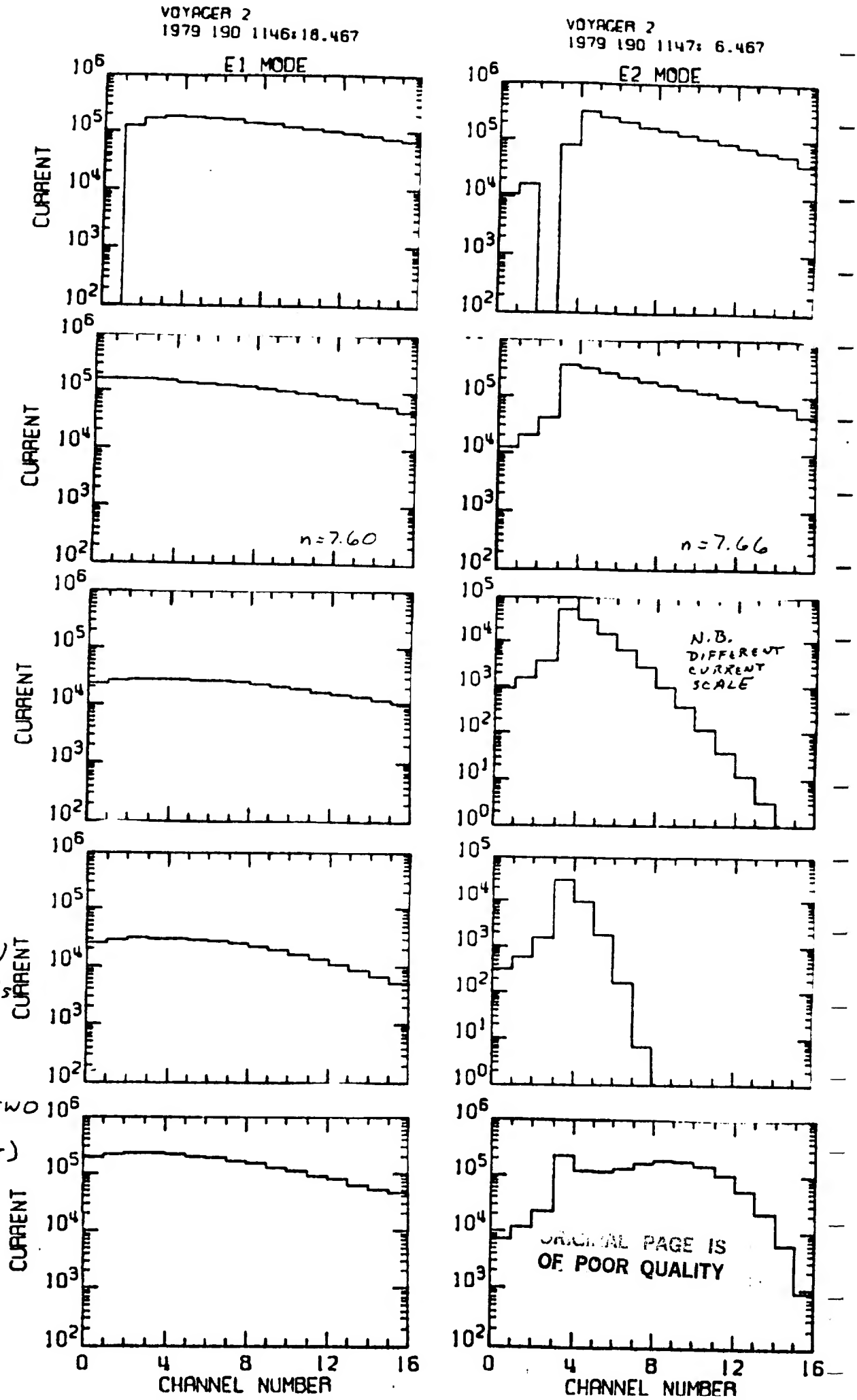
VOYAGER 2
1979 190 1146:18.467
E1 MODE
VOYAGER 2
1979 190 1147: 6.467
E2 MODE
CURRENT
DATA
PMODEL
K = 1.5
W MOST PROB = 2500 km/s (17.8 eV)
n = 7.66 cm⁻³
n = 7.60
n = 7.66
PMODEL
K = 5.5
W MOST PROB = 3500 km/s (34.8eV)
n = 1.0 cm⁻³
N.B. DIFFERENT CURRENT SCALE
PMODEL MAXWELLIAN
Wth = 300 km/s (T = 34.8eV)
n = 1.0 cm⁻³
GSFC FIT TO TWO MAXWELLIANS (NSSDC DATA SET) PMODEL
n_c = 7.113 | n_H = 0.883
T_c = 32.3 | T_H = 573
(W_th = 3369.7) | (W_th = 14,196.)
ORIGINAL PAGE IS OF POOR QUALITY
0 4 8 12 16
CHANNEL NUMBER

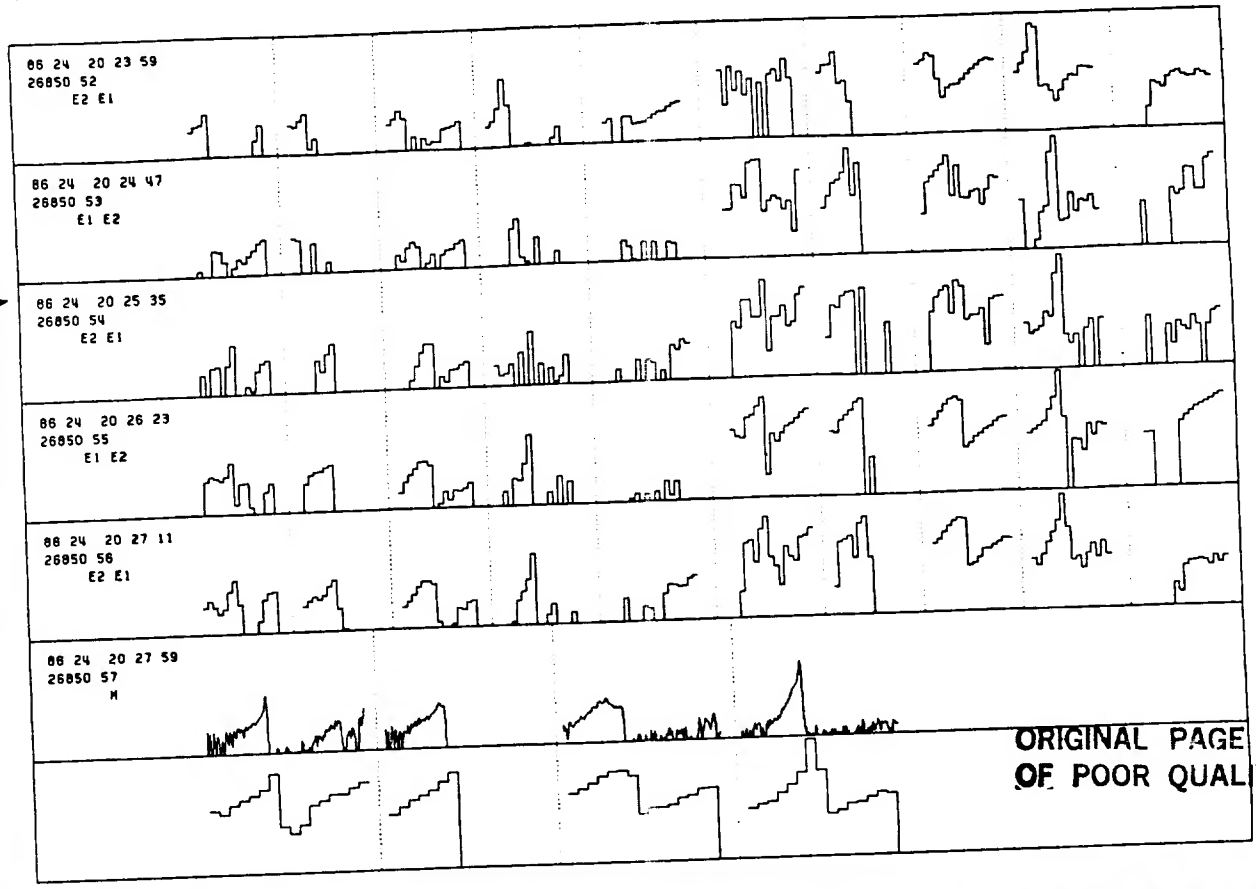

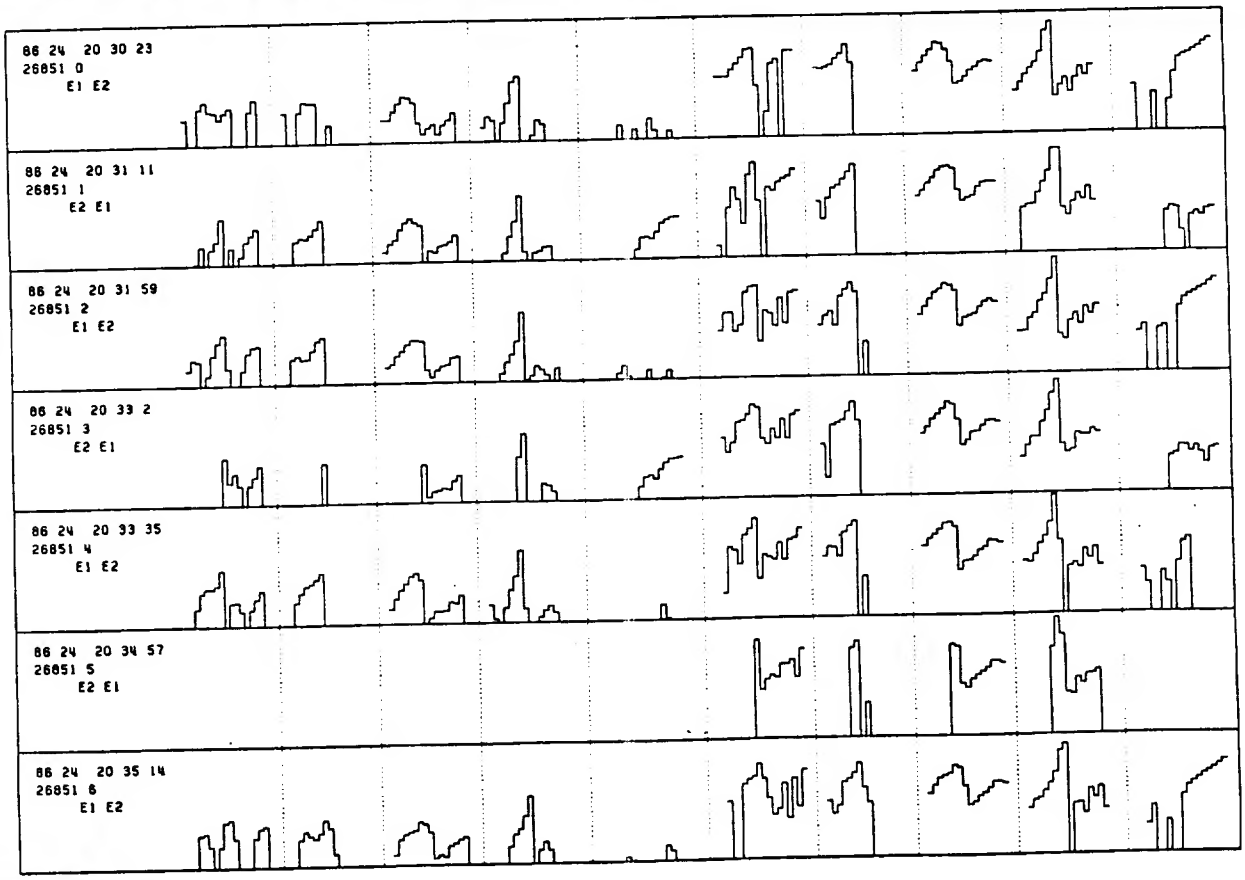

Figure 102

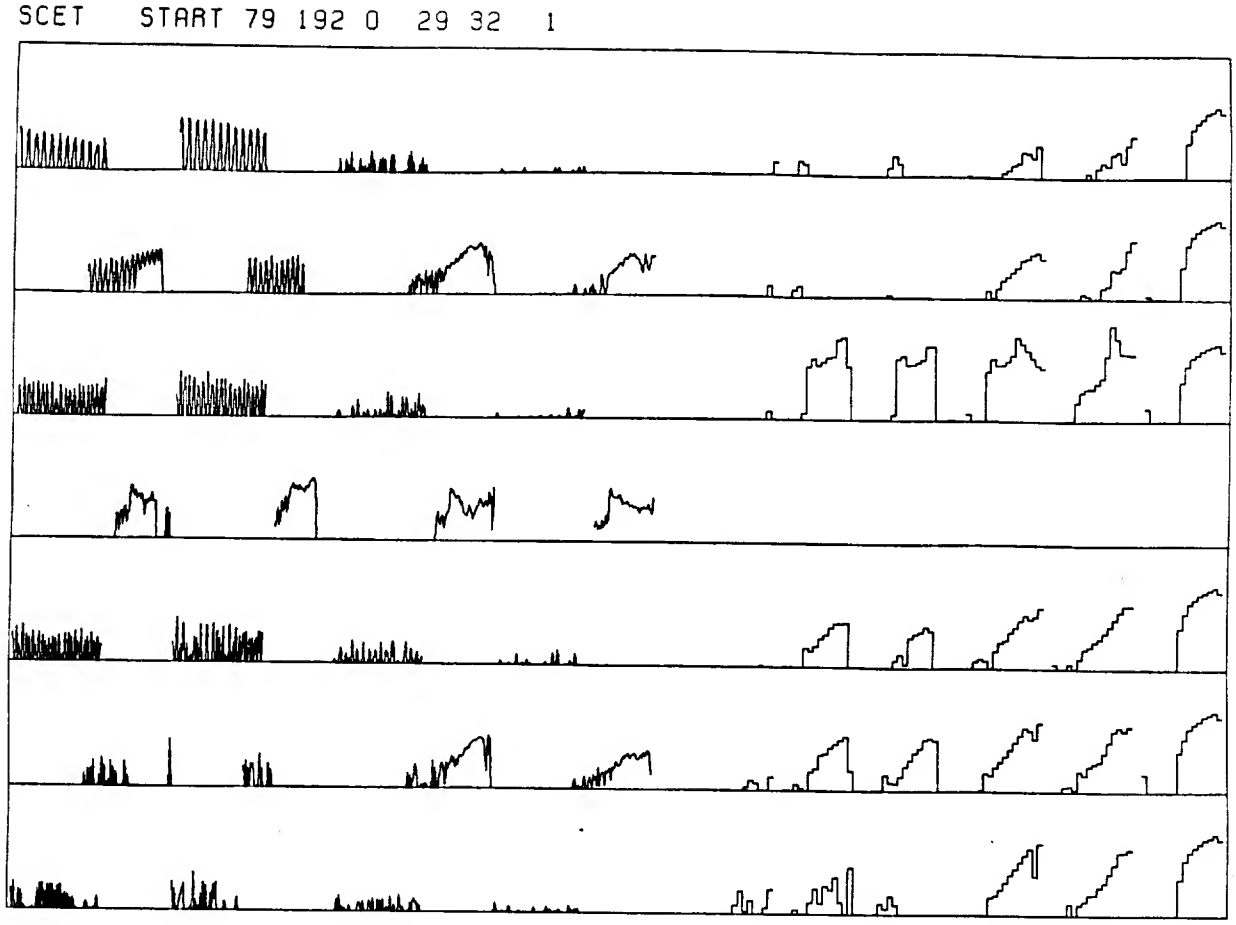

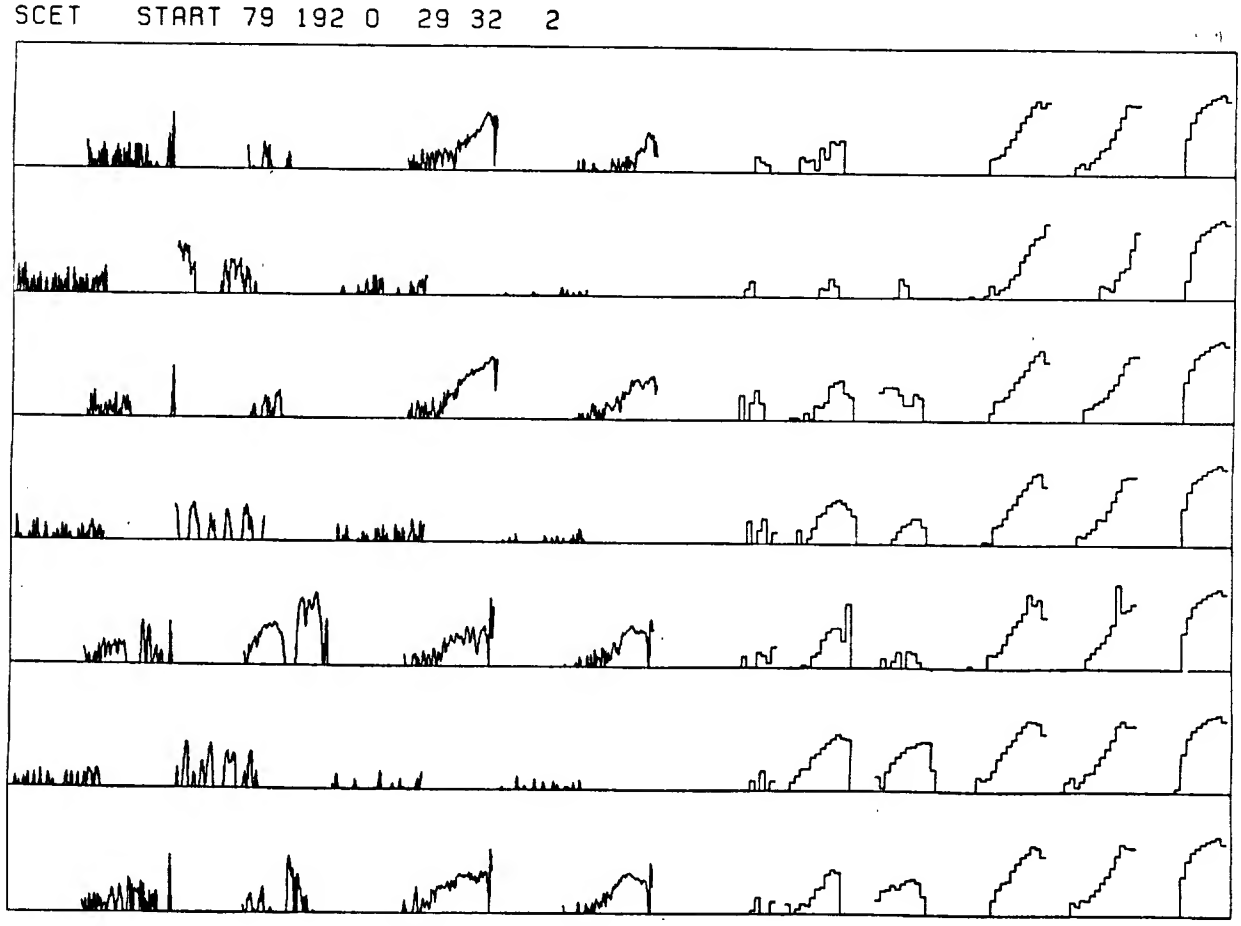

Figure 103

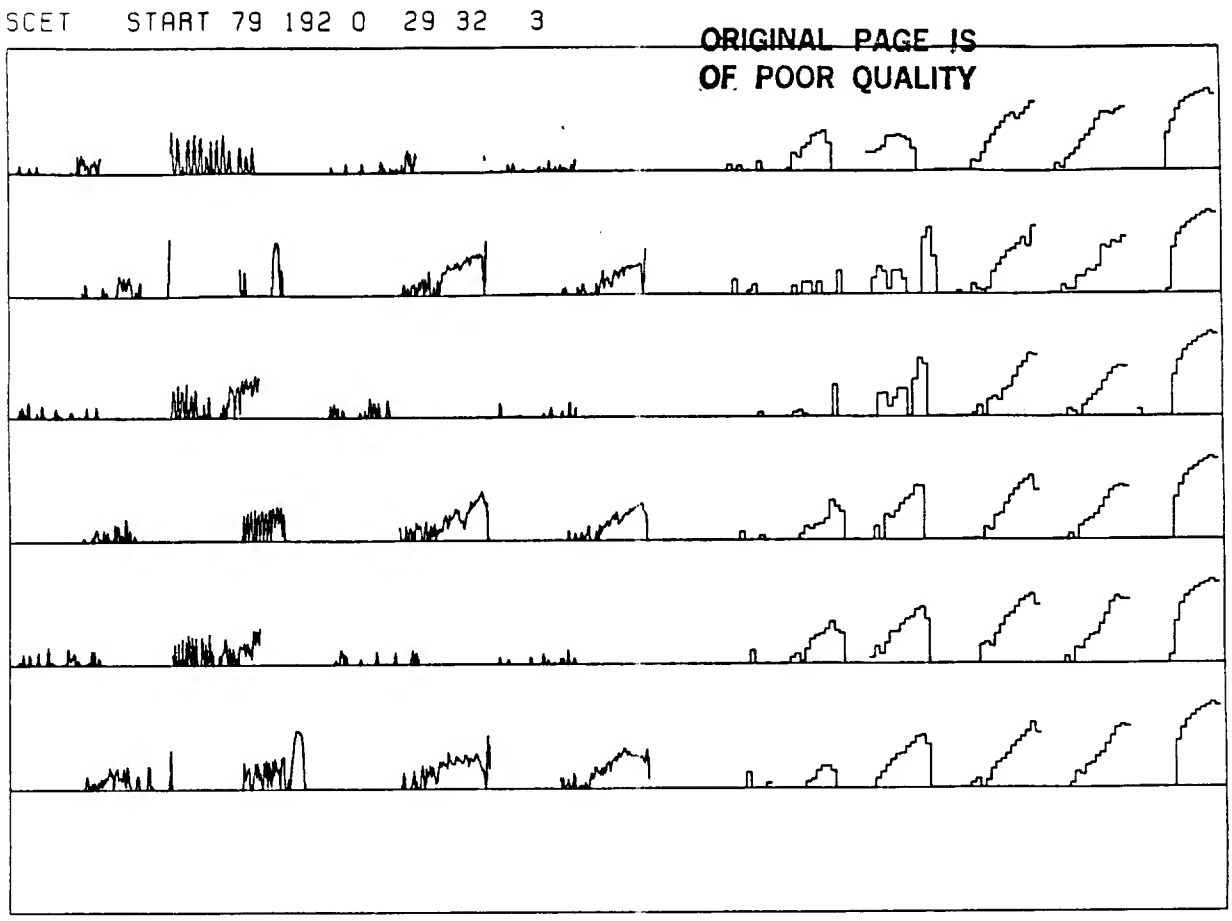

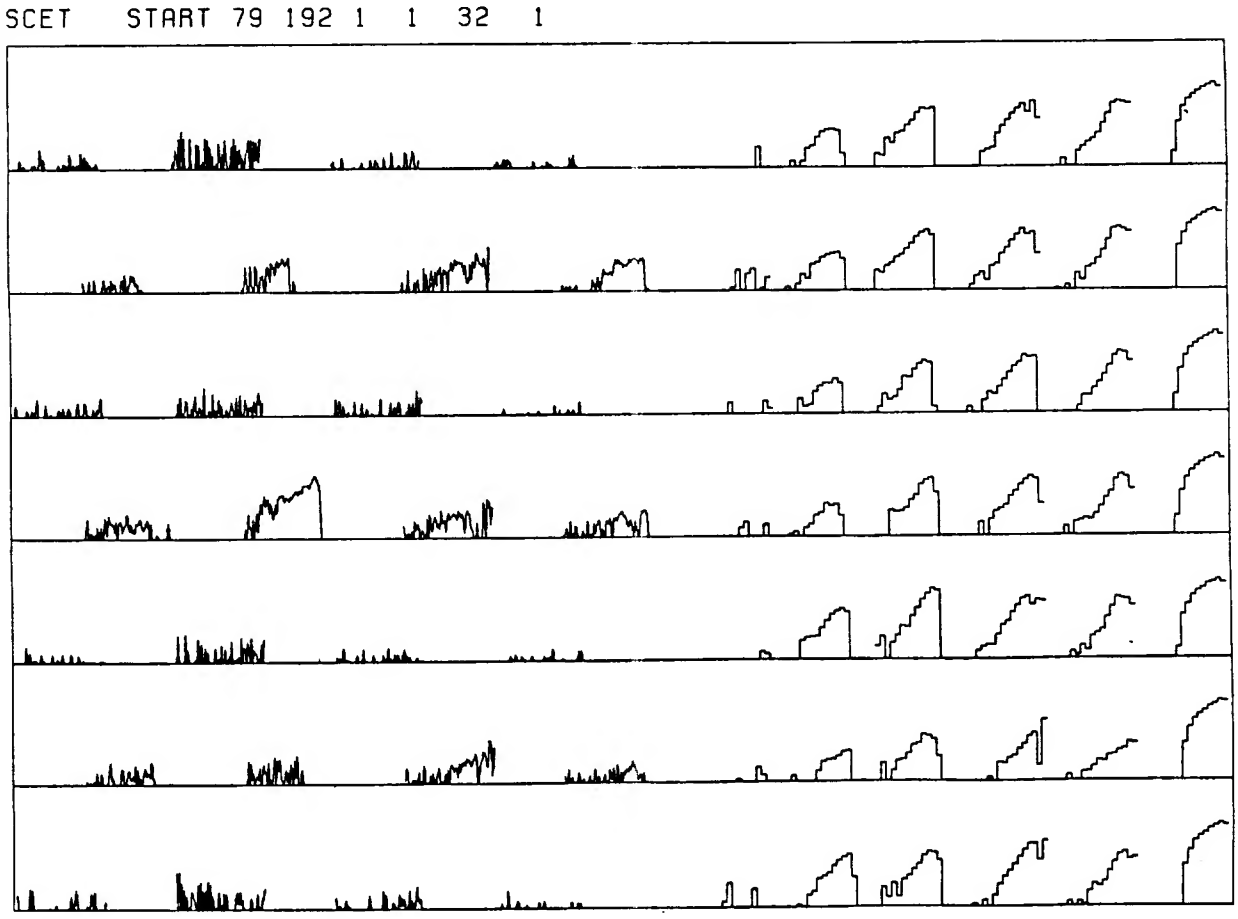

Figure 104

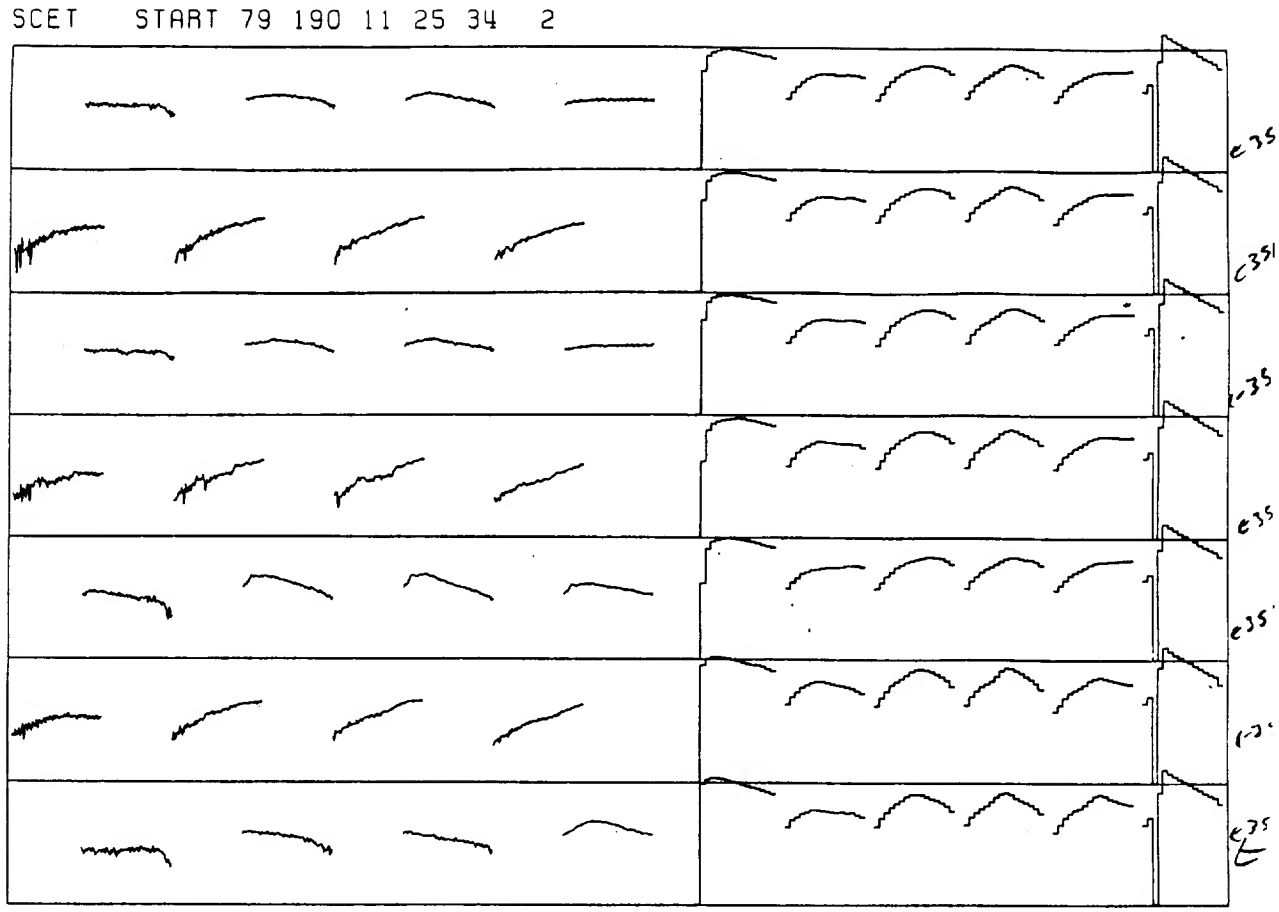

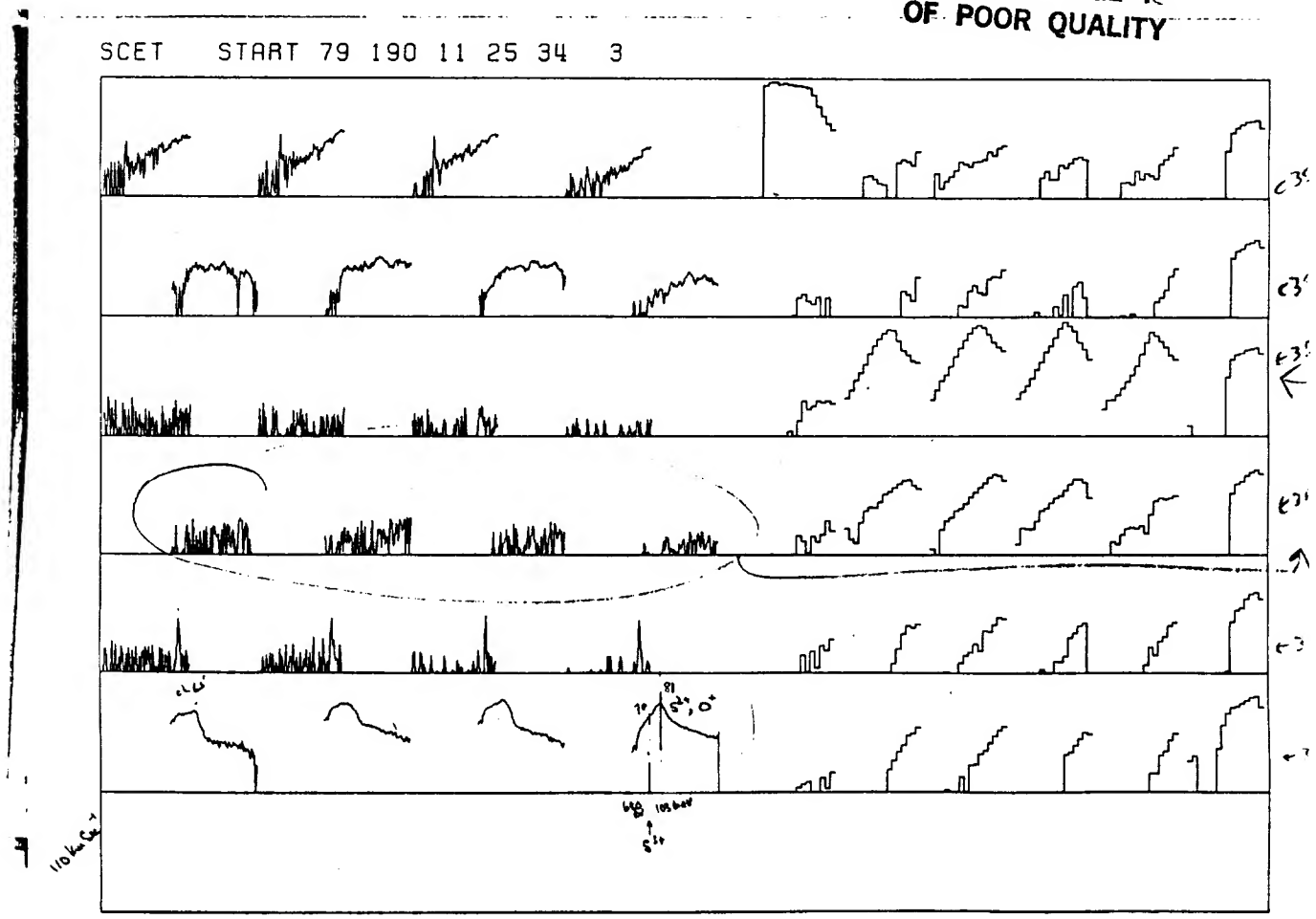

Figure 105

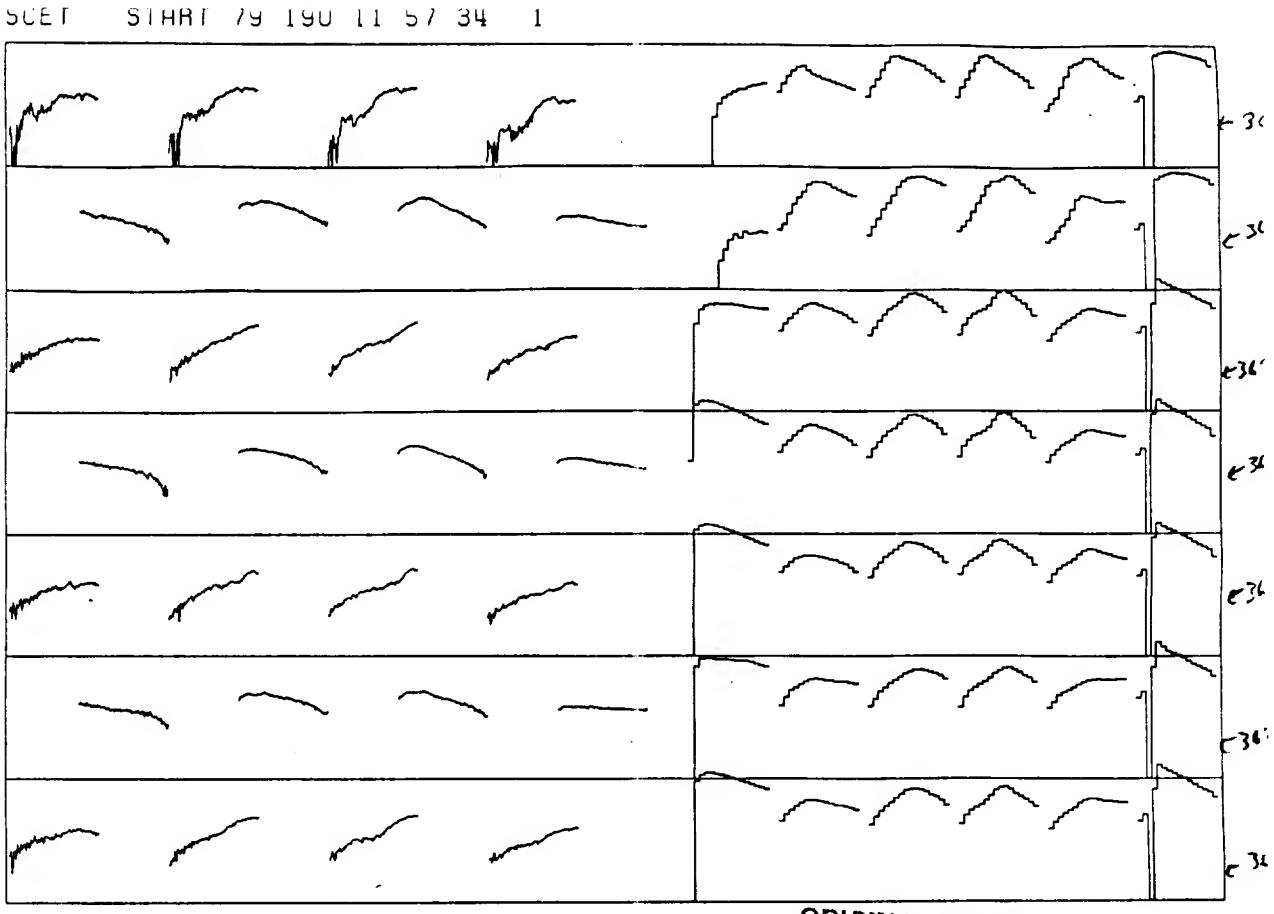

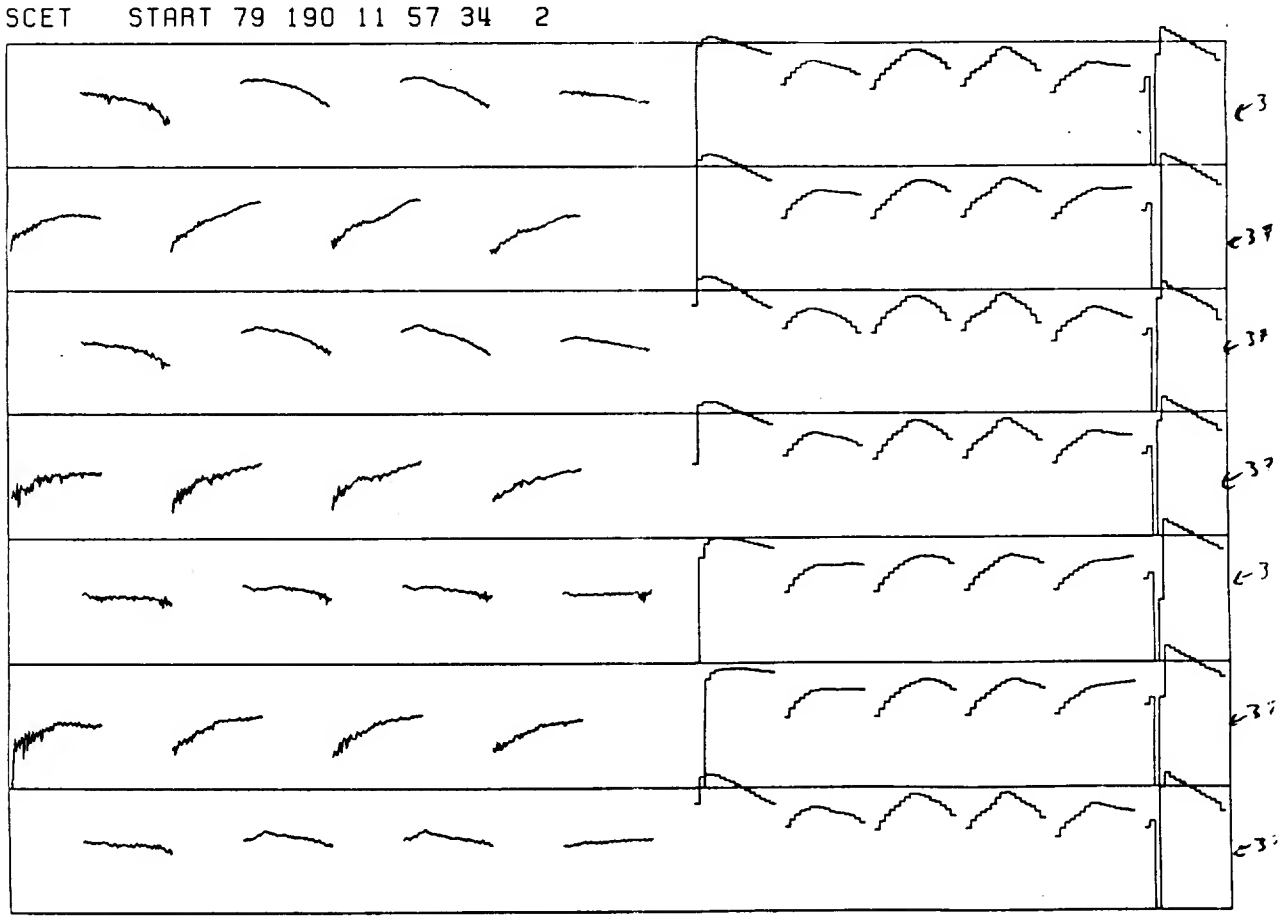

Figure 106

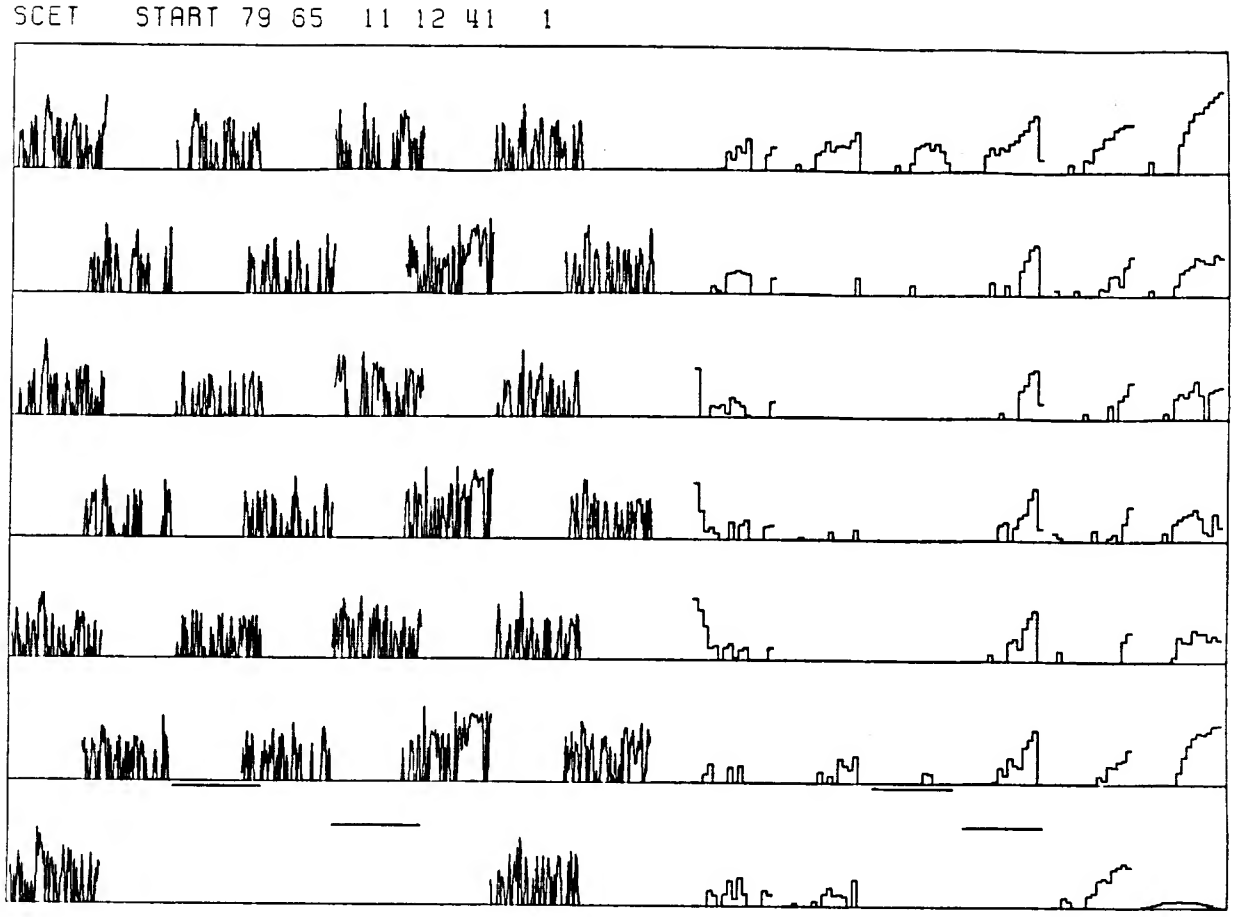

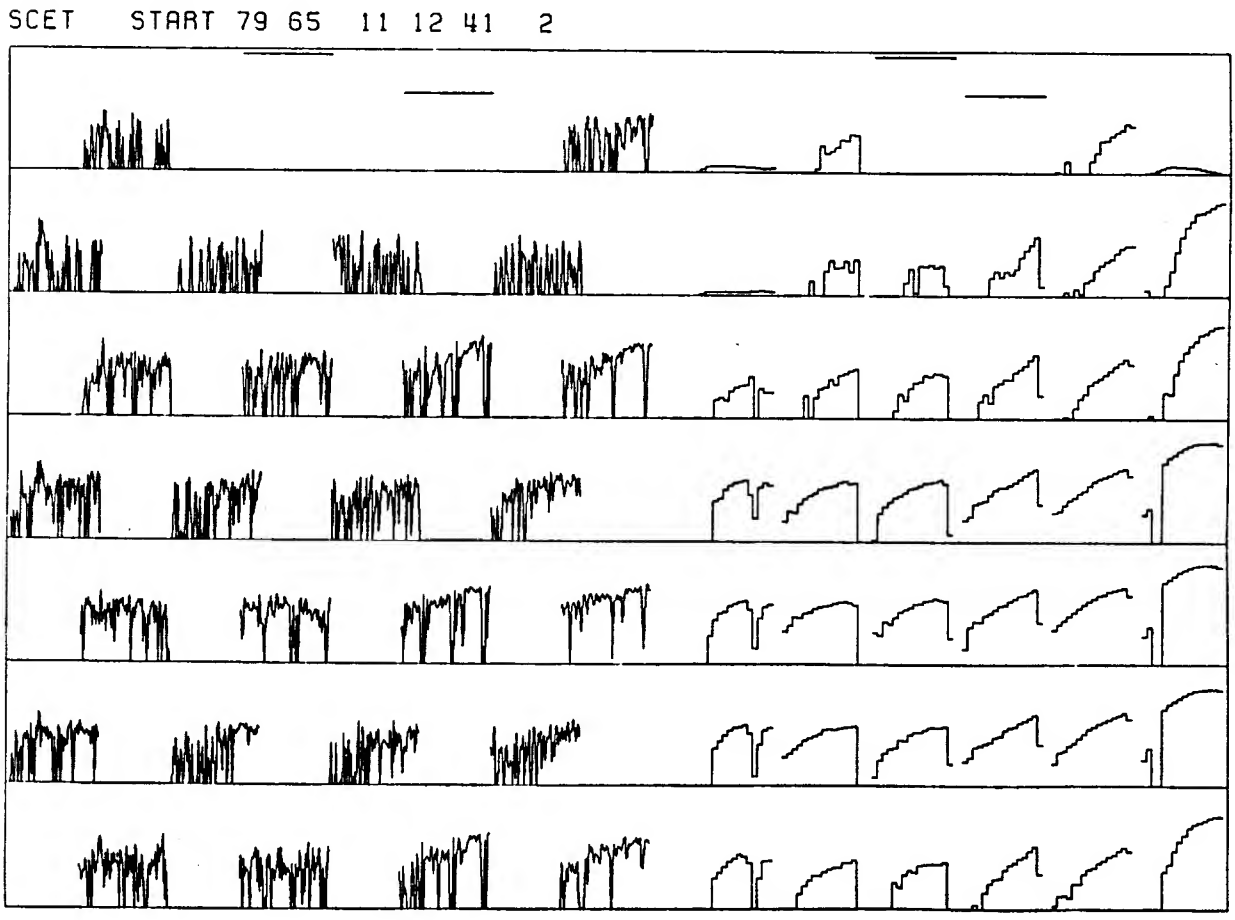

Figure 107

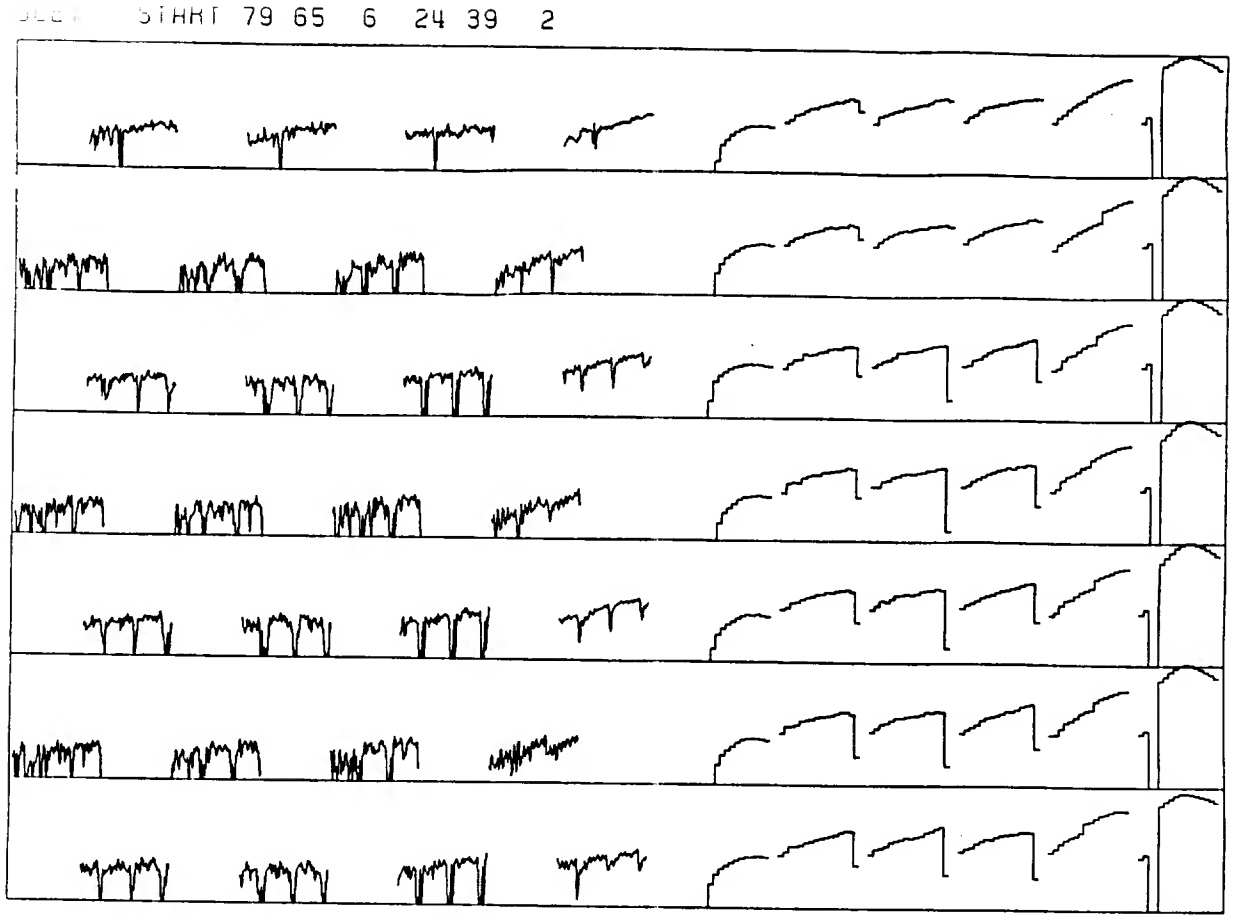

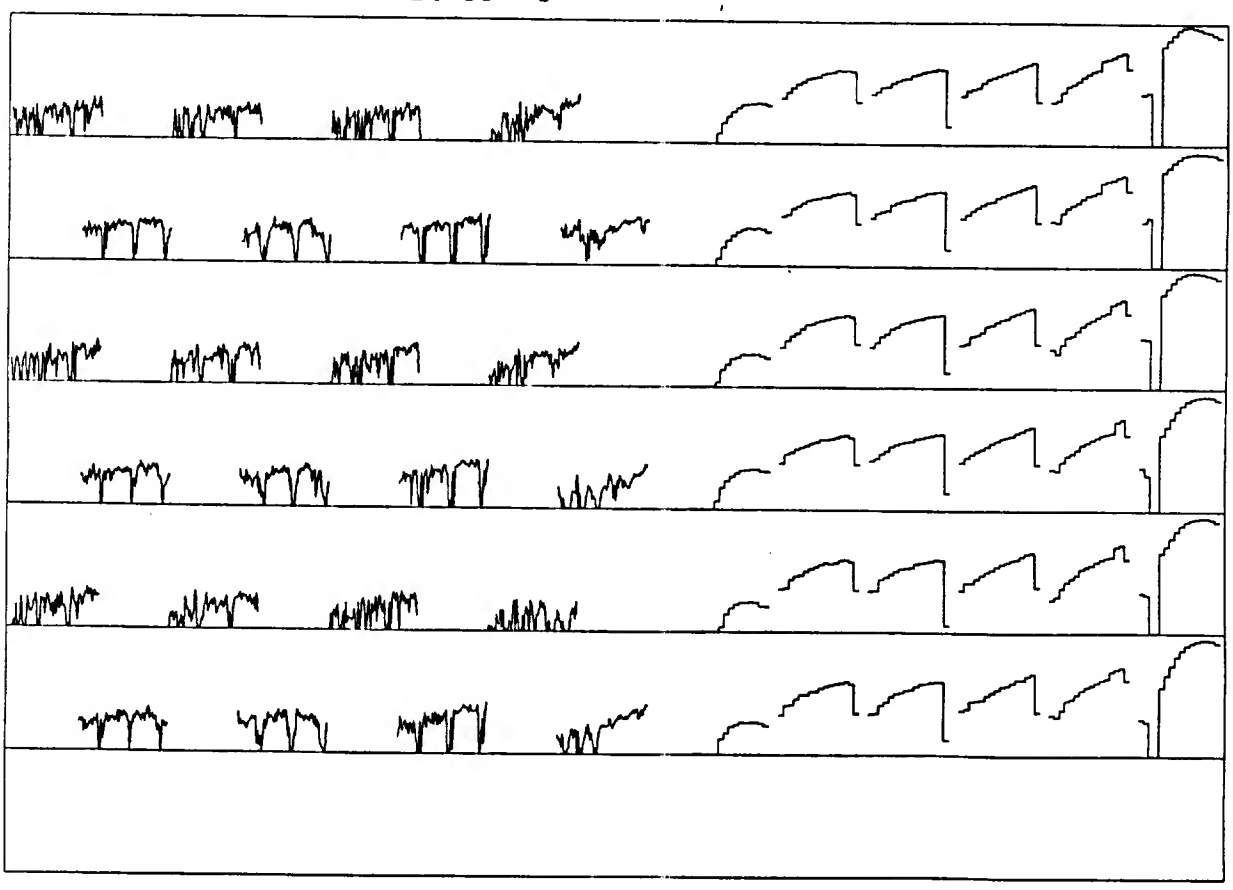

Figure 108

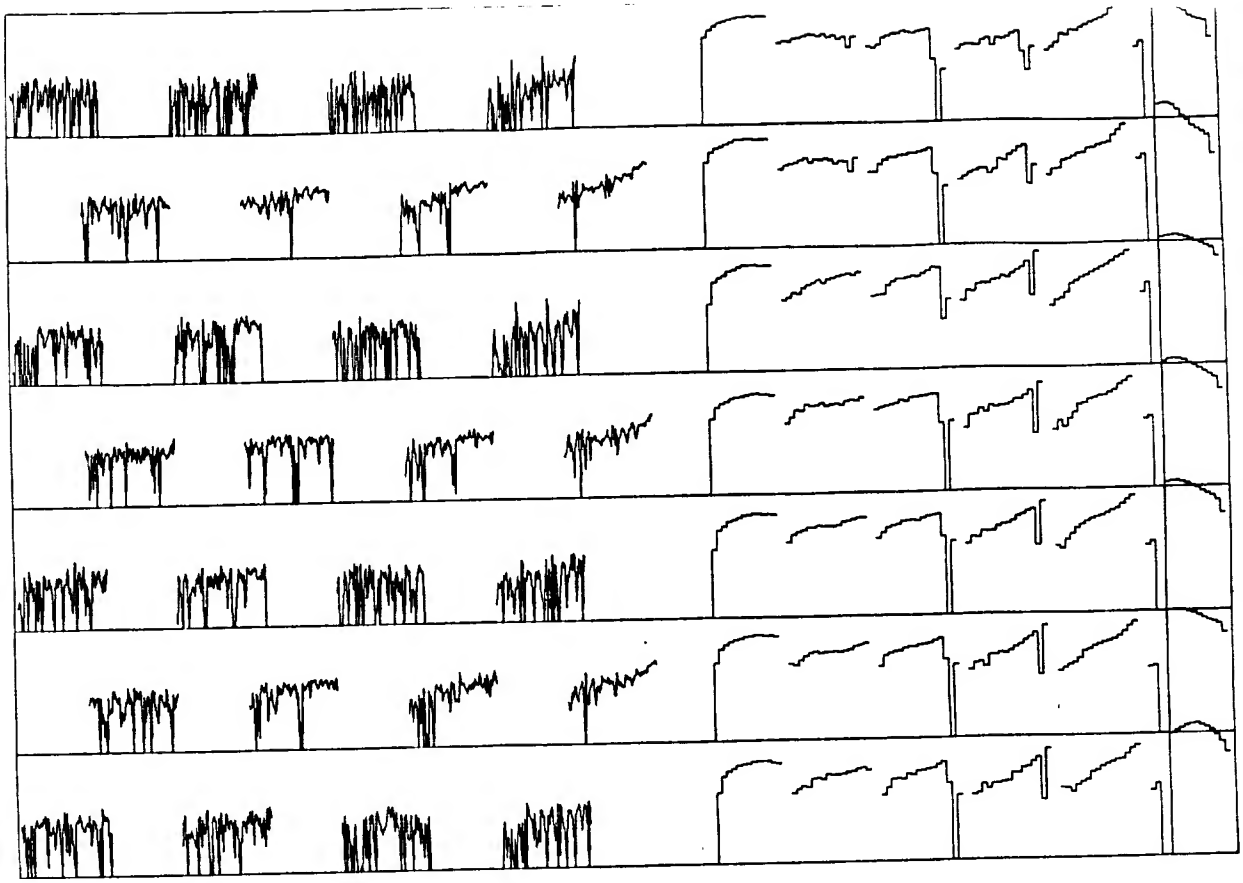

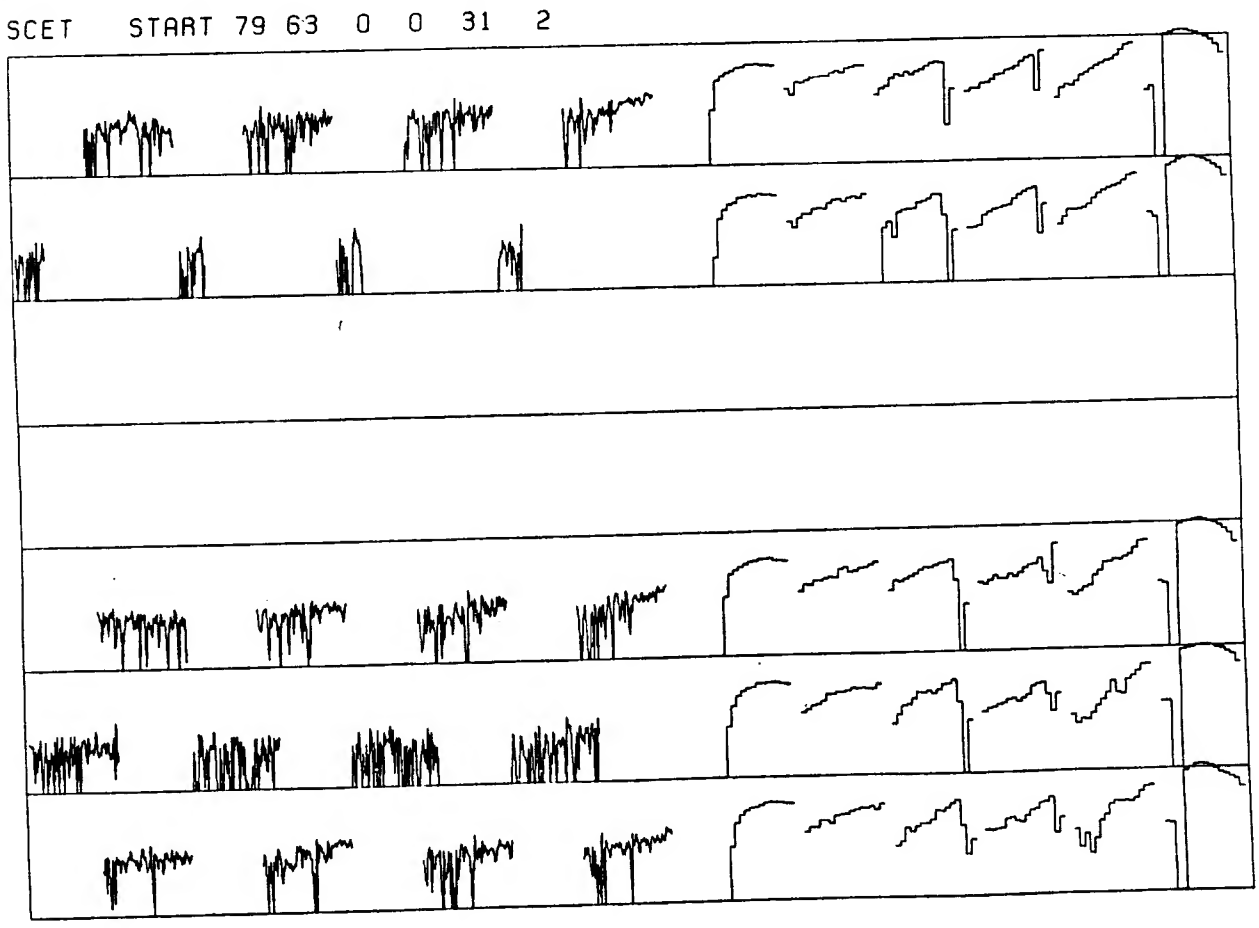

Figure 109

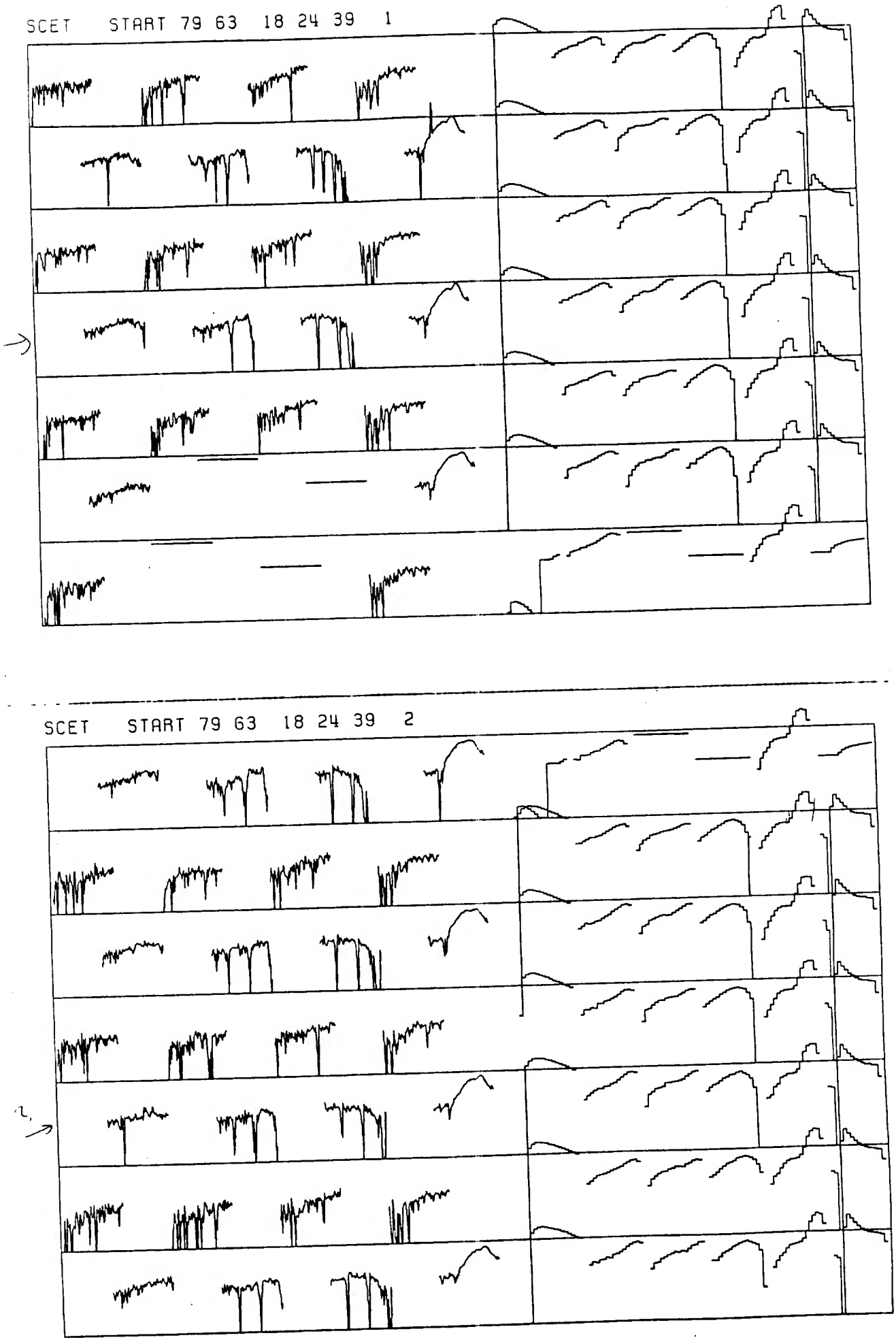

Figure 110

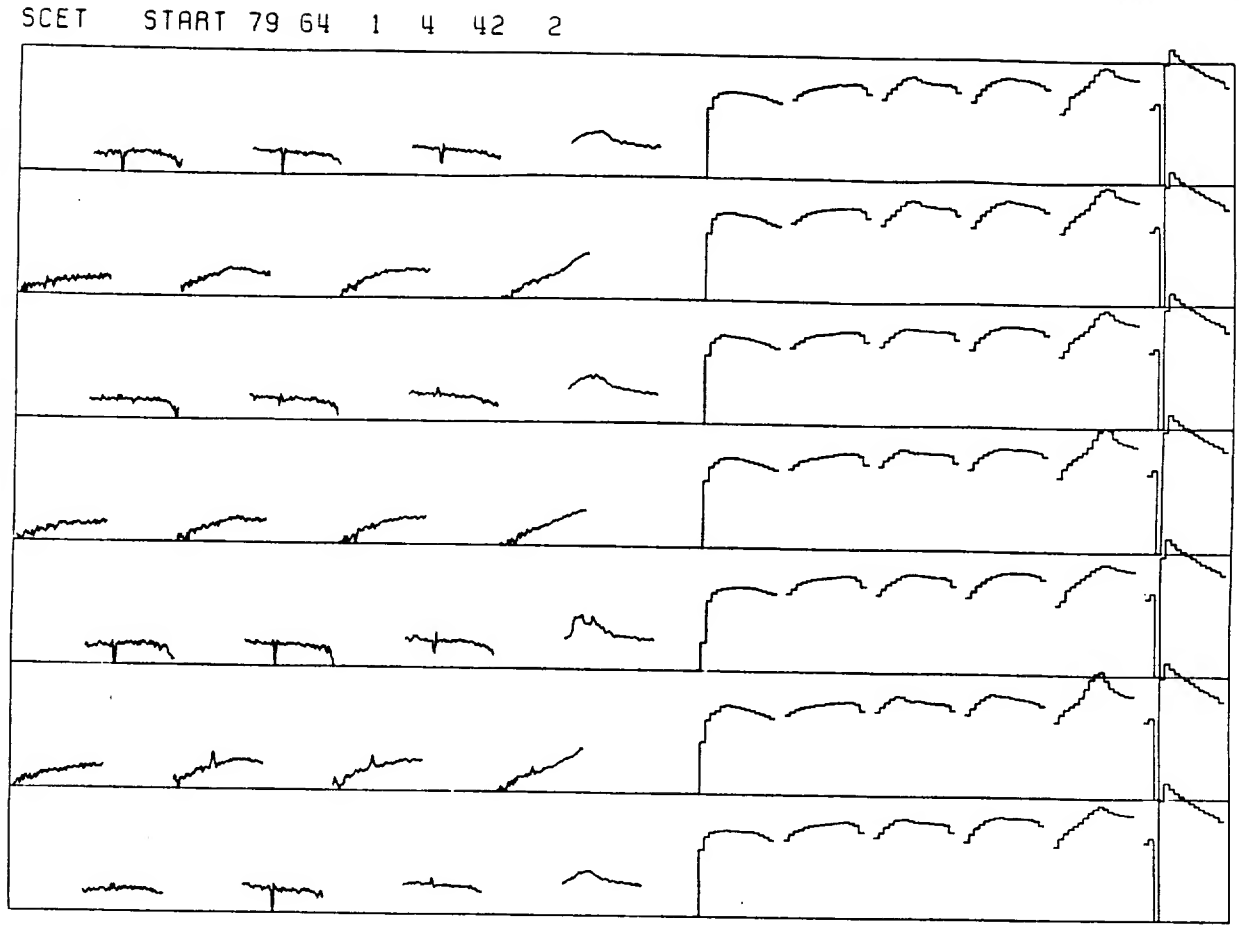

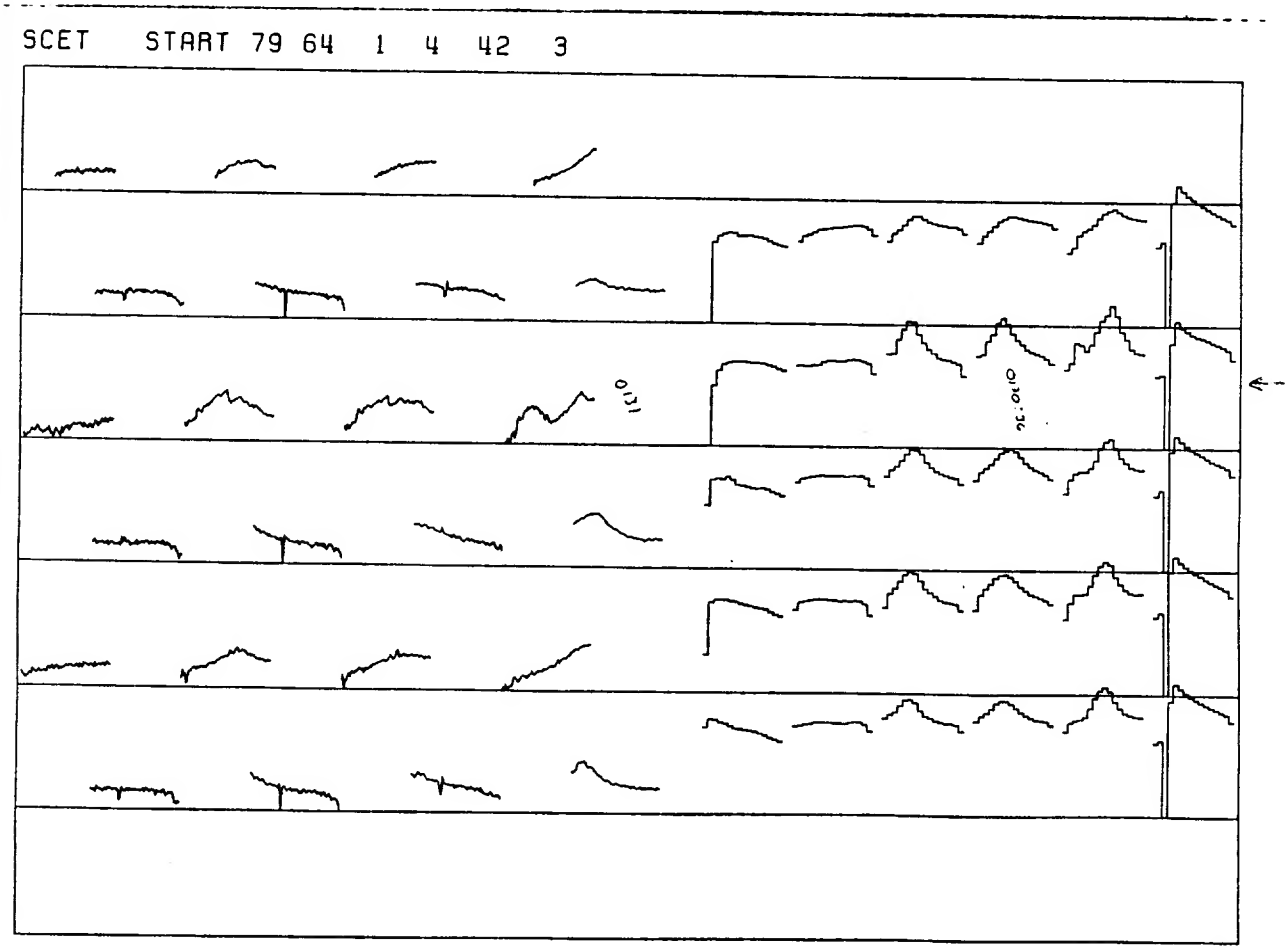

Fig. 111

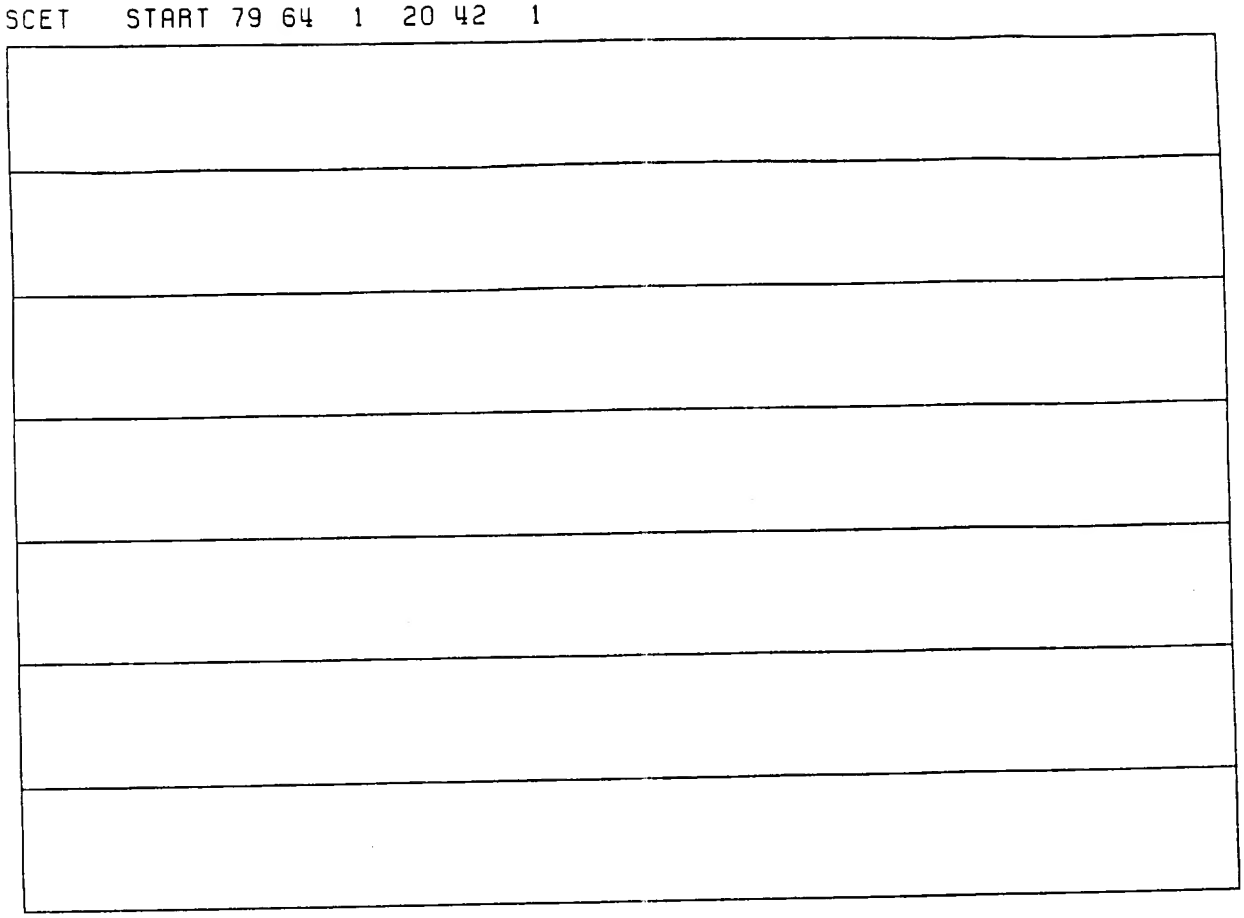

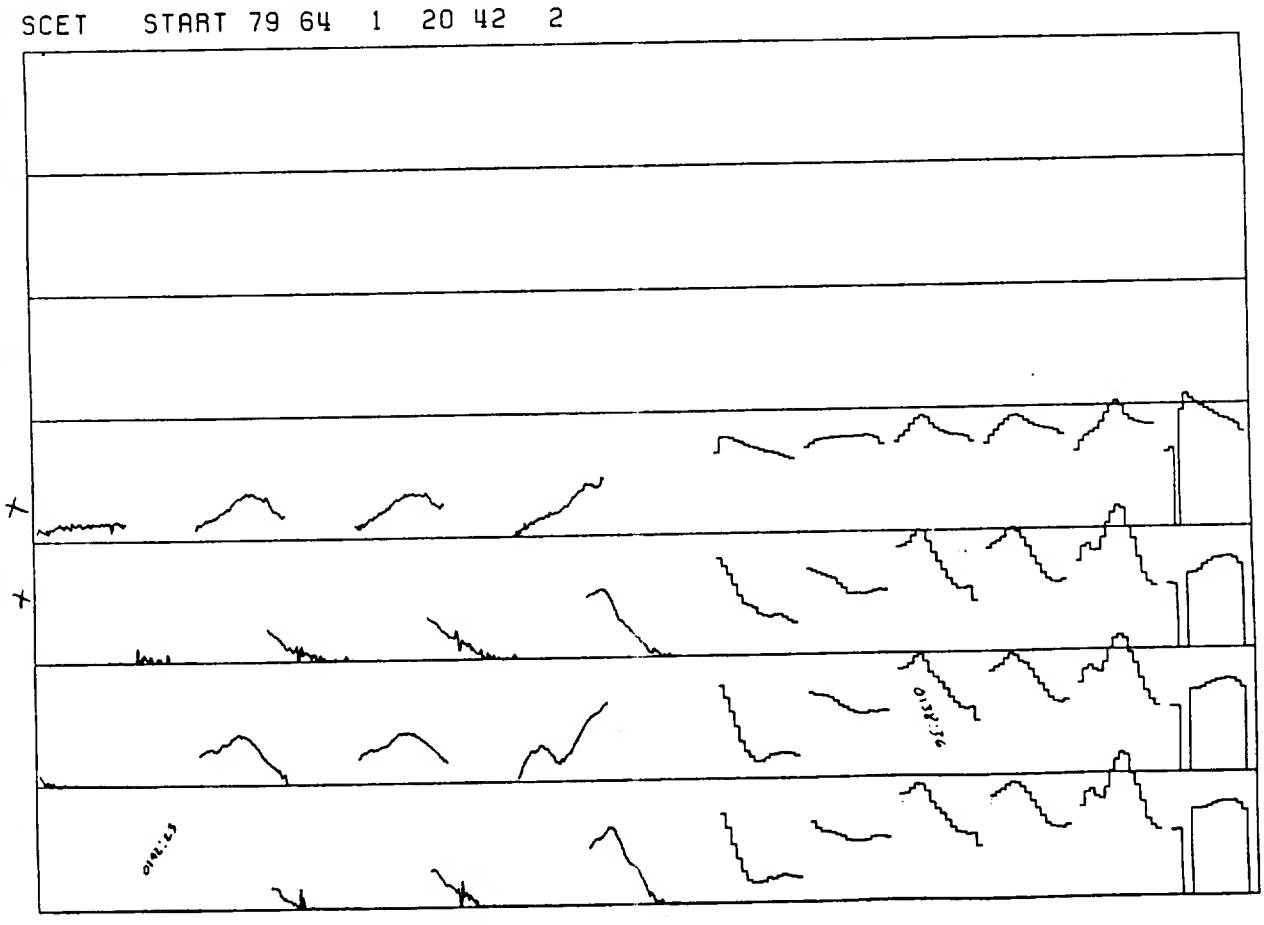

Fig. 112

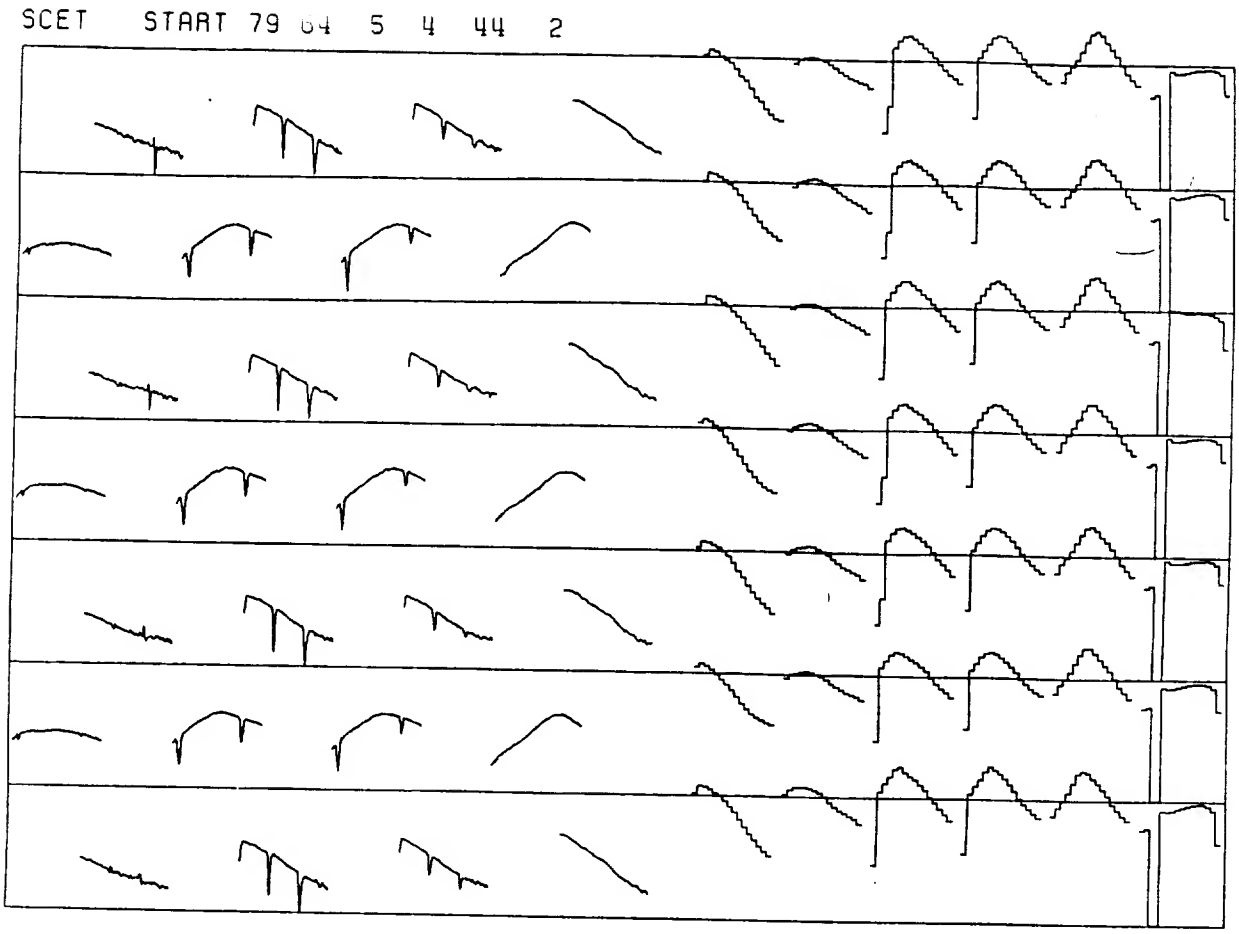

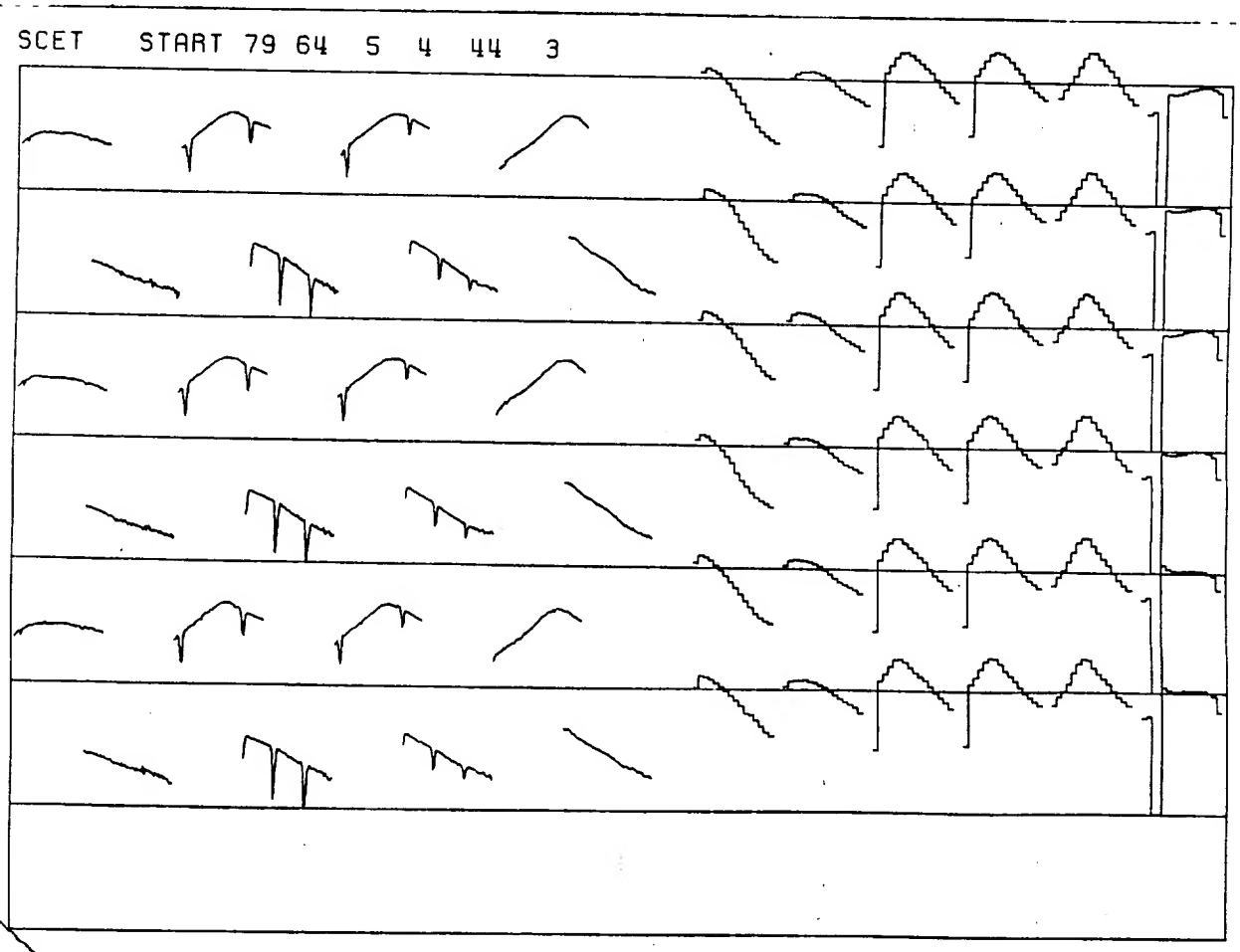

Fig. 113

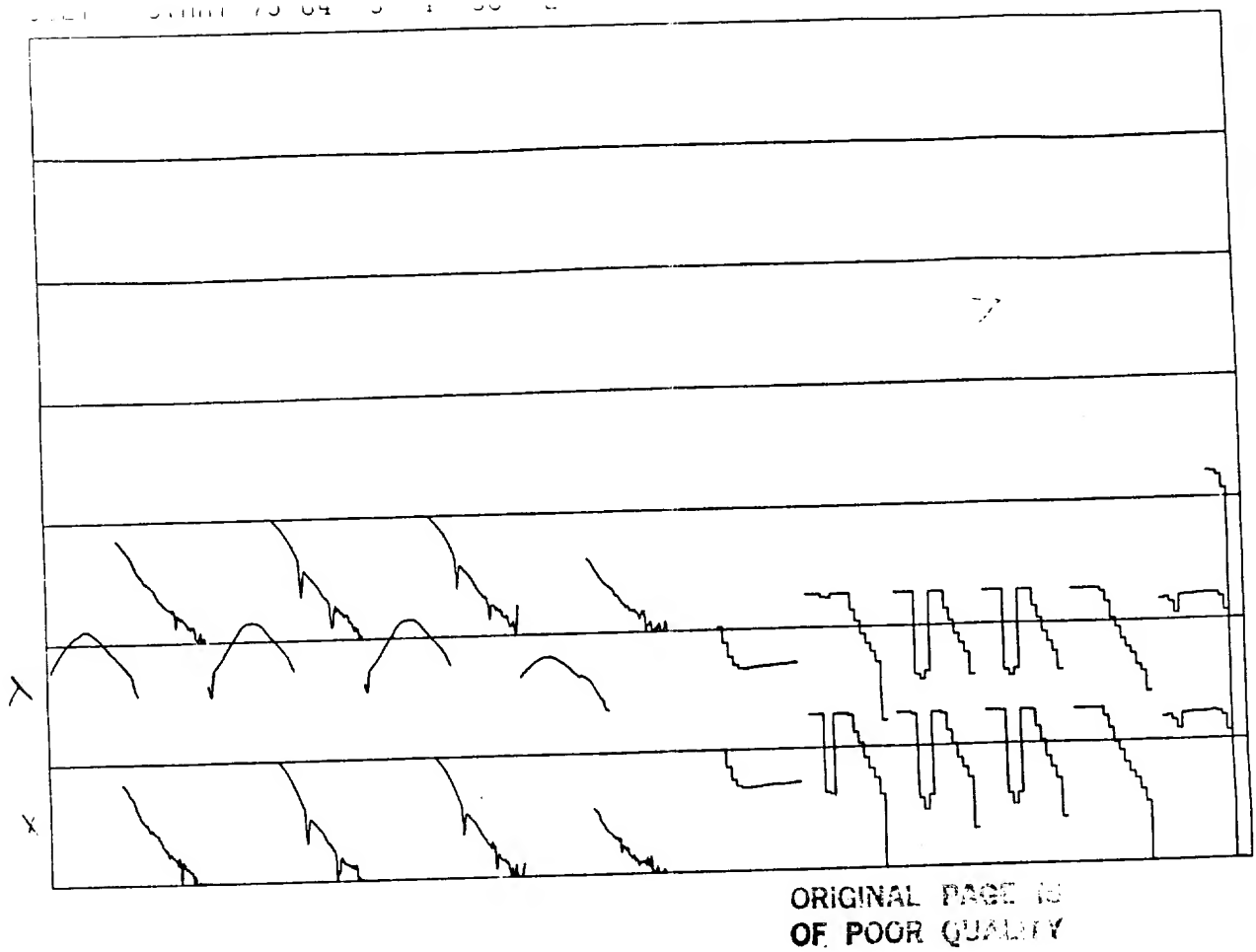

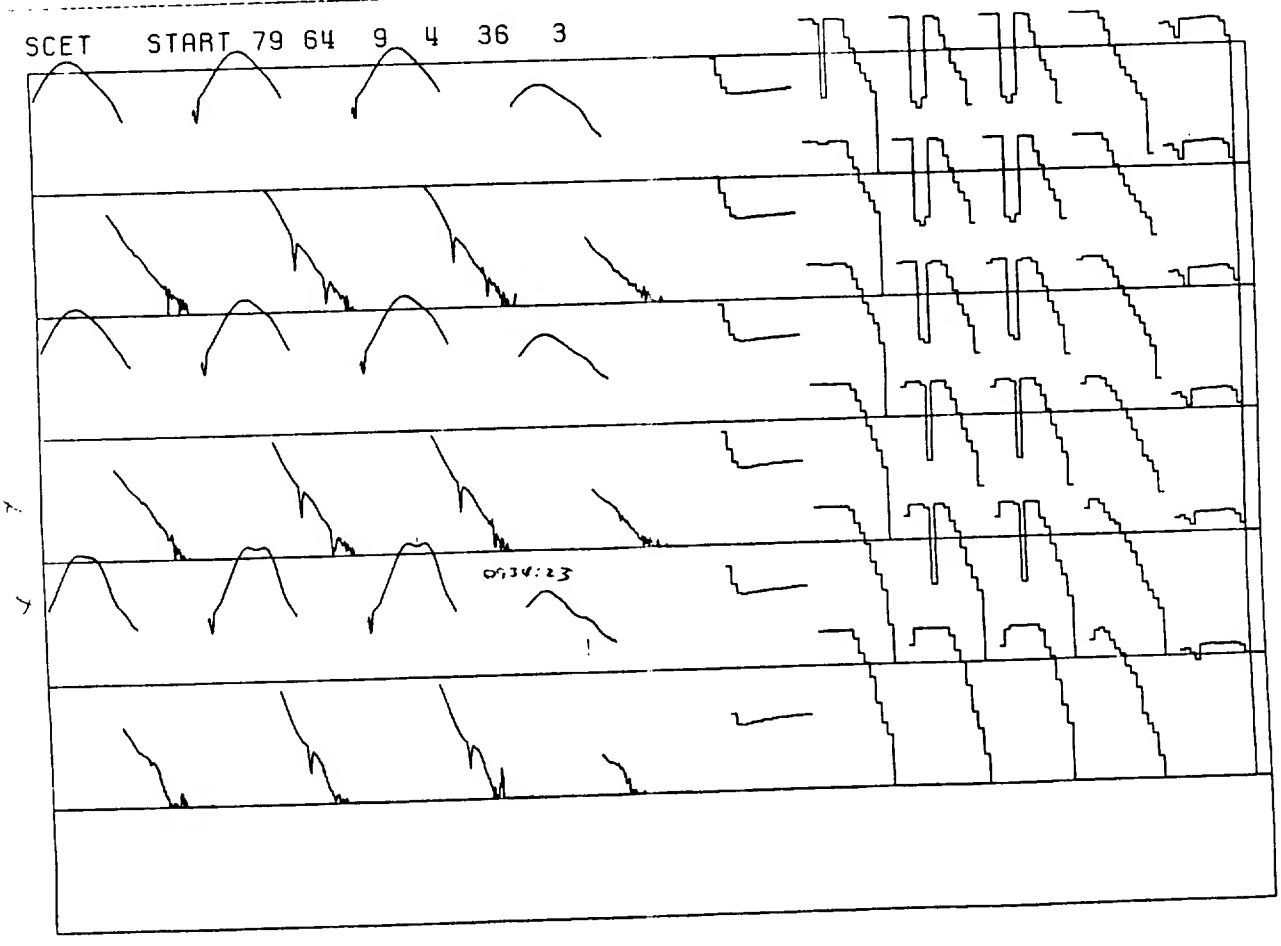

Fig. 114

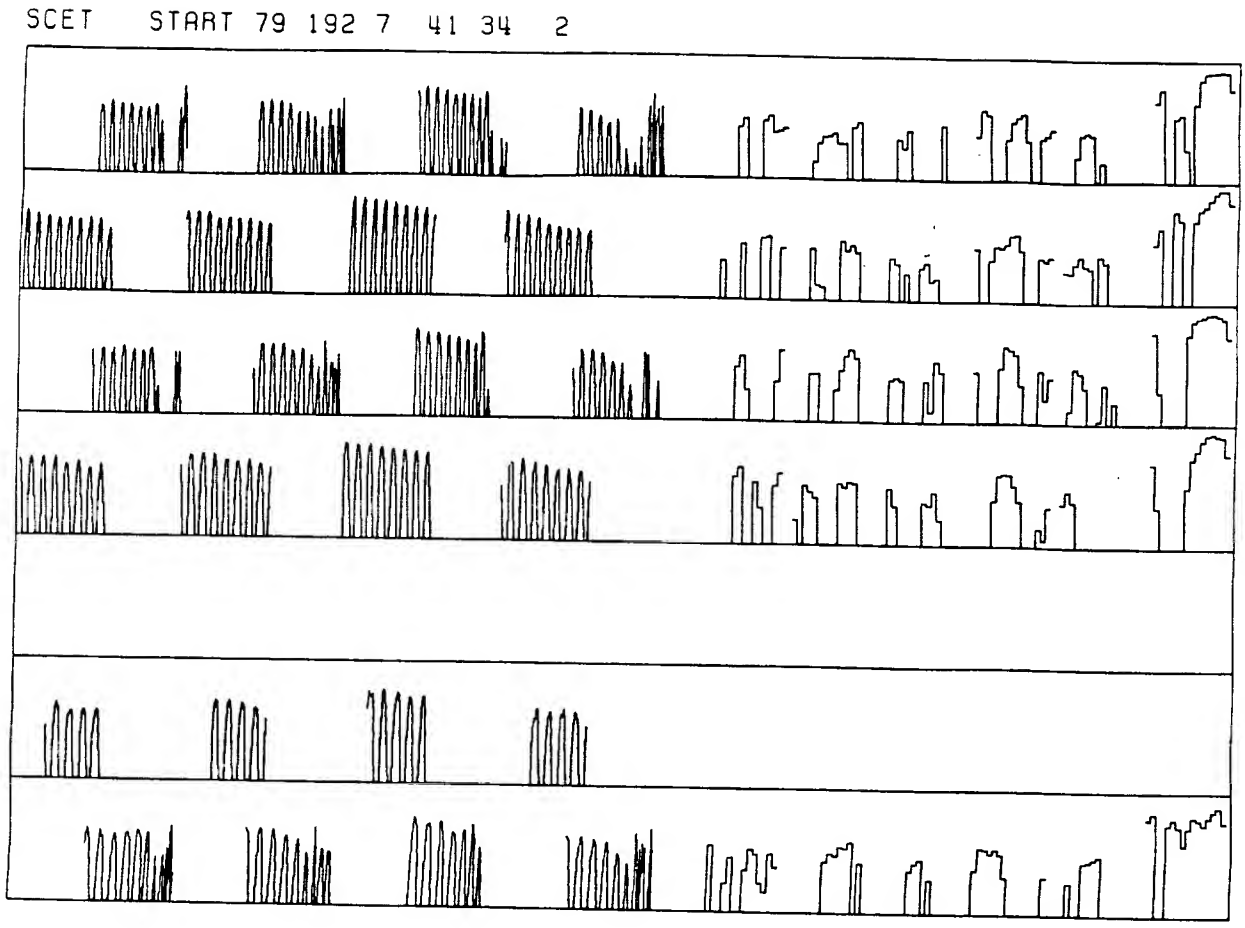

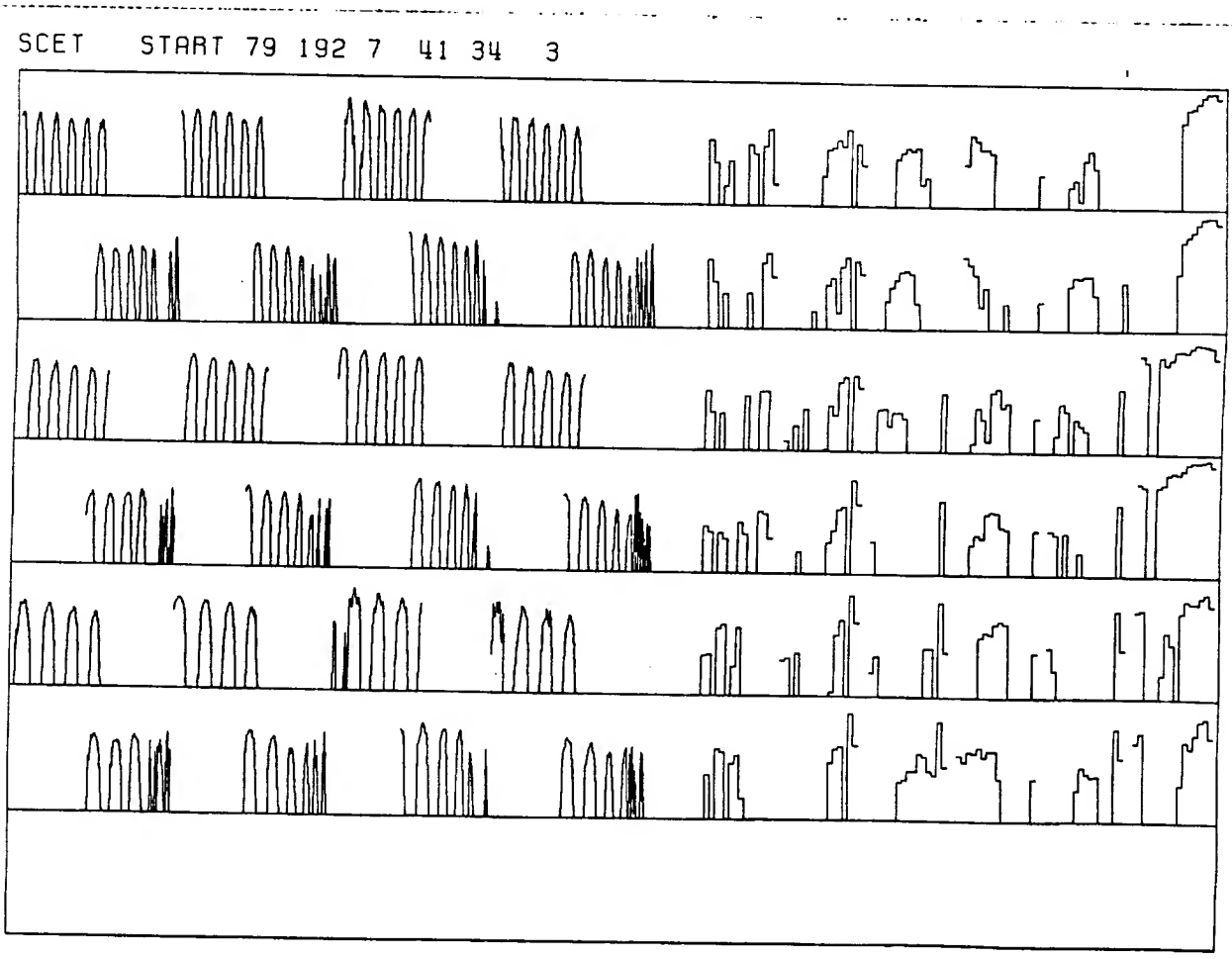

Fig. 115

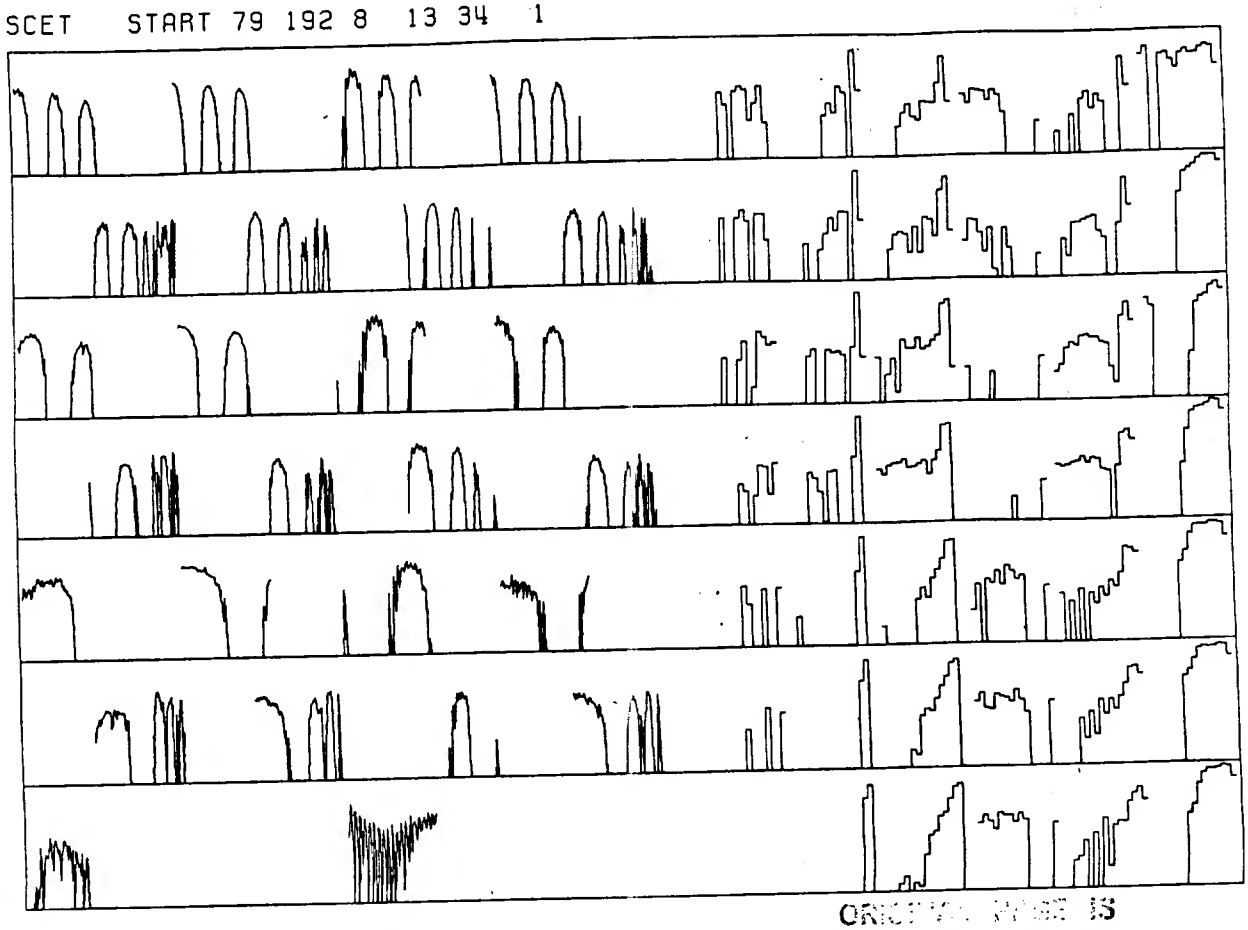

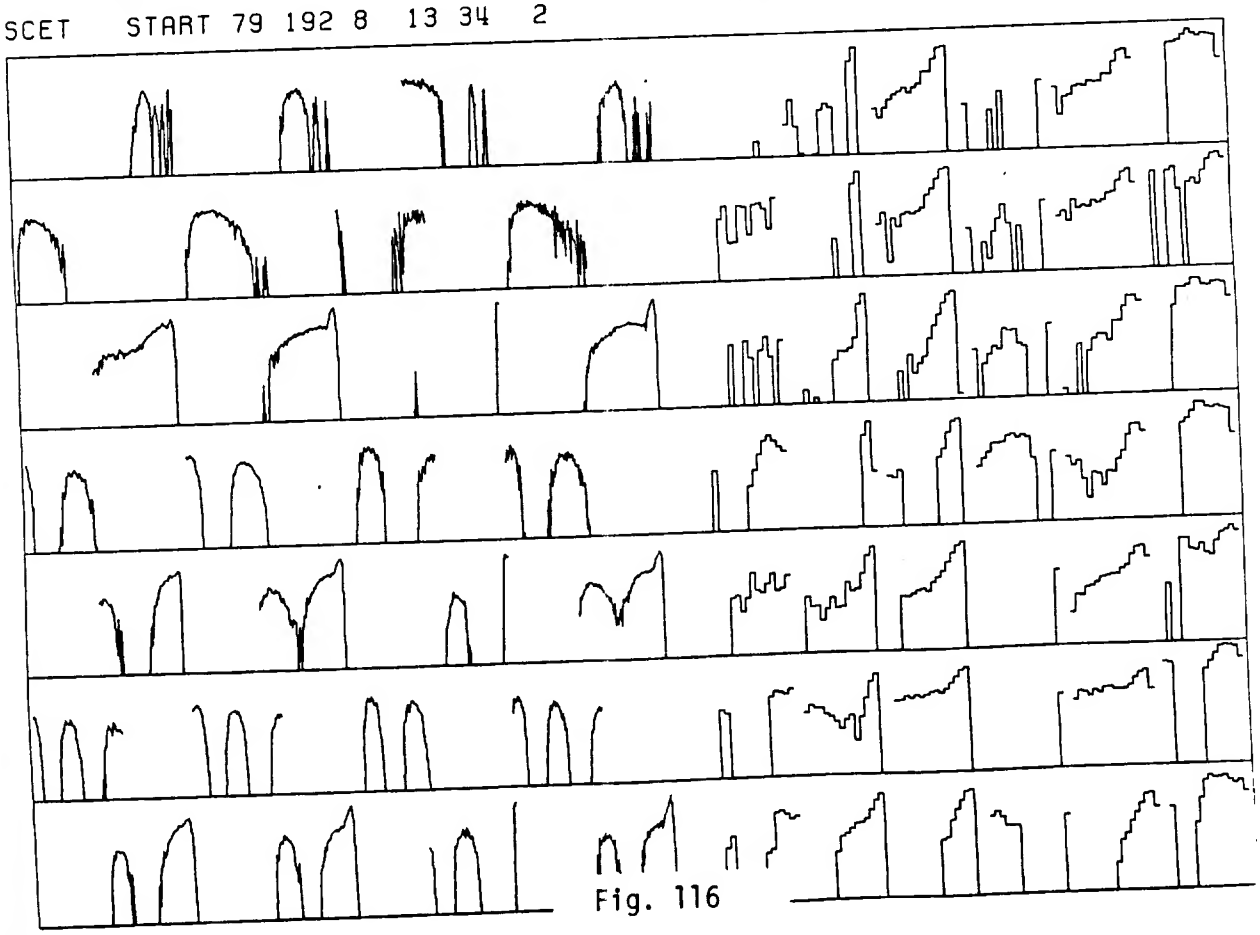

Fig. 116

APPENDIX A

jpl → MJS 77 TELEMETRY CALIBRATION

S/S ABBREV.	MEASUREMENT TITLE		TTS NO.
PLS	PLS SEN T		E-622
SUBASSEMBLY NAME	SUBASSY. REF NO.	SUBASSY. SER. NO.	CALIBRATION TEMP.
Plasma Subsystem	2032	002	N/A
SENSING DEVICE: ☒ TRANSDUCER ☐ OTHER	TRANSDUCER TYPE	TRANSDUCER PART NO: ST 11785-0004	TRANSDUCER SER NO: 8676
CALIBRATED BY: C. Odd	DATE: 10/21/77	APPROVED BY: A.R. Zeiger	DATE: 10/25/77

CALIBRATION: LOAD IMPEDANCE USED: _____ MEGOHMS, _____ TRANSD. EXCITATION _____

MEASURAND (UNITS Deg. C)	OUTPUT (UNITS DN)	MEASURAND (UNITS Deg. C)	OUTPUT (UNITS CN)
-157.59	83	68.299	224
-137.50	102	89.00	232
-116.29	120	108.19	239
- 96.699	135	128.50	246
- 75.199	150	150.19	253
- 55.00	163		
- 34.70	175		
- 14.499	186		
+ 5.100	196		
26.199	206		
46.500	215		

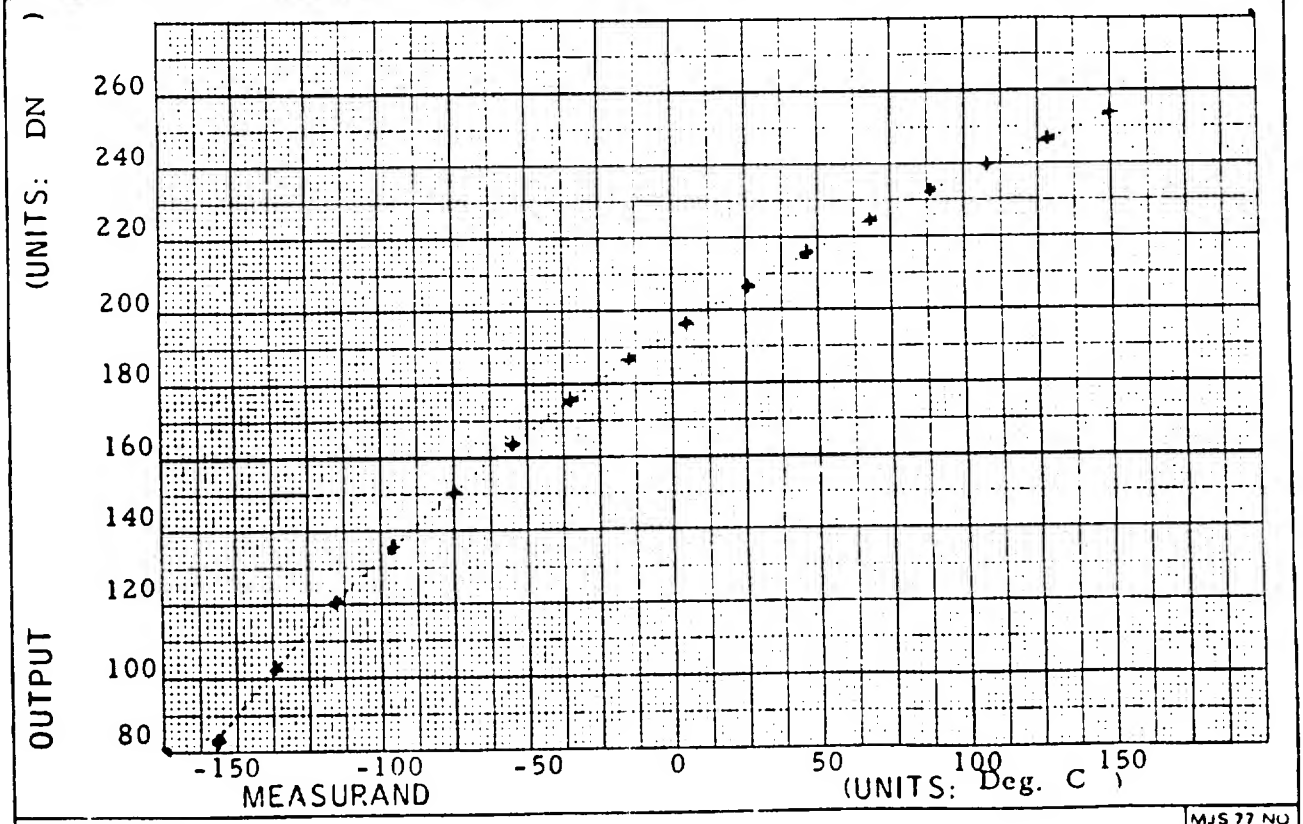

COMMENTS
Table Lookup Coefficients

ORIGINAL PAGE IS OF POOR QUALITY

E-622

MJS 77 NO -2
S/C-31
VGR-1

SC 31

RUN 0697 0022PLS

MJS77 SERIAL NO..... MJS-2
MJS77 FUNCTION ..... PLS SENSOR TEMP

FDS TREESWITCH ID .. 70
FDS RANGE ..... 25-800 OHMS
FDS SERIAL NO..... 2

SUBASSY REF NO..... 2032
SUBASSY SERIAL NO... 002

MEAS CALIB RANGE ... -70 TO 100 DEG C
MEAS CALIB TEMP .... -

XDUCER SERIAL NO.... B676
XDUCER IMPEDANCE ... -
XDUCER CALIB DATE .. 9 OCT 74

DATA PREPARED BY ... ROSEMONT ENG CO
APPROVED BY ... -
APPROVED BY ... R. ROTTER
RUN DATE 0697 0022PLS

STANDARD DEVIATION . .5664324B-01

COEFFICIENT A0 ..... -.20276987+03
COEFFICIENT A1 ..... .52035174+00
COEFFICIENT A2 25540733-03
COEFFICIENT A3 12712726-04

MEASURAND EU	OUTPUT DN	F(X) PRIME	DELTA
-70.00	154.15	-69.9296	-.070376
-60.00	160.56	-60.0212	.021169
-50.00	166.69	-50.0593	.059255
-40.00	172.55	-40.0605	.060527
-30.00	178.18	-30.0336	.033602
-20.00	183.57	-20.0041	.004107
-10.00	188.75	-9.9694	-.030637
.00	193.73	.0513	-.051264
10.00	198.52	10.0619	-.061867
20.00	203.15	20.0596	-.059597
30.00	207.62	30.0397	-.039662
40.00	211.94	40.0054	-.005437
50.00	216.13	49.9684	.031590
60.00	220.20	59.9328	.067192
70.00	224.17	69.9159	.084074
80.00	228.04	79.9327	.067263
90.00	231.83	89.9904	.009581
100.00	235.55	100.1195	-.119519

DATA NUMBER

FRAME 15

	0	2	4	6	8
0	-202.77	-201.73	-200.68	-199.64	-198.58
10	-197.53	-196.47	-195.40	-194.33	-193.25
20	-192.16	-191.06	-189.96	-188.84	-187.72
30	-186.59	-185.44	-184.28	-183.11	-181.93
40	-180.73	-179.52	-178.30	-177.06	-175.80
50	-174.52	-173.23	-171.92	-170.60	-169.25
60	-167.88	-166.50	-165.09	-163.66	-162.21
70	-160.73	-159.24	-157.71	-156.17	-154.60
80	-153.00	-151.37	-149.72	-148.04	-146.34
90	-144.60	-142.84	-141.04	-139.21	-137.36
100	-135.47	-133.55	-131.59	-129.60	-127.58
110	-125.52	-123.43	-121.30	-119.13	-116.92
120	-114.68	-112.40	-110.08	-107.72	-105.32
130	-102.88	-100.39	-97.87	-95.30	-92.69
140	-90.03	-87.33	-84.58	-81.79	-78.95
150	-76.06	-73.13	-70.15	-67.12	-64.04
160	-60.90	-57.72	-54.49	-51.20	-47.86
170	-44.47	-41.03	-37.53	-33.97	-30.36
180	-26.69	-22.97	-19.18	-15.34	-11.44
190	-7.49	-3.47	.61	4.75	8.95
200	13.22	17.55	21.94	26.39	30.91
210	35.50	40.15	44.87	49.66	54.51
220	59.43	64.43	69.49	74.62	79.82
230	85.10	90.44	95.86	101.36	106.92
240	112.57	118.28	124.08	129.95	135.89
250	141.92	148.02	154.20	160.46	

DEG C

E-622

PLS SEN T

SC31

ORIGINAL PAGE IS
OF POOR QUALITY

RUN 0697 0022PLS

FRAME 16

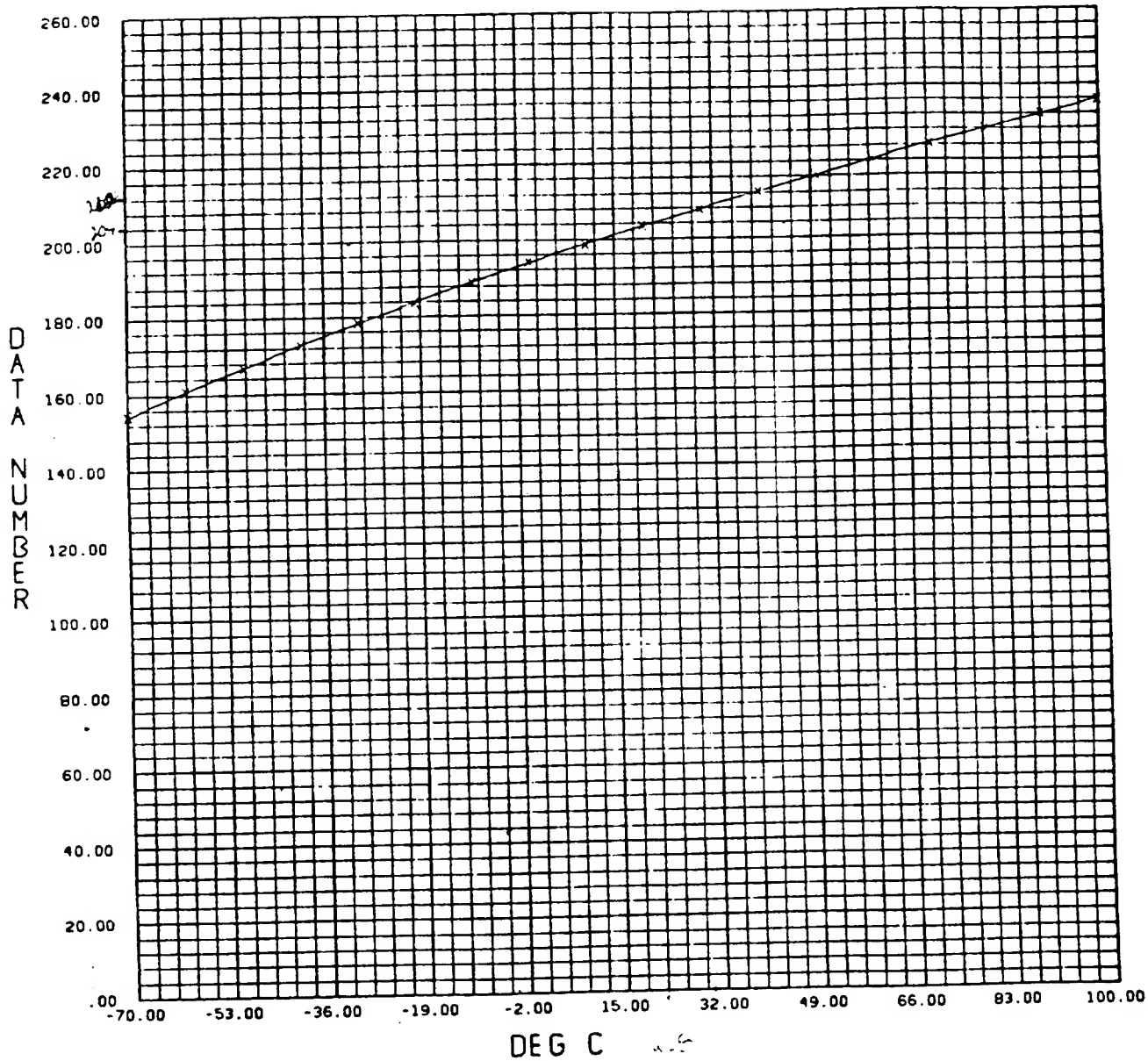

E-622 PLS SEN T

SC 31

ORIGINAL PAGE IS
OF POOR QUALITY

RUN 0397 0022PLS

MUX SERIAL NO..... MUS-2
MUX FUNCTION ..... PLS MODULATOR TEMP

FDS TREESWITCH ID .. 58
FDS RANGE ..... 350-700 OHMS
FDS SERIAL NO..... 2

SUB-ASSY REF NO..... 2036
SUB-ASSY SERIAL NO... 002

MEAS CALIB RANGE ... -70 TO 100 DEG C
MEAS CALIB TEMP .... -

XDUCER SERIAL NO.... LA55
XDUCER IMPEDANCE ... -
XDUCER CALIB DATE .. 11 NOV 74

DATA PREPARED BY ... ROSEMONT ENG CO
APPROVED BY ... -
APPROVED BY ... R. ROTTER
RUN DATE 0397 0022PLS

STANDARD DEVIATION . .34950328+00

COEFFICIENT A0 ..... -.79657113+02
COEFFICIENT A1 ..... .70390205+00

MEASURED EU	OUTPUT DN	F(X) PRIME	DELTA
-70.00	12.74	-70.6907	.690693
-60.00	27.32	-60.4288	.428842
-50.00	41.84	-50.2076	.207632
-40.00	56.30	-40.0271	.027062
-30.00	70.71	-29.8921	-.117947
-20.00	85.06	-19.7675	-.232475
-10.00	99.40	-9.6986	-.311442
.00	113.69	.3599	-.359927
10.00	127.92	10.3830	-.393015
20.00	142.12	20.3907	-.380699
30.00	156.28	30.3479	-.347901
40.00	170.40	40.2937	-.269705
50.00	184.48	50.2010	-.201028
60.00	198.53	60.0970	.096950
70.00	212.53	69.9424	.057608
80.00	226.49	79.7724	.227567
90.00	240.42	89.5771	.422926
100.00	254.31	99.3512	.648767

DATA NUMBER

FRAME 7

	0	2	4	6	8
0	-79.66	-78.25	-76.84	-75.43	-74.03
10	-72.62	-71.21	-69.80	-68.39	-66.99
20	-65.58	-64.17	-62.76	-61.36	-59.95
30	-58.54	-57.13	-55.72	-54.32	-52.91
40	-51.50	-50.09	-48.69	-47.28	-45.87
50	-44.46	-43.05	-41.65	-40.24	-38.83
60	-37.42	-36.02	-34.61	-33.20	-31.79
70	-30.38	-28.98	-27.57	-26.16	-24.75
80	-23.34	-21.94	-20.53	-19.12	-17.71
90	-16.31	-14.90	-13.49	-12.08	-10.67
100	-9.27	-7.86	-6.45	-5.04	-3.64
110	-2.23	-.82	.59	2.00	3.40
120	4.81	6.22	7.63	9.03	10.44
130	11.85	13.26	14.67	16.07	17.48
140	18.89	20.30	21.70	23.11	24.52
150	25.93	27.34	28.74	30.15	31.56
160	32.97	34.38	35.78	37.19	38.60
170	40.01	41.41	42.82	44.23	45.64
180	47.05	48.45	49.86	51.27	52.68
190	54.08	55.49	56.90	58.31	59.72
200	61.12	62.53	63.94	65.35	66.75
210	68.16	69.57	70.98	72.39	73.79
220	75.20	76.61	78.02	79.42	80.83
230	82.24	83.65	85.06	86.46	87.87
240	89.28	90.69	92.09	93.50	94.91
250	96.32	97.73	99.13	100.54	

DEG C

E-623

PLS MOD T

SCJ1

ORIGINAL PAGE IS
OF POOR QUALITY

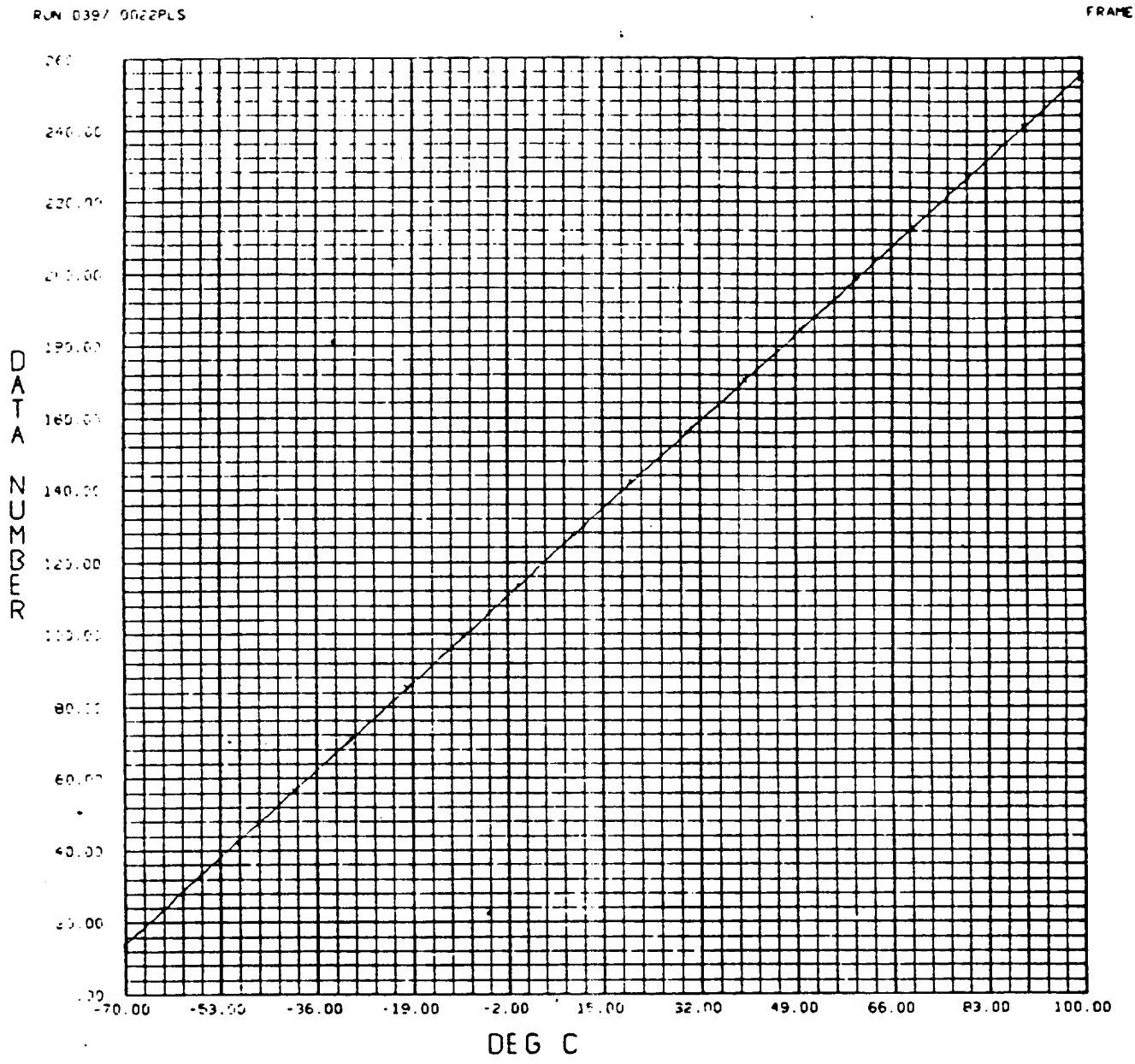

E-623 PLS MOD T

Sc 31

ORIGINAL PAGE IS
OF POOR QUALITY

RUN 0397 0022PLS

MJS77 SERIAL NO..... MJS-2
MJS77 FUNCTION ..... PLS ELECTRONICS TEMP

FDS TREESWITCH ID .. F6
FDS RANGE ..... 350-700 OHMS
FDS SERIAL NO..... 2

SUBASSY REF NO..... 2032
SUBASSY SERIAL NO... 002

MEAS CALIB RANGE ... -70 TO 100 DEG C
MEAS CALIB TEMP .... -

XDUCER SERIAL NO.... 6135
XDUCER IMPEDANCE ... -
XDUCER CALIB DATE .. 3 MAR 72

DATA PREPARED BY ... ROSEMONT ENG CO
APPROVED BY ... -
APPROVED BY ... R. ROTTER
RUN DATE 0397 0022PLS

STANDARD DEVIATION . .34991763+00

COEFFICIENT A0 ..... -.80105934+02
COEFFICIENT A1 ..... .70414370+00

MEASURAND EU	OUTPUT DN	F(X) PRIME	DELTA
-70.00	13.37	-70.6930	.692955
-60.00	27.94	-60.4312	.431180
-50.00	42.46	-50.2050	.204986
-40.00	56.92	-40.0245	.024534
-30.00	71.33	-29.8797	-.120341
-20.00	85.69	-19.7704	-.229637
-10.00	100.00	-9.6916	-.308435
.00	114.28	.3618	-.361824
10.00	128.51	10.3847	-.384717
20.00	142.71	20.3822	-.382193
30.00	156.86	30.3492	-.349177
40.00	170.98	40.2857	-.285661
50.00	185.06	50.2018	-.201819
60.00	199.10	60.0875	-.087479
70.00	213.09	69.9426	.057352
80.00	227.05	79.7724	.227600
90.00	240.98	89.5767	.423261
100.00	254.86	99.3506	.649419

DATA NUMBER

FRAME

	0	2	4	6	8
0	-80.11	-78.70	-77.29	-75.88	-74.47
10	-73.06	-71.66	-70.25	-68.84	-67.43
20	-66.02	-64.61	-63.21	-61.80	-60.39
30	-58.98	-57.57	-56.17	-54.76	-53.35
40	-51.94	-50.53	-49.12	-47.72	-46.31
50	-44.90	-43.49	-42.08	-40.67	-39.27
60	-37.86	-36.45	-35.04	-33.63	-32.22
70	-30.82	-29.41	-28.00	-26.59	-25.18
80	-23.77	-22.37	-20.96	-19.55	-18.14
90	-16.73	-15.32	-13.92	-12.51	-11.10
100	-9.69	-8.28	-6.87	-5.47	-4.06
110	-2.65	-1.24	.17	1.57	2.98
120	4.39	5.80	7.21	8.62	10.02
130	11.43	12.84	14.25	15.66	17.07
140	18.47	19.88	21.29	22.70	24.11
150	25.52	26.92	28.33	29.74	31.15
160	32.56	33.97	35.37	36.78	38.19
170	39.60	41.01	42.42	43.82	45.23
180	46.64	48.05	49.46	50.86	52.27
190	53.68	55.09	56.50	57.91	59.31
200	60.72	62.13	63.54	64.95	66.36
210	67.76	69.17	70.58	71.99	73.40
220	74.81	76.21	77.62	79.03	80.44
230	81.85	83.26	84.66	86.07	87.48
240	88.89	90.30	91.71	93.11	94.52
250	95.93	97.34	98.75	100.15	

DEG C

E-621

PLS EL T

SC31

ORIGINAL PAGE IS
OF POOR QUALITY

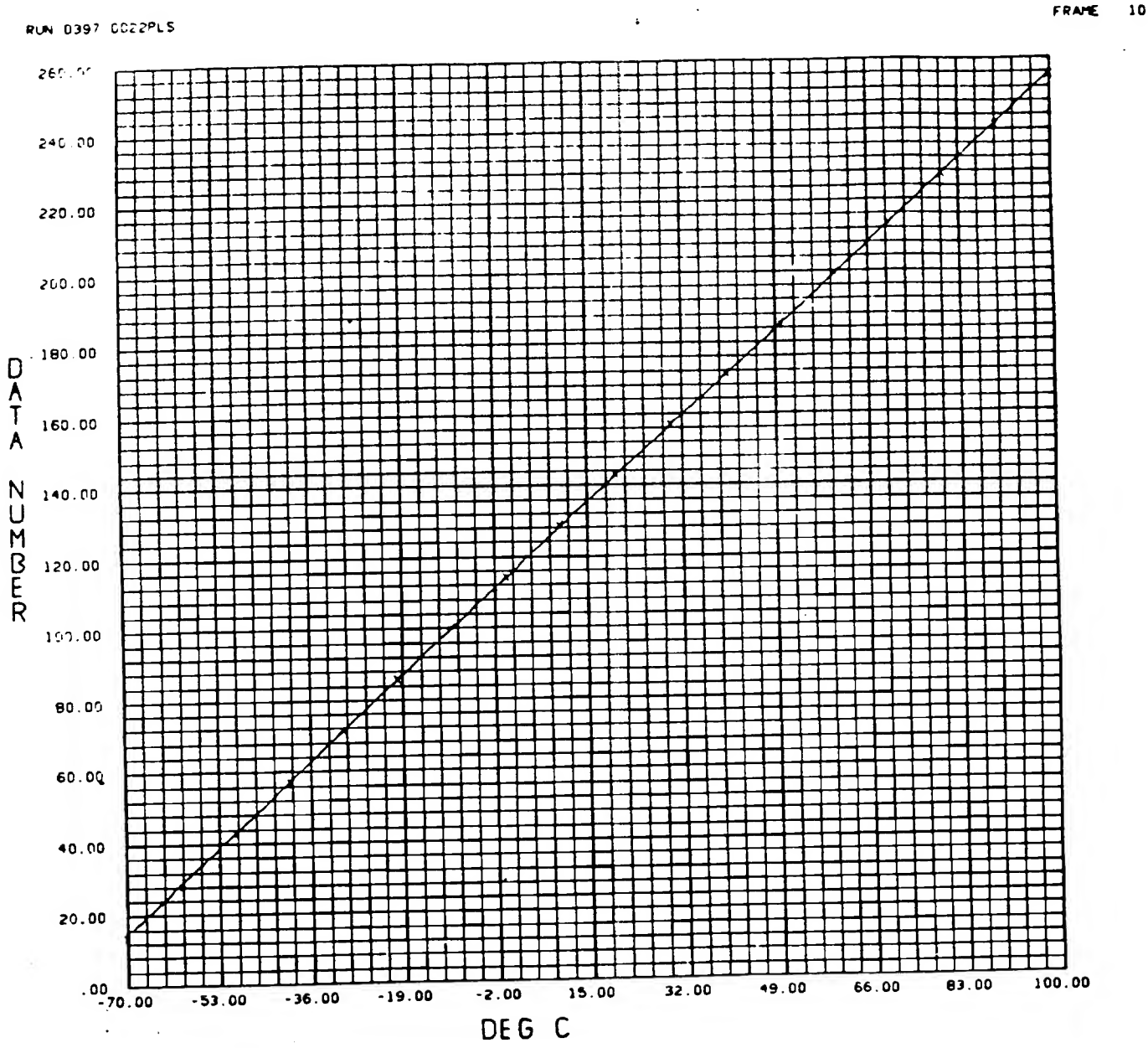

E-621

PLS EL T

APPENDIX B

```
space /usr4/gsg/src/test
Fri May 15 15:40:15 EDT 1987

 ds =   0.99600000000000   d =  0.   volts =   7.70000000000000  e0 =
  2.50000000000000
 rlmint(  0.  ) =    7.6731593544950d-02
 rlmint(    2.4804687500000d-02  ) =    7.6731593544950d-02
 rlmint(    4.9609375000000d-02  ) =    7.6731593544950d-02
 rlmint(    7.4414062500000d-02  ) =    7.6731593544950d-02
 rlmint(    9.9218750000000d-02  ) =    7.6731593544950d-02
 rlmint(   0.12402343750000  ) =    7.6731593544950d-02
 rlmint(   0.14882812500000  ) =    7.6731593544950d-02
 rlmint(   0.17363281250000  ) =    7.6731593544950d-02
 rlmint(   0.19843750000000  ) =    7.6731593544950d-02
 rlmint(   0.22324218750000  ) =    7.6731593544950d-02
 rlmint(   0.24804687500000  ) =    7.6731593544950d-02
 rlmint(   0.27285156250000  ) =    7.6731593544950d-02
 rlmint(   0.29765625000000  ) =    7.6731593544950d-02
 rlmint(   0.32246093750000  ) =    7.6731593544950d-02
 rlmint(   0.34726562500000  ) =    7.6731593544950d-02
 rlmint(   0.37207031250000  ) =    7.6731593544950d-02
 rlmint(   0.39687500000000  ) =    7.6731593544950d-02
 rlmint(   0.42167968750000  ) =    7.6731593544950d-02
 rlmint(   0.44648437500000  ) =    7.6731593544950d-02
 rlmint(   0.47128906250000  ) =    7.6731593544950d-02
 rlmint(   0.49609375000000  ) =    7.6731593544950d-02
 rlmint(   0.52089843750000  ) =    7.6731593544950d-02
 rlmint(   0.54570312500000  ) =    7.6731593544950d-02
 rlmint(   0.57050781250000  ) =    7.6731593544950d-02
 rlmint(   0.59531250000000  ) =    7.6731593544950d-02
 rlmint(   0.62011718750000  ) =    7.6731593544950d-02
 rlmint(   0.64492187500000  ) =    7.6731593544950d-02
 rlmint(   0.66972656250000  ) =    7.6731593544950d-02
 rlmint(   0.69453125000000  ) =    7.6731593544950d-02
 rlmint(   0.71933593750000  ) =    7.6731593544950d-02
 rlmint(   0.74414062500000  ) =    7.6731593544950d-02
 rlmint(   0.76894531250000  ) =    7.6731593544950d-02
 rlmint(   0.79375000000000  ) =    7.6731593544950d-02
 rlmint(   0.81855468750000  ) =    7.6731593544950d-02
 rlmint(   0.84335937500000  ) =    7.6731593544950d-02
 rlmint(   0.86816406250000  ) =    7.6731593544950d-02
 rlmint(   0.89296875000000  ) =    7.6731593544950d-02
 rlmint(   0.91777343750000  ) =    7.6731593544950d-02
 rlmint(   0.94257812500000  ) =    7.6731593544950d-02
 rlmint(   0.96738281250000  ) =    7.6731593544950d-02
 rlmint(   0.99218750000000  ) =    7.6731593544950d-02
 rlmint(   1.01699218750000  ) =    7.6731593544950d-02
 rlmint(   1.04179687500000  ) =    7.6731593544950d-02
 rlmint(   1.06660156250000  ) =    7.6731593544950d-02
 rlmint(   1.09140625000000  ) =    7.6731593544950d-02
 rlmint(   1.11621093750000  ) =    7.6731593544950d-02
 rlmint(   1.14101562500000  ) =    7.6731593544950d-02
 rlmint(   1.16582031250000  ) =    7.6731593544950d-02
 rlmint(   1.19062500000000  ) =    7.6731593544950d-02
 rlmint(   1.21542968750000  ) =    7.6731593544950d-02
 rlmint(   1.24023437500000  ) =    7.6731593544950d-02
 rlmint(   1.26503906250000  ) =    7.6731593544950d-02
 rlmint(   1.28984375000000  ) =    7.6731593544950d-02
 rlmint(   1.31464843750000  ) =    7.6731593544950d-02
 rlmint(   1.33945312500000  ) =    7.6731593544950d-02
 rlmint(   1.36425781250000  ) =    7.6731593544950d-02
 rlmint(   1.38906250000000  ) =    7.6731593544950d-02
 rlmint(   1.41386718750000  ) =    7.6731593544950d-02
 rlmint(   1.43867187500000  ) =    7.6731593544950d-02
 rlmint(   1.46347656250000  ) =    7.6731593544950d-02
 rlmint(   1.48828125000000  ) =    7.6731593544950d-02
 rlmint(   1.51308593750000  ) =    7.6731593544950d-02
 rlmint(   1.53789062500000  ) =    7.6731593544950d-02
 rlmint(   1.56269531250000  ) =    7.6731593544950d-02
 rlmint(   1.58750000000000  ) =    7.6731593544950d-02
 rlmint(   1.61230468750000  ) =    7.6731593544950d-02
 rlmint(   1.63710937500000  ) =    7.6731593544950d-02
 rlmint(   1.66191406250000  ) =    7.6731593544950d-02
 rlmint(   1.68671875000000  ) =    7.6731593544950d-02
 rlmint(   1.71152343750000  ) =    7.6731593544950d-02
 rlmint(   1.73632812500000  ) =    7.6731593544950d-02
 rlmint(   1.76113281250000  ) =    7.6731593544950d-02
 rlmint(   1.78593750000000  ) =    7.6731593544950d-02
 rlmint(   1.81074218750000  ) =    7.6731593544950d-02
 rlmint(   1.83554687500000  ) =    7.6731593544950d-02
 rlmint(   1.86035156250000  ) =    7.6731593544950d-02
 rlmint(   1.88515625000000  ) =    7.6731593544950d-02
 rlmint(   1.90996093750000  ) =    7.6731593544950d-02
 rlmint(   1.93476562500000  ) =    7.6731593544950d-02
 rlmint(   1.95957031250000  ) =    7.6731593544950d-02
 rlmint(   1.98437500000000  ) =    7.6731593544950d-02
 rlmint(   2.00917968750000  ) =    7.6731593544950d-02
 rlmint(   2.03398437500000  ) =    7.6731593544950d-02
 rlmint(   2.05878906250000  ) =    7.6731593544950d-02
 rlmint(   2.08359375000000  ) =    7.6731593544950d-02
 rlmint(   2.10839843750000  ) =    7.6731593544950d-02
 rlmint(   2.13320312500000  ) =    7.6731593544950d-02
 rlmint(   2.15800781250000  ) =    7.6731593544950d-02
 rlmint(   2.18281250000000  ) =    7.6731593544950d-02
 rlmint(   2.20761718750000  ) =    7.6731593544950d-02
 rlmint(   2.23242187500000  ) =    7.6731593544950d-02
 rlmint(   2.25722656250000  ) =    7.6731593544950d-02
 rlmint(   2.28203125000000  ) =    7.6731593544950d-02
 rlmint(   2.30683593750000  ) =    7.6731593544950d-02
 rlmint(   2.33164062500000  ) =    7.6731593544950d-02
 rlmint(   2.35644531250000  ) =    7.6731593544950d-02
 rlmint(   2.38125000000000  ) =    7.6731593544950d-02
 rlmint(   2.40605468750000  ) =    7.6731593544950d-02
 rlmint(   2.43085937500000  ) =    7.6731593544950d-02
 rlmint(   2.45566406250000  ) =    7.6731593544950d-02
 rlmint(   2.48046875000000  ) =    7.6731593544950d-02
 rlmint(   2.50527343750000  ) =    7.6731593544950d-02
 rlmint(   2.53007812500000  ) =    7.6731593544950d-02
 rlmint(   2.55488281250000  ) =    7.6731593544950d-02
 rlmint(   2.57968750000000  ) =    7.6731593544950d-02
 rlmint(   2.60449218750000  ) =    7.6731593544950d-02
 rlmint(   2.62929687500000  ) =    7.6731593544950d-02
 rlmint(   2.65410156250000  ) =    7.6731593544950d-02
 rlmint(   2.67890625000000  ) =    7.6731593544950d-02
 rlmint(   2.70371093750000  ) =    7.6731593544950d-02
 rlmint(   2.72851562500000  ) =    7.6731593544950d-02
 rlmint(   2.75332031250000  ) =    7.6731593544950d-02
 rlmint(   2.77812500000000  ) =    7.6731593544950d-02
 rlmint(   2.80292968750000  ) =    7.6731593544950d-02
 rlmint(   2.82773437500000  ) =    7.6731593544950d-02
 rlmint(   2.85253906250000  ) =    7.6731593544950d-02
 rlmint(   2.87734375000000  ) =    7.6731593544950d-02
 rlmint(   2.90214843750000  ) =    7.6731593544950d-02
 rlmint(   2.92695312500000  ) =    7.6731593544950d-02
 rlmint(   2.95175781250000  ) =    7.6731593544950d-02
 rlmint(   2.97656250000000  ) =    7.6731593544950d-02
 rlmint(   3.00136718750000  ) =    7.6731593544950d-02
 rlmint(   3.02617187500000  ) =    7.6731593544950d-02
 rlmint(   3.05097656250000  ) =    7.6731593544950d-02
 rlmint(   3.07578125000000  ) =    7.6731593544950d-02
 rlmint(   3.10058593750000  ) =    7.6731593544950d-02
 rlmint(   3.12539062500000  ) =    7.6731593544950d-02
```

```
rlmint(  3.15019531250000 ) =  7.67315935449500d-02
rlmint(  3.17500000000000 ) =  7.67315935449500d-02
rlmint(  3.19980468750000 ) =  7.67315935449500d-02
rlmint(  3.22460937500000 ) =  7.67315935449500d-02
rlmint(  3.24941406250000 ) =  7.67315935449500d-02
rlmint(  3.27421875000000 ) =  7.67315935449500d-02
rlmint(  3.29902343750000 ) =  7.67315935449500d-02
rlmint(  3.32382812500000 ) =  7.67315935449500d-02
rlmint(  3.34863281250000 ) =  7.67315935449500d-02
rlmint(  3.37343750000000 ) =  7.67315935449500d-02
rlmint(  3.39824218750000 ) =  7.67315935449500d-02
rlmint(  3.42304687500000 ) =  7.67315935449500d-02
rlmint(  3.44785156250000 ) =  7.67315935449500d-02
rlmint(  3.47265625000000 ) =  7.67315935449500d-02
rlmint(  3.49746093750000 ) =  7.67315935449500d-02
rlmint(  3.52226562500000 ) =  7.67315935449500d-02
rlmint(  3.54707031250000 ) =  7.67315935449500d-02
rlmint(  3.57187500000000 ) =  7.67315935449500d-02
rlmint(  3.59667968750000 ) =  7.67315935449500d-02
rlmint(  3.62148437500000 ) =  7.67315935449500d-02
rlmint(  3.64628906250000 ) =  7.67315935449500d-02
rlmint(  3.67109375000000 ) =  7.67315935449500d-02
rlmint(  3.69589843750000 ) =  7.67315935449500d-02
rlmint(  3.72070312500000 ) =  7.67315935449500d-02
rlmint(  3.74550781250000 ) =  7.67315935449500d-02
rlmint(  3.77031250000000 ) =  7.67315935449500d-02
rlmint(  3.79511718750000 ) =  7.67315935449500d-02
rlmint(  3.81992187500000 ) =  7.67315935449500d-02
rlmint(  3.84472656250000 ) =  7.67315935449500d-02
rlmint(  3.86953125000000 ) =  7.67315935449500d-02
rlmint(  3.89433593750000 ) =  7.67315935449500d-02
rlmint(  3.91914062500000 ) =  7.67315935449500d-02
rlmint(  3.94394531250000 ) =  7.67315935449500d-02
rlmint(  3.96875000000000 ) =  7.67315935449500d-02
rlmint(  3.99355468750000 ) =  7.67315935449500d-02
rlmint(  4.01835937500000 ) =  7.67315935449500d-02
rlmint(  4.04316406250000 ) =  7.67315935449500d-02
rlmint(  4.06796875000000 ) =  7.67315935449500d-02
rlmint(  4.09277343750000 ) =  7.67315935449500d-02
rlmint(  4.11757812500000 ) =  7.67315935449500d-02
rlmint(  4.14238281250000 ) =  7.67315935449500d-02
rlmint(  4.16718750000000 ) =  7.67315935449500d-02
rlmint(  4.19199218750000 ) =  7.67315935449500d-02
rlmint(  4.21679687500000 ) =  7.67315935449500d-02
rlmint(  4.24160156250000 ) =  7.67315935449500d-02
rlmint(  4.26640625000000 ) =  7.67315935449500d-02
rlmint(  4.29121093750000 ) =  7.67315935449500d-02
rlmint(  4.31601562500000 ) =  7.67315935449500d-02
rlmint(  4.34082031250000 ) =  7.67315935449500d-02
rlmint(  4.36562500000000 ) =  7.67323268591260-02
rlmint(  4.39042968750000 ) =  7.67434077467010-02
rlmint(  4.41523437500000 ) =  7.67681287968660-02
rlmint(  4.44003906250000 ) =  7.68070555155370-02
rlmint(  4.46484375000000 ) =  7.68606730172960-02
rlmint(  4.48964843750000 ) =  7.69295987678780-02
rlmint(  4.51445312500000 ) =  7.70143429591220-02
rlmint(  4.53925781250000 ) =  7.71155609173990-02
rlmint(  4.56406250000000 ) =  7.72339443061210-02
rlmint(  4.58886718750000 ) =  7.73698953907890-02
rlmint(  4.61367187500000 ) =  7.75243701069390-02
rlmint(  4.63847656250000 ) =  7.76979418839720-02
rlmint(  4.66328125000000 ) =  7.78914316648330-02
rlmint(  4.68808593750000 ) =  7.81055559656850-02
rlmint(  4.71289062500000 ) =  7.83411726505440-02
rlmint(  4.73769531250000 ) =  7.85989952236600-02
rlmint(  4.76250000000000 ) =  7.88801707767020-02
```

```
rlmint(  4.78730468750000 ) =  7.91851156150840-02
rlmint(  4.81210937500000 ) =  7.95153154040840-02
rlmint(  4.83691406250000 ) =  7.98713871915790-02
rlmint(  4.86171875000000 ) =  8.02546275174000-02
rlmint(  4.88652343750000 ) =  8.06659104399710-02
rlmint(  4.91132812500000 ) =  8.11063274349580-02
rlmint(  4.93613281250000 ) =  8.15772945184700-02
rlmint(  4.96093750000000 ) =  8.20798023329340-02
rlmint(  4.98574218750000 ) =  8.26153709974580-02
rlmint(  5.01054687500000 ) =  8.31848607621010-02
rlmint(  5.03535156250000 ) =  8.37901015864250-02
rlmint(  5.06015625000000 ) =  8.44322750250280-02
rlmint(  5.08496093750000 ) =  8.51136912790900-02
rlmint(  5.10976562500000 ) =  8.58341458444640-02
rlmint(  5.13457031250000 ) =  8.65969758836670-02
rlmint(  5.15937500000000 ) =  8.74033109928580-02
rlmint(  5.18417968750000 ) =  8.82545764422110-02
rlmint(  5.20898437500000 ) =  8.91533932590010-02
rlmint(  5.23378906250000 ) =  9.01013181653290-02
rlmint(  5.25859375000000 ) =  9.11001691345040-02
rlmint(  5.28339843750000 ) =  9.21524964553020-02
rlmint(  5.30820312500000 ) =  9.32602605423080-02
rlmint(  5.33300781250000 ) =  9.44262735607210-02
rlmint(  5.35781250000000 ) =  9.56530755056790-02
rlmint(  5.38261718750000 ) =  9.69417571958950-02
rlmint(  5.40742187500000 ) =  9.82967410994280-02
rlmint(  5.43222656250000 ) =  9.97221862182520-02
rlmint(  5.45703125000000 ) =  0.10121663289664
rlmint(  5.48183593750000 ) =  0.10278808421754
rlmint(  5.50664062500000 ) =  0.10443491785702
rlmint(  5.53144531250000 ) =  0.10616594647115
rlmint(  5.55625000000000 ) =  0.10797922153414
rlmint(  5.58105468750000 ) =  0.10988324694824
rlmint(  5.60585937500000 ) =  0.11188051580954
rlmint(  5.63066406250000 ) =  0.11397688980564
rlmint(  5.65546875000000 ) =  0.11617387895009
rlmint(  5.68027343750000 ) =  0.11847879212444
rlmint(  5.70507812500000 ) =  0.12089567084906
rlmint(  5.72988281250000 ) =  0.12343056435038
rlmint(  5.75468750000000 ) =  0.12609007494260
rlmint(  5.77949218750000 ) =  0.12887881088675
rlmint(  5.80429687500000 ) =  0.13180460983751
rlmint(  5.82910156250000 ) =  0.13487488843892
rlmint(  5.85390625000000 ) =  0.13809786456791
rlmint(  5.87871093750000 ) =  0.14148007271744
rlmint(  5.90351562500000 ) =  0.14503427952668
rlmint(  5.92832031250000 ) =  0.14876580120656
rlmint(  5.95312500000000 ) =  0.15269112877155
rlmint(  5.97792968750000 ) =  0.15681705034003
rlmint(  6.00273437500000 ) =  0.16116125354395
rlmint(  6.02753906250000 ) =  0.16573820214378
rlmint(  6.05234375000000 ) =  0.17056240357683
rlmint(  6.07714843750000 ) =  0.17565593440218
rlmint(  6.10195312500000 ) =  0.18104295091813
rlmint(  6.12675781250000 ) =  0.18675099658267
rlmint(  6.15156250000000 ) =  0.19280451830508
rlmint(  6.17636718750000 ) =  0.19925340109637
rlmint(  6.20117187500000 ) =  0.20614030938983
rlmint(  6.22597656250000 ) =  0.21353735268176
rlmint(  6.25078125000000 ) =  0.22152789813563
rlmint(  6.27558593750000 ) =  0.23025503234183
rlmint(  6.30039062500000 ) =  0.23994858757454
rlmint(  6.32519531250000 ) =  0.25108802357000
rlmint(  6.35000000000000 ) =  0.26593460029604
```

ds = 0.41700000000000 d = 0.99600000000000 volts = 8.05000000000000

```
e0 =    2.50000000000000
rlmint(  0.  ) =   0.18440317748644
rlmint(    2.48046875000000d-02  ) =   0.18440391376210
rlmint(    4.96093750000000d-02  ) =   0.18440766514007
rlmint(    7.44140625000000d-02  ) =   0.18441243775700
rlmint(    9.92187500000000d-02  ) =   0.18441988449604
rlmint(   0.12402343750000  ) =   0.18443300208589
rlmint(   0.14882812500000  ) =   0.18444554548340
rlmint(   0.17363281250000  ) =   0.18446365591619
rlmint(   0.19843750000000  ) =   0.18448174228485
rlmint(   0.22324218750000  ) =   0.18450231212140
rlmint(   0.24804687500000  ) =   0.18452618183704
rlmint(   0.27285156250000  ) =   0.18455284281321
rlmint(   0.29765625000000  ) =   0.18458209947740
rlmint(   0.32246093750000  ) =   0.18461418909764
rlmint(   0.34726562500000  ) =   0.18464579842489
rlmint(   0.37207031250000  ) =   0.18468286622018
rlmint(   0.39687500000000  ) =   0.18472093582598
rlmint(   0.42167968750000  ) =   0.18476155408312
rlmint(   0.44648437500000  ) =   0.18480630377541
rlmint(   0.47128906250000  ) =   0.18485739565247
rlmint(   0.49609375000000  ) =   0.18490258672535
rlmint(   0.52089843750000  ) =   0.18496307722119
rlmint(   0.54570312500000  ) =   0.18500727826865
rlmint(   0.57050781250000  ) =   0.18506361119791
rlmint(   0.59531250000000  ) =   0.18512567450937
rlmint(   0.62011718750000  ) =   0.18518611674616
rlmint(   0.64492187500000  ) =   0.18525107423679
rlmint(   0.66972656250000  ) =   0.18531588649033
rlmint(   0.69453125000000  ) =   0.18538412759935
rlmint(   0.71933593750000  ) =   0.18545954084704
rlmint(   0.74414062500000  ) =   0.18553178342485
rlmint(   0.76894531250000  ) =   0.18560930140933
rlmint(   0.79375000000000  ) =   0.18569047103882
rlmint(   0.81855468750000  ) =   0.18578040686385
rlmint(   0.84335937500000  ) =   0.18585956172326
rlmint(   0.86816406250000  ) =   0.18594701877636
rlmint(   0.89296875000000  ) =   0.18603705770547
rlmint(   0.91777343750000  ) =   0.18613232231711
rlmint(   0.94257812500000  ) =   0.18622248244370
rlmint(   0.96738281250000  ) =   0.18632505378232
rlmint(   0.99218750000000  ) =   0.18642847999566
rlmint(   1.01699218750000  ) =   0.18653183752620
rlmint(   1.04179687500000  ) =   0.18663867047543
rlmint(   1.06660156250000  ) =   0.18674965155563
rlmint(   1.09140625000000  ) =   0.18686182385471
rlmint(   1.11621093750000  ) =   0.18697811653618
rlmint(   1.14101562500000  ) =   0.18709707670574
rlmint(   1.16582031250000  ) =   0.18721823223359
rlmint(   1.19062500000000  ) =   0.18734298169893
rlmint(   1.21542968750000  ) =   0.18746991403956
rlmint(   1.24023437500000  ) =   0.18760014080667
rlmint(   1.26503906250000  ) =   0.18773356378440
rlmint(   1.28984375000000  ) =   0.18786907463861
rlmint(   1.31464843750000  ) =   0.18800803144415
rlmint(   1.33945312500000  ) =   0.18815112397515
rlmint(   1.36425781250000  ) =   0.18829591276779
rlmint(   1.38906250000000  ) =   0.18844462987498
rlmint(   1.41386718750000  ) =   0.18859641607845
rlmint(   1.43867187500000  ) =   0.18874447546823
rlmint(   1.46347656250000  ) =   0.18890830672650
rlmint(   1.48828125000000  ) =   0.18906853330694
rlmint(   1.51308593750000  ) =   0.18923257970773
rlmint(   1.53789062500000  ) =   0.18939887284522
rlmint(   1.56269531250000  ) =   0.18956987443321
rlmint(   1.58750000000000  ) =   0.18974400033010
rlmint(   1.61230468750000  ) =   0.18992130305093
rlmint(   1.63710937500000  ) =   0.19010133395338
rlmint(   1.66191406250000  ) =   0.19028290850744
rlmint(   1.68671875000000  ) =   0.19047164188239
rlmint(   1.71152343750000  ) =   0.19066211384724
rlmint(   1.73632812500000  ) =   0.19085542916694
rlmint(   1.76113281250000  ) =   0.19105234047665
rlmint(   1.78593750000000  ) =   0.19125321177235
rlmint(   1.81074218750000  ) =   0.19145772737133
rlmint(   1.83554687500000  ) =   0.19166595891299
rlmint(   1.86035156250000  ) =   0.19187759513398
rlmint(   1.88515625000000  ) =   0.19209208911333
rlmint(   1.90996093750000  ) =   0.19231125596624
rlmint(   1.93476562500000  ) =   0.19253309666938
rlmint(   1.95957031250000  ) =   0.19275799639185
rlmint(   1.98437500000000  ) =   0.19298797897773
rlmint(   2.00917968750000  ) =   0.19322227906966
rlmint(   2.03398437500000  ) =   0.19345971083543
rlmint(   2.05878906250000  ) =   0.19370067290669
rlmint(   2.08359375000000  ) =   0.19394564801386
rlmint(   2.10839843750000  ) =   0.19419430590640
rlmint(   2.13320312500000  ) =   0.19444752051903
rlmint(   2.15800781250000  ) =   0.19470374012131
rlmint(   2.18281250000000  ) =   0.19496607824232
rlmint(   2.20761718750000  ) =   0.19522871309184
rlmint(   2.23242187500000  ) =   0.19549735772540
rlmint(   2.25722656250000  ) =   0.19577185525271
rlmint(   2.28203125000000  ) =   0.19605044428885
rlmint(   2.30683593750000  ) =   0.19633186444210
rlmint(   2.33164062500000  ) =   0.19661914949297
rlmint(   2.35644531250000  ) =   0.19690936682955
rlmint(   2.38125000000000  ) =   0.19720348780806
rlmint(   2.40605468750000  ) =   0.19750369269500
rlmint(   2.43085937500000  ) =   0.19780598665411
rlmint(   2.45566406250000  ) =   0.19811431895685
rlmint(   2.48046875000000  ) =   0.19842880425615
rlmint(   2.50527343750000  ) =   0.19874513052326
rlmint(   2.53007812500000  ) =   0.19906760114479
rlmint(   2.55488281250000  ) =   0.19939527790724
rlmint(   2.57968750000000  ) =   0.19972594929160
rlmint(   2.60449218750000  ) =   0.20006282108983
rlmint(   2.62929687500000  ) =   0.20040361791020
rlmint(   2.65410156250000  ) =   0.20075101811523
rlmint(   2.67890625000000  ) =   0.20110135649728
rlmint(   2.70371093750000  ) =   0.20145826556244
rlmint(   2.72851562500000  ) =   0.20181994881401
rlmint(   2.75332031250000  ) =   0.20218580190407
rlmint(   2.77812500000000  ) =   0.20255876145501
rlmint(   2.80292968750000  ) =   0.20293457114944
rlmint(   2.82773437500000  ) =   0.20331657150559
rlmint(   2.85253906250000  ) =   0.20370455132889
rlmint(   2.87734375000000  ) =   0.20409814036883
rlmint(   2.90214843750000  ) =   0.20449622517049
rlmint(   2.92695312500000  ) =   0.20489932009928
rlmint(   2.95175781250000  ) =   0.20530885207016
rlmint(   2.97656250000000  ) =   0.20572516185861
rlmint(   3.00136718750000  ) =   0.20614391428960
rlmint(   3.02617187500000  ) =   0.20656852630498
rlmint(   3.05097656250000  ) =   0.20700173744074
rlmint(   3.07578125000000  ) =   0.20743977713064
rlmint(   3.10058593750000  ) =   0.20788485941180
rlmint(   3.12539062500000  ) =   0.20833473553784
rlmint(   3.15019531250000  ) =   0.20879287887025
rlmint(   3.17500000000000  ) =   0.20925542202221
rlmint(   3.19980468750000  ) =   0.20972104149470
rlmint(   3.22460937500000  ) =   0.21019700273824
```

```
rlmint(   3.24941406250000  ) =   0.21067826856595
rlmint(   3.27421875000000  ) =   0.21116010407147
rlmint(   3.29902343750000  ) =   0.21165752724181
rlmint(   3.32382812500000  ) =   0.21215719992376
rlmint(   3.34863281250000  ) =   0.21266325848612
rlmint(   3.37343750000000  ) =   0.21317392788040
rlmint(   3.39824218750000  ) =   0.21369419047287
rlmint(   3.42304687500000  ) =   0.21421916027593
rlmint(   3.44785156250000  ) =   0.21474964492661
rlmint(   3.47265625000000  ) =   0.21528884794440
rlmint(   3.49746093750000  ) =   0.21583561483176
rlmint(   3.52226562500000  ) =   0.21638618788862
rlmint(   3.54707031250000  ) =   0.21694511932584
rlmint(   3.57187500000000  ) =   0.21751110022944
rlmint(   3.59667968750000  ) =   0.21808399490457
rlmint(   3.62148437500000  ) =   0.21866315473487
rlmint(   3.64628906250000  ) =   0.21924989519244
rlmint(   3.67109375000000  ) =   0.21984359284676
rlmint(   3.69589843750000  ) =   0.22044382113124
rlmint(   3.72070312500000  ) =   0.22105106908997
rlmint(   3.74550781250000  ) =   0.22166583913202
rlmint(   3.77031250000000  ) =   0.22228797419029
rlmint(   3.79511718750000  ) =   0.22291602240226
rlmint(   3.81992187500000  ) =   0.22355127431795
rlmint(   3.84472656250000  ) =   0.22419354892997
rlmint(   3.86953125000000  ) =   0.22484416844950
rlmint(   3.89433593750000  ) =   0.22550024227310
rlmint(   3.91914062500000  ) =   0.22616553973387
rlmint(   3.94394531250000  ) =   0.22683515675447
rlmint(   3.96875000000000  ) =   0.22751442244911
rlmint(   3.99355468750000  ) =   0.22820002988445
rlmint(   4.01835937500000  ) =   0.22889426921568
rlmint(   4.04316406250000  ) =   0.22959447783734
rlmint(   4.06796875000000  ) =   0.23030105654195
rlmint(   4.09277343750000  ) =   0.23101582268934
rlmint(   4.11757812500000  ) =   0.23173691308108
rlmint(   4.14238281250000  ) =   0.23246516808721
rlmint(   4.16718750000000  ) =   0.23320503755063
rlmint(   4.19199218750000  ) =   0.23394800688498
rlmint(   4.21679687500000  ) =   0.23470228787188
rlmint(   4.24160156250000  ) =   0.23546091752095
rlmint(   4.26640625000000  ) =   0.23622590305246
rlmint(   4.29121093750000  ) =   0.23699637004472
rlmint(   4.31601562500000  ) =   0.23777464869327
rlmint(   4.34082031250000  ) =   0.23856196423083
rlmint(   4.36562500000000  ) =   0.23935614459018
rlmint(   4.39042968750000  ) =   0.24015716419990
rlmint(   4.41523437500000  ) =   0.24096513264800
rlmint(   4.44003906250000  ) =   0.24177971287889
rlmint(   4.46484375000000  ) =   0.24260224173777
rlmint(   4.48964843750000  ) =   0.24342910090903
rlmint(   4.51445312500000  ) =   0.24426903793893
rlmint(   4.53925781250000  ) =   0.24511437139839
rlmint(   4.56406250000000  ) =   0.24596562397251
rlmint(   4.58886718750000  ) =   0.24682267285281
rlmint(   4.61367187500000  ) =   0.24768424783559
rlmint(   4.63847656250000  ) =   0.24855333013332
rlmint(   4.66328125000000  ) =   0.24943081143081
rlmint(   4.68808593750000  ) =   0.25031365314240
rlmint(   4.71289062500000  ) =   0.25120182577590
rlmint(   4.73769531250000  ) =   0.25209688573202
rlmint(   4.76250000000000  ) =   0.25299724696496
rlmint(   4.78730468750000  ) =   0.25390595115194
rlmint(   4.81210937500000  ) =   0.25481858806990
rlmint(   4.83691406250000  ) =   0.25573866354993
rlmint(   4.86171875000000  ) =   0.25666228868067
rlmint(   4.88652343750000  ) =   0.25759463620698
rlmint(   4.91132812500000  ) =   0.25852983070561
rlmint(   4.93613281250000  ) =   0.25946737401354
rlmint(   4.96093750000000  ) =   0.26041811378233
rlmint(   4.98574218750000  ) =   0.26137144474047
rlmint(   5.01054687500000  ) =   0.26233049749123
rlmint(   5.03535156250000  ) =   0.26329407203746
rlmint(   5.06015625000000  ) =   0.26426213416962
rlmint(   5.08496093750000  ) =   0.26523952568367
rlmint(   5.10976562500000  ) =   0.26621815746099
rlmint(   5.13457031250000  ) =   0.26720176466817
rlmint(   5.15937500000000  ) =   0.26819228151979
rlmint(   5.18417968750000  ) =   0.26918916017567
rlmint(   5.20898437500000  ) =   0.27018558840287
rlmint(   5.23378906250000  ) =   0.27119062539593
rlmint(   5.25859375000000  ) =   0.27219625690113
rlmint(   5.28339843750000  ) =   0.27320779323166
rlmint(   5.30820312500000  ) =   0.27422156801467
rlmint(   5.33300781250000  ) =   0.27524906432660
rlmint(   5.35781250000000  ) =   0.27627304038715
rlmint(   5.38261718750000  ) =   0.27729927901608
rlmint(   5.40742187500000  ) =   0.27833042754196
rlmint(   5.43222656250000  ) =   0.27936216450116
rlmint(   5.45703125000000  ) =   0.28040068372630
rlmint(   5.48183593750000  ) =   0.28144041279117
rlmint(   5.50664062500000  ) =   0.28248613222529
rlmint(   5.53144531250000  ) =   0.28353256454167
rlmint(   5.55625000000000  ) =   0.28458123966336
rlmint(   5.58105468750000  ) =   0.28563290527785
rlmint(   5.60585937500000  ) =   0.28669027630783
rlmint(   5.63066406250000  ) =   0.28774709588112
rlmint(   5.65546875000000  ) =   0.28880735881119
rlmint(   5.68027343750000  ) =   0.28986917838974
rlmint(   5.70507812500000  ) =   0.29093224774388
rlmint(   5.72988281250000  ) =   0.29199823683421
rlmint(   5.75468750000000  ) =   0.29306640907010
rlmint(   5.77949218750000  ) =   0.29413585013208
rlmint(   5.80429687500000  ) =   0.29520610873333
rlmint(   5.82910156250000  ) =   0.29627795526465
rlmint(   5.85390625000000  ) =   0.29735090590704
rlmint(   5.87871093750000  ) =   0.29842497590404
rlmint(   5.90351562500000  ) =   0.29949970818354
rlmint(   5.92832031250000  ) =   0.30057469581972
rlmint(   5.95312500000000  ) =   0.30165001578666
rlmint(   5.97792968750000  ) =   0.30272667231551
rlmint(   6.00273437500000  ) =   0.30380365456432
rlmint(   6.02753906250000  ) =   0.30488143126777
rlmint(   6.05234375000000  ) =   0.30595947532538
rlmint(   6.07714843750000  ) =   0.30703738207993
rlmint(   6.10195312500000  ) =   0.30811486706131
rlmint(   6.12675781250000  ) =   0.30919284721517
rlmint(   6.15156250000000  ) =   0.31027071153077
rlmint(   6.17636718750000  ) =   0.31134766180004
rlmint(   6.20117187500000  ) =   0.31242341602150
rlmint(   6.22597656250000  ) =   0.31349754043453
rlmint(   6.25078125000000  ) =   0.31457286337628
rlmint(   6.27558593750000  ) =   0.31564440020832
rlmint(   6.30039062500000  ) =   0.31671587630871
rlmint(   6.32519531250000  ) =   0.31778695016102
rlmint(   6.35000000000000  ) =   0.31885559656964

ds =   0.99600000000000   d =  0.   volts =   85.9000000000000  e0 =
 2.50000000000000
rlmint(  0.  ) =  0.
rlmint(    2.4804687500000d-02  ) =  0.
rlmint(    4.9609375000000d-02  ) =  0.
```

```
rlmint(   7.44140625000000d-02  ) =  0.
rlmint(   9.92187500000000d-02  ) =  0.
rlmint(  0.12402343750000  ) =  0.
rlmint(  0.14882812500000  ) =  0.
rlmint(  0.17363281250000  ) =  0.
rlmint(  0.19843750000000  ) =  0.
rlmint(  0.22324218750000  ) =  0.
rlmint(  0.24804687500000  ) =  0.
rlmint(  0.27285156250000  ) =  0.
rlmint(  0.29765625000000  ) =  0.
rlmint(  0.32246093750000  ) =  0.
rlmint(  0.34726562500000  ) =  0.
rlmint(  0.37207031250000  ) =  0.
rlmint(  0.39687500000000  ) =  0.
rlmint(  0.42167968750000  ) =  0.
rlmint(  0.44648437500000  ) =  0.
rlmint(  0.47128906250000  ) =  0.
rlmint(  0.49609375000000  ) =  0.
rlmint(  0.52089843750000  ) =  0.
rlmint(  0.54570312500000  ) =  0.
rlmint(  0.57050781250000  ) =  0.
rlmint(  0.59531250000000  ) =  0.
rlmint(  0.62011718750000  ) =  0.
rlmint(  0.64492187500000  ) =  0.
rlmint(  0.66972656250000  ) =  0.
rlmint(  0.69453125000000  ) =  0.
rlmint(  0.71933593750000  ) =  0.
rlmint(  0.74414062500000  ) =  0.
rlmint(  0.76894531250000  ) =  0.
rlmint(  0.79375000000000  ) =  0.
rlmint(  0.81855468750000  ) =  0.
rlmint(  0.84335937500000  ) =  0.
rlmint(  0.86816406250000  ) =  0.
rlmint(  0.89296875000000  ) =  0.
rlmint(  0.91777343750000  ) =  0.
rlmint(  0.94257812500000  ) =  0.
rlmint(  0.96738281250000  ) =  0.
rlmint(  0.99218750000000  ) =  0.
rlmint(  1.01699218750000  ) =  0.
rlmint(  1.04179687500000  ) =  0.
rlmint(  1.06660156250000  ) =  0.
rlmint(  1.09140625000000  ) =  0.
rlmint(  1.11621093750000  ) =  0.
rlmint(  1.14101562500000  ) =  0.
rlmint(  1.16582031250000  ) =  0.
rlmint(  1.19062500000000  ) =  0.
rlmint(  1.21542968750000  ) =  0.
rlmint(  1.24023437500000  ) =  0.
rlmint(  1.26503906250000  ) =  0.
rlmint(  1.28984375000000  ) =  0.
rlmint(  1.31464843750000  ) =  0.
rlmint(  1.33945312500000  ) =  0.
rlmint(  1.36425781250000  ) =  0.
rlmint(  1.38906250000000  ) =  0.
rlmint(  1.41386718750000  ) =  0.
rlmint(  1.43867187500000  ) =  0.
rlmint(  1.46347656250000  ) =  0.
rlmint(  1.48828125000000  ) =  0.
rlmint(  1.51308593750000  ) =  0.
rlmint(  1.53789062500000  ) =  0.
rlmint(  1.56269531250000  ) =  0.
rlmint(  1.58750000000000  ) =  0.
rlmint(  1.61230468750000  ) =  0.
rlmint(  1.63710937500000  ) =  0.
rlmint(  1.66191406250000  ) =  0.
rlmint(  1.68671875000000  ) =  0.
rlmint(  1.71152343750000  ) =  0.
rlmint(  1.73632812500000  ) =  0.
rlmint(  1.76113281250000  ) =  0.
rlmint(  1.78593750000000  ) =  0.
rlmint(  1.81074218750000  ) =  0.
rlmint(  1.83554687500000  ) =  0.
rlmint(  1.86035156250000  ) =  0.
rlmint(  1.88515625000000  ) =  0.
rlmint(  1.90996093750000  ) =  0.
rlmint(  1.93476562500000  ) =  0.
rlmint(  1.95957031250000  ) =  0.
rlmint(  1.98437500000000  ) =  0.
rlmint(  2.00917968750000  ) =  0.
rlmint(  2.03398437500000  ) =  0.
rlmint(  2.05878906250000  ) =  0.
rlmint(  2.08359375000000  ) =  0.
rlmint(  2.10839843750000  ) =  0.
rlmint(  2.13320312500000  ) =  0.
rlmint(  2.15800781250000  ) =  0.
rlmint(  2.18281250000000  ) =  0.
rlmint(  2.20761718750000  ) =  0.
rlmint(  2.23242187500000  ) =  0.
rlmint(  2.25722656250000  ) =  0.
rlmint(  2.28203125000000  ) =  0.
rlmint(  2.30683593750000  ) =  0.
rlmint(  2.33164062500000  ) =  0.
rlmint(  2.35644531250000  ) =  0.
rlmint(  2.38125000000000  ) =  0.
rlmint(  2.40605468750000  ) =  0.
rlmint(  2.43085937500000  ) =  0.
rlmint(  2.45566406250000  ) =  0.
rlmint(  2.48046875000000  ) =  0.
rlmint(  2.50527343750000  ) =  0.
rlmint(  2.53007812500000  ) =  0.
rlmint(  2.55488281250000  ) =  0.
rlmint(  2.57968750000000  ) =  0.
rlmint(  2.60449218750000  ) =  0.
rlmint(  2.62929687500000  ) =  0.
rlmint(  2.65410156250000  ) =  0.
rlmint(  2.67890625000000  ) =  0.
rlmint(  2.70371093750000  ) =  0.
rlmint(  2.72851562500000  ) =  0.
rlmint(  2.75332031250000  ) =  0.
rlmint(  2.77812500000000  ) =  0.
rlmint(  2.80292968750000  ) =  0.
rlmint(  2.82773437500000  ) =  0.
rlmint(  2.85253906250000  ) =  0.
rlmint(  2.87734375000000  ) =  0.
rlmint(  2.90214843750000  ) =  0.
rlmint(  2.92695312500000  ) =  0.
rlmint(  2.95175781250000  ) =  0.
rlmint(  2.97656250000000  ) =  0.
rlmint(  3.00136718750000  ) =  0.
rlmint(  3.02617187500000  ) =  0.
rlmint(  3.05097656250000  ) =  0.
rlmint(  3.07578125000000  ) =  0.
rlmint(  3.10058593750000  ) =  0.
rlmint(  3.12539062500000  ) =  0.
rlmint(  3.15019531250000  ) =  0.
rlmint(  3.17500000000000  ) =  0.
rlmint(  3.19980468750000  ) =  0.
rlmint(  3.22460937500000  ) =  0.
rlmint(  3.24941406250000  ) =  0.
rlmint(  3.27421875000000  ) =  0.
rlmint(  3.29902343750000  ) =  0.
rlmint(  3.32382812500000  ) =  0.
```

```
rlmint(   3.34863281250000  ) =  0.
rlmint(   3.37343750000000  ) =  0.
rlmint(   3.39824218750000  ) =  0.
rlmint(   3.42304687500000  ) =  0.
rlmint(   3.44785156250000  ) =  0.
rlmint(   3.47265625000000  ) =  0.
rlmint(   3.49746093750000  ) =  0.
rlmint(   3.52226562500000  ) =  0.
rlmint(   3.54707031250000  ) =  0.
rlmint(   3.57187500000000  ) =  0.
rlmint(   3.59667968750000  ) =  0.
rlmint(   3.62148437500000  ) =  0.
rlmint(   3.64628906250000  ) =  0.
rlmint(   3.67109375000000  ) =  0.
rlmint(   3.69589843750000  ) =  0.
rlmint(   3.72070312500000  ) =  0.
rlmint(   3.74550781250000  ) =  0.
rlmint(   3.77031250000000  ) =  0.
rlmint(   3.79511718750000  ) =  0.
rlmint(   3.81992187500000  ) =  0.
rlmint(   3.84472656250000  ) =  0.
rlmint(   3.86953125000000  ) =  0.
rlmint(   3.89433593750000  ) =  0.
rlmint(   3.91914062500000  ) =  0.
rlmint(   3.94394531250000  ) =  0.
rlmint(   3.96875000000000  ) =  0.
rlmint(   3.99355468750000  ) =  0.
rlmint(   4.01835937500000  ) =  0.
rlmint(   4.04316406250000  ) =  0.
rlmint(   4.06796875000000  ) =  0.
rlmint(   4.09277343750000  ) =  0.
rlmint(   4.11757812500000  ) =  0.
rlmint(   4.14238281250000  ) =  0.
rlmint(   4.16718750000000  ) =  0.
rlmint(   4.19199218750000  ) =  0.
rlmint(   4.21679687500000  ) =  0.
rlmint(   4.24160156250000  ) =  0.
rlmint(   4.26640625000000  ) =  0.
rlmint(   4.29121093750000  ) =  0.
rlmint(   4.31601562500000  ) =  0.
rlmint(   4.34082031250000  ) =  0.
rlmint(   4.36562500000000  ) =  0.
rlmint(   4.39042968750000  ) =  0.
rlmint(   4.41523437500000  ) =  0.
rlmint(   4.44003906250000  ) =  0.
rlmint(   4.46484375000000  ) =  0.
rlmint(   4.48964843750000  ) =  0.
rlmint(   4.51445312500000  ) =  0.
rlmint(   4.53925781250000  ) =  0.
rlmint(   4.56406250000000  ) =  0.
rlmint(   4.58886718750000  ) =  0.
rlmint(   4.61367187500000  ) =  0.
rlmint(   4.63847656250000  ) =  0.
rlmint(   4.66328125000000  ) =  0.
rlmint(   4.68808593750000  ) =  0.
rlmint(   4.71289062500000  ) =  0.
rlmint(   4.73769531250000  ) =  0.
rlmint(   4.76250000000000  ) =  0.
rlmint(   4.78730468750000  ) =  0.
rlmint(   4.81210937500000  ) =  0.
rlmint(   4.83691406250000  ) =  0.
rlmint(   4.86171875000000  ) =  0.
rlmint(   4.88652343750000  ) =  0.
rlmint(   4.91132812500000  ) =  0.
rlmint(   4.93613281250000  ) =  0.
rlmint(   4.96093750000000  ) =  0.
rlmint(   4.98574218750000  ) =  0.
rlmint(   5.01054687500000  ) =  0.
rlmint(   5.03535156250000  ) =  0.
rlmint(   5.06015625000000  ) =  0.
rlmint(   5.08496093750000  ) =  0.
rlmint(   5.10976562500000  ) =  0.
rlmint(   5.13457031250000  ) =  0.
rlmint(   5.15937500000000  ) =  0.
rlmint(   5.18417968750000  ) =  0.
rlmint(   5.20898437500000  ) =  0.
rlmint(   5.23378906250000  ) =  0.
rlmint(   5.25859375000000  ) =  0.
rlmint(   5.28339843750000  ) =  0.
rlmint(   5.30820312500000  ) =  0.
rlmint(   5.33300781250000  ) =  0.
rlmint(   5.35781250000000  ) =  0.
rlmint(   5.38261718750000  ) =  0.
rlmint(   5.40742187500000  ) =  0.
rlmint(   5.43222656250000  ) =  0.
rlmint(   5.45703125000000  ) =  0.
rlmint(   5.48183593750000  ) =  0.
rlmint(   5.50664062500000  ) =  0.
rlmint(   5.53144531250000  ) =  0.
rlmint(   5.55625000000000  ) =  0.
rlmint(   5.58105468750000  ) =  0.
rlmint(   5.60585937500000  ) =  0.
rlmint(   5.63066406250000  ) =  0.
rlmint(   5.65546875000000  ) =  0.
rlmint(   5.68027343750000  ) =  0.
rlmint(   5.70507812500000  ) =  0.
rlmint(   5.72988281250000  ) =  0.
rlmint(   5.75468750000000  ) =  0.
rlmint(   5.77949218750000  ) =  0.
rlmint(   5.80429687500000  ) =  0.
rlmint(   5.82910156250000  ) =  0.
rlmint(   5.85390625000000  ) =  0.
rlmint(   5.87871093750000  ) =  0.
rlmint(   5.90351562500000  ) =  0.
rlmint(   5.92832031250000  ) =  0.
rlmint(   5.95312500000000  ) =  0.
rlmint(   5.97792968750000  ) =  0.
rlmint(   6.00273437500000  ) =    2.0548195954240d-08
rlmint(   6.02753906250000  ) =    4.5727547916405d-05
rlmint(   6.05234375000000  ) =    2.1106464451148d-04
rlmint(   6.07714843750000  ) =    5.6268124743790d-04
rlmint(   6.10195312500000  ) =    1.2036389052673d-03
rlmint(   6.12675781250000  ) =    2.2935283406668d-03
rlmint(   6.15156250000000  ) =    4.0801288193314d-03
rlmint(   6.17636718750000  ) =    6.9496723916246d-03
rlmint(   6.20117187500000  ) =    1.1504442841205d-02
rlmint(   6.22597656250000  ) =    1.8698235236351d-02
rlmint(   6.25078125000000  ) =    3.0050915560921d-02
rlmint(   6.27558593750000  ) =    4.8049621690909d-02
rlmint(   6.30039062500000  ) =    7.6955725468348d-02
rlmint(   6.32519531250000  ) =   0.12500563772985
rlmint(   6.35000000000000  ) =   0.22258035173082

ds =   0.41700000000000   d =   0.99600000000000   volts =   95.2000000000000
e0 =   2.50000000000000
rlmint(  0.  ) =   0.13321328586100
rlmint(    2.4804687500000d-02  ) =   0.13321377718942
rlmint(    4.9609375000000d-02  ) =   0.13321582134221
rlmint(    7.4414062500000d-02  ) =   0.13322120735239
rlmint(    9.9218750000000d-02  ) =   0.13323341268871
rlmint(   0.12402343750000  ) =   0.13324440941273
rlmint(   0.14882812500000  ) =   0.13325929404050
```

```
rlmint(  0.17363281250000 ) =  0.13327643528132
rlmint(  0.19843750000000 ) =  0.13329368041485
rlmint(  0.22324218750000 ) =  0.13331488204967
rlmint(  0.24804687500000 ) =  0.13334221848069
rlmint(  0.27285156250000 ) =  0.13336839771654
rlmint(  0.29765625000000 ) =  0.13339683647018
rlmint(  0.32246093750000 ) =  0.13342714147237
rlmint(  0.34726562500000 ) =  0.13346209226172
rlmint(  0.37207031250000 ) =  0.13350960082939
rlmint(  0.39687500000000 ) =  0.13354399159724
rlmint(  0.42167968750000 ) =  0.13358716883217
rlmint(  0.44648437500000 ) =  0.13363071130208
rlmint(  0.47128906250000 ) =  0.13367577822921
rlmint(  0.49609375000000 ) =  0.13372448912375
rlmint(  0.52089843750000 ) =  0.13377863683824
rlmint(  0.54570312500000 ) =  0.13383574617735
rlmint(  0.57050781250000 ) =  0.13389170806191
rlmint(  0.59531250000000 ) =  0.13394852939806
rlmint(  0.62011718750000 ) =  0.13401726679807
rlmint(  0.64492187500000 ) =  0.13408140948929
rlmint(  0.66972656250000 ) =  0.13415007230864
rlmint(  0.69453125000000 ) =  0.13422221561946
rlmint(  0.71933593750000 ) =  0.13429708096996
rlmint(  0.74414062500000 ) =  0.13437522862895
rlmint(  0.76894531250000 ) =  0.13444291005494
rlmint(  0.79375000000000 ) =  0.13453014880513
rlmint(  0.81855468750000 ) =  0.13461748495003
rlmint(  0.84335937500000 ) =  0.13470854373024
rlmint(  0.86816406250000 ) =  0.13480017912502
rlmint(  0.89296875000000 ) =  0.13489088298064
rlmint(  0.91777343750000 ) =  0.13499130115675
rlmint(  0.94257812500000 ) =  0.13508699997550
rlmint(  0.96738281250000 ) =  0.13518815407657
rlmint(  0.99218750000000 ) =  0.13529194851491
rlmint(  1.01699218750000 ) =  0.13540384680557
rlmint(  1.04179687500000 ) =  0.13550865058059
rlmint(  1.06660156250000 ) =  0.13562187649202
rlmint(  1.09140625000000 ) =  0.13573840483300
rlmint(  1.11621093750000 ) =  0.13585628611224
rlmint(  1.14101562500000 ) =  0.13597860915217
rlmint(  1.16582031250000 ) =  0.13609960392818
rlmint(  1.19062500000000 ) =  0.13623049661102
rlmint(  1.21542968750000 ) =  0.13636064696259
rlmint(  1.24023437500000 ) =  0.13649485239398
rlmint(  1.26503906250000 ) =  0.13662856398947
rlmint(  1.28984375000000 ) =  0.13677205080168
rlmint(  1.31464843750000 ) =  0.13691099206616
rlmint(  1.33945312500000 ) =  0.13705689146979
rlmint(  1.36425781250000 ) =  0.13720324916028
rlmint(  1.38906250000000 ) =  0.13735461517705
rlmint(  1.41386718750000 ) =  0.13750881067565
rlmint(  1.43867187500000 ) =  0.13766556667051
rlmint(  1.46347656250000 ) =  0.13782575695121
rlmint(  1.48828125000000 ) =  0.13798914213899
rlmint(  1.51308593750000 ) =  0.13815508565176
rlmint(  1.53789062500000 ) =  0.13832817587551
rlmint(  1.56269531250000 ) =  0.13850142139434
rlmint(  1.58750000000000 ) =  0.13868139487686
rlmint(  1.61230468750000 ) =  0.13886201486536
rlmint(  1.63710937500000 ) =  0.13904523576484
rlmint(  1.66191406250000 ) =  0.13923262850787
rlmint(  1.68671875000000 ) =  0.13941868214708
rlmint(  1.71152343750000 ) =  0.13961464156359
rlmint(  1.73632812500000 ) =  0.13981317261300
rlmint(  1.76113281250000 ) =  0.14001083487117
rlmint(  1.78593750000000 ) =  0.14021511636337
rlmint(  1.81074218750000 ) =  0.14042090712728
rlmint(  1.83554687500000 ) =  0.14063289796588
rlmint(  1.86035156250000 ) =  0.14084697308637
rlmint(  1.88515625000000 ) =  0.14106516807317
rlmint(  1.90996093750000 ) =  0.14128857774378
rlmint(  1.93476562500000 ) =  0.14151480909833
rlmint(  1.95957031250000 ) =  0.14173819930112
rlmint(  1.98437500000000 ) =  0.14197387334589
rlmint(  2.00917968750000 ) =  0.14220847851176
rlmint(  2.03398437500000 ) =  0.14244863697400
rlmint(  2.05878906250000 ) =  0.14269225792195
rlmint(  2.08359375000000 ) =  0.14294497548872
rlmint(  2.10839843750000 ) =  0.14319054414175
rlmint(  2.13320312500000 ) =  0.14344707793580
rlmint(  2.15800781250000 ) =  0.14370063416404
rlmint(  2.18281250000000 ) =  0.14397078704696
rlmint(  2.20761718750000 ) =  0.14423601413440
rlmint(  2.23242187500000 ) =  0.14450716206037
rlmint(  2.25722656250000 ) =  0.14478338601409
rlmint(  2.28203125000000 ) =  0.14506318525273
rlmint(  2.30683593750000 ) =  0.14534550996619
rlmint(  2.33164062500000 ) =  0.14563287744233
rlmint(  2.35644531250000 ) =  0.14592740146821
rlmint(  2.38125000000000 ) =  0.14622008107803
rlmint(  2.40605468750000 ) =  0.14652391505096
rlmint(  2.43085937500000 ) =  0.14683082956281
rlmint(  2.45566406250000 ) =  0.14713932466163
rlmint(  2.48046875000000 ) =  0.14745369369023
rlmint(  2.50527343750000 ) =  0.14777471039976
rlmint(  2.53007812500000 ) =  0.14809758169365
rlmint(  2.55488281250000 ) =  0.14842802080527
rlmint(  2.57968750000000 ) =  0.14875874929548
rlmint(  2.60449218750000 ) =  0.14909449173773
rlmint(  2.62929687500000 ) =  0.14943319037121
rlmint(  2.65410156250000 ) =  0.14977909266917
rlmint(  2.67890625000000 ) =  0.15013856482407
rlmint(  2.70371093750000 ) =  0.15049183279493
rlmint(  2.72851562500000 ) =  0.15085557069813
rlmint(  2.75332031250000 ) =  0.15122872942635
rlmint(  2.77812500000000 ) =  0.15159678735987
rlmint(  2.80292968750000 ) =  0.15197722544610
rlmint(  2.82773437500000 ) =  0.15235789528090
rlmint(  2.85253906250000 ) =  0.15274534563692
rlmint(  2.87734375000000 ) =  0.15313866792968
rlmint(  2.90214843750000 ) =  0.15353677900906
rlmint(  2.92695312500000 ) =  0.15394294162879
rlmint(  2.95175781250000 ) =  0.15435211088805
rlmint(  2.97656250000000 ) =  0.15476697785263
rlmint(  3.00136718750000 ) =  0.15518716662747
rlmint(  3.02617187500000 ) =  0.15561657540180
rlmint(  3.05097656250000 ) =  0.15604552365388
rlmint(  3.07578125000000 ) =  0.15648846560373
rlmint(  3.10058593750000 ) =  0.15693325726112
rlmint(  3.12539062500000 ) =  0.15738177805153
rlmint(  3.15019531250000 ) =  0.15784131948010
rlmint(  3.17500000000000 ) =  0.15830434906732
rlmint(  3.19980468750000 ) =  0.15877136448536
rlmint(  3.22460937500000 ) =  0.15924561928974
rlmint(  3.24941406250000 ) =  0.15972862529050
rlmint(  3.27421875000000 ) =  0.16021411615732
rlmint(  3.29902343750000 ) =  0.16070447552131
rlmint(  3.32382812500000 ) =  0.16120204296510
rlmint(  3.34863281250000 ) =  0.16170987754751
rlmint(  3.37343750000000 ) =  0.16223961417904
rlmint(  3.39824218750000 ) =  0.16276334140898
rlmint(  3.42304687500000 ) =  0.16328888593827
```

```
rlmint(   3.44785156250000  ) =   0.16382653711056
rlmint(   3.47265625000000  ) =   0.16436771621747
rlmint(   3.49746093750000  ) =   0.16491926978282
rlmint(   3.52226562500000  ) =   0.16547971017388
rlmint(   3.54707031250000  ) =   0.16604471520557
rlmint(   3.57187500000000  ) =   0.16661343869390
rlmint(   3.59667968750000  ) =   0.16719541012560
rlmint(   3.62148437500000  ) =   0.16778590997602
rlmint(   3.64628906250000  ) =   0.16838211524493
rlmint(   3.67109375000000  ) =   0.16898886377375
rlmint(   3.69589843750000  ) =   0.16959829869640
rlmint(   3.72070312500000  ) =   0.17021670319846
rlmint(   3.74550781250000  ) =   0.17084507237861
rlmint(   3.77031250000000  ) =   0.17147956250865
rlmint(   3.79511718750000  ) =   0.17212457896878
rlmint(   3.81992187500000  ) =   0.17277883357013
rlmint(   3.84472656250000  ) =   0.17344186543045
rlmint(   3.86953125000000  ) =   0.17411045416804
rlmint(   3.89433593750000  ) =   0.17478455556018
rlmint(   3.91914062500000  ) =   0.17547475468326
rlmint(   3.94394531250000  ) =   0.17616679429421
rlmint(   3.96875000000000  ) =   0.17685789464518
rlmint(   3.99355468750000  ) =   0.17759202823000
rlmint(   4.01835937500000  ) =   0.17833060417847
rlmint(   4.04316406250000  ) =   0.17905691140509
rlmint(   4.06796875000000  ) =   0.17979690210030
rlmint(   4.09277343750000  ) =   0.18055291420231
rlmint(   4.11757812500000  ) =   0.18131463272578
rlmint(   4.14238281250000  ) =   0.18208644939609
rlmint(   4.16718750000000  ) =   0.18286460741270
rlmint(   4.19199218750000  ) =   0.18365618049930
rlmint(   4.21679687500000  ) =   0.18446027847964
rlmint(   4.24160156250000  ) =   0.18527376466130
rlmint(   4.26640625000000  ) =   0.18609864196121
rlmint(   4.29121093750000  ) =   0.18693242392952
rlmint(   4.31601562500000  ) =   0.18777598239119
rlmint(   4.34082031250000  ) =   0.18863243583991
rlmint(   4.36562500000000  ) =   0.18949673500205
rlmint(   4.39042968750000  ) =   0.19036816876621
rlmint(   4.41523437500000  ) =   0.19125064561349
rlmint(   4.44003906250000  ) =   0.19214001991496
rlmint(   4.46484375000000  ) =   0.19303640350978
rlmint(   4.48964843750000  ) =   0.19393678390529
rlmint(   4.51445312500000  ) =   0.19491794968241
rlmint(   4.53925781250000  ) =   0.19586169177451
rlmint(   4.56406250000000  ) =   0.19681469198152
rlmint(   4.58886718750000  ) =   0.19778253569055
rlmint(   4.61367187500000  ) =   0.19875855915978
rlmint(   4.63847656250000  ) =   0.19974860284445
rlmint(   4.66328125000000  ) =   0.20074808561300
rlmint(   4.68808593750000  ) =   0.20176022788963
rlmint(   4.71289062500000  ) =   0.20278593986592
rlmint(   4.73769531250000  ) =   0.20382382931125
rlmint(   4.76250000000000  ) =   0.20486690300481
rlmint(   4.78730468750000  ) =   0.20592438561595
rlmint(   4.81210937500000  ) =   0.20699209429325
rlmint(   4.83691406250000  ) =   0.20808705677356
rlmint(   4.86171875000000  ) =   0.20917831103752
rlmint(   4.88652343750000  ) =   0.21029381167123
rlmint(   4.91132812500000  ) =   0.21141171644219
rlmint(   4.93613281250000  ) =   0.21254698186006
rlmint(   4.96093750000000  ) =   0.21369032462670
rlmint(   4.98574218750000  ) =   0.21484797903836
rlmint(   5.01054687500000  ) =   0.21601599977730
rlmint(   5.03535156250000  ) =   0.21720060307764
rlmint(   5.06015625000000  ) =   0.21839765267207
rlmint(   5.08496093750000  ) =   0.21960519390033
rlmint(   5.10976562500000  ) =   0.22081588752705
rlmint(   5.13457031250000  ) =   0.22205496047167
rlmint(   5.15937500000000  ) =   0.22329912708766
rlmint(   5.18417968750000  ) =   0.22455185703396
rlmint(   5.20898437500000  ) =   0.22582108232454
rlmint(   5.23378906250000  ) =   0.22711677905036
rlmint(   5.25859375000000  ) =   0.22838957867523
rlmint(   5.28339843750000  ) =   0.22969441655014
rlmint(   5.30820312500000  ) =   0.23100602161120
rlmint(   5.33300781250000  ) =   0.23233046918484
rlmint(   5.35781250000000  ) =   0.23366874401365
rlmint(   5.38261718750000  ) =   0.23501133135254
rlmint(   5.40742187500000  ) =   0.23637543391761
rlmint(   5.43222656250000  ) =   0.23774183226523
rlmint(   5.45703125000000  ) =   0.23912030214812
rlmint(   5.48183593750000  ) =   0.24051360717115
rlmint(   5.50664062500000  ) =   0.24191265061164
rlmint(   5.53144531250000  ) =   0.24332303737585
rlmint(   5.55625000000000  ) =   0.24474595732921
rlmint(   5.58105468750000  ) =   0.24617618115326
rlmint(   5.60585937500000  ) =   0.24762008527980
rlmint(   5.63066406250000  ) =   0.24906186184152
rlmint(   5.65546875000000  ) =   0.25051987461417
rlmint(   5.68027343750000  ) =   0.25198886489566
rlmint(   5.70507812500000  ) =   0.25346126157714
rlmint(   5.72988281250000  ) =   0.25494486724251
rlmint(   5.75468750000000  ) =   0.25643343070938
rlmint(   5.77949218750000  ) =   0.25792879516842
rlmint(   5.80429687500000  ) =   0.25943347459063
rlmint(   5.82910156250000  ) =   0.26094219025376
rlmint(   5.85390625000000  ) =   0.26246065985873
rlmint(   5.87871093750000  ) =   0.26397877899990
rlmint(   5.90351562500000  ) =   0.26550380232769
rlmint(   5.92832031250000  ) =   0.26703674382490
rlmint(   5.95312500000000  ) =   0.26857728044769
rlmint(   5.97792968750000  ) =   0.27012149119691
rlmint(   6.00273437500000  ) =   0.27167055801178
rlmint(   6.02753906250000  ) =   0.27322349714236
rlmint(   6.05234375000000  ) =   0.27477355919883
rlmint(   6.07714843750000  ) =   0.27632678393851
rlmint(   6.10195312500000  ) =   0.27788768825522
rlmint(   6.12675781250000  ) =   0.27944827073028
rlmint(   6.15156250000000  ) =   0.28100556098391
rlmint(   6.17636718750000  ) =   0.28256782169160
rlmint(   6.20117187500000  ) =   0.28413671179241
rlmint(   6.22597656250000  ) =   0.28570204432840
rlmint(   6.25078125000000  ) =   0.28726199708691
rlmint(   6.27558593750000  ) =   0.28882470589783
rlmint(   6.30039062500000  ) =   0.29039010632664
rlmint(   6.32519531250000  ) =   0.29194406386722
rlmint(   6.35000000000000  ) =   0.29350265854525
Sun May 17 07:10:40 EDT 1987
```

```
plas2 /usr4/gsg/src/test
Fri May 15 15:39:11 EDT 1987

 ds =  0.99600000000000  d =  0.  volts =  7.70000000000000  e0 =
  2.50000000000000
 rlmint(  0.  ) =   7.6731593544950d-02
 rlmint(   2.4804687500000d-02  ) =   7.6731593544950d-02
 rlmint(   4.9609375000000d-02  ) =   7.6731593544950d-02
 rlmint(   7.4414062500000d-02  ) =   7.6731593544950d-02
 rlmint(   9.9218750000000d-02  ) =   7.6731593544950d-02
 rlmint(  0.12402343750000  ) =   7.6731593544950d-02
 rlmint(  0.14882812500000  ) =   7.6731593544950d-02
 rlmint(  0.17363281250000  ) =   7.6731593544950d-02
 rlmint(  0.19843750000000  ) =   7.6731593544950d-02
 rlmint(  0.22324218750000  ) =   7.6731593544950d-02
 rlmint(  0.24804687500000  ) =   7.6731593544950d-02
 rlmint(  0.27285156250000  ) =   7.6731593544950d-02
 rlmint(  0.29765625000000  ) =   7.6731593544950d-02
 rlmint(  0.32246093750000  ) =   7.6731593544950d-02
 rlmint(  0.34726562500000  ) =   7.6731593544950d-02
 rlmint(  0.37207031250000  ) =   7.6731593544950d-02
 rlmint(  0.39687500000000  ) =   7.6731593544950d-02
 rlmint(  0.42167968750000  ) =   7.6731593544950d-02
 rlmint(  0.44648437500000  ) =   7.6731593544950d-02
 rlmint(  0.47128906250000  ) =   7.6731593544950d-02
 rlmint(  0.49609375000000  ) =   7.6731593544950d-02
 rlmint(  0.52089843750000  ) =   7.6731593544950d-02
 rlmint(  0.54570312500000  ) =   7.6731593544950d-02
 rlmint(  0.57050781250000  ) =   7.6731593544950d-02
 rlmint(  0.59531250000000  ) =   7.6731593544950d-02
 rlmint(  0.62011718750000  ) =   7.6731593544950d-02
 rlmint(  0.64492187500000  ) =   7.6731593544950d-02
 rlmint(  0.66972656250000  ) =   7.6731593544950d-02
 rlmint(  0.69453125000000  ) =   7.6731593544950d-02
 rlmint(  0.71933593750000  ) =   7.6731593544950d-02
 rlmint(  0.74414062500000  ) =   7.6731593544950d-02
 rlmint(  0.76894531250000  ) =   7.6731593544950d-02
 rlmint(  0.79375000000000  ) =   7.6731593544950d-02
 rlmint(  0.81855468750000  ) =   7.6731593544950d-02
 rlmint(  0.84335937500000  ) =   7.6731593544950d-02
 rlmint(  0.86816406250000  ) =   7.6731593544950d-02
 rlmint(  0.89296875000000  ) =   7.6731593544950d-02
 rlmint(  0.91777343750000  ) =   7.6731593544950d-02
 rlmint(  0.94257812500000  ) =   7.6731593544950d-02
 rlmint(  0.96738281250000  ) =   7.6731593544950d-02
 rlmint(  0.99218750000000  ) =   7.6731593544950d-02
 rlmint(  1.01699218750000  ) =   7.6731593544950d-02
 rlmint(  1.04179687500000  ) =   7.6731593544950d-02
 rlmint(  1.06660156250000  ) =   7.6731593544950d-02
 rlmint(  1.09140625000000  ) =   7.6731593544950d-02
 rlmint(  1.11621093750000  ) =   7.6731593544950d-02
 rlmint(  1.14101562500000  ) =   7.6731593544950d-02
 rlmint(  1.16582031250000  ) =   7.6731593544950d-02
 rlmint(  1.19062500000000  ) =   7.6731593544950d-02
 rlmint(  1.21542968750000  ) =   7.6731593544950d-02
 rlmint(  1.24023437500000  ) =   7.6731593544950d-02
 rlmint(  1.26503906250000  ) =   7.6731593544950d-02
 rlmint(  1.28984375000000  ) =   7.6731593544950d-02
 rlmint(  1.31464843750000  ) =   7.6731593544950d-02
 rlmint(  1.33945312500000  ) =   7.6731593544950d-02
 rlmint(  1.36425781250000  ) =   7.6731593544950d-02
 rlmint(  1.38906250000000  ) =   7.6731593544950d-02
 rlmint(  1.41386718750000  ) =   7.6731593544950d-02
 rlmint(  1.43867187500000  ) =   7.6731593544950d-02
 rlmint(  1.46347656250000  ) =   7.6731593544950d-02
 rlmint(  1.48828125000000  ) =   7.6731593544950d-02
 rlmint(  1.51308593750000  ) =   7.6731593544950d-02
 rlmint(  1.53789062500000  ) =   7.6731593544950d-02
 rlmint(  1.56269531250000  ) =   7.6731593544950d-02
 rlmint(  1.58750000000000  ) =   7.6731593544950d-02
 rlmint(  1.61230468750000  ) =   7.6731593544950d-02
 rlmint(  1.63710937500000  ) =   7.6731593544950d-02
 rlmint(  1.66191406250000  ) =   7.6731593544950d-02
 rlmint(  1.68671875000000  ) =   7.6731593544950d-02
 rlmint(  1.71152343750000  ) =   7.6731593544950d-02
 rlmint(  1.73632812500000  ) =   7.6731593544950d-02
 rlmint(  1.76113281250000  ) =   7.6731593544950d-02
 rlmint(  1.78593750000000  ) =   7.6731593544950d-02
 rlmint(  1.81074218750000  ) =   7.6731593544950d-02
 rlmint(  1.83554687500000  ) =   7.6731593544950d-02
 rlmint(  1.86035156250000  ) =   7.6731593544950d-02
 rlmint(  1.88515625000000  ) =   7.6731593544950d-02
 rlmint(  1.90996093750000  ) =   7.6731593544950d-02
 rlmint(  1.93476562500000  ) =   7.6731593544950d-02
 rlmint(  1.95957031250000  ) =   7.6731593544950d-02
 rlmint(  1.98437500000000  ) =   7.6731593544950d-02
 rlmint(  2.00917968750000  ) =   7.6731593544950d-02
 rlmint(  2.03398437500000  ) =   7.6731593544950d-02
 rlmint(  2.05878906250000  ) =   7.6731593544950d-02
 rlmint(  2.08359375000000  ) =   7.6731593544950d-02
 rlmint(  2.10839843750000  ) =   7.6731593544950d-02
 rlmint(  2.13320312500000  ) =   7.6731593544950d-02
 rlmint(  2.15800781250000  ) =   7.6731593544950d-02
 rlmint(  2.18281250000000  ) =   7.6731593544950d-02
 rlmint(  2.20761718750000  ) =   7.6731593544950d-02
 rlmint(  2.23242187500000  ) =   7.6731593544950d-02
 rlmint(  2.25722656250000  ) =   7.6731593544950d-02
 rlmint(  2.28203125000000  ) =   7.6731593544950d-02
 rlmint(  2.30683593750000  ) =   7.6731593544950d-02
 rlmint(  2.33164062500000  ) =   7.6731593544950d-02
 rlmint(  2.35644531250000  ) =   7.6731593544950d-02
 rlmint(  2.38125000000000  ) =   7.6731593544950d-02
 rlmint(  2.40605468750000  ) =   7.6731593544950d-02
 rlmint(  2.43085937500000  ) =   7.6731593544950d-02
 rlmint(  2.45566406250000  ) =   7.6731593544950d-02
 rlmint(  2.48046875000000  ) =   7.6731593544950d-02
 rlmint(  2.50527343750000  ) =   7.6731593544950d-02
 rlmint(  2.53007812500000  ) =   7.6731593544950d-02
 rlmint(  2.55488281250000  ) =   7.6731593544950d-02
 rlmint(  2.57968750000000  ) =   7.6731593544950d-02
 rlmint(  2.60449218750000  ) =   7.6731593544950d-02
 rlmint(  2.62929687500000  ) =   7.6731593544950d-02
 rlmint(  2.65410156250000  ) =   7.6731593544950d-02
 rlmint(  2.67890625000000  ) =   7.6731593544950d-02
 rlmint(  2.70371093750000  ) =   7.6731593544950d-02
 rlmint(  2.72851562500000  ) =   7.6731593544950d-02
 rlmint(  2.75332031250000  ) =   7.6731593544950d-02
 rlmint(  2.77812500000000  ) =   7.6731593544950d-02
 rlmint(  2.80292968750000  ) =   7.6731593544950d-02
 rlmint(  2.82773437500000  ) =   7.6731593544950d-02
 rlmint(  2.85253906250000  ) =   7.6731593544950d-02
 rlmint(  2.87734375000000  ) =   7.6731593544950d-02
 rlmint(  2.90214843750000  ) =   7.6731593544950d-02
 rlmint(  2.92695312500000  ) =   7.6731593544950d-02
 rlmint(  2.95175781250000  ) =   7.6731593544950d-02
 rlmint(  2.97656250000000  ) =   7.6731593544950d-02
 rlmint(  3.00136718750000  ) =   7.6731593544950d-02
 rlmint(  3.02617187500000  ) =   7.6731593544950d-02
 rlmint(  3.05097656250000  ) =   7.6731593544950d-02
 rlmint(  3.07578125000000  ) =   7.6731593544950d-02
 rlmint(  3.10058593750000  ) =   7.6731593544950d-02
 rlmint(  3.12539062500000  ) =   7.6731593544950d-02
```

```
rlmint(   3.15019531250000  ) =    7.6731593544950d-02
rlmint(   3.17500000000000  ) =    7.6731593544950d-02
rlmint(   3.19980468750000  ) =    7.6731593544950d-02
rlmint(   3.22460937500000  ) =    7.6731593544950d-02
rlmint(   3.24941406250000  ) =    7.6731593544950d-02
rlmint(   3.27421875000000  ) =    7.6731593544950d-02
rlmint(   3.29902343750000  ) =    7.6731593544950d-02
rlmint(   3.32382812500000  ) =    7.6731593544950d-02
rlmint(   3.34863281250000  ) =    7.6731593544950d-02
rlmint(   3.37343750000000  ) =    7.6731593544950d-02
rlmint(   3.39824218750000  ) =    7.6731593544950d-02
rlmint(   3.42304687500000  ) =    7.6731593544950d-02
rlmint(   3.44785156250000  ) =    7.6731593544950d-02
rlmint(   3.47265625000000  ) =    7.6731593544950d-02
rlmint(   3.49746093750000  ) =    7.6731593544950d-02
rlmint(   3.52226562500000  ) =    7.6731593544950d-02
rlmint(   3.54707031250000  ) =    7.6731593544950d-02
rlmint(   3.57187500000000  ) =    7.6731593544950d-02
rlmint(   3.59667968750000  ) =    7.6731593544950d-02
rlmint(   3.62148437500000  ) =    7.6731593544950d-02
rlmint(   3.64628906250000  ) =    7.6731593544950d-02
rlmint(   3.67109375000000  ) =    7.6731593544950d-02
rlmint(   3.69589843750000  ) =    7.6731593544950d-02
rlmint(   3.72070312500000  ) =    7.6731593544950d-02
rlmint(   3.74550781250000  ) =    7.6731593544950d-02
rlmint(   3.77031250000000  ) =    7.6731593544950d-02
rlmint(   3.79511718750000  ) =    7.6731593544950d-02
rlmint(   3.81992187500000  ) =    7.6731593544950d-02
rlmint(   3.84472656250000  ) =    7.6731593544950d-02
rlmint(   3.86953125000000  ) =    7.6731593544950d-02
rlmint(   3.89433593750000  ) =    7.6731593544950d-02
rlmint(   3.91914062500000  ) =    7.6731593544950d-02
rlmint(   3.94394531250000  ) =    7.6731593544950d-02
rlmint(   3.96875000000000  ) =    7.6731593544950d-02
rlmint(   3.99355468750000  ) =    7.6731593544950d-02
rlmint(   4.01835937500000  ) =    7.6731593544950d-02
rlmint(   4.04316406250000  ) =    7.6731593544950d-02
rlmint(   4.06796875000000  ) =    7.6731593544950d-02
rlmint(   4.09277343750000  ) =    7.6731593544950d-02
rlmint(   4.11757812500000  ) =    7.6731593544950d-02
rlmint(   4.14238281250000  ) =    7.6731593544950d-02
rlmint(   4.16718750000000  ) =    7.6731593544950d-02
rlmint(   4.19199218750000  ) =    7.6731593544950d-02
rlmint(   4.21679687500000  ) =    7.6731593544950d-02
rlmint(   4.24160156250000  ) =    7.6731593544950d-02
rlmint(   4.26640625000000  ) =    7.6731593544950d-02
rlmint(   4.29121093750000  ) =    7.6731593544950d-02
rlmint(   4.31601562500000  ) =    7.6731593544950d-02
rlmint(   4.34082031250000  ) =    7.6731593544950d-02
rlmint(   4.36562500000000  ) =    7.6732630068955d-02
rlmint(   4.39042968750000  ) =    7.6748266554323d-02
rlmint(   4.41523437500000  ) =    7.6783073479017d-02
rlmint(   4.44003906250000  ) =    7.6837755255019d-02
rlmint(   4.46484375000000  ) =    7.6912897105025d-02
rlmint(   4.48964843750000  ) =    7.7009265035402d-02
rlmint(   4.51445312500000  ) =    7.7127467693544d-02
rlmint(   4.53925781250000  ) =    7.7268311909779d-02
rlmint(   4.56406250000000  ) =    7.7432528373401d-02
rlmint(   4.58886718750000  ) =    7.7620912269929d-02
rlmint(   4.61367187500000  ) =    7.7834473107101d-02
rlmint(   4.63847656250000  ) =    7.8073506215912d-02
rlmint(   4.66328125000000  ) =    7.8339490537203d-02
rlmint(   4.68808593750000  ) =    7.8633090963972d-02
rlmint(   4.71289062500000  ) =    7.8955776578581d-02
rlmint(   4.73769531250000  ) =    7.9307225043808d-02
rlmint(   4.76250000000000  ) =    7.9689756832254d-02
rlmint(   4.78730468750000  ) =    8.0103869179654d-02
rlmint(   4.81210937500000  ) =    8.0550931704123d-02
rlmint(   4.83691406250000  ) =    8.1031868696487d-02
rlmint(   4.86171875000000  ) =    8.1548080525572d-02
rlmint(   4.88652343750000  ) =    8.2100521091697d-02
rlmint(   4.91132812500000  ) =    8.2690848707981d-02
rlmint(   4.93613281250000  ) =    8.3320192925510d-02
rlmint(   4.96093750000000  ) =    8.3990082807873d-02
rlmint(   4.98574218750000  ) =    8.4701362209386d-02
rlmint(   5.01054687500000  ) =    8.5457323184250d-02
rlmint(   5.03535156250000  ) =    8.6255896497942d-02
rlmint(   5.06015625000000  ) =    8.7102360429514d-02
rlmint(   5.08496093750000  ) =    8.7996934190889d-02
rlmint(   5.10976562500000  ) =    8.8941117444956d-02
rlmint(   5.13457031250000  ) =    8.9937250822482d-02
rlmint(   5.15937500000000  ) =    9.0986769607182d-02
rlmint(   5.18417968750000  ) =    9.2092555771829d-02
rlmint(   5.20898437500000  ) =    9.3255051939546d-02
rlmint(   5.23378906250000  ) =    9.4477006586989d-02
rlmint(   5.25859375000000  ) =    9.5761235652809d-02
rlmint(   5.28339843750000  ) =    9.7109810625023d-02
rlmint(   5.30820312500000  ) =    9.8523749357225d-02
rlmint(   5.33300781250000  ) =   0.10000695049508
rlmint(   5.35781250000000  ) =   0.10156129488304
rlmint(   5.38261718750000  ) =   0.10318945581532
rlmint(   5.40742187500000  ) =   0.10489440514539
rlmint(   5.43222656250000  ) =   0.10668067773362
rlmint(   5.45703125000000  ) =   0.10854531050606
rlmint(   5.48183593750000  ) =   0.11049707678713
rlmint(   5.50664062500000  ) =   0.11253747179281
rlmint(   5.53144531250000  ) =   0.11466914209828
rlmint(   5.55625000000000  ) =   0.11689591677427
rlmint(   5.58105468750000  ) =   0.11922150693796
rlmint(   5.60585937500000  ) =   0.12164943188412
rlmint(   5.63066406250000  ) =   0.12418237497252
rlmint(   5.65546875000000  ) =   0.12682543994575
rlmint(   5.68027343750000  ) =   0.12958324118933
rlmint(   5.70507812500000  ) =   0.13245796802432
rlmint(   5.72988281250000  ) =   0.13545531272831
rlmint(   5.75468750000000  ) =   0.13858020022799
rlmint(   5.77949218750000  ) =   0.14183605566640
rlmint(   5.80429687500000  ) =   0.14522820585012
rlmint(   5.82910156250000  ) =   0.14876309680691
rlmint(   5.85390625000000  ) =   0.15244306574462
rlmint(   5.87871093750000  ) =   0.15627781072400
rlmint(   5.90351562500000  ) =   0.16026680814260
rlmint(   5.92832031250000  ) =   0.16442262730329
rlmint(   5.95312500000000  ) =   0.16874721811278
rlmint(   5.97792968750000  ) =   0.17324656379943
rlmint(   6.00273437500000  ) =   0.17793050954438
rlmint(   6.02753906250000  ) =   0.18280218047162
rlmint(   6.05234375000000  ) =   0.18787170929024
rlmint(   6.07714843750000  ) =   0.19314472599471
rlmint(   6.10195312500000  ) =   0.19862763939146
rlmint(   6.12675781250000  ) =   0.20433184919285
rlmint(   6.15156250000000  ) =   0.21026134762984
rlmint(   6.17636718750000  ) =   0.21642718023568
rlmint(   6.20117187500000  ) =   0.22283800194414
rlmint(   6.22597656250000  ) =   0.22950259276781
rlmint(   6.25078125000000  ) =   0.23642930747948
rlmint(   6.27558593750000  ) =   0.24362989732037
rlmint(   6.30039062500000  ) =   0.25111276542583
rlmint(   6.32519531250000  ) =   0.25888904192709
rlmint(   6.35000000000000  ) =   0.26696988827882

ds =   0.41700000000000   d =   0.99600000000000   volts =   8.05000000000000
```

```
e0 =    2.50000000000000
rlmint(  0.  ) =   0.10417620614540
rlmint(    2.48046875000000d-02  ) =   0.10417699414509
rlmint(    4.96093750000000d-02  ) =   0.10418014509053
rlmint(    7.44140625000000d-02  ) =   0.10418521313879
rlmint(    9.92187500000000d-02  ) =   0.10419246587746
rlmint(   0.12402343750000  ) =   0.10420011662945
rlmint(   0.14882812500000  ) =   0.10421306149284
rlmint(   0.17363281250000  ) =   0.10422656986225
rlmint(   0.19843750000000  ) =   0.10424208513502
rlmint(   0.22324218750000  ) =   0.10425908284245
rlmint(   0.24804687500000  ) =   0.10427904047568
rlmint(   0.27285156250000  ) =   0.10430071624019
rlmint(   0.29765625000000  ) =   0.10432444042792
rlmint(   0.32246093750000  ) =   0.10435046578477
rlmint(   0.34726562500000  ) =   0.10437817311838
rlmint(   0.37207031250000  ) =   0.10440884945596
rlmint(   0.39687500000000  ) =   0.10444071423508
rlmint(   0.42167968750000  ) =   0.10447486567511
rlmint(   0.44648437500000  ) =   0.10451181515561
rlmint(   0.47128906250000  ) =   0.10455050405628
rlmint(   0.49609375000000  ) =   0.10459114872967
rlmint(   0.52089843750000  ) =   0.10463394675236
rlmint(   0.54570312500000  ) =   0.10467884178196
rlmint(   0.57050781250000  ) =   0.10472623123666
rlmint(   0.59531250000000  ) =   0.10477555602539
rlmint(   0.62011718750000  ) =   0.10482700738933
rlmint(   0.64492187500000  ) =   0.10488521337151
rlmint(   0.66972656250000  ) =   0.10493728007955
rlmint(   0.69453125000000  ) =   0.10499578721529
rlmint(   0.71933593750000  ) =   0.10505901702359
rlmint(   0.74414062500000  ) =   0.10512004813758
rlmint(   0.76894531250000  ) =   0.10518643351886
rlmint(   0.79375000000000  ) =   0.10525180212648
rlmint(   0.81855468750000  ) =   0.10532230829954
rlmint(   0.84335937500000  ) =   0.10539391123297
rlmint(   0.86816406250000  ) =   0.10548255104834
rlmint(   0.89296875000000  ) =   0.10554766940770
rlmint(   0.91777343750000  ) =   0.10562451864724
rlmint(   0.94257812500000  ) =   0.10570565698789
rlmint(   0.96738281250000  ) =   0.10578930262327
rlmint(   0.99218750000000  ) =   0.10587594383341
rlmint(   1.01699218750000  ) =   0.10596510911338
rlmint(   1.04179687500000  ) =   0.10605655119089
rlmint(   1.06660156250000  ) =   0.10614967310181
rlmint(   1.09140625000000  ) =   0.10624551249990
rlmint(   1.11621093750000  ) =   0.10634697872064
rlmint(   1.14101562500000  ) =   0.10644806230784
rlmint(   1.16582031250000  ) =   0.10655257176222
rlmint(   1.19062500000000  ) =   0.10665943144265
rlmint(   1.21542968750000  ) =   0.10676933542296
rlmint(   1.24023437500000  ) =   0.10688147988429
rlmint(   1.26503906250000  ) =   0.10699666570693
rlmint(   1.28984375000000  ) =   0.10711428287548
rlmint(   1.31464843750000  ) =   0.10723518645486
rlmint(   1.33945312500000  ) =   0.10735832227374
rlmint(   1.36425781250000  ) =   0.10748501008164
rlmint(   1.38906250000000  ) =   0.10761428616695
rlmint(   1.41386718750000  ) =   0.10774429970241
rlmint(   1.43867187500000  ) =   0.10788129142549
rlmint(   1.46347656250000  ) =   0.10801988086456
rlmint(   1.48828125000000  ) =   0.10816092710868
rlmint(   1.51308593750000  ) =   0.10830509072437
rlmint(   1.53789062500000  ) =   0.10845233388797
rlmint(   1.56269531250000  ) =   0.10860285044206
rlmint(   1.58750000000000  ) =   0.10875648596099
rlmint(   1.61230468750000  ) =   0.10891282245319
rlmint(   1.63710937500000  ) =   0.10907379580858
rlmint(   1.66191406250000  ) =   0.10923733238813
rlmint(   1.68671875000000  ) =   0.10940420538430
rlmint(   1.71152343750000  ) =   0.10957465752457
rlmint(   1.73632812500000  ) =   0.10974844720609
rlmint(   1.76113281250000  ) =   0.10992711901497
rlmint(   1.78593750000000  ) =   0.11010628212945
rlmint(   1.81074218750000  ) =   0.11029074627017
rlmint(   1.83554687500000  ) =   0.11047892866612
rlmint(   1.86035156250000  ) =   0.11066078950133
rlmint(   1.88515625000000  ) =   0.11086624815842
rlmint(   1.90996093750000  ) =   0.11106583965100
rlmint(   1.93476562500000  ) =   0.11126907304723
rlmint(   1.95957031250000  ) =   0.11147405565313
rlmint(   1.98437500000000  ) =   0.11168726814309
rlmint(   2.00917968750000  ) =   0.11190245212156
rlmint(   2.03398437500000  ) =   0.11212194662238
rlmint(   2.05878906250000  ) =   0.11234478411329
rlmint(   2.08359375000000  ) =   0.11257316032816
rlmint(   2.10839843750000  ) =   0.11280515716862
rlmint(   2.13320312500000  ) =   0.11304153316324
rlmint(   2.15800781250000  ) =   0.11328247096906
rlmint(   2.18281250000000  ) =   0.11352847755574
rlmint(   2.20761718750000  ) =   0.11377814335696
rlmint(   2.23242187500000  ) =   0.11403233762912
rlmint(   2.25722656250000  ) =   0.11429178690638
rlmint(   2.28203125000000  ) =   0.11455537056526
rlmint(   2.30683593750000  ) =   0.11482479407801
rlmint(   2.33164062500000  ) =   0.11509822046013
rlmint(   2.35644531250000  ) =   0.11537795418124
rlmint(   2.38125000000000  ) =   0.11566115618842
rlmint(   2.40605468750000  ) =   0.11595108096100
rlmint(   2.43085937500000  ) =   0.11624582622090
rlmint(   2.45566406250000  ) =   0.11654577377586
rlmint(   2.48046875000000  ) =   0.11685148844609
rlmint(   2.50527343750000  ) =   0.11716351646989
rlmint(   2.53007812500000  ) =   0.11747943051960
rlmint(   2.55488281250000  ) =   0.11780182268231
rlmint(   2.57968750000000  ) =   0.11813053678951
rlmint(   2.60449218750000  ) =   0.11846569551661
rlmint(   2.62929687500000  ) =   0.11880646788638
rlmint(   2.65410156250000  ) =   0.11915247167840
rlmint(   2.67890625000000  ) =   0.11950612709302
rlmint(   2.70371093750000  ) =   0.11986392464871
rlmint(   2.72851562500000  ) =   0.12022979835586
rlmint(   2.75332031250000  ) =   0.12060253848973
rlmint(   2.77812500000000  ) =   0.12098086453457
rlmint(   2.80292968750000  ) =   0.12136669736819
rlmint(   2.82773437500000  ) =   0.12175970180467
rlmint(   2.85253906250000  ) =   0.12216062714712
rlmint(   2.87734375000000  ) =   0.12256502640318
rlmint(   2.90214843750000  ) =   0.12297917717111
rlmint(   2.92695312500000  ) =   0.12340193623034
rlmint(   2.95175781250000  ) =   0.12382920943904
rlmint(   2.97656250000000  ) =   0.12426668814097
rlmint(   3.00136718750000  ) =   0.12471023356439
rlmint(   3.02617187500000  ) =   0.12516233342599
rlmint(   3.05097656250000  ) =   0.12562219601772
rlmint(   3.07578125000000  ) =   0.12609063006044
rlmint(   3.10058593750000  ) =   0.12656740718283
rlmint(   3.12539062500000  ) =   0.12705224120507
rlmint(   3.15019531250000  ) =   0.12754595073245
rlmint(   3.17500000000000  ) =   0.12804781386432
rlmint(   3.19980468750000  ) =   0.12855850244606
rlmint(   3.22460937500000  ) =   0.12907870752341
```

```
rlmint(   3.24941406250000  ) =   0.12960773595743
rlmint(   3.27421875000000  ) =   0.13014484765245
rlmint(   3.29902343750000  ) =   0.13069313025458
rlmint(   3.32382812500000  ) =   0.13124999598741
rlmint(   3.34863281250000  ) =   0.13181629555451
rlmint(   3.37343750000000  ) =   0.13239286341167
rlmint(   3.39824218750000  ) =   0.13297926648564
rlmint(   3.42304687500000  ) =   0.13357544405361
rlmint(   3.44785156250000  ) =   0.13418200678315
rlmint(   3.47265625000000  ) =   0.13479904525036
rlmint(   3.49746093750000  ) =   0.13542633095267
rlmint(   3.52226562500000  ) =   0.13606470681417
rlmint(   3.54707031250000  ) =   0.13671304623218
rlmint(   3.57187500000000  ) =   0.13737254602635
rlmint(   3.59667968750000  ) =   0.13804308809024
rlmint(   3.62148437500000  ) =   0.13872541470265
rlmint(   3.64628906250000  ) =   0.13941832647695
rlmint(   3.67109375000000  ) =   0.14012366247882
rlmint(   3.69589843750000  ) =   0.14083893187990
rlmint(   3.72070312500000  ) =   0.14156753618560
rlmint(   3.74550781250000  ) =   0.14230728059415
rlmint(   3.77031250000000  ) =   0.14305859893556
rlmint(   3.79511718750000  ) =   0.14382298736229
rlmint(   3.81992187500000  ) =   0.14459862240850
rlmint(   3.84472656250000  ) =   0.14538695653817
rlmint(   3.86953125000000  ) =   0.14618828876137
rlmint(   3.89433593750000  ) =   0.14700200747672
rlmint(   3.91914062500000  ) =   0.14782767777354
rlmint(   3.94394531250000  ) =   0.14866654643507
rlmint(   3.96875000000000  ) =   0.14951868838673
rlmint(   3.99355468750000  ) =   0.15038411486987
rlmint(   4.01835937500000  ) =   0.15126219733132
rlmint(   4.04316406250000  ) =   0.15215357611902
rlmint(   4.06796875000000  ) =   0.15305846762708
rlmint(   4.09277343750000  ) =   0.15397690265931
rlmint(   4.11757812500000  ) =   0.15490892455264
rlmint(   4.14238281250000  ) =   0.15585415307739
rlmint(   4.16718750000000  ) =   0.15681296070509
rlmint(   4.19199218750000  ) =   0.15778526868817
rlmint(   4.21679687500000  ) =   0.15877180342306
rlmint(   4.24160156250000  ) =   0.15977247733454
rlmint(   4.26640625000000  ) =   0.16078716707287
rlmint(   4.29121093750000  ) =   0.16181569414985
rlmint(   4.31601562500000  ) =   0.16285907066287
rlmint(   4.34082031250000  ) =   0.16391543495056
rlmint(   4.36562500000000  ) =   0.16498603232222
rlmint(   4.39042968750000  ) =   0.16607083721773
rlmint(   4.41523437500000  ) =   0.16716965265041
rlmint(   4.44003906250000  ) =   0.16828445818466
rlmint(   4.46484375000000  ) =   0.16941194277571
rlmint(   4.48964843750000  ) =   0.17055464596118
rlmint(   4.51445312500000  ) =   0.17171079242971
rlmint(   4.53925781250000  ) =   0.17288117671464
rlmint(   4.56406250000000  ) =   0.17406591171774
rlmint(   4.58886718750000  ) =   0.17526610685197
rlmint(   4.61367187500000  ) =   0.17647901225294
rlmint(   4.63847656250000  ) =   0.17770672151073
rlmint(   4.66328125000000  ) =   0.17894746307710
rlmint(   4.68808593750000  ) =   0.18020325724155
rlmint(   4.71289062500000  ) =   0.18147343658394
rlmint(   4.73769531250000  ) =   0.18275750570586
rlmint(   4.76250000000000  ) =   0.18405524232254
rlmint(   4.78730468750000  ) =   0.18536614557272
rlmint(   4.81210937500000  ) =   0.18669248395841
rlmint(   4.83691406250000  ) =   0.18803160165119
rlmint(   4.861[illegible]  ) =   0.18938498470142

rlmint(   4.88652343750000  ) =   0.19075069704972
rlmint(   4.91132812500000  ) =   0.19213188041037
rlmint(   4.93613281250000  ) =   0.19352467339732
rlmint(   4.96093750000000  ) =   0.19493078172976
rlmint(   4.98574218750000  ) =   0.19635062462274
rlmint(   5.01054687500000  ) =   0.19778270982782
rlmint(   5.03535156250000  ) =   0.19922787496929
rlmint(   5.06015625000000  ) =   0.20068565976276
rlmint(   5.08496093750000  ) =   0.20215575274197
rlmint(   5.10976562500000  ) =   0.20363743210379
rlmint(   5.13457031250000  ) =   0.20513288650247
rlmint(   5.15937500000000  ) =   0.20663941268026
rlmint(   5.18417968750000  ) =   0.20815419608148
rlmint(   5.20898437500000  ) =   0.20968412360710
rlmint(   5.23378906250000  ) =   0.21122611546284
rlmint(   5.25859375000000  ) =   0.21277898667128
rlmint(   5.28339843750000  ) =   0.21434292728693
rlmint(   5.30820312500000  ) =   0.21591638938274
rlmint(   5.33300781250000  ) =   0.21750033144740
rlmint(   5.35781250000000  ) =   0.21909573589849
rlmint(   5.38261718750000  ) =   0.22070466943549
rlmint(   5.40742187500000  ) =   0.22231415768263
rlmint(   5.43222656250000  ) =   0.22393693733015
rlmint(   5.45703125000000  ) =   0.22557032860317
rlmint(   5.48183593750000  ) =   0.22721238544943
rlmint(   5.50664062500000  ) =   0.22886330612269
rlmint(   5.53144531250000  ) =   0.23052198195348
rlmint(   5.55625000000000  ) =   0.23218913376843
rlmint(   5.58105468750000  ) =   0.23386450088281
rlmint(   5.60585937500000  ) =   0.23554693331009
rlmint(   5.63066406250000  ) =   0.23723646964944
rlmint(   5.65546875000000  ) =   0.23893259243528
rlmint(   5.68027343750000  ) =   0.24063540970833
rlmint(   5.70507812500000  ) =   0.24234463466975
rlmint(   5.72988281250000  ) =   0.24406025374140
rlmint(   5.75468750000000  ) =   0.24578189269804
rlmint(   5.77949218750000  ) =   0.24750800553855
rlmint(   5.80429687500000  ) =   0.24924047952576
rlmint(   5.82910156250000  ) =   0.25097726873656
rlmint(   5.85390625000000  ) =   0.25271665536050
rlmint(   5.87871093750000  ) =   0.25446125545884
rlmint(   5.90351562500000  ) =   0.25620964678172
rlmint(   5.92832031250000  ) =   0.25796104274371
rlmint(   5.95312500000000  ) =   0.25971574113785
rlmint(   5.97792968750000  ) =   0.26147302096753
rlmint(   6.00273437500000  ) =   0.26323254802354
rlmint(   6.02753906250000  ) =   0.26499446841402
rlmint(   6.05234375000000  ) =   0.26675760460595
rlmint(   6.07714843750000  ) =   0.26852219779445
rlmint(   6.10195312500000  ) =   0.27028731211485
rlmint(   6.12675781250000  ) =   0.27205326482176
rlmint(   6.15156250000000  ) =   0.27381875996620
rlmint(   6.17636718750000  ) =   0.27558349620932
rlmint(   6.20117187500000  ) =   0.27734688845611
rlmint(   6.22597656250000  ) =   0.27911490852610
rlmint(   6.25078125000000  ) =   0.28087645060860
rlmint(   6.27558593750000  ) =   0.28263649374879
rlmint(   6.30039062500000  ) =   0.28438111998137
rlmint(   6.32519531250000  ) =   0.28615401805931
rlmint(   6.35000000000000  ) =   0.28790855112959

ds =   0.99600000000000   d =  0.   volts =   85.9000000000000  e0 =
 2.50000000000000
rlmint(  0.  ) =  0.
rlmint(    2.48046875000000d-02  ) =  0.
rlmint(    4.96093750000000d-02  ) =  0.
```

rlmint(7.4414062500000d-02) = 0.
rlmint(9.9218750000000d-02) = 0.
rlmint(0.12402343750000) = 0.
rlmint(0.14882812500000) = 0.
rlmint(0.17363281250000) = 0.
rlmint(0.19843750000000) = 0.
rlmint(0.22324218750000) = 0.
rlmint(0.24804687500000) = 0.
rlmint(0.27285156250000) = 0.
rlmint(0.29765625000000) = 0.
rlmint(0.32246093750000) = 0.
rlmint(0.34726562500000) = 0.
rlmint(0.37207031250000) = 0.
rlmint(0.39687500000000) = 0.
rlmint(0.42167968750000) = 0.
rlmint(0.44648437500000) = 0.
rlmint(0.47128906250000) = 0.
rlmint(0.49609375000000) = 0.
rlmint(0.52089843750000) = 0.
rlmint(0.54570312500000) = 0.
rlmint(0.57050781250000) = 0.
rlmint(0.59531250000000) = 0.
rlmint(0.62011718750000) = 0.
rlmint(0.64492187500000) = 0.
rlmint(0.66972656250000) = 0.
rlmint(0.69453125000000) = 0.
rlmint(0.71933593750000) = 0.
rlmint(0.74414062500000) = 0.
rlmint(0.76894531250000) = 0.
rlmint(0.79375000000000) = 0.
rlmint(0.81855468750000) = 0.
rlmint(0.84335937500000) = 0.
rlmint(0.86816406250000) = 0.
rlmint(0.89296875000000) = 0.
rlmint(0.91777343750000) = 0.
rlmint(0.94257812500000) = 0.
rlmint(0.96738281250000) = 0.
rlmint(0.99218750000000) = 0.
rlmint(1.01699218750000) = 0.
rlmint(1.04179687500000) = 0.
rlmint(1.06660156250000) = 0.
rlmint(1.09140625000000) = 0.
rlmint(1.11621093750000) = 0.
rlmint(1.14101562500000) = 0.
rlmint(1.16582031250000) = 0.
rlmint(1.19062500000000) = 0.
rlmint(1.21542968750000) = 0.
rlmint(1.24023437500000) = 0.
rlmint(1.26503906250000) = 0.
rlmint(1.28984375000000) = 0.
rlmint(1.31464843750000) = 0.
rlmint(1.33945312500000) = 0.
rlmint(1.36425781250000) = 0.
rlmint(1.38906250000000) = 0.
rlmint(1.41386718750000) = 0.
rlmint(1.43867187500000) = 0.
rlmint(1.46347656250000) = 0.
rlmint(1.48828125000000) = 0.
rlmint(1.51308593750000) = 0.
rlmint(1.53789062500000) = 0.
rlmint(1.56269531250000) = 0.
rlmint(1.58750000000000) = 0.
rlmint(1.61230468750000) = 0.
rlmint(1.63710937500000) = 0.
rlmint(1.66191406250000) = 0.
rlmint(1.68671875000000) = 0.
rlmint(1.71152343750000) = 0.
rlmint(1.73632812500000) = 0.
rlmint(1.76113281250000) = 0.
rlmint(1.78593750000000) = 0.
rlmint(1.81074218750000) = 0.
rlmint(1.83554687500000) = 0.
rlmint(1.86035156250000) = 0.
rlmint(1.88515625000000) = 0.
rlmint(1.90996093750000) = 0.
rlmint(1.93476562500000) = 0.
rlmint(1.95957031250000) = 0.
rlmint(1.98437500000000) = 0.
rlmint(2.00917968750000) = 0.
rlmint(2.03398437500000) = 0.
rlmint(2.05878906250000) = 0.
rlmint(2.08359375000000) = 0.
rlmint(2.10839843750000) = 0.
rlmint(2.13320312500000) = 0.
rlmint(2.15800781250000) = 0.
rlmint(2.18281250000000) = 0.
rlmint(2.20761718750000) = 0.
rlmint(2.23242187500000) = 0.
rlmint(2.25722656250000) = 0.
rlmint(2.28203125000000) = 0.
rlmint(2.30683593750000) = 0.
rlmint(2.33164062500000) = 0.
rlmint(2.35644531250000) = 0.
rlmint(2.38125000000000) = 0.
rlmint(2.40605468750000) = 0.
rlmint(2.43085937500000) = 0.
rlmint(2.45566406250000) = 0.
rlmint(2.48046875000000) = 0.
rlmint(2.50527343750000) = 0.
rlmint(2.53007812500000) = 0.
rlmint(2.55488281250000) = 0.
rlmint(2.57968750000000) = 0.
rlmint(2.60449218750000) = 0.
rlmint(2.62929687500000) = 0.
rlmint(2.65410156250000) = 0.
rlmint(2.67890625000000) = 0.
rlmint(2.70371093750000) = 0.
rlmint(2.72851562500000) = 0.
rlmint(2.75332031250000) = 0.
rlmint(2.77812500000000) = 0.
rlmint(2.80292968750000) = 0.
rlmint(2.82773437500000) = 0.
rlmint(2.85253906250000) = 0.
rlmint(2.87734375000000) = 0.
rlmint(2.90214843750000) = 0.
rlmint(2.92695312500000) = 0.
rlmint(2.95175781250000) = 0.
rlmint(2.97656250000000) = 0.
rlmint(3.00136718750000) = 0.
rlmint(3.02617187500000) = 0.
rlmint(3.05097656250000) = 0.
rlmint(3.07578125000000) = 0.
rlmint(3.10058593750000) = 0.
rlmint(3.12539062500000) = 0.
rlmint(3.15019531250000) = 0.
rlmint(3.17500000000000) = 0.
rlmint(3.19980468750000) = 0.
rlmint(3.22460937500000) = 0.
rlmint(3.24941406250000) = 0.
rlmint(3.27421875000000) = 0.
rlmint(3.29902343750000) = 0.
rlmint(3.32382812500000) = 0.

```
rlmint(   3.34863281250000  ) =  0.
rlmint(   3.37343750000000  ) =  0.
rlmint(   3.39824218750000  ) =  0.
rlmint(   3.42304687500000  ) =  0.
rlmint(   3.44785156250000  ) =  0.
rlmint(   3.47265625000000  ) =  0.
rlmint(   3.49746093750000  ) =  0.
rlmint(   3.52226562500000  ) =  0.
rlmint(   3.54707031250000  ) =  0.
rlmint(   3.57187500000000  ) =  0.
rlmint(   3.59667968750000  ) =  0.
rlmint(   3.62148437500000  ) =  0.
rlmint(   3.64628906250000  ) =  0.
rlmint(   3.67109375000000  ) =  0.
rlmint(   3.69589843750000  ) =  0.
rlmint(   3.72070312500000  ) =  0.
rlmint(   3.74550781250000  ) =  0.
rlmint(   3.77031250000000  ) =  0.
rlmint(   3.79511718750000  ) =  0.
rlmint(   3.81992187500000  ) =  0.
rlmint(   3.84472656250000  ) =  0.
rlmint(   3.86953125000000  ) =  0.
rlmint(   3.89433593750000  ) =  0.
rlmint(   3.91914062500000  ) =  0.
rlmint(   3.94394531250000  ) =  0.
rlmint(   3.96875000000000  ) =  0.
rlmint(   3.99355468750000  ) =  0.
rlmint(   4.01835937500000  ) =  0.
rlmint(   4.04316406250000  ) =  0.
rlmint(   4.06796875000000  ) =  0.
rlmint(   4.09277343750000  ) =  0.
rlmint(   4.11757812500000  ) =  0.
rlmint(   4.14238281250000  ) =  0.
rlmint(   4.16718750000000  ) =  0.
rlmint(   4.19199218750000  ) =  0.
rlmint(   4.21679687500000  ) =  0.
rlmint(   4.24160156250000  ) =  0.
rlmint(   4.26640625000000  ) =  0.
rlmint(   4.29121093750000  ) =  0.
rlmint(   4.31601562500000  ) =  0.
rlmint(   4.34082031250000  ) =  0.
rlmint(   4.36562500000000  ) =  0.
rlmint(   4.39042968750000  ) =  0.
rlmint(   4.41523437500000  ) =  0.
rlmint(   4.44003906250000  ) =  0.
rlmint(   4.46484375000000  ) =  0.
rlmint(   4.48964843750000  ) =  0.
rlmint(   4.51445312500000  ) =  0.
rlmint(   4.53925781250000  ) =  0.
rlmint(   4.56406250000000  ) =  0.
rlmint(   4.58886718750000  ) =  0.
rlmint(   4.61367187500000  ) =  0.
rlmint(   4.63847656250000  ) =  0.
rlmint(   4.66328125000000  ) =  0.
rlmint(   4.68808593750000  ) =  0.
rlmint(   4.71289062500000  ) =  0.
rlmint(   4.73769531250000  ) =  0.
rlmint(   4.76250000000000  ) =  0.
rlmint(   4.78730468750000  ) =  0.
rlmint(   4.81210937500000  ) =  0.
rlmint(   4.83691406250000  ) =  0.
rlmint(   4.86171875000000  ) =  0.
rlmint(   4.88652343750000  ) =  0.
rlmint(   4.91132812500000  ) =  0.
rlmint(   4.93613281250000  ) =  0.
rlmint(   4.96093750000000  ) =  0.
rlmint(   4.98574218750000  ) =  0.
rlmint(   5.01054687500000  ) =  0.
rlmint(   5.03535156250000  ) =  0.
rlmint(   5.06015625000000  ) =  0.
rlmint(   5.08496093750000  ) =  0.
rlmint(   5.10976562500000  ) =  0.
rlmint(   5.13457031250000  ) =  0.
rlmint(   5.15937500000000  ) =  0.
rlmint(   5.18417968750000  ) =  0.
rlmint(   5.20898437500000  ) =  0.
rlmint(   5.23378906250000  ) =  0.
rlmint(   5.25859375000000  ) =  0.
rlmint(   5.28339843750000  ) =  0.
rlmint(   5.30820312500000  ) =  0.
rlmint(   5.33300781250000  ) =  0.
rlmint(   5.35781250000000  ) =  0.
rlmint(   5.38261718750000  ) =  0.
rlmint(   5.40742187500000  ) =  0.
rlmint(   5.43222656250000  ) =  0.
rlmint(   5.45703125000000  ) =  0.
rlmint(   5.48183593750000  ) =  0.
rlmint(   5.50664062500000  ) =  0.
rlmint(   5.53144531250000  ) =  0.
rlmint(   5.55625000000000  ) =  0.
rlmint(   5.58105468750000  ) =  0.
rlmint(   5.60585937500000  ) =  0.
rlmint(   5.63066406250000  ) =  0.
rlmint(   5.65546875000000  ) =  0.
rlmint(   5.68027343750000  ) =  0.
rlmint(   5.70507812500000  ) =  0.
rlmint(   5.72988281250000  ) =  0.
rlmint(   5.75468750000000  ) =  0.
rlmint(   5.77949218750000  ) =  0.
rlmint(   5.80429687500000  ) =  0.
rlmint(   5.82910156250000  ) =  0.
rlmint(   5.85390625000000  ) =  0.
rlmint(   5.87871093750000  ) =  0.
rlmint(   5.90351562500000  ) =  0.
rlmint(   5.92832031250000  ) =  0.
rlmint(   5.95312500000000  ) =  0.
rlmint(   5.97792968750000  ) =  0.
rlmint(   6.00273437500000  ) =    2.9053489909986d-08
rlmint(   6.02753906250000  ) =    6.4081960566067d-05
rlmint(   6.05234375000000  ) =    2.9316439650252d-04
rlmint(   6.07714843750000  ) =    7.7461601007190d-04
rlmint(   6.10195312500000  ) =    1.6421076253913d-03
rlmint(   6.12675781250000  ) =    3.1003157095612d-03
rlmint(   6.15156250000000  ) =    5.4626098672410d-03
rlmint(   6.17636718750000  ) =    9.2121148825668d-03
rlmint(   6.20117187500000  ) =    1.5073054128408d-02
rlmint(   6.22597656250000  ) =    2.4180352203379d-02
rlmint(   6.25078125000000  ) =    3.8251229347637d-02
rlmint(   6.27558593750000  ) =    5.9921943891055d-02
rlmint(   6.30039062500000  ) =    9.3227483926073d-02
rlmint(   6.32519531250000  ) =   0.14434634833284
rlmint(   6.35000000000000  ) =   0.22272644394631

ds =   0.41700000000000   d =   0.99600000000000   volts =   95.2000000000000
e0 =    2.50000000000000
rlmint(  0.  ) =    4.0011430243717d-02
rlmint(    2.4804687500000d-02  ) =    4.0011967979964d-02
rlmint(    4.9609375000000d-02  ) =    4.0014284896820d-02
rlmint(    7.4414062500000d-02  ) =    4.0021304164998d-02
rlmint(    9.9218750000000d-02  ) =    4.0027518711969d-02
rlmint(   0.12402343750000  ) =    4.0036102257406d-02
rlmint(   0.14882812500000  ) =    4.0048289797943d-02
```

```
rlmint(  0.17363281250000  ) =   4.0061947826793d-02
rlmint(  0.19843750000000  ) =   4.0076266806580d-02
rlmint(  0.22324218750000  ) =   4.0093279683997d-02
rlmint(  0.24804687500000  ) =   4.0114434112450d-02
rlmint(  0.27285156250000  ) =   4.0135766724776d-02
rlmint(  0.29765625000000  ) =   4.0158779168620d-02
rlmint(  0.32246093750000  ) =   4.0181833085371d-02
rlmint(  0.34726562500000  ) =   4.0211841567082d-02
rlmint(  0.37207031250000  ) =   4.0242187798907d-02
rlmint(  0.39687500000000  ) =   4.0275617044957d-02
rlmint(  0.42167968750000  ) =   4.0308479659859d-02
rlmint(  0.44648437500000  ) =   4.0344559651222d-02
rlmint(  0.47128906250000  ) =   4.0383120139908d-02
rlmint(  0.49609375000000  ) =   4.0423387983204d-02
rlmint(  0.52089843750000  ) =   4.0467056537684d-02
rlmint(  0.54570312500000  ) =   4.0514207566583d-02
rlmint(  0.57050781250000  ) =   4.0557772290848d-02
rlmint(  0.59531250000000  ) =   4.0607466577849d-02
rlmint(  0.62011718750000  ) =   4.0658349853514d-02
rlmint(  0.64492187500000  ) =   4.0711176730458d-02
rlmint(  0.66972656250000  ) =   4.0767413606909d-02
rlmint(  0.69453125000000  ) =   4.0824540938000d-02
rlmint(  0.71933593750000  ) =   4.0884895392911d-02
rlmint(  0.74414062500000  ) =   4.0948263141003d-02
rlmint(  0.76894531250000  ) =   4.1010975250509d-02
rlmint(  0.79375000000000  ) =   4.1077455401464d-02
rlmint(  0.81855468750000  ) =   4.1147084553881d-02
rlmint(  0.84335937500000  ) =   4.1218967752985d-02
rlmint(  0.86816406250000  ) =   4.1292959284591d-02
rlmint(  0.89296875000000  ) =   4.1397835229626d-02
rlmint(  0.91777343750000  ) =   4.1454949368420d-02
rlmint(  0.94257812500000  ) =   4.1527397019146d-02
rlmint(  0.96738281250000  ) =   4.1610968752398d-02
rlmint(  0.99218750000000  ) =   4.1695507355378d-02
rlmint(  1.01699218750000  ) =   4.1785493850439d-02
rlmint(  1.04179687500000  ) =   4.1874786063939d-02
rlmint(  1.06660156250000  ) =   4.1966930022196d-02
rlmint(  1.09140625000000  ) =   4.2062261692506d-02
rlmint(  1.11621093750000  ) =   4.2159962382960d-02
rlmint(  1.14101562500000  ) =   4.2260319222526d-02
rlmint(  1.16582031250000  ) =   4.2361362745786d-02
rlmint(  1.19062500000000  ) =   4.2468241979710d-02
rlmint(  1.21542968750000  ) =   4.2575578299290d-02
rlmint(  1.24023437500000  ) =   4.2687406574092d-02
rlmint(  1.26503906250000  ) =   4.2798339602349d-02
rlmint(  1.28984375000000  ) =   4.2916343035180d-02
rlmint(  1.31464843750000  ) =   4.3033282955218d-02
rlmint(  1.33945312500000  ) =   4.3155230057833d-02
rlmint(  1.36425781250000  ) =   4.3277990166485d-02
rlmint(  1.38906250000000  ) =   4.3405056489518d-02
rlmint(  1.41386718750000  ) =   4.3535545391930d-02
rlmint(  1.43867187500000  ) =   4.3667613411485d-02
rlmint(  1.46347656250000  ) =   4.3802146267392d-02
rlmint(  1.48828125000000  ) =   4.3940283440451d-02
rlmint(  1.51308593750000  ) =   4.4079983056826d-02
rlmint(  1.53789062500000  ) =   4.4223853653105d-02
rlmint(  1.56269531250000  ) =   4.4370079481513d-02
rlmint(  1.58750000000000  ) =   4.4521752826142d-02
rlmint(  1.61230468750000  ) =   4.4674446898257d-02
rlmint(  1.63710937500000  ) =   4.4830512269379d-02
rlmint(  1.66191406250000  ) =   4.4989539328273d-02
rlmint(  1.68671875000000  ) =   4.5152173175975d-02
rlmint(  1.71152343750000  ) =   4.5318994551831d-02
rlmint(  1.73632812500000  ) =   4.5486158820849d-02
rlmint(  1.76113281250000  ) =   4.5656489619398d-02
rlmint(  1.78593750000000  ) =   4.5834098202152d-02
rlmint(  1.81074218750000  ) =   4.6011430810565d-02
rlmint(  1.83554687500000  ) =   4.6193960782575d-02
rlmint(  1.86035156250000  ) =   4.6350500885167d-02
rlmint(  1.88515625000000  ) =   4.6567669869872d-02
rlmint(  1.90996093750000  ) =   4.6762585099131d-02
rlmint(  1.93476562500000  ) =   4.6957850741829d-02
rlmint(  1.95957031250000  ) =   4.7157532725586d-02
rlmint(  1.98437500000000  ) =   4.7359662245858d-02
rlmint(  2.00917968750000  ) =   4.7568049683815d-02
rlmint(  2.03398437500000  ) =   4.7778781172683d-02
rlmint(  2.05878906250000  ) =   4.7993798776841d-02
rlmint(  2.08359375000000  ) =   4.8212893444719d-02
rlmint(  2.10839843750000  ) =   4.8435935534880d-02
rlmint(  2.13320312500000  ) =   4.8663493675985d-02
rlmint(  2.15800781250000  ) =   4.8893064659635d-02
rlmint(  2.18281250000000  ) =   4.9126631927465d-02
rlmint(  2.20761718750000  ) =   4.9367062514842d-02
rlmint(  2.23242187500000  ) =   4.9611136425520d-02
rlmint(  2.25722656250000  ) =   4.9861158834733d-02
rlmint(  2.28203125000000  ) =   5.0111061444139d-02
rlmint(  2.30683593750000  ) =   5.0368816776541d-02
rlmint(  2.33164062500000  ) =   5.0629529350736d-02
rlmint(  2.35644531250000  ) =   5.0895378519061d-02
rlmint(  2.38125000000000  ) =   5.1165376702871d-02
rlmint(  2.40605468750000  ) =   5.1440351453996d-02
rlmint(  2.43085937500000  ) =   5.1721094592213d-02
rlmint(  2.45566406250000  ) =   5.2005059597446d-02
rlmint(  2.48046875000000  ) =   5.2295386812048d-02
rlmint(  2.50527343750000  ) =   5.2590794117184d-02
rlmint(  2.53007812500000  ) =   5.2890473088976d-02
rlmint(  2.55488281250000  ) =   5.3197361794524d-02
rlmint(  2.57968750000000  ) =   5.3507311633455d-02
rlmint(  2.60449218750000  ) =   5.3814645598442d-02
rlmint(  2.62929687500000  ) =   5.4145304373720d-02
rlmint(  2.65410156250000  ) =   5.4471015121614d-02
rlmint(  2.67890625000000  ) =   5.4803834133847d-02
rlmint(  2.70371093750000  ) =   5.5141606917016d-02
rlmint(  2.72851562500000  ) =   5.5486374723219d-02
rlmint(  2.75332031250000  ) =   5.5837909956953d-02
rlmint(  2.77812500000000  ) =   5.6194464141849d-02
rlmint(  2.80292968750000  ) =   5.6557323082586d-02
rlmint(  2.82773437500000  ) =   5.6925550848384d-02
rlmint(  2.85253906250000  ) =   5.7301168648310d-02
rlmint(  2.87734375000000  ) =   5.7682143319844d-02
rlmint(  2.90214843750000  ) =   5.8069150275158d-02
rlmint(  2.92695312500000  ) =   5.8464424948553d-02
rlmint(  2.95175781250000  ) =   5.8866544294969d-02
rlmint(  2.97656250000000  ) =   5.9274402568326d-02
rlmint(  3.00136718750000  ) =   5.9690090635398d-02
rlmint(  3.02617187500000  ) =   6.0113718000041d-02
rlmint(  3.05097656250000  ) =   6.0543545325909d-02
rlmint(  3.07578125000000  ) =   6.0982366043710d-02
rlmint(  3.10058593750000  ) =   6.1427535167814d-02
rlmint(  3.12539062500000  ) =   6.1880085640069d-02
rlmint(  3.15019531250000  ) =   6.2341716465702d-02
rlmint(  3.17500000000000  ) =   6.2810341010869d-02
rlmint(  3.19980468750000  ) =   6.3289707045169d-02
rlmint(  3.22460937500000  ) =   6.3772284134639d-02
rlmint(  3.24941406250000  ) =   6.4271202323924d-02
rlmint(  3.27421875000000  ) =   6.4767853280885d-02
rlmint(  3.29902343750000  ) =   6.5280092626730d-02
rlmint(  3.32382812500000  ) =   6.5798939607644d-02
rlmint(  3.34863281250000  ) =   6.6327901009125d-02
rlmint(  3.37343750000000  ) =   6.6866544107864d-02
rlmint(  3.39824218750000  ) =   6.7414943275891d-02
rlmint(  3.42304687500000  ) =   6.7972389929507d-02
```

```
rlmint(   3.44785156250000  ) =    6.8538789952733d-02
rlmint(   3.47265625000000  ) =    6.9116621048270d-02
rlmint(   3.49746093750000  ) =    6.9702453287593d-02
rlmint(   3.52226562500000  ) =    7.0299684187666d-02
rlmint(   3.54707031250000  ) =    7.0907863456248d-02
rlmint(   3.57187500000000  ) =    7.1526722216909d-02
rlmint(   3.59667968750000  ) =    7.2157540832584d-02
rlmint(   3.62148437500000  ) =    7.2798973138406d-02
rlmint(   3.64628906250000  ) =    7.3450189850796d-02
rlmint(   3.67109375000000  ) =    7.4112758330186d-02
rlmint(   3.69589843750000  ) =    7.4788137053086d-02
rlmint(   3.72070312500000  ) =    7.5475882281355d-02
rlmint(   3.74550781250000  ) =    7.6175323060417d-02
rlmint(   3.77031250000000  ) =    7.6886898973129d-02
rlmint(   3.79511718750000  ) =    7.7611409565858d-02
rlmint(   3.81992187500000  ) =    7.8350429412208d-02
rlmint(   3.84472656250000  ) =    7.9100477198159d-02
rlmint(   3.86953125000000  ) =    7.9863421174934d-02
rlmint(   3.89433593750000  ) =    8.0638716503271d-02
rlmint(   3.91914062500000  ) =    8.1430466224205d-02
rlmint(   3.94394531250000  ) =    8.2234428656127d-02
rlmint(   3.96875000000000  ) =    8.3053409919720d-02
rlmint(   3.99355468750000  ) =    8.3888765032424d-02
rlmint(   4.01835937500000  ) =    8.4735952263292d-02
rlmint(   4.04316406250000  ) =    8.5599431704577d-02
rlmint(   4.06796875000000  ) =    8.6479087474647d-02
rlmint(   4.09277343750000  ) =    8.7372136541157d-02
rlmint(   4.11757812500000  ) =    8.8283168994546d-02
rlmint(   4.14238281250000  ) =    8.9209616572416d-02
rlmint(   4.16718750000000  ) =    9.0152714673896d-02
rlmint(   4.19199218750000  ) =    9.1112584672439d-02
rlmint(   4.21679687500000  ) =    9.2089925341502d-02
rlmint(   4.24160156250000  ) =    9.3081841425532d-02
rlmint(   4.26640625000000  ) =    9.4096206128575d-02
rlmint(   4.29121093750000  ) =    9.5123675144164d-02
rlmint(   4.31601562500000  ) =    9.6173959007386d-02
rlmint(   4.34082031250000  ) =    9.7240555287394d-02
rlmint(   4.36562500000000  ) =    9.8321621737157d-02
rlmint(   4.39042968750000  ) =    9.9425420397581d-02
rlmint(   4.41523437500000  ) =   0.10054744224483
rlmint(   4.44003906250000  ) =   0.10169100493293
rlmint(   4.46484375000000  ) =   0.10285361313772
rlmint(   4.48964843750000  ) =   0.10403531138192
rlmint(   4.51445312500000  ) =   0.10523732026966
rlmint(   4.53925781250000  ) =   0.10646323123916
rlmint(   4.56406250000000  ) =   0.10770748168958
rlmint(   4.58886718750000  ) =   0.10897416334504
rlmint(   4.61367187500000  ) =   0.11025910242613
rlmint(   4.63847656250000  ) =   0.11156806757619
rlmint(   4.66328125000000  ) =   0.11290138106085
rlmint(   4.68808593750000  ) =   0.11425654298876
rlmint(   4.71289062500000  ) =   0.11563326317740
rlmint(   4.73769531250000  ) =   0.11703637834104
rlmint(   4.76250000000000  ) =   0.11845029893015
rlmint(   4.78730468750000  ) =   0.11990346001197
rlmint(   4.81210937500000  ) =   0.12137455794868
rlmint(   4.83691406250000  ) =   0.12286857007173
rlmint(   4.86171875000000  ) =   0.12438533607687
rlmint(   4.88652343750000  ) =   0.12592970987433
rlmint(   4.91132812500000  ) =   0.12750522563749
rlmint(   4.93613281250000  ) =   0.12909101535385
rlmint(   4.96093750000000  ) =   0.13070615935510
rlmint(   4.98574218750000  ) =   0.13235185151040
rlmint(   5.01054687500000  ) =   0.13402279864215
rlmint(   5.03535156250000  ) =   0.13571882401392
rlmint(   5.06015625000000  ) =   0.13742590346827
rlmint(   5.08496093750000  ) =   0.13916934642838
rlmint(   5.10976562500000  ) =   0.14093946798689
rlmint(   5.13457031250000  ) =   0.14273508455726
rlmint(   5.15937500000000  ) =   0.14455657607238
rlmint(   5.18417968750000  ) =   0.14640280608327
rlmint(   5.20898437500000  ) =   0.14827566894662
rlmint(   5.23378906250000  ) =   0.15018119162855
rlmint(   5.25859375000000  ) =   0.15209578062575
rlmint(   5.28339843750000  ) =   0.15404811846970
rlmint(   5.30820312500000  ) =   0.15602437851382
rlmint(   5.33300781250000  ) =   0.15802576964389
rlmint(   5.35781250000000  ) =   0.16005328852739
rlmint(   5.38261718750000  ) =   0.16210308919232
rlmint(   5.40742187500000  ) =   0.16417715954438
rlmint(   5.43222656250000  ) =   0.16628098740945
rlmint(   5.45703125000000  ) =   0.16840355679697
rlmint(   5.48183593750000  ) =   0.17055145749457
rlmint(   5.50664062500000  ) =   0.17273009177139
rlmint(   5.53144531250000  ) =   0.17492742571023
rlmint(   5.55625000000000  ) =   0.17714784778244
rlmint(   5.58105468750000  ) =   0.17938900347298
rlmint(   5.60585937500000  ) =   0.18165402045717
rlmint(   5.63066406250000  ) =   0.18393746975382
rlmint(   5.65546875000000  ) =   0.18624571926091
rlmint(   5.68027343750000  ) =   0.18857781277038
rlmint(   5.70507812500000  ) =   0.19092533204397
rlmint(   5.72988281250000  ) =   0.19329369419686
rlmint(   5.75468750000000  ) =   0.19568222076161
rlmint(   5.77949218750000  ) =   0.19809132716725
rlmint(   5.80429687500000  ) =   0.20051177638464
rlmint(   5.82910156250000  ) =   0.20295051578627
rlmint(   5.85390625000000  ) =   0.20541248910328
rlmint(   5.87871093750000  ) =   0.20787722142062
rlmint(   5.90351562500000  ) =   0.21036414750549
rlmint(   5.92832031250000  ) =   0.21286239819950
rlmint(   5.95312500000000  ) =   0.21537405622175
rlmint(   5.97792968750000  ) =   0.21789786844764
rlmint(   6.00273437500000  ) =   0.22043311775735
rlmint(   6.02753906250000  ) =   0.22297804795507
rlmint(   6.05234375000000  ) =   0.22552786081034
rlmint(   6.07714843750000  ) =   0.22809087634848
rlmint(   6.10195312500000  ) =   0.23065893678546
rlmint(   6.12675781250000  ) =   0.23323404030092
rlmint(   6.15156250000000  ) =   0.23581363401176
rlmint(   6.17636718750000  ) =   0.23839231078562
rlmint(   6.20117187500000  ) =   0.24098280288960
rlmint(   6.22597656250000  ) =   0.24357137707999
rlmint(   6.25078125000000  ) =   0.24616863211522
rlmint(   6.27558593750000  ) =   0.24874417058539
rlmint(   6.30039062500000  ) =   0.25133923248523
rlmint(   6.32519531250000  ) =   0.25389477428857
rlmint(   6.35000000000000  ) =   0.25649940230824
Sun May 17 07:56:07 EDT 1987
```

APPENDIX C

cpresp.f

```
C          03/21/84    16:14:04       03/21/84    14:46:26       $380300.MJS
      FUNCTION CPRESP(V,UU,SUP,ZCU,AEVV,III)                              CPRESP
C    11/12/78    VMV
C       REVISED 12/30/78    VMV
C    COMPUTES RESPONSE FUNCTION OF VOYAGER CUP, IN (CURRENT UNIT)CM**3/SC
C    V(3)=VELOCITY VECTOR, CM/SEC
C    UU=EFFECTIVE MODULATOR VOLTAGE (VOLTS*Z, INCLUDING SIGN)
C    SUP= SUPPRESSOR VOLTAGE
C    ZCU= PARTICLE CHARGE
C    AEVV=PARTICLE MASS  (AEVV*V**2=ENERGY IN EV)
C    III=CUP INDEX  1=A, 2=B, 3=C, 4=D PROTON MODE, 5=D ELECTRON MODE
C
C    SUBPROGRAMS CALLED  - - - TRANSN,TRANSD,DIPLN,DISPLD,ARMAIN,ARSIDE
C
c      REAL*8 $$$DT(6) /'$$DATE$$','03/21/84','14:46:26',
c     | '  CPRESP','  FORTRAN','MJS       '/
c
      DIMENSION V(3)
         common     /comellos/  ilossm,ilossd,ilossi
c         ilossm 1 for e1 voltage, 2 for e2 or ion voltages
c         ilossd 0 no losses, 1 isotropic secondaries, 2 cosine law
         data   dm1   /1.6153/, ame   /3.553513e-19/
      VZ=V(3)
      IF(VZ.LE.0.)GO TO 99
      U=AEVV*VZ**2
C    GET TRANSPARENCY AND BEAM DISPLACEMENT FACTOR
      IF(III.GE.4)GO TO 5
      TR=TRANSN(V,U,UU,SUP)
      BDSPL=DISPLN(U,UU,SUP)
C    GET AREA
      X=BDSPL*V(1)/VZ
      Y=BDSPL*V(2)/VZ
      AR=ARMAIN(X,Y)
         alossd = 0.0
      GO TO 20
C    COME HERE FOR SIDE SENSOR
5     TR=TRANSD(V,U,UU,SUP)
      CALL DISPLD(V,U,UU,SUP,X,Y)
      AR=ARSIDE(X,Y,aloss,ilossi)
      if ( ar*aloss .eq. 0.0) then
                  alossd = 0.0
      else
                  vt2 = v(1)**2 + v(2)**2
                  vt = sqrt(vt2)
                  vz2 = vz**2
                  vv2 = vt2 + vz2
                  vv = sqrt(vv2)
                  epem = ame*(vt2 + vz2)
                  costhp = vz/vv
                  del = dm1/costhp*epem**-0.35*
     |                  (1.0-exp(-2.28*costhp*epem**1.35))
                  alossd = 1.0*del*aloss
      end if
      if (ilossd .lt. 0) then
                  ar = 0.0
                  alossd = -alossd
      end if
20    CONTINUE
C    PUT IT ALL TOGETHER
      CPRESP=ZCU*VZ*TR*(AR - alossd)
C    CHANGE SIGN OF CURRENT IN ELECTRON MODE, TO KEEP OUTPUT SIGNAL POSIT
```

FOR AREA CORRECTION

$I = \int \vec{F} \cdot d\vec{S}$

$= FS\cos\theta$

$= (F\cos\theta)\,S$

where F is unit flux

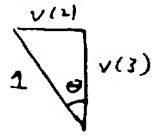

V(1) = 0.0
V(2) = SIN θ
V(3) = COS θ

FOR INCOMING PHOTONS AT ANGLE θ

SET U = 0.0, P = 0.0

GIVES CORRECT TRANSPARENCY AND "DISPLACEMENT" TO FIND AREA OF COLLECTOR ACTUALLY ILLUMINATED

ILOSSI = 7 (NORM. SUPP., ION)

3

EFFECTIVE LOSS AREA including correction for angle of incidence

This quantity multiplied by the photo current density to get current

YIELD PER INCIDENT ELECTRON

PUT AEVV = 1, ZCU = 1

ILOSSD = 1, 2

ILOSSM = 2

III = 4

RELEVANT OUTPUT QUANTITY IS (aloss)(TR)

ORIGINAL PAGE IS
OF POOR QUALITY

cpresp.f

```
C                                                                    IVE
      IF(III.EQ.5)CPRESP=-CPRESP
      RETURN
99    CPRESP=0.
      RETURN
      END
```

arside.f

```
C            03/22/85    14:01:55        03/22/85    13:52:09        $380300.MJS
      FUNCTION ARSIDE(DAS,DSC,aloss,ils)                                    ARSIDE
C    12/30/78
C    COMPUTES AREA IN SQ.CM. OF VOYAGER SIDE SENSOR
C    DAS-RELATIVE DISPLACEMENT OF APERTURE AND SHIELD CIRCLE CELTERS, CM
C    DSC-RELATIVE DISPLACEMENT OF SHIELD AND COLLECTOR CIRCLE CENTERS, CM
c    aloss is loss function from secondary electrons on collector
C
C
CCC
CCCCCCCCC
C
C       HERR SULLIVAN SOLL DIESES PROGRAM SCHREIBEN
c       REAL*8 $$$DT(6) /'$$DATE$$','03/22/85','13:52:09',
c      | '  ARSIDE','FORTRAN','MJS       '/
      COMMON /SDTABL/TABLSD(25,25),NDAS,NDSC,DDAS,DDSC
C LOOK-UP TABLE FOR AREA OF SIDE SENSOR
C TABLSD(IAS,ISC) = AREA OF SIDE SENSOR AT (DAS,DSC)
C NDAS,NDSC SIZE OF ARRAY
C DDAS,DDSC RESPECTIVE STEP SIZEA
        common   /sidloss/  tablls(25,25,8)
c       tabel of losses for secondary electrons
c       same indicies as for tablsd
c       third index is for type of configuration
c       i=0 noloss, i=odd normal surpressor, even reverse supressos
c       i< 5 isotropic secondary production, i>4 cosine law secondary
c       i=1,2,5,6 e1 voltages, i=3,4,7,8 e2 or ion voltages
C
      LOGICAL INIT
      data      INIT/.TRUE./
      IF (INIT) CALL REDART
      INIT = .FALSE.
      ARSIDE = 0
      XAS = DAS/DDAS+1.0
      XSC = DSC/DDSC+1.0
      NAS = XAS
      NSC = XSC
      IF(NAS+1.GE.NDAS.OR.NSC+1.GE.NDSC) RETURN
      IF(NAS.GT.0.AND.NSC.GT.0) GO TO 10
      RETURN
 10   CONTINUE
C FOUR POINT BIVARIATE INTERPOLATION
      DXAS = XAS-NAS
      CXAS = 1.0-DXAS
      DXSC = XSC-NSC
      CXSC = 1.0-DXSC
         if ( ils .ne. 0) then
            aloss = (TABLls(NAS,NSC,ils)*CXAS+TABLls(NAS+1,NSC,ils)*
     |              DXAS)*CXSC+
     1      (TABLls(NAS,NSC+1,ils)*CXAS+TABLls(NAS+1,NSC+1,ils)*DXAS)*
     |              DXSC
         else
            aloss = 0.0
         end if
      ARSIDE = (TABLSD(NAS,NSC)*CXAS+TABLSD(NAS+1,NSC)*DXAS)*CXSC+
     1    (TABLSD(NAS,NSC+1)*CXAS+TABLSD(NAS+1,NSC+1)*DXAS)*DXSC
      RETURN
      END
```

```
C           01/16/85    16:04:22       01/16/85    10.11:39       $380300.MJS
      SUBROUTINE REDART
C CMS VERSION OF SETART FOR READING IN AREA TABLES PREVIOUSLY GENERATED
C WITH ARGEN.
C
C FT21F001 FOR MAIN SENSOR
C FT22F001 FOR SIDE SENSOR
C
C FILEDEF FT21F001 X DSN CSR $380300 ARMAIN DATA (PERM RECFM VBS
C BLKSIZE 19069 DSORG PS
C FILEDEF FT22F001 X DSN CSR $380300 ARSIDE DATA (PERM RECFM VBS
C BLKSIZE 19069 DSORG PS
C
c       REAL*8 $$$DT(6) /'$$DATE$$','01/16/85','10:11:39',
c      | '  REDART','  FORTRAN','MJS       '/
       COMMON /MNTABL/TABLMN(32,32),NSTPX,NSTPY,DSTPX,DSTPY,XMAX,YMIN,
      *    YMAX
C    LOOK-UP TABLE FOR AREA OF MAIN SENSOR
C    TABLMN(IX,IY)= AREA OF MAIN SENSOR AT X=VX/VZ8 Y=VY/VZ
C    NSTPX, NSTPY SIZE OF ARRAY IN X,Y
C    DSTPX= STEP SIZE IN X,     DSTPY= STEP SIZE IN Y
C    XMAX,YMIN,YMAX    LIMITS BEYOND WHICH AREA IS ZERO
C    PRESUME  XMIN=0.       AREA SAME FOR +X,-X
CCC
       COMMON /SDTABL/TABLSD(25,25),NDAS,NDSC,DDAS,DDSC
C LOOK-UP TABLE FOR AREA OF SIDE SENSOR
C TABLSD(IAS,ISC) = AREA OF SIDE SENSOR AT (DAS,DSC)
C NDAS,NDSC SIZE OF ARRAY
C DDAS,DDSC RESPECTIVE STEP SIZEA
c
          common   /sidloss/  tablls(25,25,8)
          real t1(25,25),t2(25,25),t3(25,25),t4(25,25)
          real t5(25,25),t6(25,25),t7(25,25),t8(25,25)
          equivalence   (t1(1,1),tablls(1,1,1))
          equivalence   (t2(1,1),tablls(1,1,2))
          equivalence   (t3(1,1),tablls(1,1,3))
          equivalence   (t4(1,1),tablls(1,1,4))
          equivalence   (t5(1,1),tablls(1,1,5))
          equivalence   (t6(1,1),tablls(1,1,6))
          equivalence   (t7(1,1),tablls(1,1,7))
          equivalence   (t8(1,1),tablls(1,1,8))
c          tabel of losses for secondary electrons
c          same indicies as for tablsd
c          third index is for type of configuration
c          i=0 noloss, i=odd normal surpressor, even reverse supressos
c          i< 5 isotropic secondary production, i>4 cosine law secondary
c          i=1,2,5,6 e1 voltages, i=3,4,7,8 e2 or ion voltages
c
       LOGICAL FIRST
          integer ia,ib
       data      FIRST/.FALSE./
       IF (FIRST) RETURN
       FIRST = .TRUE.
c          open(21,file="redart.data",form="unformatted")
          ia = -31
          call init( 1, ia, ib)
c
       READ (31) TABLMN,                DSTPX,DSTPY,XMAX,YMIN,YMAX
c                 1024    1      1      1     1     1     1     1
c                 1024    1      2      1     2     3     4     5
       READ (31) TABLSD,             DDAS,DDSC
```

redart.f

```
c                    625     1     1     1     1
c                    625     1     2     1     2
          read (31)
     | NDAS,NDSC
     | ,                          NSTPX,NSTPY
c
          call   initex( 1, ia, ib)
          read    (31,end=100) t1
          read    (31,end=100) t2
          read    (31,end=100) t3
          read    (31,end=100) t4
          read    (31,end=100) t5
          read    (31,end=100) t6
          read    (31,end=100) t7
          read    (31,end=100) t8
          return
 100      continue
          write (6,*) ' do loss table read'
        RETURN
        END
```

APPENDIX D

S/C 31 YEAR	DOY	TYPE OF MANEUVER	# 360 YAW TURNS	# 360 ROLL TURNS	Comments
1978	048	CRSMVR	10	25	ABORTED
1978	257	CRSMVR	10	25	
1979	034	CRSMVR	10	25	
1979	288/9	CRSMVR	10	25	
1980	004	MAG-ROLL		1	
1980	031	CRSMVR	10	25	
1980	121	MAG-ROLL	0	1	
1980	168	CRSMVR	10	25	
1980	189	MAG-ROLL	0	1	
1980	235	Mini-CRSMVR	4	4	
1980	334	MAG-ROLL	0	1	
1981	041	CRSMVR	10	25	
1981	117	MAG-ROLL	0	1	
1981	134	CRSMVR	10	25	
1981	195	MAG-ROLL	0	1	
1981	321	CRSMVR	10	25	
1981	351	MAG-ROLL	0	2	
1982	089	CRSMVR	10	25	
1982	218	MAG-ROLL	0	2	
1982	300	Mini-CRSMVR	4	4	
1983	117	CRSMVR	10	25	
1983	145	MAG-ROLL	0	4	
1983	306	Mini-CRSMVR	4	4	
1984	011	Mini-CRSMVR	4	4	
1984	116	Mini-CRSMVR	4	4	
1984	193	Mini-CRSMVR	4	4	
1984	312	Mini-CRSMVR	4	4	
1985	059	Mini-CRSMVR	0	0	CANCELLED
1985	213	MAG-ROLL & ABCAL	0	4	
1985	238	MAG-YAW	4	0	
1985	283	Mini-CRSMVR	4	4	
1986	093/4	Mini-CRSMVR	4	4	
1986	155/6	Mini-CRSMVR	4	4	
1986	264/7	Mini-CRSMVR	4	4	
1986	309	Mini-CRSMVR	4	4	
1987	016	Mini-CRSMVR	4	4	
1987	155/6	Mini-CRSMVR	4	4	SCHEDULED

S/C 32 YEAR	DOY	TYPE OF MANEUVER	# 360 YAW TURNS	# 360 ROLL TURNS	Comments
1977	362	CRSMVR	10	25	
1978	275	CRSMVR	10	25	
1979	155	Mini-CRSMVR	4	4	
1980	024	CRSMVR	10	25	
1980	136	CRSMVR	10	25	
1980	192	MAG-ROLL	0	4	
1980	249	MAG-ROLL	0	1	
1980	341	MAG-ROLL	0	1	
1980	351	Mini-CRSMVR	4	4	
1981	077	Mini-CRSMVR	4	4	
1981	148	CRSMVR	10	25	
1981	302	Mini-CRSMVR	4	4	
1982	103	CRSMVR	10	25	
1982	293	Mini-CRSMVR	4	4	
1983	132	Mini-CRSMVR	4	4	
1983	188	MAG-ROLL	0	4	
1983	313	Mini-CRSMVR	4	4	
1984	020	MAG-ROLL	0	4	
1984	145	Mini-CRSMVR	4	4	
1984	206	MAG-ROLL	0	4	
1984	329	Mini-CRSMVR	4	4	
1985	036	MAG-ROLL	0	0	MISSED
1985	112	MAG-ROLL	0	4	
1985	150	Mini-CRSMVR	4	4	
1985	170	MAG-ROLL & ABCAL	0	4	
1985	231	MAG-ROLL & ABCAL	0	4	
1985	330	Mini-CRSMVR	4	4	
1986	036	Mini-CRSMVR	4	4	
1986	113	Mini-CRSMVR	4	4	
1986	197	Mini-CRSMVR	4	4	
1986	273	Mini-CRSMVR	4	4	
1986	339	Mini-CRSMVR	4	4	
1987	042	Mini-CRSMVR	4	4	
1987	133	Mini-CRSMVR	4	4	

MASSACHUSETTS INSTITUTE OF TECHNOLOGY
CENTER FOR SPACE RESEARCH
CAMBRIDGE, MASSACHUSETTS 02139

June 14, 1978

MEMORANDUM

To: J. Belcher, G. Gordon, A. Lazarus

From: J. D. Sullivan

Subject: Nominal Cruise Science Maneuver (CRSMVR)

1. A science maneuver comprises 10 yaw turns and 26 roll turns; it is possible to do an intial partial roll before commencing the yaw turns. We have requested partial rolls to bring the side sensor across the sun, and to sweep the main cluster through the ecliptic on different CRSMVR.

2. The schedule for yaw turns is:

Turn 1	AJ15	normal plasma
2	AJ15	normal plasma
3	AJ03	plasma, reversed grid
4	AJ15	normal plasma
5	AJ10	current cal. mod off
6	AJ11	current cal. mod on
7	AJ13	IDC mod on normal grid
8	AJ15	normal plasma
9	AJ15	normal plasma
10	AJ15	normal plasma

The purpose of the calibrations is to determine the modulator pickup with no plasma input and to measure the net photo current. To really clean this up, we probably should do a turn with IDC mod on reversed grid.

3. The schedule for roll turns is:

Turn 1 - 25	AJ15	normal plasma
26	AJ10	current cal. mod off

The prime roll turn calibration goal is intermeasurement chain calibration.

APPENDIX E

```
C          03/21/84    16:14:04      03/21/84    14:46:26      $380300.MJS
c       FUNCTION CPRESP(V,UU,SUP,ZCU,AEVV,III)
c          modified to compute respons to sunlight
C    11/12/78    VMV
C       REVISED 12/30/78    VMV
C    COMPUTES RESPONSE FUNCTION OF VOYAGER CUP, IN (CURRENT UNIT)CM**3/SC
C    V(3)=VELOCITY VECTOR, CM/SEC
C    UU=EFFECTIVE MODULATOR VOLTAGE (VOLTS*Z, INCLUDING SIGN)
C    SUP= SUPPRESSOR VOLTAGE
C    ZCU= PARTICLE CHARGE
C    AEVV=PARTICLE MASS  (AEVV*V**2=ENERGY IN EV)
C    III=CUP INDEX  1=A, 2=B, 3=C, 4=D PROTON MODE, 5=D ELECTRON MODE
C
C    SUBPROGRAMS CALLED  - - - TRANSN,TRANSD,DIPLN,DISPLD,ARMAIN,ARSIDE
C
c       REAL*8 $$$DT(6) /'$$DATE$$','03/21/84','14:46:26',
c      | '  CPRESP','  FORTRAN','MJS       '/
c
       DIMENSION V(3)
          common     /comellos/  ilossm,ilossd,ilossi
c          ilossm 1 for e1 voltage, 2 for e2 or ion voltages
c          ilossd 0 no losses, 1 isotropic secondaries, 2 cosine law
          real ara(2),alossa(2)
          data   dm1   /1.6153/, ame   /3.553513e-19/
          data th1 /40./, th2 /80./, dth /0.5/ degrad /1.74533e-2/
          th = th1
 1        continue
          v(1) = 0.0
          tt = th*degrad
          v(2) = sin(tt)
          v(3) = cos(tt)
          uu = 0.0
          sup = 0.0
          zcu = 1.0
          aevv = 1.0
          iii = 4
       VZ=V(3)
c       IF(VZ.LE.0.)GO TO 99
       U=AEVV*VZ**2
5      TR=TRANSD(V,U,UU,SUP)
       CALL DISPLD(V,U,UU,SUP,X,Y)
          ilossm=2
          do 10 ilossd=1,2
          if (ilossd .eq. 1 ) then
                    ilossi = 3
          else
                    ilossi = 7
          end if
       AR=ARSIDE(X,Y,aloss,ilossi)
          ara(ilossd) = ar
          alossa(ilossd) = aloss
 10       continue

          write ( 6,16) th, x, y, tr, ara, alossa
 16       format(f6.2,1x,2f6.2,2x,pe13.3,2x,2e13.3,2x,2e13.3)
          if ( th .gt. th2) go to 20
          th = th+dth
          go to 1
20     CONTINUE
C    PUT IT ALL TOGETHER
          call exit
```

CPRESP

D-CUP CURRENTS FOR IDC MOD ON WHEN FACING SUN

ORIGINAL PAGE IS OF POOR QUALITY

cprlm.f

```
c       CPRESP=ZCU*VZ*TR*(AR - alossd)
cC    CHANGE SIGN OF CURRENT IN ELECTRON MODE, TO KEEP OUTPUT SIGNAL POSIT
cC                                                                    IVE
c       IF(III.EQ.5)CPRESP=-CPRESP
c       RETURN
c99     CPRESP=0.
c       RETURN
        END
```

ANGLE FROM D-CUP NORMAL	DAS	DSC	TRANSPARENCY	OVERLAP AREA		EFF. LOSS AREA ISOTROPIC SECONDARIES	EFF. LOSS AREA COSINE DISTRIBUTION
40.00	3.87	1.22	0.639e+00	0.497e+02	0.497e+02	0.925e+01	0.497e+01
40.50	3.94	1.24	0.638e+00	0.490e+02	0.490e+02	0.915e+01	0.495e+01
41.00	4.01	1.26	0.637e+00	0.483e+02	0.483e+02	0.906e+01	0.493e+01
41.50	4.08	1.28	0.636e+00	0.475e+02	0.475e+02	0.896e+01	0.490e+01
42.00	4.15	1.31	0.634e+00	0.468e+02	0.468e+02	0.886e+01	0.488e+01
42.50	4.22	1.33	0.633e+00	0.460e+02	0.460e+02	0.876e+01	0.486e+01
43.00	4.30	1.35	0.631e+00	0.452e+02	0.452e+02	0.865e+01	0.484e+01
43.50	4.37	1.38	0.630e+00	0.444e+02	0.444e+02	0.855e+01	0.481e+01
44.00	4.45	1.40	0.628e+00	0.436e+02	0.436e+02	0.844e+01	0.479e+01
44.50	4.53	1.43	0.627e+00	0.428e+02	0.428e+02	0.833e+01	0.476e+01
45.00	4.61	1.45	0.625e+00	0.419e+02	0.419e+02	0.820e+01	0.471e+01
45.50	4.69	1.48	0.623e+00	0.410e+02	0.410e+02	0.805e+01	0.465e+01
46.00	4.77	1.50	0.622e+00	0.400e+02	0.400e+02	0.789e+01	0.459e+01
46.50	4.86	1.53	0.620e+00	0.389e+02	0.389e+02	0.773e+01	0.452e+01
47.00	4.94	1.56	0.618e+00	0.379e+02	0.379e+02	0.756e+01	0.445e+01
47.50	5.03	1.58	0.616e+00	0.369e+02	0.369e+02	0.740e+01	0.438e+01
48.00	5.12	1.61	0.615e+00	0.358e+02	0.358e+02	0.723e+01	0.431e+01
48.50	5.21	1.64	0.613e+00	0.348e+02	0.348e+02	0.705e+01	0.423e+01
49.00	5.30	1.67	0.611e+00	0.337e+02	0.337e+02	0.687e+01	0.416e+01
49.50	5.39	1.70	0.609e+00	0.326e+02	0.326e+02	0.669e+01	0.408e+01
50.00	5.49	1.73	0.607e+00	0.314e+02	0.314e+02	0.650e+01	0.399e+01
50.50	5.59	1.76	0.604e+00	0.303e+02	0.303e+02	0.631e+01	0.390e+01
51.00	5.69	1.79	0.602e+00	0.291e+02	0.291e+02	0.612e+01	0.381e+01
51.50	5.79	1.82	0.600e+00	0.280e+02	0.280e+02	0.591e+01	0.372e+01
52.00	5.90	1.86	0.598e+00	0.268e+02	0.268e+02	0.570e+01	0.362e+01
52.50	6.00	1.89	0.595e+00	0.256e+02	0.256e+02	0.549e+01	0.351e+01
53.00	6.11	1.92	0.593e+00	0.243e+02	0.243e+02	0.527e+01	0.340e+01
53.50	6.23	1.96	0.590e+00	0.230e+02	0.230e+02	0.503e+01	0.327e+01
54.00	6.34	2.00	0.588e+00	0.217e+02	0.217e+02	0.478e+01	0.314e+01
54.50	6.46	2.03	0.585e+00	0.204e+02	0.204e+02	0.454e+01	0.301e+01
55.00	6.58	2.07	0.582e+00	0.191e+02	0.191e+02	0.428e+01	0.287e+01
55.50	6.70	2.11	0.580e+00	0.177e+02	0.177e+02	0.402e+01	0.272e+01
56.00	6.83	2.15	0.577e+00	0.164e+02	0.164e+02	0.376e+01	0.257e+01
56.50	6.96	2.19	0.574e+00	0.151e+02	0.151e+02	0.350e+01	0.242e+01
57.00	7.10	2.23	0.571e+00	0.137e+02	0.137e+02	0.322e+01	0.226e+01
57.50	7.23	2.28	0.567e+00	0.124e+02	0.124e+02	0.295e+01	0.209e+01
58.00	7.37	2.32	0.564e+00	0.111e+02	0.111e+02	0.267e+01	0.192e+01
58.50	7.52	2.37	0.561e+00	0.973e+01	0.973e+01	0.238e+01	0.174e+01
59.00	7.67	2.41	0.557e+00	0.842e+01	0.842e+01	0.209e+01	0.155e+01
59.50	7.82	2.46	0.554e+00	0.718e+01	0.718e+01	0.181e+01	0.136e+01
60.00	7.98	2.51	0.550e+00	0.594e+01	0.594e+01	0.152e+01	0.116e+01
60.50	8.14	2.56	0.546e+00	0.475e+01	0.475e+01	0.124e+01	0.964e+00
61.00	8.31	2.62	0.542e+00	0.365e+01	0.365e+01	0.964e+00	0.762e+00
61.50	8.49	2.67	0.538e+00	0.255e+01	0.255e+01	0.689e+00	0.556e+00
62.00	8.67	2.73	0.534e+00	0.164e+01	0.164e+01	0.450e+00	0.368e+00
62.50	8.85	2.79	0.530e+00	0.828e+00	0.828e+00	0.230e+00	0.191e+00
63.00	9.04	2.85	0.525e+00	0.215e+00	0.215e+00	0.614e-01	0.525e-01
63.50	9.24	2.91	0.521e+00	0.679e-01	0.679e-01	0.197e-01	0.170e-01
64.00	9.45	2.97	0.516e+00	0.000e+00	0.000e+00	0.000e+00	0.000e+00
64.50	9.66	3.04	0.511e+00	0.000e+00	0.000e+00	0.000e+00	0.000e+00
65.00	9.88	3.11	0.506e+00	0.000e+00	0.000e+00	0.000e+00	0.000e+00
65.50	10.11	3.18	0.501e+00	0.000e+00	0.000e+00	0.000e+00	0.000e+00
66.00	10.35	3.26	0.495e+00	0.000e+00	0.000e+00	0.000e+00	0.000e+00
66.50	10.60	3.34	0.490e+00	0.000e+00	0.000e+00	0.000e+00	0.000e+00
67.00	10.85	3.42	0.484e+00	0.000e+00	0.000e+00	0.000e+00	0.000e+00
67.50	11.12	3.50	0.478e+00	0.000e+00	0.000e+00	0.000e+00	0.000e+00
68.00	11.40	3.59	0.471e+00	0.000e+00	0.000e+00	0.000e+00	0.000e+00
68.50	11.70	3.68	0.465e+00	0.000e+00	0.000e+00	0.000e+00	0.000e+00
69.00	12.00	3.78	0.458e+00	0.000e+00	0.000e+00	0.000e+00	0.000e+00
69.50	12.32	3.88	0.451e+00	0.000e+00	0.000e+00	0.000e+00	0.000e+00
70.00	12.66	3.98	0.444e+00	0.000e+00	0.000e+00	0.000e+00	0.000e+00
70.50	13.01	4.10	0.436e+00	0.000e+00	0.000e+00	0.000e+00	0.000e+00
71.00	13.38	4.21	0.428e+00	0.000e+00	0.000e+00	0.000e+00	0.000e+00
71.50	13.77	4.33	0.420e+00	0.000e+00	0.000e+00	0.000e+00	0.000e+00
72.00	14.18	4.46	0.412e+00	0.000e+00	0.000e+00	0.000e+00	0.000e+00
72.50	14.61	4.60	0.403e+00	0.000e+00	0.000e+00	0.000e+00	0.000e+00
73.00	15.07	4.74	0.393e+00	0.000e+00	0.000e+00	0.000e+00	0.000e+00
73.50	15.55	4.90	0.384e+00	0.000e+00	0.000e+00	0.000e+00	0.000e+00
74.00	16.07	5.06	0.374e+00	0.000e+00	0.000e+00	0.000e+00	0.000e+00
74.50	16.61	5.23	0.363e+00	0.000e+00	0.000e+00	0.000e+00	0.000e+00
75.00	17.20	5.41	0.352e+00	0.000e+00	0.000e+00	0.000e+00	0.000e+00
75.50	17.82	5.61	0.341e+00	0.000e+00	0.000e+00	0.000e+00	0.000e+00
76.00	18.48	5.82	0.329e+00	0.000e+00	0.000e+00	0.000e+00	0.000e+00
76.50	19.19	6.04	0.317e+00	0.000e+00	0.000e+00	0.000e+00	0.000e+00
77.00	19.96	6.28	0.304e+00	0.000e+00	0.000e+00	0.000e+00	0.000e+00
77.50	20.78	6.54	0.291e+00	0.000e+00	0.000e+00	0.000e+00	0.000e+00
78.00	21.68	6.82	0.277e+00	0.000e+00	0.000e+00	0.000e+00	0.000e+00
78.50	22.65	7.13	0.263e+00	0.000e+00	0.000e+00	0.000e+00	0.000e+00
79.00	23.70	7.46	0.248e+00	0.000e+00	0.000e+00	0.000e+00	0.000e+00
79.50	24.86	7.83	0.232e+00	0.000e+00	0.000e+00	0.000e+00	0.000e+00
80.00	26.13	8.23	0.216e+00	0.000e+00	0.000e+00	0.000e+00	0.000e+00
80.50	27.53	8.67	0.199e+00	0.000e+00	0.000e+00	0.000e+00	0.000e+00

APPENDIX F

FRINGE FIELD CALCULATIONS NEAR NEGATIVE MODULATOR GRID SUPPORT

From: G. S. Gordon Jr.

Date: January 6, 1988

The directory /usr4/rlm/fringe contains the programs for computing the fringing field in the region near the negative modulator grid for the side sensor; some more generally usefull programs are also included. All of the programs are compiled and linked using make and are run by direct invocation. The user must set up any environmental variables by hand, although some sample files (e.g., setft[123]) exist which can be run with the source command.

The most important programs are:

elec

ELEC calls initvolt to read in the potential field from unit ft10. From specified initial conditions (stdin), ELEC then integrates an electron trajectory through the electric field to the plane containing the shield ring and supressor grid (the assumed potential there is zero as in the reversed supressor configuration). If ft11 is defined, the trajectory is written out on ft11 in a format suitable for mongo. Note that the voltage is normally negative and the the external units are in inches while the internal dimensions are in meters. Note that TRAJ is a logical part of ELEC, and that the PARAMETERs must match. VOLTAGE computes the E field from the read in potential field. It should be noted the the field at the very edge is not correct as the first equipotential contour does not lie exactly on the metal conductor, i.e., at the exact boundary.

pltxy

PLTXY plots out the potential contours, E field lines, or the inverse of the conformal map(real,imaginary), depending upon the type of plot specified: 1, 2, 3, 4. PLTXY does its plotting with mongo coutours, and it will plot to several devices, s=sun, t=tek, l=landscape laser, p=portrait laser, with different contour integrval which are documented (some what) in the program.

wfromz

WFROMZ inverts the function ZFUNC using a variation on Newton Rapson method. ZFUNC is $z\,(w)$ which is the solution of

$$\frac{dz}{dw} = \frac{k\sqrt{w-1}}{\pi\, w\sqrt{w-c}} \tag{1}$$

with $k \equiv hc^{-1/2}$ and $c > 1$, $k > 0$. The solution is given by

$$z\,(w) = \frac{k}{\pi}\left[\cosh^{-1}\left[\frac{2w-c-1}{c-1}\right] - \frac{1}{\sqrt{c}}\cosh^{-1}\left[\frac{[c+1]\,w-2c}{[c-1]\,w}\right]\right] \tag{2}$$

In this problem $k = 0.452$ inches, $h = 0.312$ inches, and $c = 2.0988$. This solution is given on p.161 of H. Korber [*Dictionary of Conformal Representations*, Dover Publications, Inc., 1957] and in problem 10.21 on p.1315 of Morse and Feshbach [*Methods of Theoretical Physics*, Mc Graw-Hill Book Co., Inc., New York, 1953]. The inversion method tries using both the numerical and analytic derivatives to find the solution and accepts the closer iteration; however, if both iterations are farther from the solution than the initial guess, the method checks in the immediate vicinity of the initial guess for a better solution. WFROMZ also changes the size of the interval both for computing the derivative and for what it considers the immediate vicinity. It returns when either the max iterations have been run or the

required accuracy achieved (defined as moving less than derr on the last iteration or if the number of iterations is more than jmax/2 being within a specified error of z); both W and Z of the final point are returned.

acosh

ACOSH compute the inverse sin, cos, sinh, cosh for complex*16 arguments. It shold be noted that the cutlines used may not be what are expected as they were made for this probleem.

cone.f

CONE computes and stores the potential field as is used by ELEC.

con[f12]?

These programs are closely related to one another. They all compute the conformal maps much as CONE does, only where cone and conf compute the inverse map, con and con1 compute the forward map; con1 and con2 plot out the contours.

APPENDIX G

11/17/87

①

Modulator grid pickup
(RFM)

σ_i = charge per unit area on grid i
ρ = grid wire radius

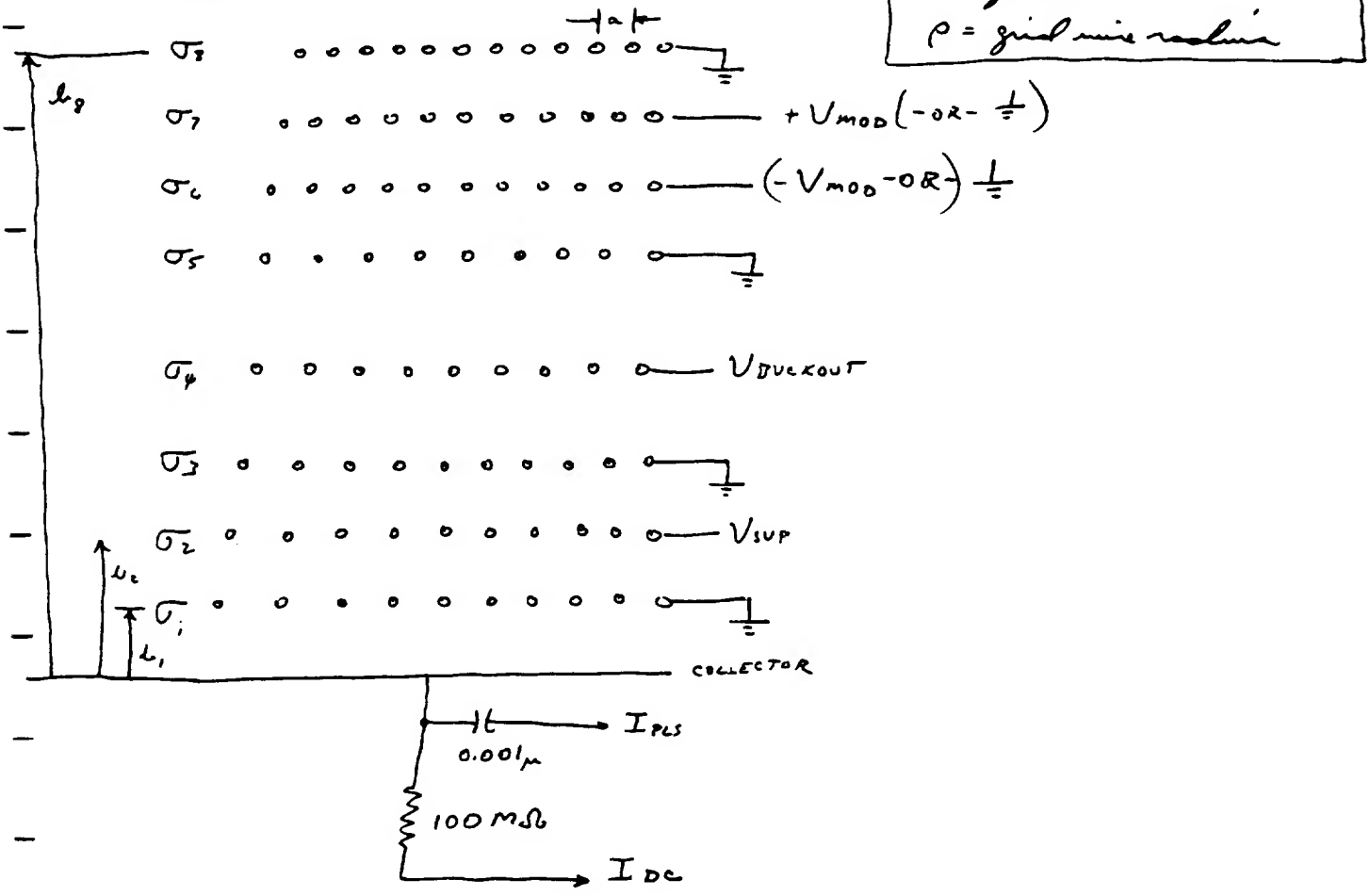

b_i = distance from collector to grid i

11/17/87

(2)

Including the eight grids and their images, the electrostatic potential (in cgs units) is given by (see Morse and Feshbach):

$$\psi = a \sum_{i=1}^{8} \sigma_i \ln \left\{ \frac{\sin^2 \frac{\pi x}{a} + \sinh^2 \left[\frac{\pi}{a} (y + b_i) \right]}{\sin^2 \frac{\pi x}{a} + \sinh^2 \left[\frac{\pi}{a} (y - b_i) \right]} \right\}$$

Enforce the ordering $\rho \ll a \ll b_i \; \forall i$ to obtain

$$V_n = 4\pi \sum_{i=1}^{8} \sigma_i b_i + 2a\sigma_n \ln \left(\frac{a}{2\pi\rho} \right)$$

$$= 4\pi \left[\sum_{i=1}^{8} \sigma_i b_i + \sigma_n \left(\frac{a}{2\pi} \ln \frac{a}{2\pi\rho} \right) \right]$$

where V_n is the potential of the nth grid.

In the same limit, the total charge on the collector plate is given by

$$\sigma_c = -\frac{1}{4\pi} \left. \frac{\partial \psi}{\partial y} \right|_{y=0} \cong -\sum_{i=1}^{8} \sigma_i \quad \text{(where the } x \text{ dependence is approximated).}$$

11/12/87

(3)

Suppose we restrict ourselves to only the oscillatory part of the σ_i's (due to the oscillatory part of the V_i's). Then we obtain the set of equations

$$\frac{1}{4\pi}\begin{pmatrix} 0 \\ 0 \\ 0 \\ \Delta V_{DUCKOUT} \\ 0 \\ 0 \\ \Delta V_{MOD} \\ 0 \end{pmatrix} = \begin{pmatrix} b_1+\varepsilon & b_1 & b_1 & \cdots & b_1 \\ b_1 & b_2+\varepsilon & b_2 & \cdots & b_2 \\ b_1 & b_2 & b_3+\varepsilon & \cdots & b_3 \\ b_1 & b_2 & b_3 & \cdots & b_4 \\ b_1 & b_2 & b_3 & \cdots & b_5 \\ b_1 & b_2 & b_3 & \cdots & b_6 \\ b_1 & b_2 & b_3 & \cdots & b_7 \\ b_1 & b_2 & b_3 & \cdots & b_8+\varepsilon \end{pmatrix} \begin{pmatrix} \sigma_1 \\ \sigma_2 \\ \sigma_3 \\ \sigma_4 \\ \sigma_5 \\ \sigma_6 \\ \sigma_7 \\ \sigma_8 \end{pmatrix}$$

↑ oscillatory part

Define $a_{j+1} \equiv \dfrac{\varepsilon a_j}{\varepsilon + a_j} + b_{j+2} - b_{j+1}$

$a_0 = b_1$

as in the limit of small ε, $a_j \to b_{j+1} - b_j$ which is just the integral spacing.

$$\varepsilon \equiv \frac{a}{2\pi} \ln \frac{a}{2\pi\rho}$$

$$\simeq 0.0299 \text{ cm}$$

11/17/87

By manipulating the equations into a triangular form and using back substitution, we obtain (after significant algebra):

$$\sum_{i=1}^{8} \sigma_i = \left(\prod_{j=0}^{5} \frac{\varepsilon}{\varepsilon + a_j} \right) \frac{1}{\varepsilon + a_6} \left(1 - \frac{\varepsilon}{\varepsilon + a_7} \frac{a_6}{\varepsilon + a_6} \right) \frac{\Delta V_{MOD}}{4\pi}$$

$$+ \left(\prod_{j=0}^{2} \frac{\varepsilon}{\varepsilon + a_j} \right) \frac{1}{\varepsilon + a_3} \left(- \frac{1}{\varepsilon + a_6} \frac{a_3}{\varepsilon + a_3} \left[\frac{\varepsilon}{\varepsilon + a_4} \right]^2 \left[\frac{\varepsilon}{\varepsilon + a_5} \right]^2 \right.$$

$$\times \left[1 + \frac{\varepsilon}{\varepsilon + a_6} \frac{\varepsilon}{\varepsilon + a_7} \right] + \left[1 + \frac{\varepsilon}{\varepsilon + a_4} \frac{a_3}{\varepsilon + a_3} \right\} - 1 + \frac{\varepsilon}{\varepsilon + a_4} \frac{\varepsilon}{\varepsilon + a_5}$$

$$\times \frac{\Delta V_{BUCKOUT}}{4\pi}$$

If we let $\varepsilon \to 0$ and only keep the lowest order, non-vanishing terms, we obtain

$$\sum_{i=1}^{8} \sigma_i \simeq \frac{1}{a_0} \frac{\varepsilon^3}{a_1 a_2 a_3} \left[\frac{\Delta V_{BUCKOUT}}{4\pi} + \frac{\varepsilon^3}{a_4 a_5 a_6} \frac{\Delta V_{MOD}}{4\pi} \right]$$

with the a_i's equal to the integral spacing.
For the side sensor

$$\varepsilon = 0.0299 \text{ cm}$$

$$\frac{\varepsilon^3}{a_0 a_1 a_2 a_3} = 3.8829 \times 10^{-4} \text{ cm}^{-1}$$

$$\frac{\varepsilon^3}{a_4 a_5 a_6} = 4.8604 \times 10^{-5}$$

11/17/87

(5)

In the L-mode for channel 16 $\Delta V_{mod} = \frac{1500}{300}$

$= 5$ at the last peak-to-peak

$\frac{\varepsilon^3}{a_v a_s a_c}(1500) = 0.0729$ volts to compensate

at this level $i_c = \frac{d\sigma_c}{dt} A$

$= 2\pi\nu A \sigma_c$

$A = 126.68\ cm^2$

$\nu = 800\pi\ s^{-1}$

$\rightarrow i_c = 7.963 \times 10^{-13}$ amperes

If the shielding of each grid is increased by a factor of 2 due to the 2D mesh

$i_c = 1.24 \times 10^{-14}$ amperes - below the thermal noise level ($\sim 5 \times 10^{-14}$ amperes)

[Exact solution of the equations gives results within ~60% of these approximate results].

For the main sensor, a rough calculation gives ~4.6 volts at the last exit grid (1500 volts pp on the modulator grid); hence, 5 volts pp last exit voltage (out of phase) gives a fair value for the compensating pick up (at the level of approximations used).